For Reference

NOT TO BE TAKEN FROM THIS ROOM

Ex libris
universitatis
albertaensis

QUAECUMQUE VERA

Digitized by the Internet Archive
in 2022 with funding from
University of Alberta Library

https://archive.org/details/Dettman1984

THE UNIVERSITY OF ALBERTA

FLUORINE NUCLEAR MAGNETIC RESONANCE STUDIES OF MICELLE AND VESICLE BOUND M13 COAT PROTEIN

by

© Heather Diane Dettman

A THESIS

SUBMITTED TO THE FACULTY OF GRADUATE STUDIES AND RESEARCH
IN PARTIAL FULFILMENT OF THE REQUIREMENTS FOR THE DEGREE
OF Doctor of Philosophy

Department of Biochemistry

EDMONTON, ALBERTA

FALL, 1984

Dedication

To my parents, Hugo and Coralie Dettman

Thank you for encouraging me to make my own decisions and supporting me, regardless of my choice.

Abstract

Structural studies of intrinsic membrane proteins, those proteins that span the lipid bilayer of cellular membranes, have been few. There has been much interest in defining the contributions of interactions with lipids, water, proteins and/or other components of the lipid and aqueous phases, to the structure and function of intrinsic proteins; structural studies of these interactions have been limited due to the insolubility in water, the low yields and the lack of knowledge of the amino acid sequence of most intrinsic proteins.

An intrinsic protein which is well characterised and can be isolated in large quantities, is the coat (gene VIII) protein of the filamentous coliphage, M13. The M13 coat protein spans the cytoplasmic membrane of its host *E. coli* during infection, hence it is an intrinsic membrane protein. The protein consists of 50 amino acids, whose sequence may be divided into three regions: an acidic N-terminus, a basic C-terminus and a hydrophobic core. The hydrophilic and hydrophobic domains of the coat protein have been biosynthetically labelled with the 3-fluoro-analogs of phenylalanine and tyrosine, respectively. Structural information was obtained by monitoring the motion and exposure of the Fphe and Ftyr residues of the DOC micelle- or vesicle-bound protein using ^{19}F NMR.

The exposure of the Fphe and Ftyr residues of the labelled coat proteins in DOC micelles, was determined from the results of proteolytic digestions, solvent isotope induced shift measurements, fluorine photo-chemically induced dynamic nuclear polarization experiments, and pH titrations. The data showed that the Fphe residues were outside of the micelle while the Ftyr residues were either at the solvent-micelle interface (Ftyr21) or within the micelle (Ftyr24). Temperature studies, monitored with both circular dichroism and ^{19}F NMR revealed that structural changes occurred with temperature in the immediate vicinities of the fluoro-residues and/or over large segments of the protein. A model dependent analysis of the Fphe and Ftyr ring motions using the ^{19}F NMR relaxation data showed that Fphe11 is slightly more mobile than Ftyr21, and Ftyr21 is slightly more mobile than Ftyr24. This result, together with the observation that water had little access to the Fphe11 fluorine suggested that the hydrophilic end(s) were structured such that Fphe11 was, at least, partially buried in a hydrophobic pocket.

The exposure of the Fphe and Ftyr residues of the labelled coat proteins reconstituted into phospholipid vesicles was determined by monitoring their accessibility to chymotrypsin and the effects of temperature on their ^{19}F NMR resonances. The results showed the Fphe residues to be outside the lipid bilayer; the Ftyr residues were inside the lipid bilayer. Qualitatively, the Ftyr ring motions were

dependent upon the phase state of the bilayer lipids; the mobility was restricted when the lipid was in the gel-state. Above the lipid phase transition temperature, the ^{19}F NMR analyses of the Fphe and Ftyr ring motions of the vesicle-bound protein showed that the Fphe residues were not much more mobile than the Ftyr residues, suggesting that, as with the DOC micelle-bound coat proteins, the hydrophilic ends were not freely diffusing in solution but were structured.

Acknowledgements

My project required the use of a variety of techniques hence it gave me the opportunity to work with a fair number of people. The first of those I would like to thank are my supervisors: Drs. Brian Sykes and Joel Weiner. Brian spent many hours discussing experimental analyses and explaining both the theoretical and practical aspects of NMR spectroscopy: I am grateful for his patience. As well, his enthusiasm, whether directed at your most recent results or your effort at baking a birthday cake, made working in Room 419 enjoyable. I especially want to thank him for helping me to "keep things in perspective" throughout the writing of this thesis. I am grateful to Joel, my co-supervisor, for the early development of the M13 project. Since I started, Joel has been a reliable source of information on the biochemical aspects of the system and a constant vigilante for the biological relevance of the experiments being done; his contributions to the project served to give me an appreciation of the biological problems which may be studied using physical techniques.

The initial experiments on the M13 project were performed by Mr. D. Scott Hagen. I wish to thank him for supervising me in my early days in the project, as it made the transition into the project easier. As well, I greatly appreciate the work done by Mr. Meyer Aaron on the solvent isotope induced shift and the fluorine photo-chemically

induced dynamic nuclear polarization projects. He "single-handedly" synthesized the N-acetylated/methyl-esterified derivatives of the fluorinated amino acids, measured the pH dependence of the SIIS's of the fluoro-amino acids and their blocked analogs, tried, in vain, to solubilize the coat protein in urea or guanidine HCl, and, aided by Dr. Brian Sykes, ran the fluoro-CIDNP of the Ftyr labelled coat protein in micelles. He also obtained the same SIIS results as I did, so what more can one want from a summer student?! A third person to whom I am indebted for his work on the M13 project is Dr. Poul Hansen. His expertise in the solvent isotope shift field and his careful experiments with model compounds, Fphe-labelled M13 coat protein in micelles and Fphe-containing coat protein fragment 1-11 has allowed us to confidently interpret the micelle-bound coat protein SIIS results. The task of continuing the M13 project after I leave, will be placed in the hands of Dr. Gillian Henry and Dr. Joe O'Neil. I thank both of them for choosing this project as it is satisfying to know that a project on which I have worked so long, will not terminate upon my departure. I would also like to thank Gillian for drawing the "artist's impression of a biological membrane" (Figure I-1); not only can she make ^{13}C-labelled coat protein, but she can draw! My only reservation is that both Gillian and Joe insist on tying knots in their dialysis tubing; this is progress!?

There are many people throughout the Biochemistry department who helped me with various segments of the M13

project, either directly or indirectly. I would like to thank Mr. Gerry McGuaid and Mr. David Corson for performing the maintenance duties for the spectrometer, Dr. Joyce Pearlstone and Dr. Clive Sanders for discussions and technical assistance with the paper electrophoresis and amino acid analysis experiments, Mr. Brian McDonough and Dr. Ruthven Lewis for supplying the fluorinated lipids, Mr. Mike Nattriss for running the amino acid analyses, Mr. Kim Oikawa for running the circular dichroism spectra, Mr. Bob Iwanicka for maintaining the 10 litre fermentors, and Mr. Roger Bradley for taking the electron micrographs of my vesicles.

I also had assistance from individuals in other departments. I would like to thank Mr. Glen Bigam, Mr. Tom Brisbane and Dr. Tom Nakashima for the use of the 400 MHz NMR spectrometer in the NMR facility of the University of Alberta Chemistry Department; Drs. Ponsy Lu and Stan Opella for the use of their 150 MHz spectrometer in Philadelphia; and Drs. Ted Schaefer and Frank Hruska and Mr. Kirk Marat for the use of their 100 MHz spectrometer in the Chemistry Department of the University of Manitoba in Winnipeg.

The execution of my thesis has left me indebted to several people. I am grateful to Mr. Perry d'Obrenan for drawing many of the figures for this thesis and for publications. As well, I would especially like to thank

Mrs. Pat McDonald for typing a major portion of my thesis and to Ms. Elke Metke for her help with entering corrections; without their assistance, I am sure I would not have been finished until Fall '85!

Aside from work, there are a number of friends who have made my grad studies days pleasant and who I will always remember fondly. Some I have already mentioned: Gillian Henry, Elke Metke, Ruthven Lewis, Clive Sanders and Brian McDonough. Others I have not: Dr. Judy Shelling and Dr. Lana Lee who were fellow graduate students in the lab; Dr. Steve Withers and Dr. John and Ms. Carol Baldo, who taught me how to enjoy the Rockies; Ms. Michele Bjornson, who has proven that SOME "Med-students" are terrific people; and Mr. Bernie Lemire and Ms. Cathy McPhalen, who will carry on the "Black Forest Cake" tradition. Last, but most important is Dr. Brian Marsden, whose love and friendship has greatly contributed to my happiness over the last few years.

Table of Contents

Chapter Page

I. Introduction 1

A. Structural Studies of Membrane Proteins 1

B. The Use of ^{19}F NMR in Studying Protein Structure 6

C. The History and Objectives of this Project 10

II. Experimental Methods 16

A. Materials 16

B. Procedures for the experiments with Fphe and Ftyr Amino Acids 16

Studies of the Effects of Bicarbonate Buffer 16

Determination of Solvent Isotope Induced Shifts 17

The synthesis of the N-acetyl-, methyl ester derivatives 18

C. Preparation of Fphe and Ftyr Labelled M13 Coat Protein 21

E. Coli Preparation 21

Phage Preparation 21

Phage Titer Determination 22

M13 Phage Growth in Ten Liter Fermentors 23

Phage Purification 24

D. Procedures for the Experiments with DOC Micelle-Bound M13 Coat Protein 26

Preparation of DOC Micelle-Bound M13 Coat Protein 26

Chymotryptic Fragment Purification 28

Solvent Isotope Induced Shifts 29

Circular Dichroism Studies 31

E. Procedures for Experiments with Vesicle-Bound M13 Coat Protein 35

Reconstitution of M13 Coat Protein into Phospholipid Vesicles 35

Determination of Phospholipid to Protein Ratios 40

Chymotryptic Fragment Purification 45

F. NMR Procedures 46

Instrument and Equipment Description and Conventions 46

Relaxation and Nuclear Overhauser Experiments 47

Fluorine Chemically Induced Dynamic Nuclear Polarization Studies 49

III. Studies of the Two Amino Acids: Fphe and Ftyr 50

A. Interaction with Carbon Dioxide in Bicarbonate Buffer 50

Introduction 50

Theory 51

Results 54

Discussion 64

B. Solvent Isotope Induced Chemical Shifts 79

Introduction 79

Theory 81

Results 84

Discussion 95

IV. Studies of Fphe and Ftyr Labelled M13 Coat Protein in DOC Micelles 103

A. Assignments of the Resonances of the ^{19}F NMR Spectrum 103

Introduction 103

Results 106

Discussion 119

B. The Exposure of Fphe and Ftyr Amino Acid Residues of M13 Coat Protein in DOC Micelles ..121

Introduction 121

Theory 124

Results 127

Discussion 145

V. Fphe and Ftyr Labelled M13 Coat Protein Reconstituted into Phospholipid Vesicles 162

A. The Exposure of the Fphe and Ftyr Residues 162

Introduction 162

Results 164

Discussion 174

B. The Analyses of Fphe and Ftyr Ring Motions 180

Introduction 181

Theory 182

Results 192

Discussion 192

Concluding Discussion 201

A. Thesis Overview 201

B. Possible Future Studies 205

Bibliography 209

Appendix A 215

Appendix B 217

List of Tables

Table Page

II-1 The molar extinction coefficients for Fphe, Ftyr, and unlabelled M13 coat protein 33

III-1 The T_1 relaxation times of Fphe and Ftyr amino acid resonances 65

III-2 The equilibrium constants used for the carbamate species analysis 73

III-3 Literature values of amino group carbamate formation constants 78

III-4 The SIIS values of Fphe, 4-Fphe, and Ftyr as functions of pH 92

IV-1 Paper electrophoresis mobilities at pH6.5 of the chymotryptic fragments of M13 coat protein 116

IV-2 The SIIS data for the Fphe and Ftyr resonances of labelled coat protein in DOC micelles 131

IV-3 The % exposure of the Fphe and Ftyr residues of the labelled coat proteins in DOC micelles as determined by SIIS 133

IV-4 The chemical shift, T_1, and linewidth data of the ^{19}F NMR resonances of Fphe- and Ftyr-labelled M13 coat proteins in DOC micelles 146

IV-5 The T_1 and linewidth results calculated using the best-fit values of D_1, D_2 and γ_0 156

V-1 T_1 and nOe of Fphe- and Ftyr-labelled M13 coat proteins reconstitutedinto phospholipid vesicles 194

V-2 The T_1, $\Delta\nu$, and nOe results obtained using the best-fit values of D_1, D_2, and γ_0 for the analyses of the Fphe and Ftyr residue ring motions in vesicle-bound coat protein 197

List of Figures

Figure Page

I-1 An artist's representation of a biological membrane, as proposed by the fluid mosaic model 2

I-2 The chemical structures of 3-fluorophenylalanine (Fphe) and 3-fluoro-tyrosine (Ftyr) 9

I-3 The amino acid sequence of M13 coat protein 12

II-1 The Sephacryl S200 elution profile of DOC micelle-bound M13 coat protein 27

II-2 The Sepharose CL-4B column elution profile of a sample containing coat protein reconstituted into phospholipid vesicles after sonication 38

III-1 The ^{19}F NMR spectrum of Fphe and Ftyr in bicarbonate buffer 55

III-2 The ^{19}F NMR spectra of Fphe and Ftyr with varying NH_4HCO_3 concentrations 57

III-3 The ^{19}F NMR spectra of Fphe in either phosphate or Tris-HCl buffer with varying pH 58

III-4 The ^{19}F NMR spectra of 3-fluoro-benzoic acid in bicarbonate buffer with varying pH 59

III-5 The ^{19}F NMR spectra of Fphe and Ftyr in bicarbonate with varying pD 60

III-6 The pD titration curves of the Fphe and Ftyr ^{19}F NMR chemical shifts in bicarbonate buffer 62

III-7 The graphs of the concentrations of the Fphe and Ftyr carbamate species as functions of pD 63

III-8 The proton NMR of H_2O and HDO in acetone-d_6 87

Figure Page

III-9 The ^1H NMR spectra at 300°K of mixtures of H_2O and 99.9% D_2O 89

III-10 The ^{19}F NMR spectra of Fphe and Ftyr as functions of % D_2O 90

III-11 The graphs of the ^{19}F NMR chemical shifts of Fphe and Ftyr as functions of % D_2O, with and without DOC 91

III-12 The graphs of the ^{19}F NMR chemical shifts of 4-Fphe and Ftyr as functions of % D_2O and pH 94

III-13 The ^{19}F NMR spectra of N- and C-blocked Fphe and Ftyr as functions of % D_2O 97

III-14 The graphs of the ^{19}F NMR chemical shifts of N- and C-blocked Fphe and Ftyr as functions of % D_2O and pH 97

IV-1 The chemical structure of deoxycholic acid 105

IV-2 The ^{19}F NMR spectrum at 297°K of Fphe and Ftyr labelled M13 coat protein in DOC micelles 107

IV-3 The amino acid sequence of the coat protein of the bacteriophage M13 108

IV-4 The ^{19}F NMR spectrum of Fphe- and Ftyr-labelled M13 coat proteins in DOC micelles with varying temperature 109

IV-5 The ^{19}F NMR spectra of the chymotryptic digestion at 277°K of Fphe- and Ftyr-labelled M13 coat proteins in DOC micelles 113

IV-6 The graph of the increase of intensity of the Fphe chymotryptic fragment resonance with digestion time 113

IV-7 The paper electrophoresis of the fragments released from the chymotryptic digestion at 277°K of Fphe- and Ftyr-labelled M13 coat proteins in DOC micelles 116

Figure Page

IV-8 The ^{19}F NMR spectra of the pronase digestion at 300°K of Fphe- and Ftyr-labelled M13 coat proteins in DOC micelles 119

IV-9 The ^{19}F NMR spectra of Fphe- and Ftyr-labelled coat protein in DOC micelles with varying D_2O content 130

IV-10 The graphs of the ^{19}F NMR chemical shifts of Fphe- and Ftyr-labelled M13 coat proteins in DOC micelles as functions of %D_2O 130

IV-11 The chemical structures of the dyes used in the photo-CIDNP experiments on Ftyr-labelled coat protein in DOC micelles 134

IV-12 The ^{19}F NMR CIDNP spectra of Ftyr labelled M13 coat protein in DOC micelles 136

IV-13 The ^{19}F NMR spectra of the pronase digestion of Fphe and Ftyr labelled M13 coat protein in DOC micelles at 277°K 137

IV-14 The CD spectra of Fphe- and Ftyr-labelled M13 coat proteins in DOC micelles as a function of temperature 140

IV-15 The graphs of the % α-helix, β-sheet and random coil in the labelled M13 coat protein in DOC micelles as a function of temperature 141

IV-16 The ^{19}F NMR spectra of the pH titration of Fphe- and Ftyr-labelled M13 coat proteins in DOC micelles 143

IV-17 The graphs of the ^{19}F NMR chemical shifts of the Fphe11 and Ftyr21/24 resonances and of the intensity of the Ftyr upfield resonances (relative to the total Ftyr resonance intensity) as functions of pH 144

V-1 The ^{19}F NMR spectrum of phospholipid vesicles containing equimolar quantities of Fphe- and Ftyr-labelled M13 coat protein 165

Figure Page

V-2 The chemical structures of dimyristoylphosphatidylcholine (DMPC), dipalmitoyl phosphatidic acid (DPPA) and cardiolipin (CL) 166

V-3 The ^{19}F NMR spectra of Fphe- and Ftyr-labelled M13 coat proteins reconstituted into 8-FDPPC-labelled vesicles at two temperatures 169

V-4 The analyses of the broad spectral component of the 8-FDPPC resonance from 8-FDPPC-labelled vesicles containing Fphe- and Ftyr-labelled M13 coat proteins with temperature 170

V-5 The plots of the linewidths of the narrow components of the ^{19}F resonances of Fphe- and Ftyr-labelled M13 coat proteins reconstituted into 8-FDPPC-labelled vesicles as a function of the inverse temperature 172

V-6 The ^{19}F NMR spectra of the chymotryptic digestion of the Fphe- and Ftyr-labelled M13 coat proteins reconstituted into vesicles 174

V-7 Diagrammatic representations of the behavior of the net magnetization of spin 1/2 nuclei in a reference frame rotating at the resonance frequency of the nuclei 183

V-8 A diagram of the rotations, angles, and possible dipolar interactions of the model assumed for the analysis of the Fphe and Ftyr relaxation data 188

V-9 The ^{19}F NMR linewidths for Fphe- and Ftyr-labelled M13 coat proteins in vesicles plotted as a function of the square of the spectrometer frequency 194

V-10 A histogram of the size distribution of vesicles containing Fphe- and Ftyr-labelled M13 coat proteins 195

List of Abbreviations and Symbols

Amino Acids

ala	alanine
arg	arginine
asn	asparagine
asp	aspartic acid
cys	cysteine
gln	glutamine
glu	glutamic acid
gly	glycine
his	histidine
ile	isoleucine
leu	leucine
lys	lysine
met	methionine
phe	phenylalanine
pro	proline
ser	serine
thr	threonine
trp	tryptophan
tyr	tyrosine
val	valine
Fphe	3-fluoro-phenylalanine
4-Fphe	4-fluoro-phenylalanine
Ftyr	3-fluoro-tyrosine

Other Abbreviations

B_0	static magnetic field
BPTI	bovine pancreatic trypsin inhibitor
CD	circular dichroism
CIDNP	chemically induced dynamic nuclear polarization
CL	cardiolipin
CM-LUM	3-N-carboxymethyl-lumiflavine

D_1	ring wobble frequency about the $\alpha\beta$-bond
D_2	ring rotation frequency about the $\beta\gamma$-bond
D_2O	deuterium oxide
DCl	deuterium chloride
dm	decimeter
DMPC	dimyristoyl-phosphatidylcholine
DNA	deoxyribonucleic acid
DOC	sodium deoxycholate
DPPA	dipalmitoyl-phosphatidic acid
DSS	sodium 2,2-dimethyl-2-silapentane-5-sulfonate
EDTA	ethylene-diamine-tetra-acetic acid
Fben	fluoro-benzoic acid
8-FDPPC	8-fluoro-dipalmitoyl-phospatidic acid
FID	free induction decay
FMN	flavin mononucleotide
g	gram
Hb	hemoglobin
H_1	the applied magnetic field
Hz	hertz (sec^{-1})
kg	kilogram
MHz	megahertz
ml	milliliter
mM	millimolar
msec	millisecond

m_r	mean residue molecular weight
NaOD	sodium deuteroxide
NMR	nuclear magnetic resonance
N_0	avogadro's number
nOe	nuclear Overhauser effect
nsec	nanosecond
pD	$-\log[{}^2H^+]$
pfu	plaque forming unit
pH	$-\log[H^+]$
ppm	parts per million
Rf	(the distance travelled by a peptide)/(the distance travelled by aspartic acid) by pH 6.5 paper electrophoresis
SDS	sodium dodecylsulfate
sec	second
SIS	solvent induced shift
SIIS	solvent isotope induced shift
T_1	spin lattice relaxation time
T_2	transverse relaxation time
TFA	trifluoro-acetic acid
TMS	tetramethyl-silane
T_m	lipid phase transition temperature
Tris	tris-(hydroxymethyl)-aminomethane

γ	gyromagnetic ratio
δ	chemical shift
δ'	grams of water bound/ gram of protein
Δ	difference
$\Delta\nu$	linewidth
ϵ	molar extinction coefficient
η	viscosity
θ	ellipticity
$[\theta]$	mean residue ellipticity
κ	grams detergent bound/ gram of protein
μsec	microseconds
$\bar{\nu}_p$	protein specific volume
$\bar{\nu}_w$	water specific volume
$\bar{\nu}_d$	detergent specific volume
σ	chemical shielding
τ_c	correlation time

I. Introduction

A. Structural Studies of Membrane Proteins

Membrane proteins are essential for cell viability. They perform many functions for the cell, including transport of ions and substrates through the hydrophobic bilayer, recognition and transfer of inter- and intra-cellular messages, and the enzymatic processes required for maintenance of membrane potential. In 1972 Singer and Nicholson proposed the fluid mosaic model for biological membranes (Singer, 1971; Singer & Nicolson, 1972). They suggested that membrane proteins are "floating in a sea of lipid" (shown in Figure I-1). Although there tends to be less lipid present relative to the amount of protein than implied by that statement, the essence of the theory has held true: the proteins are found either partially or totally embedded in the lipid bilayer.

There are two types of membrane proteins (Figure I-1). The first are called extrinsic membrane proteins. These proteins are bound at the surface of the membrane and can be dissociated from the surface by high ionic strength. Once removed, they are water-soluble and can be studied using the wide variety of techniques that have been developed for water-soluble proteins. The second type of membrane proteins are called intrinsic membrane proteins. These proteins span the lipid bilayer and require the disruption of the membrane by detergents or organic solvents to be isolated. Their

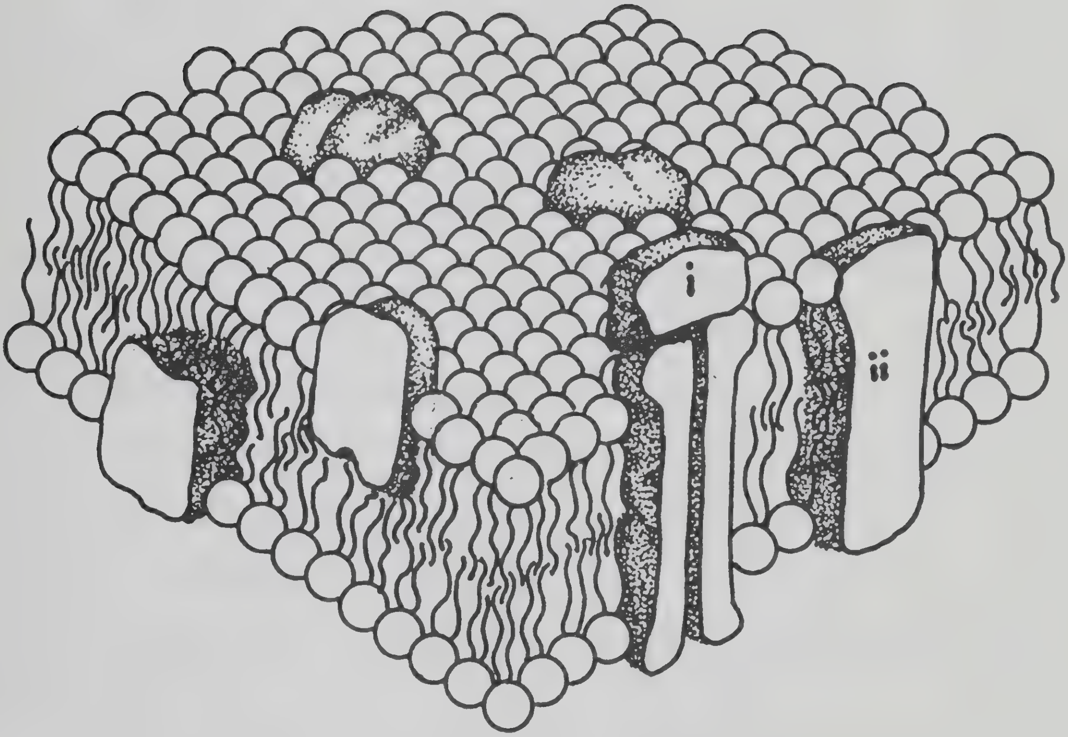

Figure I-1 An artist's representation of a biological membrane, as proposed by the fluid mosaic model. This diagram shows the two types of membrane proteins: i) extrinsic; ii) intrinsic.

study, whether kinetic, structural or chemical, has been limited due to their insolubility in aqueous media; the standard techniques used for water-soluble proteins can not be applied.

Membrane proteins, in particular, intrinsic proteins, have the potential to be the most interesting of all proteins, both structurally and biochemically. These proteins not only have the possibility to interact with proteins, substrates and cofactors in the aqueous environments on one or both sides of the membrane, but, as well, may be influenced by the components of the membrane, whether they be, for example, lipid, protein, or steroids. Structural studies of integral proteins would allow one to monitor those interactions at the molecular level, and so would determine the mechanism by which the protein performs it function.

Physical studies of membrane proteins, at present, have been mainly limited to those proteins classified as extrinsic membrane proteins (for example, cytochrome C and glucagon). X-ray and/or nuclear magnetic resonance studies have given detailed information of each of those systems. Structural studies of intrinsic proteins are few for a number of reasons. X-ray crystallography, which is capable of giving the most structural information, is also the most demanding in terms of sample preparation: the protein must be in highly ordered 3-dimensional crystals. Techniques for crystallizing intrinisic proteins are being developed, but

at present, the use of x-ray crystallography in the study of intrinsic protein structure is very limited. The second most useful technique for obtaining structural information is NMR. It is more flexible in the type of sample it may use but has other limitations. The width of a NMR spectral resonance is very dependent upon the size of the "particle": the larger the particle, the broader the linewidth. If a protein is bound by detergent or lipid, its "particle-size" may become so large that the resonance is essentially undetectable by solution NMR techniques.

These problems have led to the development of new physical approaches; the intrinsic protein that has been most used is bacteriorhodopsin, from *Halobacterium halobium*. Membrane fragments containing large quantitities of bacteriorhodopsin may be readily isolated. These 2-dimensional ordered arrays have been used by Unwin and Henderson (1975) to obtain both electron micrographs and optical diffraction patterns. Analysis of the diffraction patterns by similar methods used in the analysis of X-ray diffraction patterns have shown that bacteriorhodopsin contains 7 helices spanning the membrane; their folding in the membrane appears to be similar to the folding of peptide chains in water-soluble proteins. The internal motions of bacteriorhodopsin have been studied by solid state deuterium NMR. E. Oldfield and coworkers (Kinsey *et al.*, 1981; Keniry *et al.*, 1984) have incorporated deuterated amino acids into bacteriorhodopsin and have found residues within the

hydrophobic region of the protein (within the lipid bilayer) to be immobile while residues outside, to be very mobile on the timescale of the experiments (~1 μsec).

The EM and solid state NMR studies give information of the topology and motions present in the static system; ideally however, one would still want to observe the interactions present in a dynamic (solution) state. Some studies have been done; S. Opella and coworkers (Cross and Opella, 1979; 1980; 1981) have used proton NMR to study the coat protein of the filamentous coliphage, fd, in sodium dodecylsulfate micelles.

This thesis describes the study of the coat protein of the filamentous coliphage, M13[1] when it is either bound by sodium deoxycholate (DOC) micelles or reconstituted into phospholipid vesicles. The coat protein was biosynthetically labelled with either 3-fluoro-phenylalanine (Fphe) or 3-fluoro-tyrosine (Ftyr) thus providing specific labels of the hydrophilic and hydrophobic (membrane/micelle-bound) domains of the protein. ^{19}F NMR was used to characterize the structure of the coat protein in the DOC micelles and vesicle as inferred from the motion and exposure of those residues. The history and objectives of this project are outlined in Chapter I-C.

---

[1] the coat protein of M13 has the same amino acid sequence as the coat protein of fd.

B. The Use of ^{19}F NMR in Studying Protein Structure

Nuclear magnetic resonance (NMR) spectroscopy is a physical technique that can give information as to the motions and interactions of a particular group in a molecule provided that the NMR signal from that group is resolved from the other resonances in the spectrum. This can be a serious problem in using NMR techniques to study biological samples when nuclei such as ^1H, and natural abundance ^{13}C and ^{15}N are used. These nuclei are present in the sample, hence the larger the molecule, the more resonances will be present. As well, the larger the molecule, the slower the molecule tumbles in solution, and the broader the resonances become. The combination of these two effects results, in the worst case, in the entire spectrum becoming a broad unresolved envelope of resonances. It is difficult to obtain information from such a spectrum.

An alternative approach to doing natural abundance NMR is to selectively label residues within the macromolecule. This results in either decreasing the number of resonances (for example, Putter *et al.*, 1969, deuterated all but a few proton positions) or else giving new resonances to be studied. The latter method has been particularly useful when the new nucleus is fluorine (for reviews, see Sykes and Hull (1978) and Sykes and Weiner (1980)).

The use of fluorine labelled macromolecules has both assets and possible hazards. Fluorine (^{19}F) is a 100% abundant nucleus (with spin=1/2) which is not usually found

in biological molecules. Consequently, there is no background problem; signals only occur from synthetically incorporated fluorine nuclei. It is 94% as sensitive as proton (compared to ^{31}P (40%), ^{13}C (25%) and ^{15}N (10%)), hence spectra may be obtained with less sample and/or faster than with the naturally occurring (non-proton) nuclei. Its chemical shift range is much larger than that of proton (~±1000 ppm as compared to ~±10 ppm) so that individual resonances in the fluorine spectrum may often be resolved when they would not be resolved by proton NMR, aside from the background problem for protons. The potential problem in using fluorine substituted molecules arises from its size and its electronegativity. It is usually substituted for protons, when used to label biological macromolecules (for example, 3-fluoro-phenylalanine in a protein). Fluorine is both larger and more electronegative than a proton, hence one must be careful that the behavior seen by ^{19}F NMR, is that of the native molecule and not just due to the fluorine (Murray-Rust *et al.*, 1983).

One of the key reasons for doing an NMR experiment is to obtain information of the motions within a molecule. The motion analysis of an NMR spectrum requires that the mechanisms by which the nuclei relax be known. Fluorine has two relaxation mechanisms: dipole-dipole and chemical shift anisotropy (csa). Dipole-dipole relaxation arises from the interaction between two dipolar nuclei. For a fluorine-substituted amino acid in a protein, this is usually between

the fluorine and protons on the same residue or between the fluorine and protons on neighbouring residues. Chemical shift anisotropy is the result of the asymmetric electron distribution about the fluorine nucleus. It causes the chemical shift of the fluorine to depend on the orientation of the nucleus in the magnetic field. This mechanism causes the fluorine resonance linewidth to be proportional to the square of the magnetic field. Thus, at the higher fields available these days (300 MHz and up) chemical shift anisotropy is the dominant mechanism contributing to the fluorine linewidth (or the transverse relaxation time, T_2).

Fluorine labelled amino acids have been incorporated into proteins (for a review, see Sykes and Weiner, 1980). Of the methods available, biosynthetic incorporation of fluoro-amino acids has been very successful. 3-fluoro-tyrosine has been incorporated into alkaline phosphatase (Hull and Sykes, 1976), *lac* repressor protein (Jarema *et al.*, 1981), M13 coat protein (Hagen *et al.*, 1978), and the single-stranded DNA-binding protein of fd (Coleman and Armitage, 1977). 5-fluoro-tryptophan has been incorporated into histidine-binding protein J from *Salmonella* (Post *et al.*, 1984). In all cases, information of the structure and motions of the fluorinated residues has been obtained.

The 3-fluoro-analogues of phenylanine (Fphe) and tyrosine (Ftyr) have been used extensively in this project; their structures are shown in Figure I-2. The biosynthetic incorporation of these amino acids into M13 coat protein and

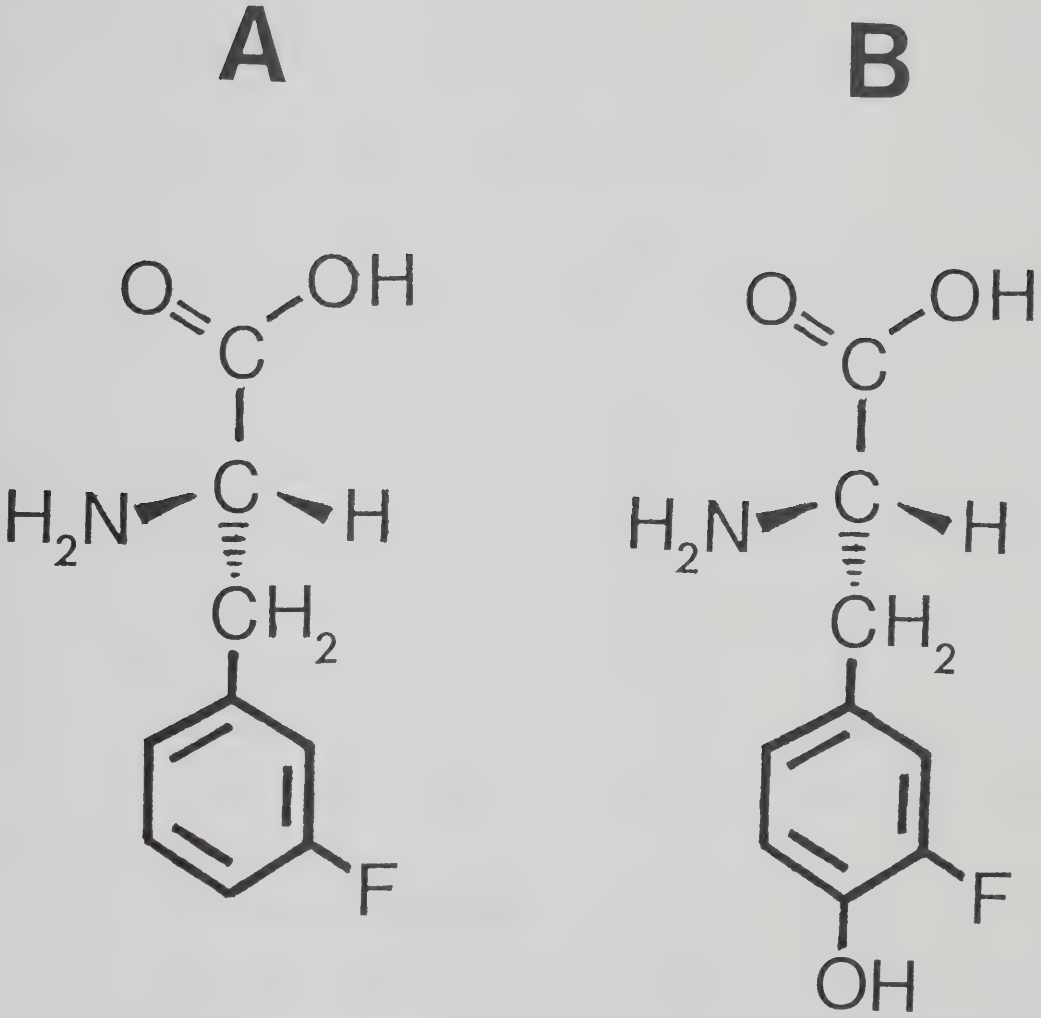

Figure I-2 The chemical structures of 3-fluorophenylalanine (Fphe) and 3-fluoro-tyrosine (Ftyr). Structure A is Fphe; structure B is Ftyr. The L-configurations of each are shown.

their observation using ^{19}F NMR has given structural information about the protein bound by DOC micelles (Chapter IV) or by phospholipid vesicles (Chapter V).

C. The History and Objectives of this Project

Exposure and mobility studies using solution NMR techniques have contributed a great deal to the understanding of the dynamic structure of water-soluble proteins. The application of this technique to the study of intrinsic membrane proteins has been severely limited for a number of reasons: the technique requires significant quantities of the protein; the amino acid sequence of the protein must be known for meaningful interpretation of results; and the "particle-size" of the protein-detergent or protein-lipid complex must not be too large. Few intrinsic proteins fulfill those criteria.

One protein that satisfies those three conditions is the coat (gene 8) protein of the filamentous bacteriophage M13 (or fd). This protein performs two functions for the coliphage. First, it forms a protective layer around the single-stranded circular DNA of the phage as it diffuses in solution; 2700 copies of the coat protein are found per phage. The second function is to transport the phage DNA through the cytoplasmic membrane of the *E. coli*, both into and out of the cell. In performing this task, the coat protein is found spanning the cytoplasmic membrane: its N-terminus is in the periplasmic space; and its C-terminus

is in the cytoplasm. Hence, it is an intrinsic membrane protein.

M13 coat protein is an ideal membrane protein for NMR structural studies. The high copy number of the coat protein on each phage and that each infected bacterium produces ~200 phage particles, results in gram-quantities of coat protein being isolated. As well, it is a small protein, comprised of only 50 amino acids; its amino acid sequence is shown in Figure I-3. An additional advantage for this membrane protein is that its synthesis requires the use of the *E. coli*-host machinery. Thus, the use of genetic mutants of *E. coli* allows the biosynthetic incorporation of labelled amino acids.

The M13 coat protein sequence can be divided into three regions (see Figure I-3): an acidic N-terminus, a basic C-terminus and a hydrophobic core. The preliminary studies to this project, performed by Mr. D. Scott Hagen (Hagen *et al.*, 1978; 1979a,b) were done with labels in the hydrophobic domain; Ftyr residues were incorporated at positions 21 and 24 of the amino acid sequence. ^{19}F NMR was used to study the motions and exposure of those residues when the coat protein was bound by either deoxycholate (DOC) micelles or phospholipid vesicles.

My project has been to obtain information of the overall structure of the "membrane-bound" form of M13 coat protein. This required the hydrophilic ends, as well as the hydrophobic core, to be monitored. For this task, Fphe was

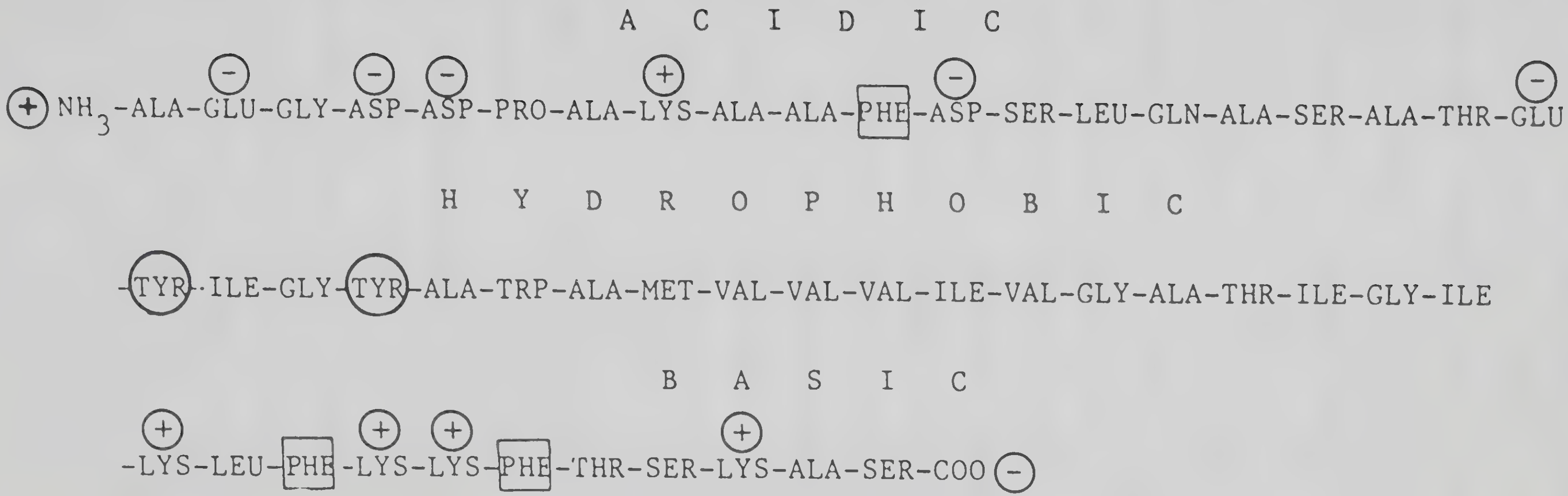
A C I D I C
+ NH3-ALA-GLU-GLY-ASP-ASP-PRO-ALA-LYS-ALA-ALA-PHE-ASP-SER-LEU-GLN-ALA-SER-ALA-THR-GLU
H Y D R O P H O B I C
-TYR-ILE-GLY-TYR-ALA-TRP-ALA-MET-VAL-VAL-VAL-ILE-VAL-GLY-ALA-THR-ILE-GLY-ILE
B A S I C
-LYS-LEU-PHE-LYS-LYS-PHE-THR-SER-LYS-ALA-SER-COO
+
−

Figure I-3 The amino acid sequence of M13 coat protein. The 3-fluoro-analogs of phenylalanine and tyrosine have been biosynthetically incorporated into the protein at the boxed and circled residues, respectively.

incorporated into both the acidic and basic domains of the protein, at positions 11, 42, and 45. Structural information has been obtained by simultaneously monitoring the motions and exposures of the Fphe- and Ftyr-residues when bound by either DOC micelles or phospholipid vesicles, using ^{19}F NMR (Dettman *et al.*, 1982; 1984)[2]. The techniques used for studies of Ftyr-labelled coat protein, including solvent isotope effects on the ^{19}F chemical shifts, digestion with pronase, and varying temperature, have been repeated, including Fphe-labelled coat protein in the preparations. Chymotryptic digestion, circular dichroism, and fluorine photo-chemically induced dynamic nuclear polarization experiments have provided additional information; improvements in the procedure for the reconstitution of the coat proteins into vesicles has allowed detailed motion analyses to be done. The results have given insight as to: the presence of structure in the vicinities of the Fphe residues; the extent to which the Ftyr ring mobilities are restricted by the solvating lipid or bile acid molecules; and the degree of protection that protein structure and/or bile acids and lipids give the Ftyr residues from the aqueous environment.

The work described in this thesis has been divided into three sections: Chapter III outlines studies of the Fphe and

---

[2] The structural information obtained from the Fphe and Ftyr residues of the M13 coat proteins, whether bound by micelles or vesicles, was assumed to be give information of the environments about the unlabelled phe and tyr residues, as well. Major evidence that the fluoro-residues were not perturbing the structure significantly, if at all, was given in the observation that both the Fphe- and Ftyr-labelled M13 phages were just as infectious as the unlabelled phage.

Ftyr amino acids; Chapter IV shows the behavior of the Fphe- and Ftyr-labelled coat proteins in DOC micelles; and Chapter V describes experiments with the Fphe- and Ftyr-labelled coat proteins in phospholipid vesicles. The amino acid studies done in Chapter III-A characterized the interactions found between bicarbonate buffer and the fluoro-amino acids. This study was performed to determine the effect, if any, that bicarbonate buffer might have on the ^{19}F NMR spectra of the Fphe- and Ftyr-residues of the coat proteins. Chapter III-B shows the effects on the ^{19}F chemical shifts of Fphe and Ftyr amino acids as the solvent was changed from water (H_2O) to deuterium oxide (D_2O). These experiments were preliminary to the use of solvent isotope exchange as a method of determining protein residue exposure when bound by DOC micelles. Chapter IV-A shows data to suggest assignments of the resonances seen in the ^{19}F NMR spectrum of the Fphe- and Ftyr-labelled coat proteins in DOC micelles. Chapter IV-B gives the motion and exposure studies of the fluoro-labelled coat proteins in DOC micelles. Chapter V-A characterizes the exposure, orientation and effects of lipid fluidity on the motions of Fphe and Ftyr residues of the labelled coat proteins in vesicles. Chapter V-B gives a quantitative discussion of ring motions of the Fphe- and Ftyr-residues of the labelled coat proteins reconstituted into phospholipid vesicles. Each Chapter has its own Introduction, Theory (if necessary) and Discussion sections. The Methods for all the experiments described in

this thesis are given in Chapter II.

II. Experimental Methods

A. Materials

The materials used in the experiments outlined in this thesis were obtained from Sigma Chemical Company, St. Louis, Missouri with the following exceptions: the deuterium oxide (99.75%) was bought from Bio-Rad Laboratories, Richmond, Ca., U.S.A.; the ammonium hydroxide from J.T. Baker Chemical Company, Phillipsburg, N.J., U.S.A.; the sodium deuteroxide and the deuterium chloride from Stohler Isotope Chemicals, Waltham, Ma, U.S.A.; the ammonium and sodium bicarbonates and the sodium mono- and di-phosphates and hydrochloric acid from Fisher Scientific Limited, Edmonton, Alta., Canada.

Escherichi coli strains KA197 (CGSC 5243, Hfr, *thi*, *phe*A97, *rel*A1) and AT2471 (CGSC 4510, Hfr, *thi*, *rel*, *tyr*A4) were obtained from Dr. Barbara Bachman, Yale University School of Medicine. The M13 bacteriophage was a gift from Dr. William Paranchych, the Department of Biochemistry, University of Alberta.

B. Procedures for the experiments with Fphe and Ftyr Amino Acids

Studies of the Effects of Bicarbonate Buffer

The samples were prepared by weighing out the appropriate amount of fluoro-amino acids, 3-fluoro-benzoic acid (Fben), sodium bicarbonate ($NaHCO_3$), ammonium bicarbonate

(NH_4HCO_3) and/or sodium mono- and di-phosphates, placing in a vial and adding 99.75% deuterium oxide (D_2O) to the correct volume. (No special drying or purification procedures were done prior to use.)

The experiments showing the effects of the bicarbonate concentration on the ^{19}F NMR resonances of Fphe and Ftyr were done by preparing two "stock" solutions: 1) no sodium bicarbonate (pH 9.0) and 2) 1.2 M sodium bicarbonate (pH 9.0). Each contained 3 mM Fphe and Ftyr and 99.75% deuterium oxide. They were mixed to obtain intermediate concentrations of the bicarbonate buffer.

The pH titrations were followed using a Radiometer (Copenhagen, Denmark) pH meter fitted with a microelectrode and the pH was adjusted by the addition of either sodium deuteroxide or deuterium chloride.

Determination of Solvent Isotope Induced Shifts

The Fphe/Ftyr amino acid samples used for the SIIS studies were prepared by first making H_2O and D_2O solutions containing Fphe, Ftyr and the other components to complete the mixtures. The two solutions were then mixed to obtain the range of D_2O/H_2O ratios. The D_2O content of the sample was calculated by:

$$\frac{\text{volume } D_2O \text{ solution} \times 99\%}{\text{volume } D_2O \text{ solution} + \text{volume } H_2O \text{ solution}} = \%D_2O$$

The D_2O used was 99.75% deuterium oxide but the amino acids and buffers were not deuterated. Only the NH_4HCO_3 contributed enough water to lower the deuterium content below 99.5%. Thus the "D_2O buffer" solution that was made using NH_4HCO_3 was taken to be 99% D_2O while that made using $NaHCO_3$ was 100%. (These were also the D_2O values used in the calculations of the D_2O contents of samples containing coat protein in micelles or vesicles.)

The errors in the SIIS values were determined as follows:

The error in the chemical shift data ($\Delta\delta$) in ppm depends upon the digital resolution, which can be calculated from the acquisition time (AT) of the spectrum and the spectrometer frequency (SF):

$$\Delta\delta = \frac{1}{(AT)(SF)}$$

The error in the SIIS values is then given by:

$$SIIS = \delta_{d_2o} - \delta_{h_2o} - SIIS_{lock}$$

$$\Delta SIIS = [(\Delta\delta_{d_2o})^2 + (\Delta\delta_{h_2o})^2 + (\Delta SIIS_{lock})^2]^{0.5}$$

The synthesis of the N-acetyl-, methyl ester derivatives

The procedure used for the synthesis of the methyl esters of Fphe and Ftyr were modified from that of Brenner and Huber (1953). The reactions were done as follows:

Three ml (74 mmole) of anhydrous methanol were cooled in a dry ice-acetone bath before dropwise addition of 0.78 ml (11 mmole) of thionyl chloride. Mechanical stirring of the methanol solution was used to achieve vigorous mixing; a stirring bar is not sufficient. 100 mg (0.5 mmole) of Fphe (or Ftyr) were then added slowly to the solution.[3] (The above steps should be done such that the temperature of the reaction never gets above -5°C.) After the addition, the suspension should be allowed to warm to room temperature, then slowly heated to 40°C (with stirring) and kept at that temperature for 2 hours. Fphe and, particularly, Ftyr are not very soluble in methanol but their methyl esters are. Thus, a clear solution indicates completion of reaction. (An alternative procedure is to allow the suspension to come to room temperature, then leave stirring for 24 h.)

The solvent was removed by rotoevaporation and the residue redissolved in a minimum amount of methanol. Ether was added, until the methyl ester hydrochloride precipitated (several volumes required), then re-rotoevaporated to dryness. White crystals were obtained. If moisture and CO_2 are eliminated during the reaction, an 83-86% yield may be expected.

The method of N-acetylation of Fphe and Ftyr was suggested by Dr. C. Hamilton (personal communication) and Huang

---

[3] The procedure of Brenner and Huber (1953) used molar ratios of 7:1:1:1 for methanol:thionyl chloride:leucine. Fphe is quite soluble in the methanol while the Ftyr is not, so an excess of methanol/thionyl chloride was used to enhance the solubility and the subsequent reaction of (particularly) Ftyr.

and Niemann (1951), as follows:

The methyl ester hydrochloride product (above) was mixed with one equivalent of anhydrous sodium acetate and 10 equivalents of acetic anhydride plus a drop of pyridine (all at 0°C). This was stirred for 1/2 hour at 0°C then allowed to come to room temperature and stirred for an additional 24 hours. To stop the reaction, the acetic anhydride was decomposed by the addition of approximately 1 ml of water containing 0.4g sodium bicarbonate. The solution was extracted with chloroform (15 ml) then the organic layer was washed with 1M HCl, then shaken with solid $NaHCO_3$. The $CHCl_3$ layer was decanted off, and dried, resulting in an oily residue. The final product was crystallized from the residue in ethyl acetate.

Synthesis of N-acetyl Ftyr results in the O-acetylation of the phenolic hydroxyl group. To remove this without removal of the methyl ester, the blocked Ftyr was dissolved in a minimum of chloroform then a catalylic amount of sodium methylate was added. Sodium methylate was prepared by adding a small piece (2 mm in length) of sodium metal to 10 ml anhydrous methanol. After it had dissolved, two drops were added to the blocked Ftyr in chloroform and left standing at room temperature for 2 hours. (At this time ^1H-NMR showed that the reaction was complete.) It was then rotoevaporated to dryness.

C. Preparation of Fphe and Ftyr Labelled M13 Coat Protein

E. Coli Preparation

Escherichia coli KA197 and AT2471 were used to synthesize Fphe or Ftyr labelled M13 coat proteins, respectively. In each case they were tested for being auxotrophic for phenylalanine or tyrosine by growing a loopful of the glycerol stab in L broth (rich medium, see Appendix A), streaking onto an L broth plate, picking isolated colonies with sterile toothpicks and streaking on two minimum medium plates (see Appendix B): one with and one without the required amino acid. The plates containing the amino acid were grown at 37°C for 24 hours, then placed in a 4°C refrigerator. The plates without the amino acid were allowed to remain at 37°C for 48 hrs. The innoculum culture was started using a picked colony that had no signs of growth (revertants) on the "minus" amino acid plate.

Phage Preparation

Before the growth of Fphe- and Ftyr-labelled M13 coat proteins, the phage was purified as follows: the phage stock solution (containing $\sim 10^{11}$ plaque forming units (pfu) / ml) was titered as described below. A "normal" plaque was removed from the agar and placed in a 1 ml early-log-phase-culture of the E.coli auxotroph that would be used. It was grown at 37°C to late log phase, then transferred to a 500 ml culture of E.coli in early log phase. When this had grown

to late log phase at 37°C, the flask was placed in the refrigerator at 4°C to cool.

The culture was centrifuged in sterile bottles at 15,000xg for 10 minutes at 4°C to remove the bacteria (the cooling of the culture improves the "pelleting" of the E.coli). The supernatant was collected and placed in a sterile flask. The titer of this stock is ~10^{11} pfu/ml.

Phage Titer Determination

The phage concentrations in culture solutions were determined by first making dilutions of the phage solution with sterile buffered saline (see Appendix A) of the order of 10^{-8}, 10^{-9} and 10^{-10}. 0.1 ml of the dilutions was added to 0.1 ml aliquots of an overnight E.coli culture and incubated for 5 minutes at 37°C. These were, in turn, added to 3.5 ml quantities of 50-55°C top agar, mixed and poured onto warm bottom agar plates. After setting, the plates were incubated at 37°C from 8 to 12 hours until confluent growth was achieved. (The plaques were visible as less opaque spots in the top agar.) The titer was calculated as:

$$\text{Titer} = \frac{\text{\# of plaques x dilution of phage stock}}{\text{0.1 ml of dilution plated}}$$

$$= \text{plaque forming units (pfu)/ml}$$

M13 Phage Growth in Ten Liter Fermentors

Both Fphe- and Ftyr-labelled M13 coat proteins were grown in 10 l fermentors[4], using the M63 minimum medium. It was found that the phe auxotroph, KA197, could grow using Fphe only, while the tyr auxotroph, AT2471, required L-tyr to be present at the start, then an excess of Ftyr added later. The details are as follows:

The fermentors were prepared the day before to allow overnight equilibration. For Fphe incorporation 100 ml of 0.8% Fphe per ten liters was used, while for Ftyr incorporation 5 ml of 0.4% L-tyr was included in the minimum media (see Apendix A). A 10 ml culture of L broth (see Appendix A) was started the morning of the day before, which was used to innoculate a ~500 ml L broth culture the night before the fermentors were to be used. 200 ml of the culture was transferred to each fermentor to obtain a starting $A_{600} \cong 0.05$. After ~3 hr, the A_{600} doubled to 0.1 (this corresponds to 1×10^8 cells/ml). At this time a 20-fold excess of M13 stock culture (see above) was added (~200 ml). For the growth of Ftyr-labelled M13 phage, 10 minutes after the addition of the phage, a 10-fold excess of Ftyr (100 ml of 0.4% D,L-Ftyr) was added. The fermentor cultures were grown until late log phase (A_{600} = 0.6 - 0.9), adding antifoam B as necessary to prevent frothing. [The fermentor settings included the air pressure = 30 (arbitrary units), stirrer = 200 rpm and the temperature = 37±0.5°C.] The temperature regulation

---

[4] P.E.C. Fermentor, Chemap AG, Mannedorf, Switzerland.

(done by the mixing of hot and cold water and its circulation through tubing in the vat) was then turned off to allow the cold water to cool the culture to ≅15°C. The *E. coli* were removed from the culture by centrifugation at 40,000 rpm with a Sharples continuous flow centrifuge[5] at 0°C.

Phage Purification

M13 phage purification involved the precipitation of the phage from the culture medium supernatant, two washes with detergents to remove lipid contamination and a CsCl-gradient centrifugation. The details are as follows (modified from that of Wickner, 1975):

The supernatant (above) was made 2.5% polyethylene glycol-6000 and 0.5 M sodium chloride, and was placed in a 4°C cold room for 5 days (or until the phage had settled). The medium was then decanted and 0.01 volume of Triton X-100 was added. This was stirred vigorously for 1 hour at room temperature; then the phage was pelleted by centrifugation at 22,100xg for 10 minutes at 1°C. The pellets were resuspended in 250 ml of 1M NaCl, 0.1 M Tris-HCl (pH 7.5) and 1% Sarkosyl 97, stirred vigorously for 1 hour at room temperature; then the phage reprecipitated by the slow addition, with stirring, of polyethylene glycol-6000 to 2.5%. The suspension was centrifuged again. The phage pellet was dissolved in ~15 ml of 0.05M Tris-HCl (pH 7.5), 1mM EDTA and 1M

---

[5] Cepa-Schnell-Zentrifuge, Carl Padberg, Lahr/Baden.

NaCl. Solid CsCl was added to a density of 1.29 g/ml, the quantity determined by the following equation:

$$\text{wt of CsCl added} = 0.4351 \times (\text{wt of sample})$$

20 g CsCl causes a volume change of 5 ml; therefore, if a certain final volume is desired:

$$\text{Final volume} = \text{volume sample} + y + \frac{(5\text{x}0.4351)(\text{wt sample} + y)}{20}$$

$$\text{wt CsCl} = 0.4351(\text{wt sample} + y)$$

y is the volume of buffer required to make the desired final volume; the density of the buffer is assumed to be ~1 g/ml, thus the volume of the buffer added is equal to its weight. To fill two Ti50 rotor tubes (10.1 ml/tube), one sets the final volume = 20.2 ml and solves the equation.

The solutions were centrifuged at 60,000xg for ~36 hours at 15°C. The tubes contained three identifiable regions upon visual inspection: a lipid crust at the surface (the more vigorous the detergent washings, the less this was); a purple-tinted band immediately below the lipid which is the phage; and pellet at the bottom of the tube. The purple band was removed from the tube by putting a capillary tube (with tygon tubing attached) to the bottom and drawing the solution out using a peristaltic pump, collecting fractions. The fractions containing the phage (by either visual or A_{260} inspection) were pooled and dialyzed against

a total of 3 l of 0.05M Tris-HCl (pH 7.5) and 0.1mM EDTA with at least 3 changes over 3 days. The phage solution was then lyophylized. Typical yields from 20 l preparations were ~350 mg Fphe- labelled phage and ~600 mg Ftyr-labelled phage (including the weight of the Tris/EDTA (~100 mg) buffer in the phage solution).

D. Procedures for the Experiments with DOC Micelle-Bound M13 Coat Protein

Preparation of DOC Micelle-Bound M13 Coat Protein

Micelle-bound coat protein was prepared as follows: 15 mg of lyophylized M13 phage (as above) was placed in a 18 x 150 mm tube. 1.0 ml of 10mM Tris-HCl (pH 8.0) was added and the mixture gently swirled to moisten and, at least, partially dissolve the phage. Then, 1 ml of 0.1M $Na(NH_4)HCO_3$, 70mM sodium deoxycholate (DOC) and 200 μl of chloroform were added. This was shaken at high speed for 3 hours (or until the solution cleared) at 37°C. The clear sample was placed on a 44 x 1.6 cm Sephacryl[6] S200 column, which had been equilibrated with 0.1M $Na(NH_4)CO_3$, 8mM DOC, and the column was run using the same buffer. A typical elution profile is given in Figure II-1. The fractions containing the coat protein in micelles were pooled and concentrated to ~1 ml using an Amicon concentrator and a YM10 Amicon[7] membrane. An aliquot of 0.1M Na(or NH_4)CO_3 (pH 9.0),

---

[6] Pharmacia Fine Chemicals, Uppsala, Sweden.
[7] Amicon Corporation, Scientific Systems Division, Danvers,

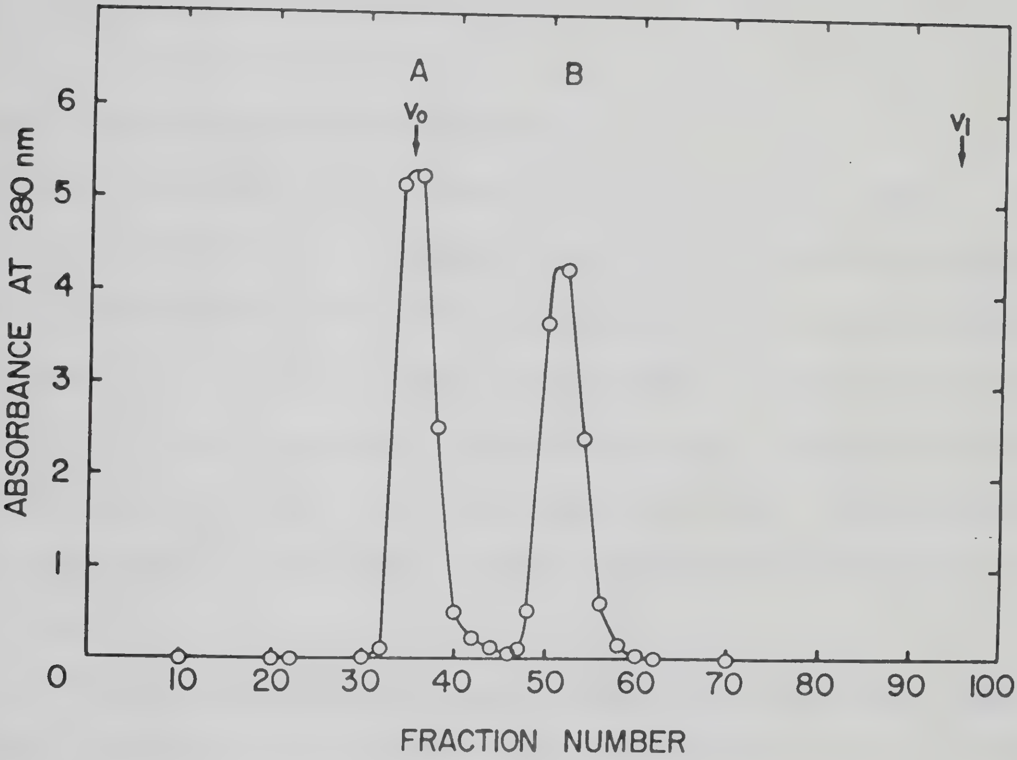

Figure II-1 The Sephacryl S200 elution profile of DOC micelle-bound M13 coat protein. The sample was prepared using 30 mg of Fphe-labelled M13 phage, using twice the amounts of buffers/$CHCl_3$ given in the text, and was run using 0.1M NH_4HCO_3 (pH 9.0)/8mM DOC. Peak A is a mixture of M13 DNA coat protein (protein B) aggregates and attachment protein (protein A). Peak B is the DOC micelle-bound coat protein. V_0 is the excluded volume of the column while V_i is the included volume (determined by including ^{3}H-cholic acid). Each fraction contained 1.5 ml and was collected using the flow rate determined by gravity. The column size was 44 x 1.6 cm.

8mM DOC, made using deuterium oxide (D_2O), was added and the sample reconcentrated to 1.3 ml to obtain D_2O in the sample for NMR spectrometer locking. The calculation of the D_2O content is given in section II-B.

Chymotryptic Fragment Purification

The chymotryptic digestion of the Fphe- and Ftyr-labelled M13 coat proteins in DOC micelles (see Chapter IV-A) were done at 277°K and monitored by ^{19}F NMR as shown in Figure IV-17. NH_4HCO_3 buffer was used for this experiment so that the buffer may be removed through lyophylization. The preparation of the digestion mixture for the paper electrophoresis separation of the hydrophilic fragments was as follows:

The micelle component may be separated from the hydrophilic fragments by either running the sample down an S200 column (the micelles elute at the void volume, indicating that aggregation has occurred, and the hydrophilic fragments elute just before the included volume), or by precipitating the micelles by the addition of 0.5 M formic acid, with stirring, until ~pH 4. The precipitation step is done regardless of whether the hydrophobic protein fragments remaining with the micelles are to be saved, to remove the bulk of the DOC from the sample. The precipitated DOC micelles were filtered by gravity filtration, wetting the paper with pH 4 distilled water / formic acid and washing

---

[7](cont'd) Ma., U.S.A.

the paper three times after the filtration. The filtrates were pooled and lyophylized. The residue was taken up in distilled water and lyophylized 4 times to remove the ammonium formate present. The residue was dissolved in 10% pyridine, 0.3% acetic acid (pH 6.5) buffer and streaked on Whatman 3 mm or 1 mm electrophoresis paper (depending on the concentration of fragments: for 1 mm paper the peptide concentration was ~15 nmole/ cm, while for 3 mm it was ~30 nmole/cm). The paper was run at 3000 volts for 50 min. After drying (~45 min.) either the whole paper (for analytical use, for example, Figure IV-7) or strips of the paper (for preparative use) were stained with 85% [1% ninhydrin in acetone], 15% [0.029M cadmium acetate, 5.8M acetic acid] and dried in an 80°C oven. For preparative paper electrophoresis, the bands indicated from the strips were cut-out and eluted with ~0.5 ml H_2O.

Amino acid analysis was done on the separated fragments to confirm their identity. This was done by performing a 20-hour acid hydrolysis of the fragments (in "constant boiling" 6N HCl, 0.1% phenol) at 100°C, evaporating the acid and having an amino acid analysis done on the resin.

Solvent Isotope Induced Shifts

The coat protein-micelle samples used for the SIIS experiments were prepared as outlined at the beginning of this section (Chapter II-D). The D_2O content for the M13 coat protein-DOC micelle samples were varied as follows: the

S200 column fractions (in 0.1M NH_4HCO_3, 8mM DOC, pH 9.0 (in H_2O) were concentrated to 1.0 ml using the usual amicon concentration procedure. An aliquot of 0.1M NH_4CO_3 and 8mM DOC (pH 9) in D_2O (D_2O buffer) was added, then the sample reconcentrated to 1.0 ml. This procedure was repeated to obtain increasing amounts of D_2O in the sample. The % D_2O of the protein-micelle samples was calculated as follows: if the volume of the sample to which the D_2O buffer is to be added is V_i and the volume of the solution after adding the D_2O buffer = $V_i + V_{d_2o} = V_f$, and if the % D_2O in the sample before the addition of the D_2O buffer is % D_2O_i, and after the addition is % D_2O_f, then the % D_2O in the new sample is[8]:

$$\frac{V_i}{V_f} \times \% \, D_2O_i + \frac{V_{d_2o}}{V_f} \times 99\% = \% \, D_2O_f$$

To start with, % D_2O_i = 0, but the D_2O content of the sample increases with the addition of D_2O buffer. Thus the % D_2O_i before the second addition of the D_2O buffer will be the value of the % D_2O after the first addition.

The % exposure values were determined by:

$$\% \text{ exposure} = \frac{\text{SIIS(protein)} \times 100}{\text{SIIS(amino acid(aa))}}$$

---

[8] See Chapter II-B, the Solvent Isotope Induced Shift section, for the definition of the D_2O content of the "D_2O buffer".

so the error was calculated as:

$$\Delta\%\text{exposure}=\%\text{exposure}\left[\left(\frac{\Delta \text{SIIS(protein)}}{\text{SIIS(protein)}}\right)^{2}+\left(\frac{\Delta \text{SIIS(aa)}}{\text{SIIS(aa)}}\right)^{2}\right]^{0.5}$$

where the error(s) in the protein SIIS values were determined by the same method used in calculating the amino acid SIIS errors (Chapter II-B).

Circular Dichroism Studies

The coat protein (micelle-bound) concentration(s) used for the CD experiments were such that the $A_{280} \cong 0.5$. This was related to the g/ml concentration of the Fphe- and Ftyr-labelled coat proteins in the solution by the use of their respective extinction coefficients, which were determined as follows:

10 mg of each of unlabelled and Fphe- and Ftyr-labelled M13 phages were used to make DOC micelle-bound protein in NH_4HCO_3 buffer. The center tube of the S200 elution fractions (see this Chapter, the DOC micelle-bound coat protein preparation section) for each type of M13 coat protein were diluted to $A_{280} \cong 0.7$, and measured. (An absorption spectrum showed that all three types of proteins had absorption maxima at 280 nm.) 100 μl aliquots from the samples were then lyophylized, acid-hydrolyzed and submitted for amino acid analysis. The concentration of the protein in the original tubes were calculated using the average of the moles of leucine hydrolyzed after 22 hours over the number

of aliquots (either two or three) that were taken of each type of protein. The molar extinction coefficients obtained are shown in Table II-1.

The CD spectra in Chapter IV-B were run using Fphe- and Ftyr-labelled M13 coat proteins in micelles that were prepared separately to allow the measurement of the concentration of each type of protein, then they were mixed. The CD spectra were run on a Cary Model 60 spectrophotometer with a CD accessory fitted, and a thermostated cell. Column-eluant buffer (0.1M NH_4HCO_3, 8 mM DOC, pH 9.0) was used to set the zero value of the instrument.

The α-helix content of the protein was calculated by averaging the CD data at three sets of two wavelengths: $\alpha(210/225)$, $\alpha(215/225)$, and $\alpha(220/225)$, as given in Chapter IV-B. The β-sheet and random coil contents were obtained using the α-helix results. The errors in the % α-helix, % β-sheet and % random coil data, given in Figure IV-15 were calculated as follows: The ellipticity (θ) is calculated by the sample ellipticity (θ_s) minus that of the blank (θ_b), thus the error in θ is:

$$\Delta\theta = [(\Delta\theta_s)^2 + (\Delta\theta_b)^2]^{0.5}$$

Table II-1

The molar extinction coefficients for Fphe, Ftyr and unlabelled M13 coat protein at 280 nm

Phage	ϵ[1]
Fphe	8630±510
Ftyr	8220±590
unlabelled	8290±460

[1] the units are $cm^{-1}M^{-1}$

The mean residue ellipticity $[\theta]$ is calculated by:

$$[\theta] = \frac{m_r \ \theta}{10(1)(c)}$$

thus

$$\Delta[\theta] = [\theta]\left[\left(\frac{\Delta\theta}{\theta}\right)^2 + \left(\frac{\Delta c}{c}\right)^2\right]^{0.5}$$

The equations for $\alpha(X/225)$, $\beta(X/225)$, and random coil(X/225) (given in Chapter IV-B), are of the form of:

$$\alpha(X/225) = \frac{([\theta]_x + K_2)K_3 + ([\theta]_{225} + K_4)K_5}{K_1}$$

$$\beta(X/225) = \frac{[\theta]_x + K_2 - (\alpha(X/225))K_6}{K_7}$$

$$\text{random coil}(X/225) = 1 - \alpha(X/225) - \beta(X/225)$$

therefore, the errors will be:

$$\Delta\alpha(X/225) = \frac{[(\Delta[\theta]_x K_3)^2 + (\Delta[\theta]_{225} K_5{}^2]^{0.5}}{K_1}$$

$$\Delta\beta(X/225) = \frac{[(\Delta[\theta]_x)^2 + (\Delta\alpha(X/225)K_6)^2]^{0.5}}{K_7}$$

$$\Delta\text{random coil}(X/225) = [(\alpha(X/225))^2 + (\beta(X/225))^2]^{0.5}$$

E. Procedures for Experiments with Vesicle-Bound M13 Coat Protein

Reconstitution of M13 Coat Protein into Phospholipid Vesicles

M13 coat protein is an ideal membrane protein for physical studies due to its small size, the ease with which "gram-quantities" of it may be purified, and its amino acid sequence is known. Its one draw-back, though, is that it does not have a measurable activity, so it is difficult to know whether a certain preparation procedure is perturbing to its structure or not. With this uncertainty in mind, I have attempted to develop the most gentle reconstitution techniques possible to produce uniformly small, unilamellar vesicles, containing sufficient quantities of coat protein to allow ^{19}F NMR studies to be done. As a result, the procedure has evolved from a urea-cholate to cholate method. Both procedures, however, required sonication to produce the small vesicles. A recent improvement, obtained by increasing the amount of cholate (modified cholate procedure) will allow the removal of the sonication step.

Urea-cholate procedure

The coat protein, whether from Fphe- or Ftyr-labelled phage, was extracted from 30 mg of phage into DOC micelles. The micelle-bound protein was dialyzed in Spectrapor 3[1] dialysis tubing against,

---

[1] Spectrum Medical Industries Inc., Los Angeles, Ca., U.S.A.

first, 4 l of 10mM NH_4HCO_3, pH 9.0, then, 4 l of H_2O over 4 days to remove the DOC. It was lyophylized to dryness.

400/50/50 mg of dimyristoyl-phosphatidyl-choline (DMPC)/dipalmitoyl-phosphatidic acid (DPPA)/cardiolipin were placed in a round bottom flask. This was rotoevaporated to ~0.5 ml, then 6 ml of benzene and 6 drops of water were added. The flask was swirled until the lipid was dissolved, then strained through glass wool in a pasteur pipette. It was rotoevaporated to dryness then placed overnight either in a vacuum chamber connected to a vacuum pump or in a desiccator with a piece of paraffin wax using the house vacuum-line.

The next day the lipid was taken up in 6 ml of urea-cholate buffer [10] and sonicated for 10 min at 60 W power[11]. 15 mg of each of the labelled lyophylized coat proteins were placed in a tube and the lipid solution was added to them. The tube was gently swirled at 37°C until the protein was dissolved. (By this time the translucent solution had become whitish, suggesting that vesicles had been formed.) It was placed in Spectropor 6[12] dialysis tubing (molecular weight cutoff=1000) and dialyzed against a total of 4 l of 10 mM Tris-HCl (pH 8.0), 0.2 mM EDTA, 10% methanol over

---

[10] Urea-cholate buffer contained 2% sodium cholate, 0.1 mM EDTA, 20 mM $(NH_4)_2SO_4$ and 5 mM Tris-HCl, pH 8.0

[11] using a Braunosonic 1510 sonicator, Canadian Laboratory Supplies Limited, Edmonton Alta.

[12] Spectrum Medical Industries Inc., Los Angeles, Ca., U.S.A.

72 hours with changes three times a day. The dialyzed protein/lipid solution was layered over 5 ml of 10 mM Tris-HCl (pH 8.0), 1 mM EDTA in each of two Ti50 tubes and centrifuged at 15°C in a Ti50 rotor at 110,000xg for 4 hours. The pellets were suspended to a total volume of 9.0 ml with 60 mM Tris-HCl, 1 mM EDTA (pH 8). The sample was then divided into 2x4.5 ml samples. Each, in turn, was flushed with nitrogen for 5 min, then sonicated at 60-100 W power for 25 min, and was run on a Sepharose CL-4B[13] column using 60 mM Tris-HCl/1 mM EDTA (pH 8) buffer. The elution profile is shown in Figure II-2. The fractions following the major peak (starting from 5 tubes after the fraction with the highest A_{300} value until $A_{300} \cong$ the baseline value) were pooled from both samples and concentrated in a dual cavity (100 ml/10 ml) Amicon concentrator[14] to 1.5 ml. 60 mM Tris-HCl/1 mM EDTA (pH 8.0) in D_2O was added for the deuterium spectrometer lock, and the sample was reconcentrated to 1.3 ml.

Cholate Procedure

The cholate procedure for making vesicles was the same as the urea-cholate procedure, except that urea was left out of the solution used to solubilize the lipids and the coat protein.

---

[13] Pharmacia Fine Chemicals, Uppsala, Sweden.
[14] Amicon Corporation, Scientific Systems Division, Danvers, Ma., U.S.A.

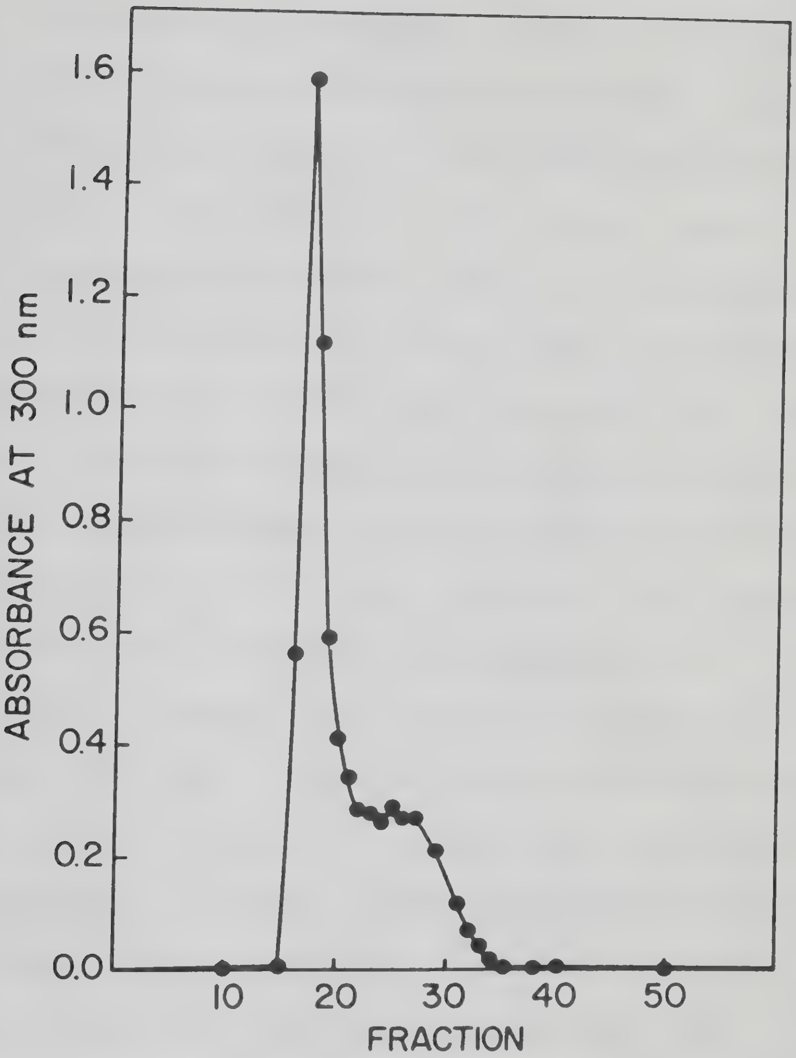

Figure II-2 The Sepharose CL-4B column elution profile of a sample containing coat protein reconstituted into phospholipid vesicles after sonication. The sample was prepared as described in the text. The major peak (fractions 16-20) contains large vesicles and lipid-protein fragments. The peak eluting just after the major peak (fractions ~22-35) is from small unilamellar vesicles (SUV)'s. The latter fractions were used to make the NMR sample. Each fraction contained 50 drops (2.4 ml) and the column was run by gravity. The column size was 55 x 1.6 cm.

Modified Cholate Procedure

The above procedures for making vesicles did not result in consistently good preparations. It was found that the problem was due to the insolubility of the coat protein in the aqueous solutions used, so two modifications were made to the Cholate procedure:

1) the amount of cholate was increased in the solution used for dissolving the protein and lipid;

2) the coat protein in micelles was added directly to the lipid/cholate solution and was not dialyzed and lyophylized as in the Cholate and Urea-cholate Procedures. The details are as follows:

100 mg, rather than 500 mg, of lipid (80 mg DMPC, 10 mg DPPA and 10 mg CL) were solubilized using 6 ml benzene and 6 drops of water, as described in the Urea-cholate procedure. After overnight evacuation, 5 ml of 60 mM Tris-HCl (pH 8.0), 1 mM EDTA was added to the lipid and the flask swirled until the lipid was suspended. A cholate/Tris-HCl/EDTA solution was prepared by adding 1 g of cholic acid to 10 ml of 60 mM Tris-HCl (pH 8.0), 1 mM EDTA and adjusting the pH with 1 M NaOH as it dissolved, so that the final pH was 8.0. The final concentrations were 46 mM Tris-HCl, 0.77 mM EDTA and 7.7% sodium cholate. 1.6 ml of this was added to the lipid suspension resulting in a change from a white suspension to an "almost clear" solution (the molar ratio of cholate:lipid was ~2).

Fifteen mg of each of Fphe- and Ftyr-labelled M13 phage were used to prepare labelled coat proteins in DOC micelles, as outlined in Chapter II-D. The fractions from the S200 column were pooled and concentrated to 1.3 ml. This was added, dropwise with stirring, to the lipid/cholate solution at room temperature. The turbidity of the resulting lipid/cholate/coat protein in DOC micelles solution did not change. The mixture was placed in Spectropor 6 dialysis tubing, as described in the urea-cholate procedure. It was dialyzed at 4°C for 87 hours against a total of 4 litres of 60 mM NH_4HCO_3 (pH˜8.2), 1 mM EDTA with 6 changes. The lipid/protein mixture went turbid after ˜24 hours, indicating vesicle formation at that time. The dialysate was layered over 4 ml of 60 mM NH_4HCO_3 (pH˜8.2)/1 mM EDTA in two Ti50 tubes and was otherwise handled by the same procedure given in the Urea-cholate procedure, except that the Sepharose CL-4B column buffer and D_2O buffer were 60 mM NH_4HCO_3[15](pH˜8.2), 1 mM EDTA.

Determination of Phospholipid to Protein Ratios

Determination of the Phospholipid Concentration

The procedure was adapted from Raheja, *et al.* (1973). It measures the phosphorus content in the

---

[15] These particular vesicles were to be digested with chymotrypsin, hence NH_4HCO_3 (without being pH adjusted) was used to allow the lyophylization of the buffer and the subsequent paper electrophoretic separation of the cleavage products.

samples, rather than the phosphate, thus problems with trace quantities of phosphate detergent in the sample tubes was not a problem. Four solutions were prepared:

Solution I contained 16 g of ammonium molybdate in 120 ml of distilled water. A few drops of HCl were required to help dissolve the molybdate.

Solution II contained 10 ml of redistilled mercury added to a mixture of 40 ml concentrated HCl and 80 ml of Solution I. The mixture was stirred for 45 min, then filtered. The reddish brown filtrate was Solution II.

Solution III, a dark green solution, was made by the careful addition, with stirring, of a mixture of 200 ml of concentrated H_2SO_4 and 40 ml of Solution I to Solution II.

Solution IV, the chromogenic solution, was prepared by the slow addition, with stirring, of 25 ml of Solution III to a mixture of 45 ml of methanol, 5 ml of chloroform and 20 ml of distilled water. (This solution has a shelf-life of at least three months.)

The assay procedure was as follows: Five aliquots were taken from each of a chloroform solution containing a known quantity of dimyristoyl-phosphatidylcholine and the aqueous solution containing the coat protein vesicles. The size of the aliquots were chosen to give a range of lipid phosphorus from 0.5 to 10 μg (usually the coat protein in vesicles sample had to be diluted ~30 times with water). The tubes were placed in a 100°C oven

until the solvents were evaporated. After cooling the tubes, 0.4 ml of chloroform and 0.2 ml of the chromogenic solution were added and vortexed for 30 sec each. The rack of tubes was placed in a boiling waterbath for 3 min, then, after cooling, 3 ml of chloroform/3% methanol was added. Each tube was vortexed for a minute. The samples were centrifuged in a counter-top centrifuge for 3 min to separate the layers, then the absorbance of the organic layer at 716 nm was measured. Chloroform containing 3% methanol must be used as the spectrophotometer blank; a sample that does not contain any lipid, but has been assayed as described above, gives an A_{716} that is not co-linear with the absorbances at 716 nm of the 0.5-10 μg lipid samples. The final colour is stable for 3 hours.

The moles of lipid present in a milliliter of a coat protein in vesicles NMR sample was calculated by, first, averaging the micrograms of phosphorus present in a unit volume of sample (Z), then solving the following equation[16]:

$$L = \frac{Z(\mu g/ml) x dilution x 10^{-6} (g/\mu g)}{31 (g\ P/mole)} \times \frac{7.29 (mole\ lipid)}{7.93 (mole\ P)}$$

---

[16] The lipids of the vesicles containing coat protein were DMPC, DPPA and CL (80:10:10). CL has two phosphorus atoms/molecule, thus the moles of phosphorus are greater than the moles of lipid by the ratio given. The ratio was determined assuming that the molecular weights of DMPC, DPPA and CL are 678 g/mole, 671 g/mole and 781 g/mole, respectively.

$$\text{where dilution} = \frac{\text{volume of diluted sample}}{\text{volume of sample assayed}}$$

The error in this calculation was determined as follows:

$$\Delta L = L \quad \frac{\Delta Z}{Z}^{2} + \frac{\Delta V_d}{V_d}^{2} + \frac{\Delta V_s}{V_s}^{2 \quad 0.5}$$

where V_d is the volume of the diluted sample and V_s is the volume of the sample that was diluted.

Determination of the Protein Concentration

The procedure used to measure the protein content of the coat protein in vesicles sample was the Hartree protein assay (a modified Lowry procedure) (Hartree, 1972). Three solutions were made:

Solution A contained 10% sodium carbonate and 0.2% sodium/potassium tartarate in 0.5 M sodium hydroxide.

Solution B had 2% sodium/potassium tartarate and 1% copper sulfate pentahydrate in 0.1 M sodium hydroxide.

Solution C was made just before using and contained 1 ml of Folin-Ciocalteau phenol reagent and 14 ml of water.

An aliquot of the coat protein in vesicles sample[17] was diluted 20 times with water and dispensed into 5 tubes. As well, aliquots of a solution containing a known amount of bovine serum albumin were measured

---

[17] The sample could not be in Tris-HCl buffer, as the Trizma base reacts with the reagents.

into 5 other tubes. In both cases the concentrations of protein were between 0 - 50μg protein/tube. Distilled water was added to all tubes to make their volumes 1 ml. 50 μl of 0.4% Triton X-100 was added to each tube. They were mixed using a vortex, then 0.9 ml of Solution A was added and mixed again. The rack of tubes was placed in a 50°C waterbath for 10 min. They were removed from the waterbath, allowed to cool; then 100 μl of Solution B was added and mixed. After sitting for at least 5 min, 3 ml of Solution C was added to each tube and immediately mixed thoroughly. The rack was placed in the 50°C waterbath again for 10 min. The tubes were removed from the waterbath, allowed to cool and their absorbance at 650 nm was measured.

The protein content in the coat protein in vesicles sample (P) was calculated by first determining the average protein content per unit volume of each sample tube (Y), then using the following relationship:

$$P(\text{mole/ml}) = \frac{Y(\mu g/\text{ml}) \times \text{dilution} \times 10^{-6}(g/\mu g)}{5240(g/\text{mole})}$$

$$\text{where dilution} = \frac{\text{volume of diluted sample}}{\text{volume of sample diluted}}$$

The error in the protein content measured was calculated using the following:

$$\Delta P = P\left[\left(\frac{\Delta Y}{Y}\right)^2 + \left(\frac{\Delta V_d}{V_d}\right)^2 + \left(\frac{\Delta V_s}{V_s}\right)^2\right]^{0.5}$$

where V_d is the volume of the diluted sample and V_s is the volume of the sample that was diluted.

The lipid to protein ratio (R) was calculated by $R = L/P$, thus the error is given by:

$$\Delta R = R\left[\left(\frac{\Delta L}{L}\right)^2 + \left(\frac{\Delta P}{P}\right)^2\right]^{0.5}$$

Chymotryptic Fragment Purification

After the chymotryptic cleavage of Fphe- and Ftyr-labelled M13 coat proteins in vesicles (see Chapter V-A), the vesicles were separated from the fragments by gel filtration on a Sephacryl S200 column (44 x 1.6 cm), equilibrated with 60 mM NH_4HCO_3 (pH~8.2). The absorbance of the fractions at 230 nm was measured, and those fractions containing the chymotryptic fragments were pooled and lyophylized. The residue was taken up in 0.5 ml of 0.1 M NH_4HCO_3 (pH 9.0), 8 mM DOC, then the DOC was precipitated and filtered as described in Chapter A II-D.[18] The filtrate was lyophylized. The residue was dissolved in 2 ml distilled

---

[18] This step was required to remove lipid contamination, which caused streaking of the paper electrophoresis.

water and lyophylized. This was repeated two more times. It was dissolved in 40 μl of pH 6.5 electrophoresis buffer, streaked over 4 cm on 1 mM paper, and the paper electrophoresis was run as described in Chapter II-D.

F. NMR Procedures

Instrument and Equipment Description and Conventions

The ^{19}F NMR spectra shown in this thesis were run on a Bruker HXS 270 MHz spectrometer, operating at 254.025 MHz for fluorine, in the fourier transform mode, unless stated otherwise. The temperature was controlled using a Bruker variable-temperature controller for temperatures above room temperature (~299°K), and the same temperature controller simultaneously with a refrigeration unit[19] for temperatures below room temperature.

^{19}F NMR spectra and/or T_1 measurements were done at two other frequencies. The spectra and T_1 data at 141 MHz were collected using the Nicolet NT150 NMR spectrometer of Drs. Ponsy Lu and Stan Opella in the Chemistry Department of the University of Pennsylvania in Philadelphia, U.S.A. The 376 MHz spectrum was run on the Bruker WH400 spectrometer of the Chemistry Department of the University of Alberta.

The ^{19}F chemical shifts were given relative to the fluorine signal of trifluoro-acetic acid (TFA) at 299°K in a solution containing 1.67 mM TFA, 15 mM potassium phosphate

---

[19] CryoCool, Neslab Instrument Incorporation, Portsmouth, N.H., U.S.A.

(dibasic) 2 mM EDTA and 50 mM potassium chloride (pH 7.0) in 99.75% deuterium oxide. The convention was taken that increasing field was decreasing frequency; Fphe and Ftyr were resonating upfield of the TFA resonance, therefore their resonances had negative chemical shifts. The chemical shifts reported were those obtained from spectra whose collection was started (at least) 20 min after the sample was placed in the magnet, unless stated otherwise ; this was found to be the equilibration time necessary for stable chemical shift values.

The acquisition parameters used in the one-pulse NMR experiments are given in the Figure legends. The acquisition parameters for the experiments using modified pulse sequences are given in the next two sections of this Chapter.

Relaxation and Nuclear Overhauser Experiments

^{19}F spin lattice relaxation times (T_1) were measured using either inversion recovery or progressive saturation techniques, without proton saturation. The inversion recovery technique monitors the relaxation of the ^{19}F spins after a 180° pulse by varying the length of time (t) waited before the 90° pulse: 180°-t-90°-acquisition. The spectral parameters used for the measurement of the Fphe and Ftyr residue T_1's of those labelled coat proteins in DOC micelles were: P_1 = 42 μsec (180°), P_2 = 21 μsec (90°), ±5000 Hz sweepwidth, 4 K data, 800 scans and a 5 sec delay between

cycles. The times (t) waited were: 0.05, 0.1, 0.2, 0.3, 0.4, 0.6, 0.8, 1.0 and 2.0 sec.

The T_1's of the Fphe and Ftyr residues of M13 coat proteins reconstituted into vesicles were measured using a progressive saturation technique. This method monitors the steady-state magnetization of the ^{19}F spins after a 90° pulse as they are allowed varying times, t, to relax: 90°-acquisition-t. Steady-state is obtained after the first few pulses. The acquistion parameters used to obtain the T_1 spectra were: P_2 = 17 μsec (90°), a sweepwidth of ±6300 Hz, 2 K data and 15,000 scans. There was no delay between transients other than the times, t: 0.15, 0.3, 0.45, 0.6, 0.8, 1.0 and 1.5 sec.

The nuclear Overhauser experiments required the saturation of the proton spins, prior to the pulse and acquisition of the fluorine spins. It was necessary to use both 270 pass/254 stop and 254 pass/270 stop cavity filters to avoid saturating the fluorine resonances with the pre-irradiation of the protons; broad-band decoupling with 2.5 W of power centered in the proton aromatic region was used. The decoupler was off during acquisition of the fluorine signal. The spectra were acquired using a 19 μsec (90°) pulse, a sweepwidth of ±6300 Hz, 4 K data and 30,000 scans. There was a delay of 400 msec between transients. The NOE's were determined relative to a spectrum that was collected using the same parameters as above, except that the decoupler was set off-resonance.

The NOE's measured at 141 MHz used cavity filters[20] to remove the fluorine frequencies from the decoupler pulse and the proton frequencies from the fluorine signal. The decoupler was gated off during fluorine acquisition. The spectral parameters were: a 25 μsec (78°) pulse, a sweepwidth of ±10,000 Hz, 30,000 scans, 8 K data, and a delay of 300 msec between transients.

Fluorine Chemically Induced Dynamic Nuclear Polarization Studies

The CIDNP of a tyrosine molecule requires the photo-excitation of a dye and its interaction with the tyrosine (see Chapter IV-B). This was monitored using the following pulse/laser sequence: D_4-L-D_3-P_2-A, where D_4 was a delay between transients (9 sec), L was the time that the laser shutter is open (1 sec), D_3 was a delay to allow the shutter to be closed (10 μsec), P_2 was the acquisition pulse (18 μsec (90°)), and A was the acquisition time. The other acquisition parameters included a sweepwidth of ±2000 Hz and 4 K data. The light and dark transients, referring to whether the laser was on or off prior to the pulse, were collected alternately.

---

[20] Sinclair Radio Laboratories Ltd., Downsview, Ontario.

III. Studies of the Two Amino Acids: Fphe and Ftyr

A. Interaction with Carbon Dioxide in Bicarbonate Buffer

Introduction

The kinetics and thermodynamics of the interaction of carbon dioxide with water and amines have been studied for many years (for a review, see Kern, 1960). Initially, the reactions of CO_2 and amines to form carbamate products were only of interest with respect to the study of the hydration kinetics of CO_2 (Faurholt, 1924). Interest in the reaction of CO_2 with amino groups increased greatly when it was postulated that this was the method by which hemoglobin (Hb) binds CO_2. Since that time researchers such as Roughton and coworkers (1966,1970), Van Kempen *et al.* (1975), and Imaizumi *et al.* (1982) have done detailed studies using amino acids, dipeptides and Hb to determine the details of the reaction. Studies of the amino acids and dipeptides have typically depended upon the measurement of the CO_2 in solution as either carbamate, using a $BaCl_2$ precipitation technique (Faurholt, 1924) or as dissolved CO_2, using a CO_2 electrode (Roughton *et al.*, 1966). Studies of Hb are often more complex, sometimes requiring the isolation of the carbamino Hb (the carbamate form of Hb) and subsequent CO_2 gas analysis of the protein (Van Kempen, 1975).

Nuclear magnetic resonance is a technique by which the concentrations of the reactants may be monitored directly.

In particular, ^{13}C NMR has been used by Gurd *et al*. (1980), O'Leary *et al*. (1979) and Morrow *et al*. (1974) to monitor carbamate formation in Hb, ribulose biphosphate carboxylase, and myoglobin, respectively (for a review, see Lorimer, 1983). We have found that ^{19}F NMR may also be used if the carbamate species are of fluoro-amino acids; the ^{19}F NMR spectra of Fphe and Ftyr, in a solution of bicarbonate buffer (pH 9.0), contain resonances from both the free amino acid and carbamate species of each amino acid. Measurement of the concentrations of the carbamate products, using the NMR peak intensities, as a function of pH has allowed the determinations of the carbamate equilibrium constants of these fluoro-amino acids.

Theory

Carbon dioxide has been shown to react with amines as follows:

$CO_2 + RNH_2 \rightleftharpoons RNHCO_2H$

$RNHCO_2H \rightleftharpoons RNHCO_2^- + H^+$

where RNH_2 is the deprotonated amino acid and $RNHCO_2H$ is the carbamate species. The overall reaction can then be written as:

$$CO_2 + RNH_2 \overset{K_c}{\rightleftharpoons} RNHCO_2^- + H^+$$

The ^{19}F NMR spectra allow the measurement of the concentrations of both the free amino acid and the carbamate form of the amino acid as a function of pH. With these data, it is possible to determine Kc, the equilibrium constant for the reaction.

From Kern (1960) and Roughton *et al.* (1966), the equilibria present in a solution containing bicarbonate buffer and amino acids (in the pH range 8 to 12) are:

$$RNH_3^+ \rightleftharpoons H^+ + RNH_2 \qquad K_z \tag{1}$$

$$RNH_2 + CO_2 \rightleftharpoons RNHCO_2^- + H^+ \qquad K_c \tag{2}$$

$$CO_2 + H_2O \rightleftharpoons H_2CO_3 \qquad K_h^{-1} \tag{3}$$

$$H_2CO_3 \rightleftharpoons H^+ + HCO_3^- \qquad K_1 \tag{4}$$

$$CO_2 + OH^- \rightleftharpoons HCO_3^- \qquad K_b^{-1} \tag{5}$$

$$HCO_3^- \rightleftharpoons H^+ + CO_3^{-2} \qquad K_2 \tag{6}$$

Reactions (3) and (5) are known as the direct hydrolysis and basic hydrolysis of carbon dioxide, respectively. Reactions (3) and (4) are the dominant equilibria below pH 6 while reactions (5) and (6) dominate above pH 10. At intermediate pH's both mechanisms are present. To solve for the concentration of the carbamate species as a function of proton concentration, equations 3 and 4, and 5 and 6 will combine to give:

$$CO_2 + H_2O \rightleftharpoons H^+ + HCO_3^- \qquad K_{1h} = K_1/K_h \tag{7}$$

$$CO_2 + OH^- \rightleftharpoons H^+ + CO_3^{-2} \qquad K_{2b} = K_2/K_b \tag{8}$$

The dissociation of H_2CO_3 described by equation (4) has a pK < pH 8 ($pK_1 = 3.76$) therefore the concentration of H_2CO_3 was assumed to be negligible. Hence,

C_0 = total concentration of carbonate species

$$= [H_2CO_3]+[HCO_3^-]+[CO_3^{-2}]+[CO_2]+[RNHCO_2^-]$$

$$\sim [HCO_3^-]+[CO_3^{-2}]+[CO_2]+[RNHCO_2^-] \qquad (9)$$

R_0 = total concentration of amino acid species

$$=[RNH_3^+]+[RNH_2]+[RNHCO_2^-] \qquad (10)$$

Writing and rearranging the equilibrium equation for equation (2), one obtains the relationship between the concentration of the carbamate product and the hydrogen ion concentration:

$$[RNHCO_2^-] = \frac{K_c\,[RNH_2]\,[CO_2]}{[H^+]} \qquad (11)$$

Substitution of equation (10) into the equilibrium equation for equation (1) and rearrangment gives:

$$[RNH_2] = \frac{K_z(R_0 - [RNHCO_2^-])}{[H^+] + K_z} \qquad (12)$$

Combining the equilibrium relationships of equations 7 and 8 with equation (9) and solving for the concentration of CO_2 results in:

$$[CO_2] = \frac{[H^+]^2(C_0-[RNHCO_2^-])}{[H^+]^2 + K_{1b}[H^+] + K_wK_{2h}} \qquad (13)$$

Finally, substituting equations (12) and (13) into (11) gives the quadratic:

$$A[RNHCO_2^-]^2 - B[RNHCO_2^-] + C = 0 \qquad (14)$$

where $A = K_cK_z[H^+]$

$B = D_1D_2 + K_cK_z[H^+](R_0 + C_0)$

$C = K_cK_zR_0C_0[H^+]$

$D_1 = [H^+] + K_z$

$D_2 = [H^+]^2 + K_{1h}[H^+] + K_wK_{2b}$

The analyses of the Fphe and Ftyr data using this relationship are given in the Discussion.

Results

The ^{19}F NMR spectrum of a sample containing Fphe, Ftyr, DOC[21] and sodium bicarbonate (pH9.0) (see Figure III-1), contains four sets of resonances: the resonances at -38.27 and -61.41 ppm have been assigned to Fphe and Ftyr, respectively; the resonances upfield of each of these, at -38.91 and -62.18 ppm, are due to Fphe and Ftyr as well, but are shifted from the major resonances indicating that the fluorines in these amino acids are in different magnetic environments. The multiplicity of each of the Fphe and Ftyr

---

[21] The deoxycholate was included in the sample so that the conditions for the acquisition of the free fluoro-amino acid spectra would be identical to the conditions of the experiments with the DOC micelle-bound, fluoro-amino acid-labelled coat protein. The presence or absence of the DOC was found to have no effect on the fluoro-amino acid ^{19}F NMR spectra.

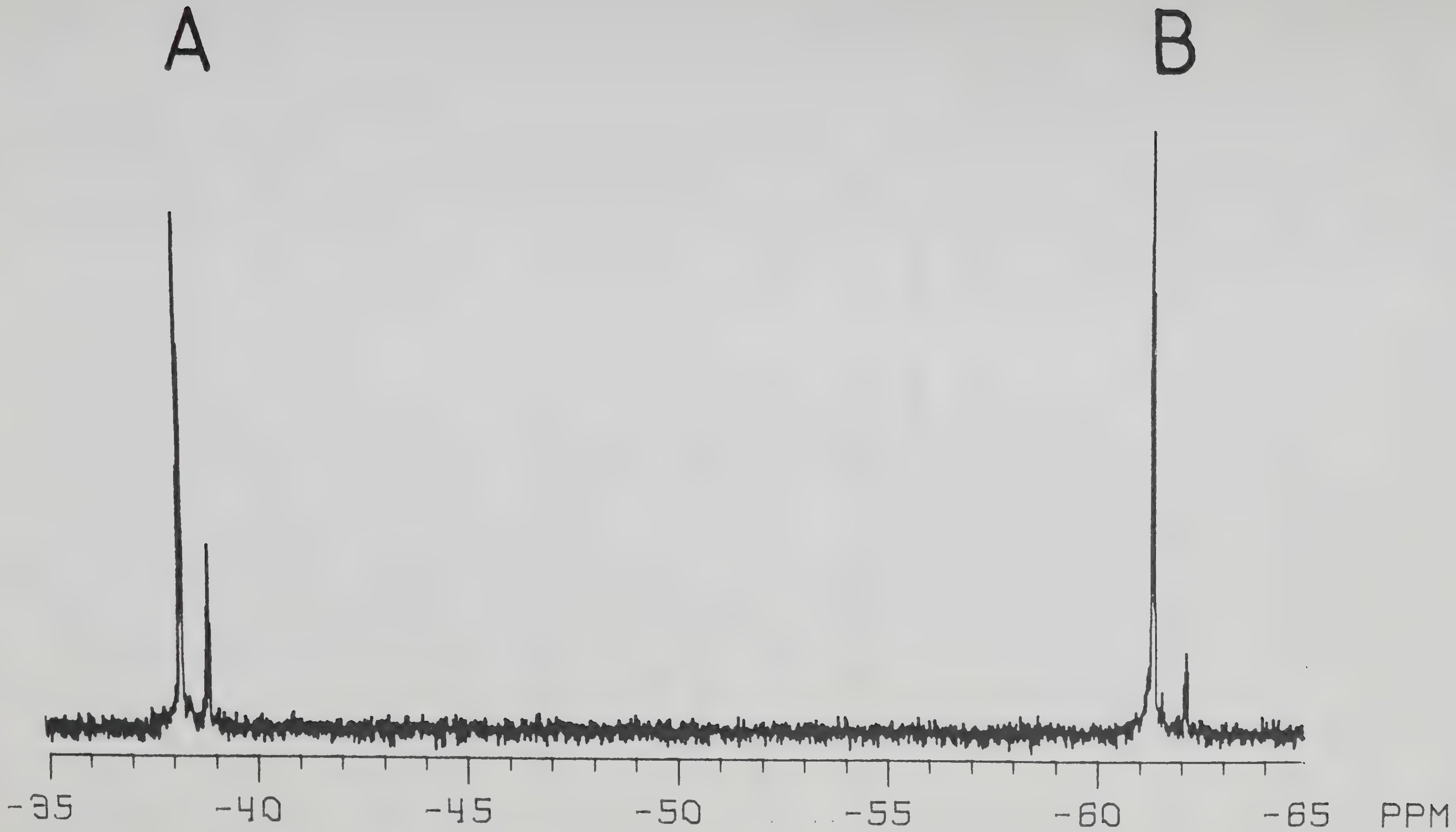

Figure III-1 The ^{19}F NMR spectrum of Fphe and Ftyr in bicarbonate buffer. The sample contained 3 mM each of Fphe and Ftyr, 0.1M $NaHCO_3$ (pH 9.0) and 8 mM DOC, in D_2O. Resonances (A) are from Fphe while resonances (B) are from Ftyr. The spectrum resulted from 2000 scans and was acquired using a 9 usec (45°) pulse, ±5000 Hz sweepwidth, 8K data and no delay between transients. 1 Hz linebroadening was used.

resonances, seen clearly in Figure III-2, is due to the coupling of the fluorine nucleus of each amino acid to neighbouring ring protons; the spectra were not proton decoupled. Figure III-2 also shows that the upfield resonances were not caused by the DOC but result from the bicarbonate buffer. A D_2O solution containing only Fphe and Ftyr at pH 9.0 did not have any upfield resonances [Figure III-2(i)]. As the buffer concentration was increased, the height of the upfield resonance relative to the "major" resonance increases until at 0.5 M, the relative heights are almost equal [Figure III-2(iv)]. At 1.0 M [Figure III-2(v)] the upfield resonance becomes the major resonance.

Figure III-3 shows the ^{19}F NMR spectra of Fphe in either sodium phosphate [Figure III-3(A)] or Tris-HCl [Figure III-3(B)] buffer, as a function of pH. There were no upfield resonances present in either buffer through a pH range of 8.0 to 11.0 with sodium phosphate and 4.0 to 9.6 with Tris-HCl.

The ^{19}F NMR spectra of 3-fluoro-benzoic acid in $NaHCO_3$ buffer are presented as a function of pH in Figure III-4. There were no upfield resonances present for this compound throughout the pH range of 8.0 to 10.0. As well, the chemical shift of the resonance at ~-38.42 ppm did not shift throughout the pH titration.

Figure III-5 shows the effect of changing the pH of a solution containing Fphe, Ftyr and $NaHCO_3$. The results of

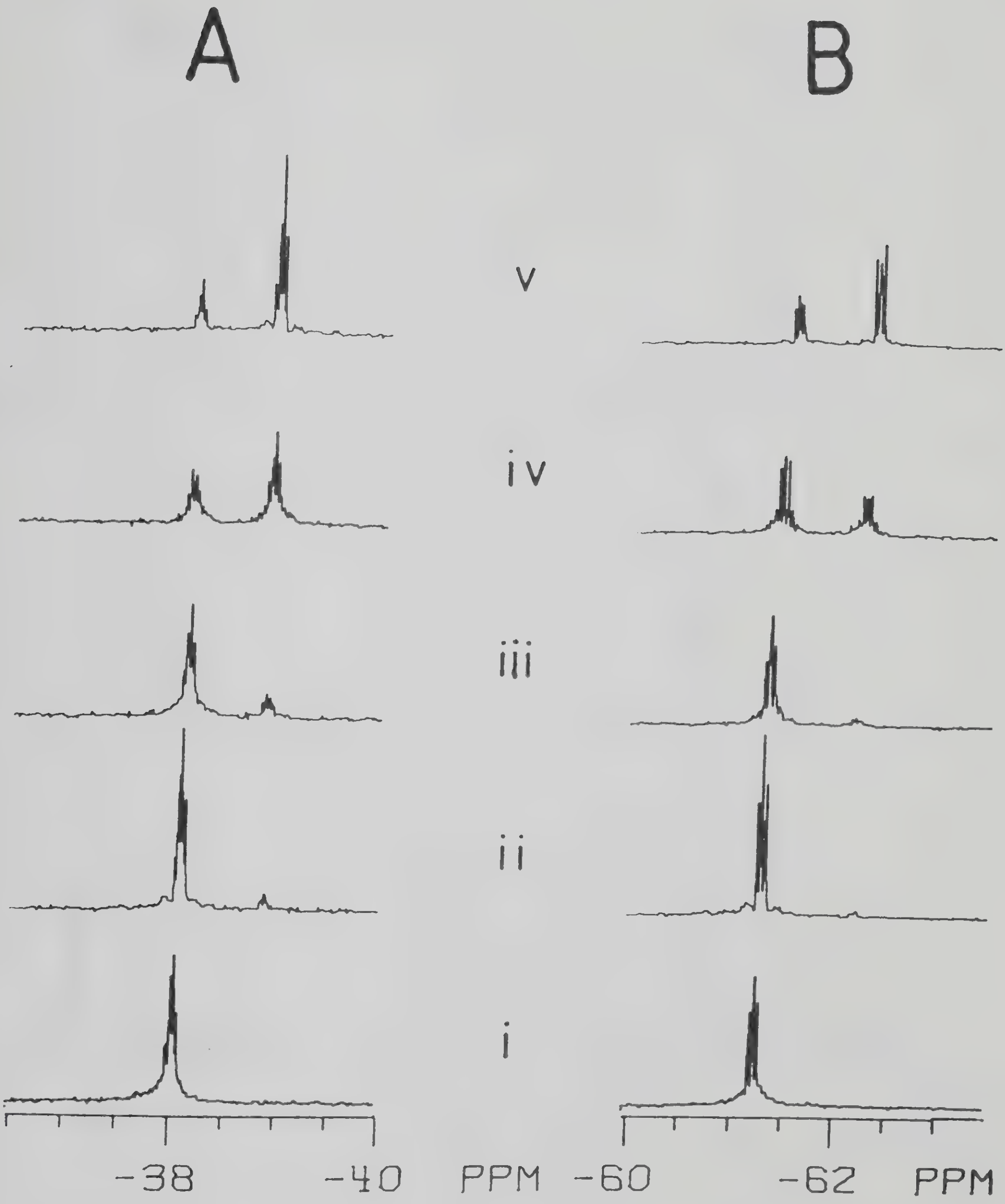

Figure III-2 The ^{19}F NMR spectra of Fphe and Ftyr with varying NH_4HCO_3 concentrations. The sample contained 3 mM each of Fphe and Ftyr and were all pH 9.0. The resonances in A are from Fphe while those in B are from Ftyr. The NH_4HCO_3 concentrations are: i) 0 M; ii) 0.05; iii) 0.1; iv) 0.5; v) 1.0. The acquisition parameters were the same as in Figure III-1.

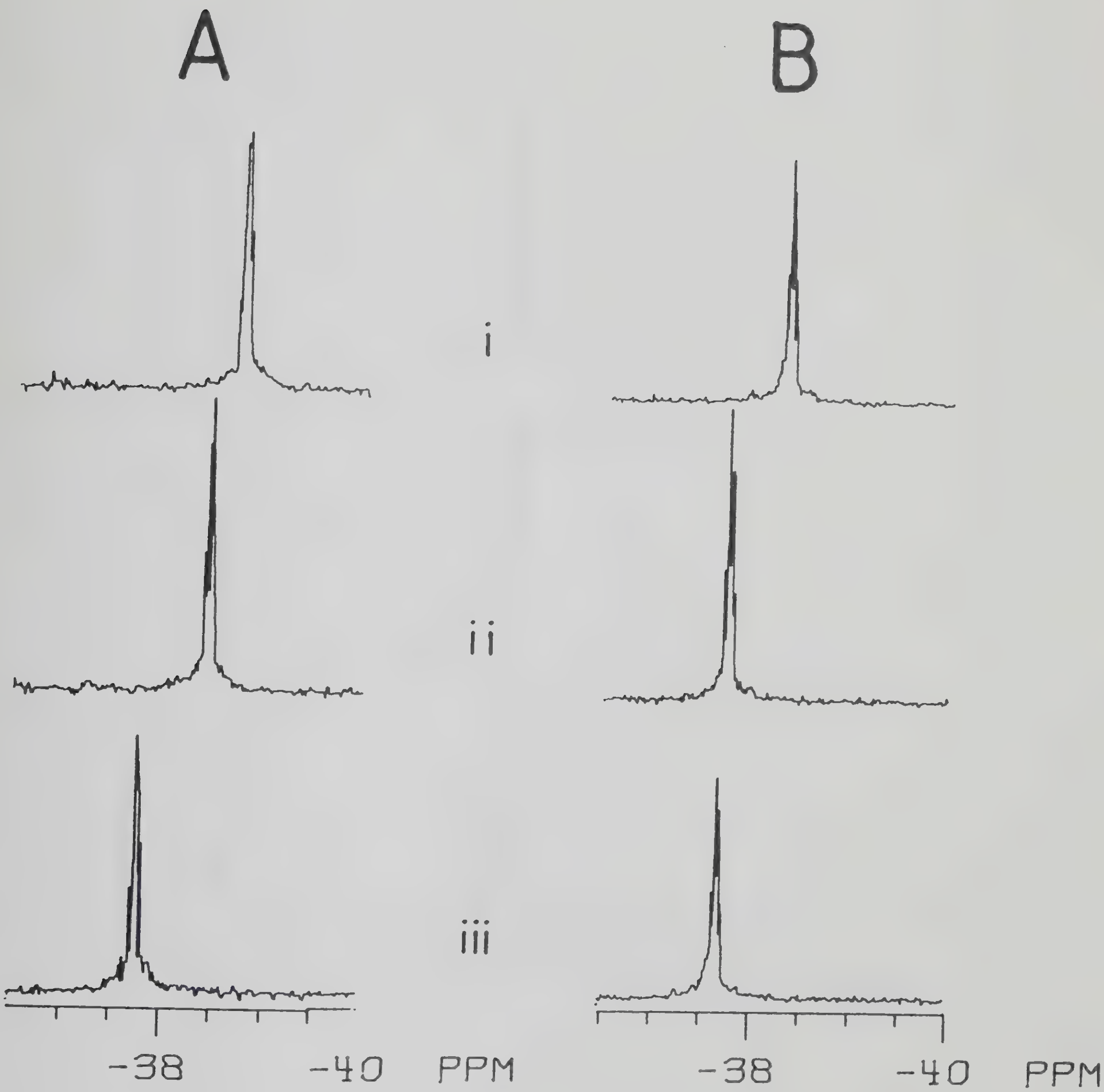

Figure III-3 The ¹⁹F NMR spectra of Fphe in either phosphate or Tris-HCl buffer with varying pH. The samples contained 3 mM of both Fphe and Ftyr (only Fphe spectra shown) and 0.1M of either A) sodium phosphate or B) Tris-HCl buffer, in D_2O. The pH values were varied as follows: A-i) 10.97; A-ii) 9.50; A-iii) 7.98; B-i) 9.60; B-ii) 7.99; B-iii) 4.04. The spectra were acquired at 297°K using the acquisition parameters given in Figure III-1.

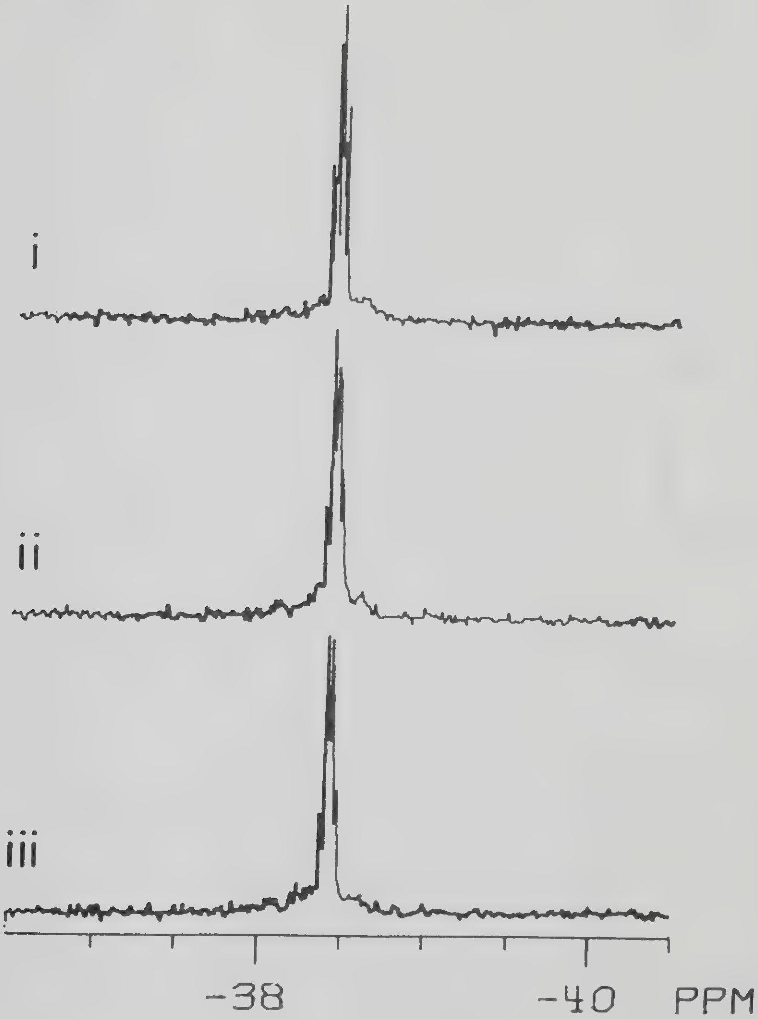

Figure III-4 The ^{19}F NMR spectra of 3-fluorobenzoic acid in bicarbonate buffer with varying pH. The sample contained 3 mM Fben and 0.1M $NaHCO_3$ buffer, in D_2O. The pH was varied as follows: i) 10.0; ii) 9.0; iii) 8.0. The spectra were collected at 297°K using the same acquisition parameters given in Figure III-1.

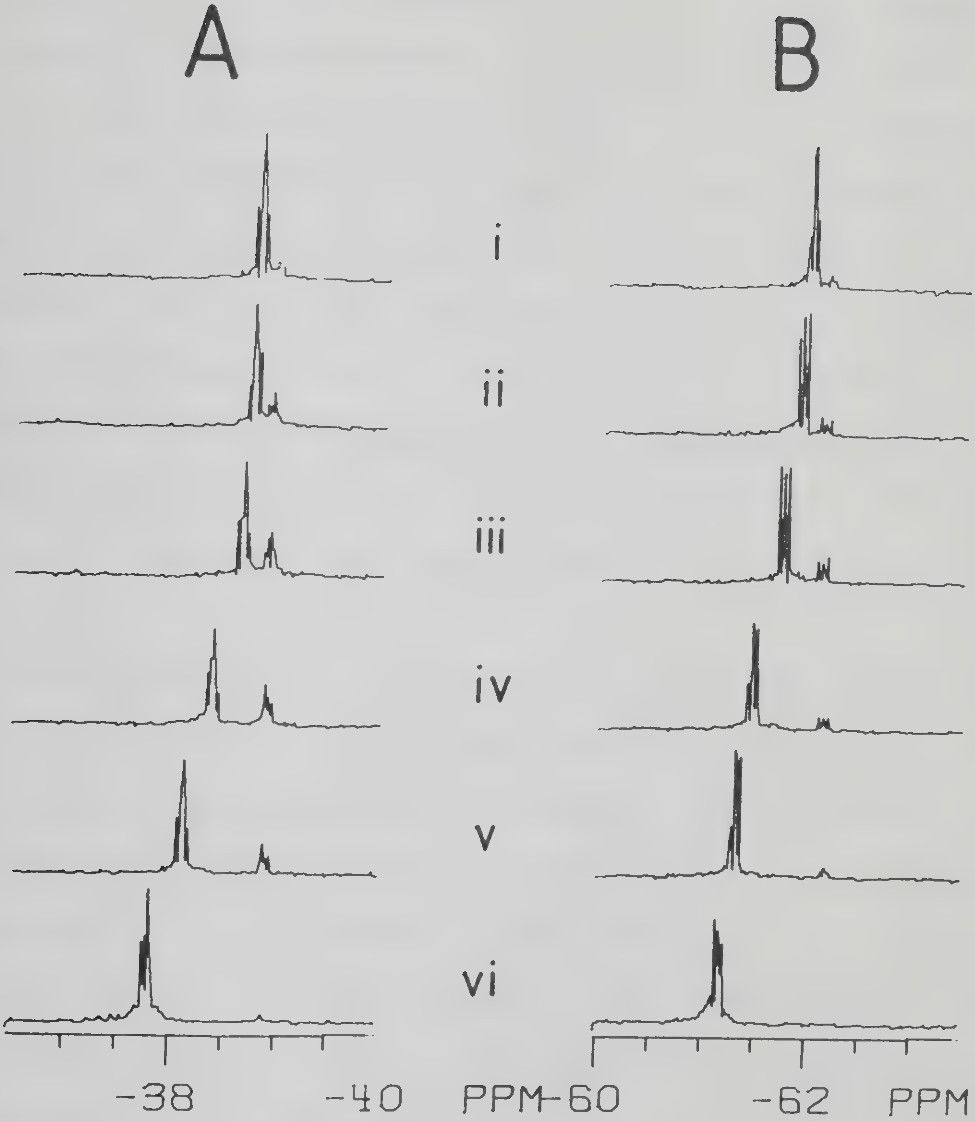

Figure III-4 The ^{19}F NMR spectra of Fphe and Ftyr in bicarbonate with varying pD. The sample contained 3 mM each of Fphe and Ftyr and 0.1M $NaHCO_3$ in D_2O. The resonances in A are from Fphe while those in B are from Ftyr. The pD values are: i) 11.69; ii) 11.08; iii) 10.54; iv) 9.89; v) 9.44; vi) 6.67. The spectra result from 1000 scans, collected at 298°K using a 7 μsec (35°) pulse, ±4000 Hz sweepwidth, 4K data, and a delay of 406 msec between transients. 0.2 Hz line-broadening was used.

this titration will be used for calculating the equilibrium constant, K^d, of the carbamate reaction in D_2O, hence, the pH values are given as the more appropriate pD values. As the pD is increased from 8.67 to 11.69, the major (downfield) resonances for both Fphe and Ftyr shift upfield. The chemical shift of the upfield Fphe resonance does not change throughout this pH range, while the Ftyr upfield resonance shifts downfield slightly. The titration behavior of the chemical shifts of the Fphe and Ftyr resonances are more clearly shown in Figure III-6. The analyses of the dissociation constants of these curves are given in the Discussion.

The spectra in Figure III-5 also show that the relative intensities of the major and upfield resonances for both Fphe and Ftyr are affected by the pD of the solution: the intensities of the upfield resonances increase with pD until a maximum at ~10.5 is reached, then they decrease. The areas of the upfield resonances were normalized relative to the total area (major + upfield resonances), then converted to concentrations of the species. The graph of the concentration of the upfield resonances as a function of pD is shown in Figure III-7. The points shown are the actual data while the curve is the computer fit to the data using the equations presented in the Theory section (see Discussion). The upper graph used the Fphe upfield peak intensities while the lower graph used the Ftyr intensities. The better fit of the upfield Fphe data compared to the upfield Ftyr data

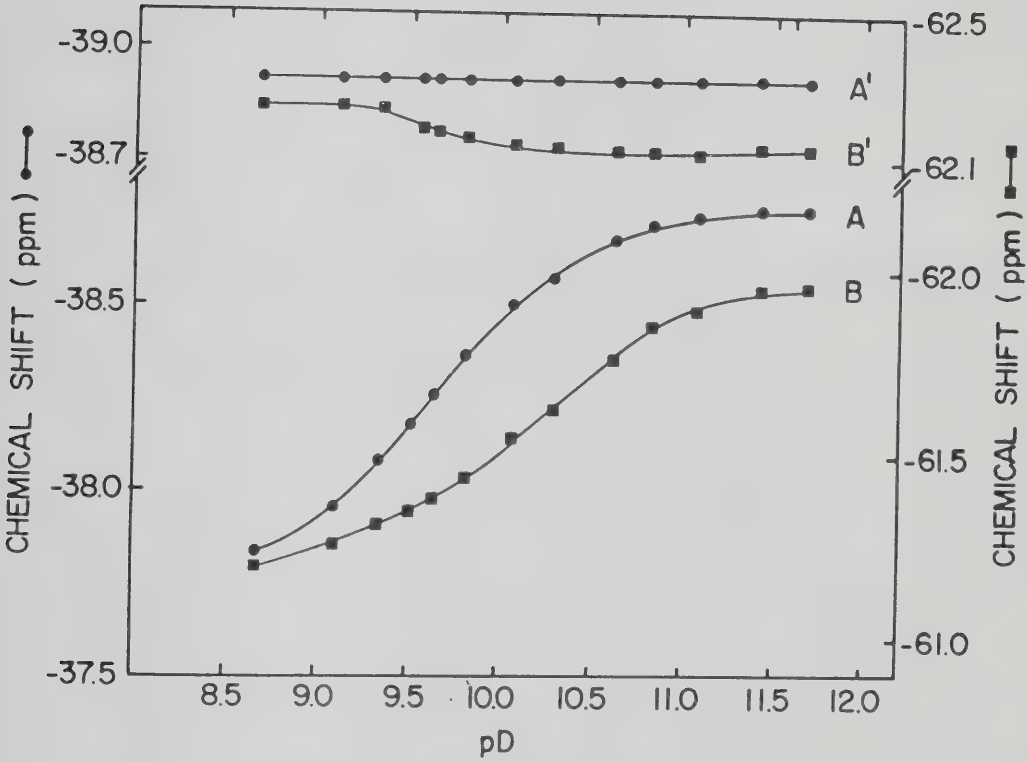

Figure III-6 The pD titration curves of the Fphe and Ftyr ¹⁹F NMR chemical shifts in bicarbonate buffer. The data were obtained from the ¹⁹F NMRpD titration of the fluoro-amino acids, six of which are shown in Figure III-5. Curves A and A' are the major and upfield Fphe resonances, respectively, while B and B' are from the major and upfield Ftyr resonances (see Figure III-5).

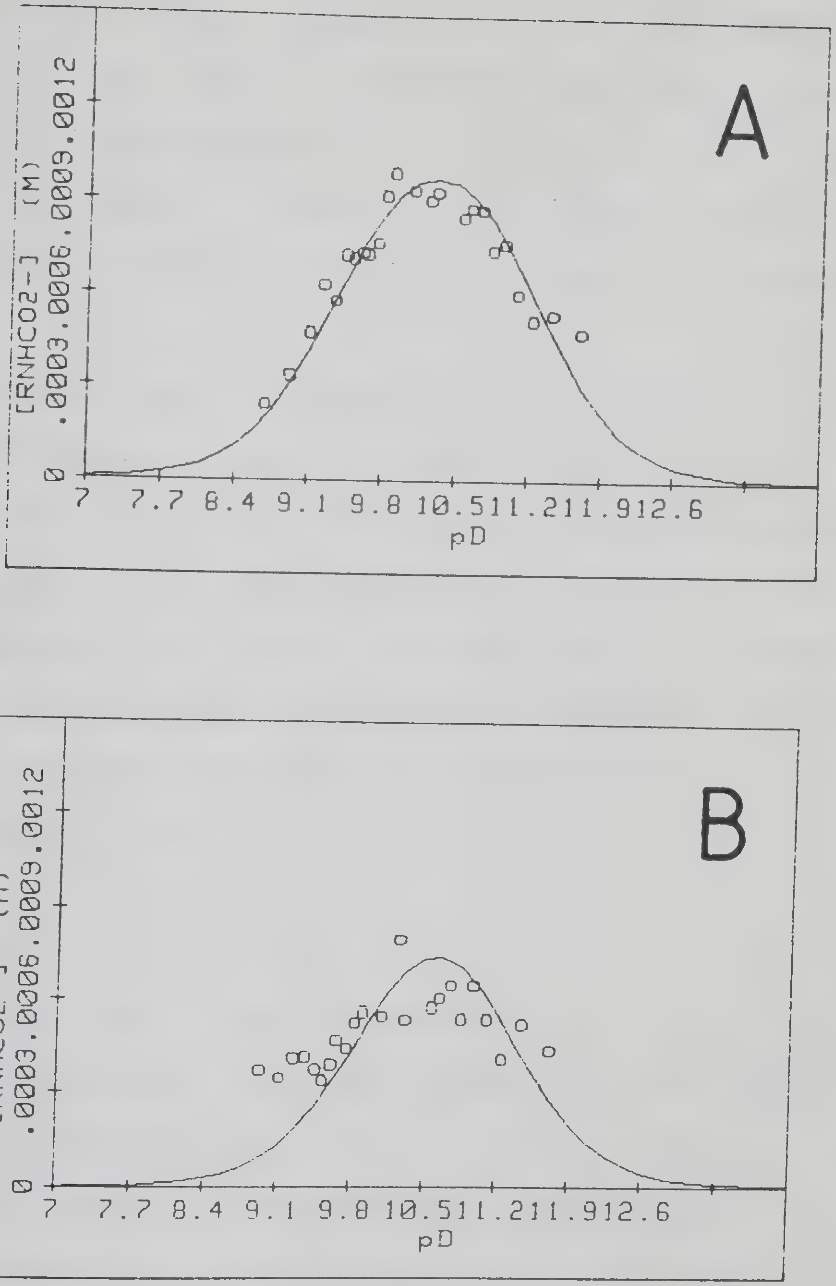

Figure III-7 The graphs of the concentrations of the Fphe and Ftyr carbamate species as functions of pD. Graph A is the Fphe data, while graph B is the Ftyr data. The data were obtained from the ^{19}F NMR resonance intensities at each of the pD values (see Figure III-5). The curves through the points are the computer fits to the data, using equation (14).

reflected the higher concentration of the upfield Fphe species in the sample; there was less than 0.3 mM of the upfield Ftyr species at most of the pD values which appeared to be the limit of detection. More scans and/or a higher concentration of Ftyr would be necessary to improve the data.

To ensure that the comparison of resonance intensities is valid, the T_1 relaxation times of the Fphe and Ftyr resonances were measured at 298°K and are shown in Table III-1. The T_1 data were acquired using a progressive saturation pulse sequence and were analyzed using a Nicolet T_1 progressive saturation curve-fitting program. The delays between transients (see Chapter II-F) were: 0.1, 0.3, 0.7, 1.5, 3, and 8.5 sec.

Discussion

Gaseous CO_2 in the presence of an aqueous solution equilibrates between the gaseous phase over the solution and the dissolved and hydrated forms in the solution. The mechanism of CO_2 hydration depends upon the solution pH: at pH <6, the direct interaction with H_2O is the dominant mechanism (equation (3)) while at pH >10, the alkaline catalysed mechanism predominates (equation (5)). It is clear from those two equations that CO_2 in a solution may be produced by either performing experiments in a CO_2 atmosphere or by starting with bicarbonate buffer.

Table III-1

The T_1 relaxation times of Fphe and Ftyr amino acid resonances

Resonance		T_1 (sec)
Fphe:	upfield	2.9 ± 0.1
	major	3.1 ± 0.2
Ftyr:	upfield	1.8 ± 0.2
	major	2.5 ± 0.1

Given that the bicarbonate buffer is a source of CO_2 and that CO_2 is known to react with amines to form carbamate products, it is reasonable to propose that the upfield resonances in the ^{19}F NMR spectra of Fphe and Ftyr in a bicarbonate solution result from the carbamate species of each of the amino acids. It is necessary however to prove that the upfield resonances depend both on a source of CO_2 and the presence of amino groups. The necessity of a "CO_2-source" is demonstated in Figures III-2 and III-3. Figure III-2(i) shows that when there is no bicarbonate buffer included in the sample, no upfield resonances are seen. As the concentration of the bicarbonate buffer is increased [Figure III-2(ii-v)], the intensities of the upfield resonances increase. This is expected if the bicarbonate buffer is providing the CO_2. Figure III-3 reiterates the conclusion from Figure III-2(i). When the ^{19}F NMR spectra of Fphe and Ftyr are run in solutions containing either sodium phosphate [Figure III-3(A)] or Tris-HCl [Figure III-3(B)] buffer, no upfield resonances are seen (only the Fphe spectra are shown). In Figure III-6, it was shown that the pH of the bicarbonate solution affects the intensities of the upfield resonances. To show that the pH of the phosphate and Tris-HCl solutions has no effect on whether or not upfield resonances are detected, the pH of those solutions was varied. The second and third pKa values of the phosphate buffer[22] are 7.21 and 12.67 respectively, while the pKa of

---

[22] *CRC Handbook of Chemistry and Physics* (1969) ed. Weast, R.C. (The Chemical Rubber Company, Cleveland,

Tris-HCl buffer[23] is 8.38. It is seen in Figure III-3 that regardless of the ionic valence of the buffer (determined by the pH) or whether the buffer is anionic or cationic (being phosphate or Tris), the upfield resonances are not detected. This suggests that the upfield resonances of the ^{19}F NMR spectra of Fphe and Ftyr in bicarbonate are not due to a nonspecific ionic interaction. These results also show that CO_2 contamination from the air (which is particularly of importance at pH>7 [Hall *et al.*, 1983]) is not significant in these experiments.

The necessity of the amino groups to the appearance of the upfield resonances was shown by the following: the ^{19}F NMR spectra of 3-fluoro-benzoic acid (Fben) in bicarbonate buffer (Figure III-4) were insensitive to the pH of the sample with respect to both the chemical shift of the resonance and the absence of an "upfield resonance". The Fphe and Ftyr resonances experience significant changes in their chemical shifts and contain upfield resonances throughout the pD range (Figures III-5 and III-6). The only difference in structure between Fphe and Fben, essentially, is that Fben does not have an amino group. Hence, the change in chemical shift of 1.05 ppm of the Fphe major resonance [Figure III-6(A)] must result from the titration of the amino group (pK_2^d = 9.64)[24]. (As well, in Chapter III-B,

---

[22] (cont'd) Ohio),pg.D-119.

[23] *CRC Handbook of Biochemistry: Selected Data for Molecular Biology* (1968) ed. Sober, H.A. (The Chemical Rubber Company, Cleveland, Ohio),pg.J-117

[24] This amino group dissociation constant was measured in D_2O. In H_2O, this constant would be 9.04 [see Marshall

Figure III-13 shows the ^{19}F NMR spectra of Fphe and Ftyr whose N- and C-termini have been N-acetylated and methyl esterified, respectively. There are no upfield resonances present, thus the necessity of the free amino group for the appearance of the upfield resonances is supported.) The titration behavior of the upfield Fphe resonance was shown in Figure III-6(A'). In this case the chemical shift did not change with pD, showing that the amino group of this Fphe species was not not titratable.

The Ftyr case is more complicated as both the phenolic hydroxyl and the amino groups are titrated in this pD region. As a result, curve B in Figure III-6 is actually a curve containing both titrations. Curve B' shows that the chemical shift of the Ftyr upfield species shifts less than that of the Ftyr resonance and in the opposite direction (shifting downfield instead of upfield). The pKa obtained from curve B' is 9.21.[25] That the amino group of the Fphe upfield species was not titrated, suggests that the titration of the Ftyr upfield species is of the hydroxyl rather than the amino group. (This pKa is low for a tyrosine hydroxyl but would be showing the effects that the fluorine has on the ring.) A comparison of curve B' to curve B assigns the lower region of curve B to the titration of the hydroxyl moiety. The upper major portion of the curve, then, corresponds to the titration of the Ftyr amino group.

---

[24] (cont'd) (1978), pp456-457, to be given].

[25] The Ftyr amino and hydroxyl group dissociation constants were determined in D_2O. Thus, in H_2O, pK = 8.62 and pK_z= 9.62 (see Marshall (1978), pp.456-457, to be given).

Analysis of pD dependence of this region of the curve results in a pK_z^d of 10.23^{25}.

The results discussed demonstrate that the presence of the upfield Fphe and Ftyr resonances in bicarbonate buffer requires both the amino groups of the amino acids, and the bicarbonate, hence the upfield resonances are due to the carbamate species of each of the amino acids. The Fphe and Ftyr carbamate resonances are well resolved from those of the amino acids so their behavior may be monitored directly. In particular, the changes in their intensity with pD reflects the changes in their concentrations with pD. These data allowed the determination of the equilibrium constants for the carbamate formation (see Theory section) for both of the fluoro-amino acids.

The desire to compare the intensities of the major and upfield resonances of the pD titration spectra prompted the measurement of the spin lattice relaxation times, (T_1's), of the resonances. Table III-1 showed that there is only approximately 1 sec difference between the longest and shortest T_1's. The spectral acquisition parameters were optimized for the longest T_1, that of the major Fphe resonance, but as the dependence of the signal to noise ratio on the T_1 is logrithmic (Ernst and Anderson, 1966), the signal to noise ratios due to the data acquisition should not be significantly different. Differences in resonance intensities, then, were due to differences in the concentrations of the Fphe and Ftyr species.

The changes in the concentrations of the carbamate species with pD for Fphe and Ftyr are shown in Figure III-7. Qualitatively the data may be explained in terms of the relative $pK_z{}^d$ values of Fphe and Ftyr and the pK_2 value of bicarbonate. The reaction of CO_2 with an amino group requires that the amino group be uncharged. Therefore, the gradual increase in the concentrations of the Fphe and Ftyr carbamate species reflect the increasing concentrations of the deprotonated amino groups as the Fphe and Ftyr $pK_z{}^d$ values are approached. The Ftyr $pK_z{}^d$ is higher than that of Fphe (10.23 compared to 9.64), thus the concentration of the deprotonated Fphe and consequently the concentration of the Fphe carbamate will be greater. Once above the amino acid $pK_z{}^d$ values, the pD approaches the pK_2 value of the bicarbonate (10.88). This equilibrium (shown by equation (6)) is intimately involved with the CO_2 concentration of the solution (through equation (5)). Once the pD is above pK_2, the concentration of the HCO_3^- ion has decreased significantly. This, in turn, draws from the CO_2 concentration (in equation (5)) which results in the reversal of the carbamate equilibrium (of equation (2)). The concentrations of the carbamate species therefore decrease with the conversion of carbamate to deprotonated amino acid and CO_2.

The quantitative discussion of the carbamate reaction uses the equilibrium formulae outlined in the Theory section. The result (equation(14)) is a relationship between the concentration of the carbamate species and the proton

concentration; the constants of the equation are all known from the literature except for K_c, the carbamate reaction equilibrium constant. This constant may be derived by the solution of equation(14).

Equilibrium constants depend upon the experimental conditions under which they were derived, hence, a discussion of the factors influencing these constants is appropriate. Three factors are particularly relevant: the temperature, the solvent (H_2O versus D_2O) and the ionic strength of the sample. The literature constants used in the calculation were determined at 25°C (298°K) and 0 ionic strength in water. The experiments described herein were also done at 298°K, so temperature is not a problem. Both the ionic strength and the solvent though, were different, so the effects will be analyzed.

Correction for the change of solvent from H_2O to D_2O is relatively straightforward. For the dissociation of an acid, the following relationships apply (Marshall, 1978):

$$pD = pH\ \text{reading} + 0.41$$

$$pK_a^d = 1.02(pK_a) + 0.42$$

Thus the conversion of K_1 and K_2 to K_1^d and K_2^d is simple. The correction of the carbon dioxide equilibrium constants, K_h and K_b require individual kinetic analysis.

Morrow *et al.* (1974) give the effects of replacing water with deuterium oxide on the constants as:

$$K_h/K_h^d = 4$$

$$K_b/K_b^d = 0.8$$

hence, K_h^d and K_b^d may be determined. The values of K_1, K_h and K_b are given in Table III-2.

The third factor that would affect the equilibria, the ionic strength, is more difficult to correct. Neuberger (1937) outlined, in detail, the protocol for determining the effects of ionic strength on equilibrium constants. Absolute equilibrium constants are given by the following:

$$K = \frac{[A^+]\ [B^-]}{[AB]} \times \frac{f_{A+}\ f_{B-}}{f_{AB}}$$

where $[A^+]$, $[B^-]$ and $[AB]$ are the equilibrium concentrations of the reactants and products, and f_{A+}, f_{B-} and f_{AB} are their respective activity coefficients. At very low ionic strength, $f_{A+} = f_{B-} = f_{AB}$, so that

$$K = \frac{[A^+]\ [B^-]}{[AB]}$$

As the ionic strength is increased, the ions become non-randomly dispersed in the solution. This causes f_{A+} and f_{B-} to be less than 1; f_{AB}, being a neutral species, is 1 until very high ionic strengths.

Table III-2

The equilibrium constants used for the carbamate species analysis

	Absolute (K)	D_2O Corrected (K^d)	Ionic Strength Corrected	
			Fphe (I=0.14M)	Ftyr (I=0.21M)
K_z	-	-	2.29×10^{-10}	5.89×10^{-11}
K_1	1.74×10^{-4}(1)	5.50×10^{-5}	1.15×10^{-4}	1.29×10^{-4}
K_2	5.62×10^{-11}(2)	1.32×10^{-11}	5.62×10^{-11}	7.40×10^{-11}
K	388(2)	97	97	97
K	2.35×10^{-8}(3)	2.94×10^{-8}	2.94×10^{-8}	2.94×10^{-8}
K	1.01×10^{-14}(4)	2.00×10^{-15}	6.33×10^{-15}	5.35×10^{-15}

[1] *CRC Handbook of Biochemistry: Selected Data for Molecular Biology*, ed. Sober, H.A. (The Chemical Rubber Company, Cleveland, Ohio)

[2] Kern (1960) : $K_1 = K_1'(1 + K_h)$, where

$$K_1' = [H^+][HCO_3^-]/([CO_2] + [H_2CO_3]) \quad (pK_1' = 6.35)$$

[3] Kern (1960) : $K = \frac{[OH^-]\,[CO_2]}{[HCO_3^-]} = \frac{k_{HCO_3^-}}{k_{OH^-}}$

[4] *CRC Handbook of Chemistry and Physics* (1969), ed. Weast, R.C. (The Chemical Rubber Company, Cleveland, Ohio)

The absolute equilibrium constant is then given by:

$$K = \frac{[A^+][B^-]}{[AB]} f_{A^+} f_{B^-} = K(I)\ f_{A^+} f_{B^-}$$

where K(I) is the equilibrium constant obtained for a solution of ionic strength, I.

Neuberger calculated f_x using the following equation:

$$-\log f_x = \frac{0.5\sqrt{I}}{1 + \sqrt{I}}$$

where I is the ionic strength of the solution. This equation was obtained through solving the Debye-Huckel equation for a temperature of 298°K, an ionic valence of 1, and an ionic radius of 3.08 Å. The concept of "ionic radius" is not clearly defined for ions that are diatomic or larger but a value of 1.5 Å was determined for HCO_3^- as the average distance of closest approach that another ion can come as it tumbles in solution, hence the equation becomes:

$$-\log f_x = Z^2 \frac{0.5\sqrt{I}}{1 + 0.5\sqrt{I}}$$

where Z is the ionic valence (for example, $Z_{CO_3^{-2}} = -2$). The equation does not change much by substituting estimates of the ionic radii of H^+, CO_3^{-2}, OH^-, etc., so that this relationship was used to calculate f_x for all of them.

The next problem is to determine the ionic strength of the solution, I.

The ionic strength of the Fphe/Ftyr/bicarbonate solution is given by:

$$
\begin{aligned}
I &= 1/2\ \Sigma M_i Z_i^2 \\
&= 1/2[[Na^+](1)^2 + [HCO_3^-](-1)^2 + [CO_3^{-2}](-2)^2 + [RNH_3^+CO_3^-](1)^2 \\
&\qquad + [RNH_2CO_2^-](-1)^2 + [RNH(CO_2^-)\ ](-2)^2]
\end{aligned}
$$

for the pH range being used. The valence of 1 for the $RNH_3^+CO_2^-$ species was discussed by Neuberger (1937). The concentration of the bicarbonate buffer was 0.1 M in these experiments while the total concentration of the fluoro-amino acids was 0.006 M, hence an approximation may be made:

$$I = 1/2[[Na^+](1)^2 + [HCO_3^-](-1)^2 + [CO_3^{-2}](-2)^2]$$

One immediately notices, however, that as the pH increases, the ionic strength increases, therefore the equilibrium constants theoretically require correction at every pH.

Figures III-6 and III-7 show that the analyses are most affected by the pH (pD) regions in the centre of the graphs. In particular, the K_z^d's are measured from the "inflection points" of the curves shown in Figure III-6, hence the ionic strength of the "inflection point" is the ionic strength of the constant; the curve does not give the absolute K_z^d but rather $K_z^d(I)$. Rather than trying to estimate the activity coefficients of the Fphe and Ftyr amino acids to convert the constant to its "ionic-strength-independent" value, it was thought more accurate to convert the absolute constants from

the literature to their $K_z(I)$ values.

To determine the ionic strengths of the Fphe and Ftyr $K_z{}^d(I)$'s, the concentrations of Na^+, $HCO_3{}^-$ and $CO_3{}^{-2}$ were calculated by:

$$K_z{}^d = \frac{[D^+][CO_3{}^{-2}]}{[DCO_3{}^{-1}]}$$

$$[Na^+] = [DCO_3{}^{-1}] + 2[CO_3{}^{-2}]$$

This is not completely accurate, as $K_z{}^d$ should be corrected for the ionic strength determined, hence a computer program was written to iterate to a $K_z{}^d(I)$ and I at which I does not change by more than 0.001 M between iterations. The ionic strength for Fphe (at $pD = pK_z{}^d(I) = 9.64$) was 0.14 M while for Ftyr [at $pD = pK_z{}^d(I) = 10.23$] the ionic strength was 0.21 M. The equilibrium constants used for the analysis, corrected for both D_2O and ionic strength effects are given in Table III-2.

Computer simulations of the concentrations of the Fphe and Ftyr carbamate species as a function of pD used equation(14) and the corrected constants in Table III-2. The best fits, shown in Figure III-7, gave the carbamate equilibrium constant $K_c{}^d(I)$ as $8.52 \pm 0.27 \times 10^{-6}$ ($pK_c{}^d(I) = 5.07 \pm 0.01$) for the Fphe reaction and $8.84 \pm 0.72 \times 10^{-6}$ ($pK_c{}^d(I) = 5.05 \pm 0.04$) for Ftyr.

Table III-2 shows that whereas the effect of D_2O as a solvent usually decreases the constants, the moderate ionic

strength of the Fphe and Ftyr derivations tends to increase them again. Hence, the $pK_c^d(I)$ values above may be compared to the values obtained for amino acids, peptides and proteins in the literature (Table III-3). As was observed by Roughton (1970) there is not much variation in pK_c between the types of amino groups being measured (protein, peptide or amino acid), even with the differences in experimental conditions and techniques. The presence of fluorines in Fphe and Ftyr, as well, does not move the carbamate constants out of the range seen in Table III-3 (the degree and direction of the effects of the fluorine would require the carbamate constants of phe and tyr to be determined).

It is apparent from these experiments that ^{19}F NMR may be used to monitor the carbamate formation of fluoro-amino acids. ^{19}F is a nucleus whose chemical shift is particularly sensitive to long range effects on its magnetic environment. This allows the ring fluorines in Fphe and Ftyr to report on the presence or absence of the carboxyl bound to the amino group. The data obtained allows the calculation of the equilibrium constant of carbamate formation. As the origins of the upfield fluoro-amino acid resonances were found to be due to the interaction of their free amino groups with CO_2, this type of interaction is not a concern for the Fphe and Ftyr amino acids when incorporated into a protein (as they are not N-terminal amino acids)[26].

---

[26] The possibility does exist however that if there are lysines or N-terminal amino groups in the vicinities of the fluoro-amino acids, anomalies may occur. This possibility was tested for the coat protein in micelles by running

Table III-3. Literature values of amino group carbamate formation constants.

Carbamate adduct		Source	[carbonate] (mM)	Temperature (°K)	Method	pKc
glycine		Roughton (1970)	<10	291	pCO_2 electrode Barium ppt. "total" equilibrium	4.90
glycine (0.5M)	in H_2O	Morrow *et al.* (1974)	50	303	^{13}C NMR	4.71±0.06
	in D_2O					5.3±0.1
glycylglycine		Roughton (1970)	<10	293	pCO_2 electrode Barium ppt. "total" equilibrium	4.85
sperm whale Myoglobin (N-terminal Val)		Morrow *et al.*(1974)	45	303	^{13}C NMR	5.1±0.1
Human H (deoxy)	Val-1-α	Gurd *et al.* (1980)	35-57	303	^{13}C NMR	4.64
	Val-1-β					4.89
Human H (CO)	Val-1-α	Gurd *et al.* (1980)	35-57	303	^{13}C NMR	5.8
	Val-1-β					5.5

B. Solvent Isotope Induced Chemical Shifts

Introduction

The chemical shifts of fluoro-compounds are very sensitive to their environment (see Chapter I-B). For example, the chemical shifts of Fphe and Ftyr are separated by ~23 ppm (Figure III-1). Given that the only difference between the structures of Fphe and Ftyr is the Ftyr hydroxyl group (see Figure I-2), there is a large intramolecular effect of the hydroxyl group on the fluorine chemical shift. Fluorine nuclei are also sensitive to intermolecular interactions. Studies with organic solvents and fluorine-containing solutes have shown that the fluorine chemical shift of the solute is dependent on the solvent in which it is dissolved. A great deal of work has been done to try to understand the mechanisms of these solvent induced shifts (SIS's) (for review, see Emsley and Phillips, 1971). Smaller, though significant, effects of solvents on fluorine chemical shifts are seen when isotopically-substituted solvents are used (solvent isotope induced shifts (SIIS's)). In particular, the effect of replacing water with deuterium oxide (D_2O) on the chemical shifts of fluoro-compounds has been studied (Hull and Sykes, 1976; Muller, 1977b; Lauterbur *et al.*, 1978).

---

[26] (cont'd) spectra using sodium borate buffer (see Figure IV-16). There was no change in the Fphe and Ftyr spectra observed compared to those obtained in the bicarbonate buffers.

With the preparation of fluoro-amino acids and their subsequent incorporation into proteins, a biological application of fluorine SIIS studies appeared. In order for a SIIS to occur, the solvent and the fluorine of the solute must interact. When the fluorine is on a protein residue, the residue must have access to the solvent; a buried residue in the hydrophobic core of the protein would have a smaller SIIS than a residue on the surface of the protein. Thus, the commparison of the SIIS's of a fully exposed residue to that of a buried residue provides a measure of the accessibility of the water (deuterium oxide) to the "buried" residue. Experiments have been done with a number of water-soluble proteins (Hull and Sykes, 1976; Lauterbur *et al.*, 1978; Gerig *et al.*, 1979). Quantitation of the fluoro-residue exposure to the solvent was achieved through comparing the protein SIIS to the SIIS of the free fluoro-amino acid as the "100% exposed" residue.

A natural extension of those studies is to determine the exposure of amino acid residues in membrane proteins. The goals would be to not only determine which residues are inaccessible to water due to protein structure and/or being protected by either detergent or lipid, but as well to gain information as to the accessibility of water into the hydrophobic domain of the detergent micelle or lipid bilayer to water. Ftyr-labelled M13 coat protein in DOC micelles has been used for such studies (Hagen *et al.*, 1978). Those experiments have been redone including Fphe-labelled protein

(see Chapter IV-B). The analyses of the SIIS's of Fphe and Ftyr amino acids as the controls for "100% exposed" protein residues, are presented herein.

Theory

Much work has been done to determine the mechanisms of the behaviors of fluorine chemical shifts (Buckingham *et al.*,1960; Evans, 1960; Emsley and Phillips, 1966; Muller, 1976, 1977(a,b)). The results have succeeded in delineating the types of interactions involved between solvent and fluoro-solute molecules that cause SIS's (and SIIS's) (see following text). The studies have also shown that the complexity of the interactions make their complete understanding impossible at this time; theory requires further development before it can be used to successfully predict the behavior of the chemical shift of a fluoro-compound in an untested solvent.

There are five types of interactions possible between the solvent and a fluoro-solute. The shielding of the fluorine nucleus due to the solvent medium, is given by:

$$\sigma_m = \sigma_b + \sigma_a + \sigma_w + \sigma_e + \sigma_c$$

(Emsley and Phillips, 1971), where σ_b is the shielding contribution from the bulk diamagnetic susceptibility of the solvent, σ_a is the shielding effect of anisotropic solvent molecules, σ_w is the van der Waals interaction contribution, σ_e is an electric field (reaction field) effect between

solute and solvent molecules having dipole moments and σ_c is the shielding effect due to the formation of complexes or hydrogen bonds. These terms are each considered below.

The first term, σ_b, results from chemical shifts not being absolute; chemical shifts of molecules are always given relative to a reference compound (for example, the fluorine chemical shifts in this thesis are relative to trifluoro-acetic acid (TFA) (see Chapter II-F). σ_b is equal to zero when the reference compound is either included in the sample or referenced through the use of the same spectrometer lock compound for the reference compound and the sample of interest. For the experiments outlined in this Chapter, the lock for both the TFA and amino acid samples was D_2O, hence $\sigma_b = 0$.

The second term, σ_a, is relevant for solvents having anisotropic diamagnetic susceptibilities, meaning that the susceptibility of the solvent molecule will vary depending upon its orientation in the magnetic field. This applies to disc-shaped molecules (for example, aromatic solvents like benzene) and rod-shaped molecules (like carbon disulphide). Water is in neither of those categories and so σ_a will be negligible for the experiments to be described.

The contribution of van der Waals solute-solvent interactions, σ_w, result from three kinds of forces: dipole orientation (Keesom) forces, induction (Debye) forces and dispersion (London) forces. In most intermolecular interactions, London forces are dominant. These depend on the

polarizability of the two molecules; the electron clouds of the approaching molecules shift so as to create an attraction for each other. Studies with fluorocompounds and varying solvents have shown that σ_w is the dominant shielding term for ^{19}F medium effects (Evans, 1960; Emsley and Phillips ,1971; Muller, 1977). Evans (1960) found that for a range of compounds, the chemical shifts were furthest upfield (most shielded) in solvents (of similar size) having the highest polarizability. The further upfield a chemical shift is, the larger the σ_m term. As only σ_w is dependent upon polarizability, van der Waals interactions are implicated as having a dominant contribution to shielding effects.

σ_e, the electric field effect created when a dipolar or quadrapolar solute is studied, has been found to have a small contribution to the overall σ_m (Emsley and Phillips, 1966). Recently Muller (1976) has questioned even the validity of including a σ_e term in the σ_m expression and suggests that a more complex theory for analyzing van der Waal interaction (σ_w) is probably more relevant than having a separate σ_e term.

The contribution to the solute chemical shift due to complex formation (for example, through charge transfer or H-bonding) is included in the σ_c term. Like σ_e, σ_c is difficult to quantitate as it is necessary to eliminate (at least) the van der Waals' term, σ_w. Historically, σ_c was taken to be a form of correction factor (Emsley and

Phillips, 1971); if the theory for the other shielding terms could not account for the chemical shift observed, then the residual shift was assigned to σ_c. More recently, the formation of complexes between organic acceptor and donor molecules (such as hexafluorobenzene and acetone, respectively) has been shown to contribute significantly to the observed ^{19}F chemical shift of the solute (Muller, 1977a). Studies of complex formation with water as a solvent are limited. In one particular example, Muller (1977b), using a fluoroalkane, 6,6,6-trifluoro-1-hexanol as the solute, assumed that σ_c was negligible in solutions of water and organic cosolvents. (This solute was previously found to be inert, even when in donor-acceptor solvent systems (Muller, 1977a).) As fluorobenzene derivatives are electron acceptors and water may act as a donor, it is not clear whether water-Fphe complexation is present. Hydrogen bonding between the Ftyr hydroxyl and water, though, seems to contribute to its chemical shift dependence on the isotope of water (see Discussion).

Results

The fluorine chemical shifts throughout this thesis are given relative to the trifluoro-acetic acid (TFA) resonance at 298°K of a sample containing TFA, potassium phosphate (dibasic), EDTA and potassium chloride in D_2O (pH 7.0) (see NMR Methods, Chapter II-F). The TFA was not included in the amino acid samples but was referenced through the mutual use

of D_2O as the lock compound; the spectrometer was frequency-locked onto D_2O for both the TFA and the fluoro-amino acid samples. The offset determined to place the TFA resonance at 0 ppm was used as the offset for the amino acid samples, thus the amino acid chemical shifts are relative to TFA. A problem with this method of referencing arises though when the compound being studied is not in 100% D_2O but contains, for example, only 50% D_2O (and 50% H_2O); the lock signal is no longer D_2O but rather HDO. The effect on the frequency of the lock signal has been determined indirectly by monitoring the effect of deuterating H_2O to HDO on the proton NMR spectrum of the water (Holmes *et al.*, 1962).

Holmes et al. (1962) found that the resonances from H_2O and HDO may be resolved from each other in the proton spectrum when dilute solutions of water were prepared in acetone. This experiment was repeated using acetone-d_6, the water spectrum being shown in Figure III-8. The downfield peak at 2.977 ppm is due to H_2O while the broader upfield resonance at 2.946 ppm is from HDO (both shifts relative to internal TMS). The HDO peak is actually a triplet; the proton resonance is split by the deuterium (spin=1). The individual peaks of the triplet are not resolved, however, as the D_2O was not ultrapure, hence impurities and/or pH≠7 have broadened the resonances. The difference in shift between the two peaks $(\delta_{dho}-\delta_{h_2o})$ in Figure III-8 is -0.033 ppm. A different sample was run obtaining a difference of -0.026 ppm, therefore the average shift is

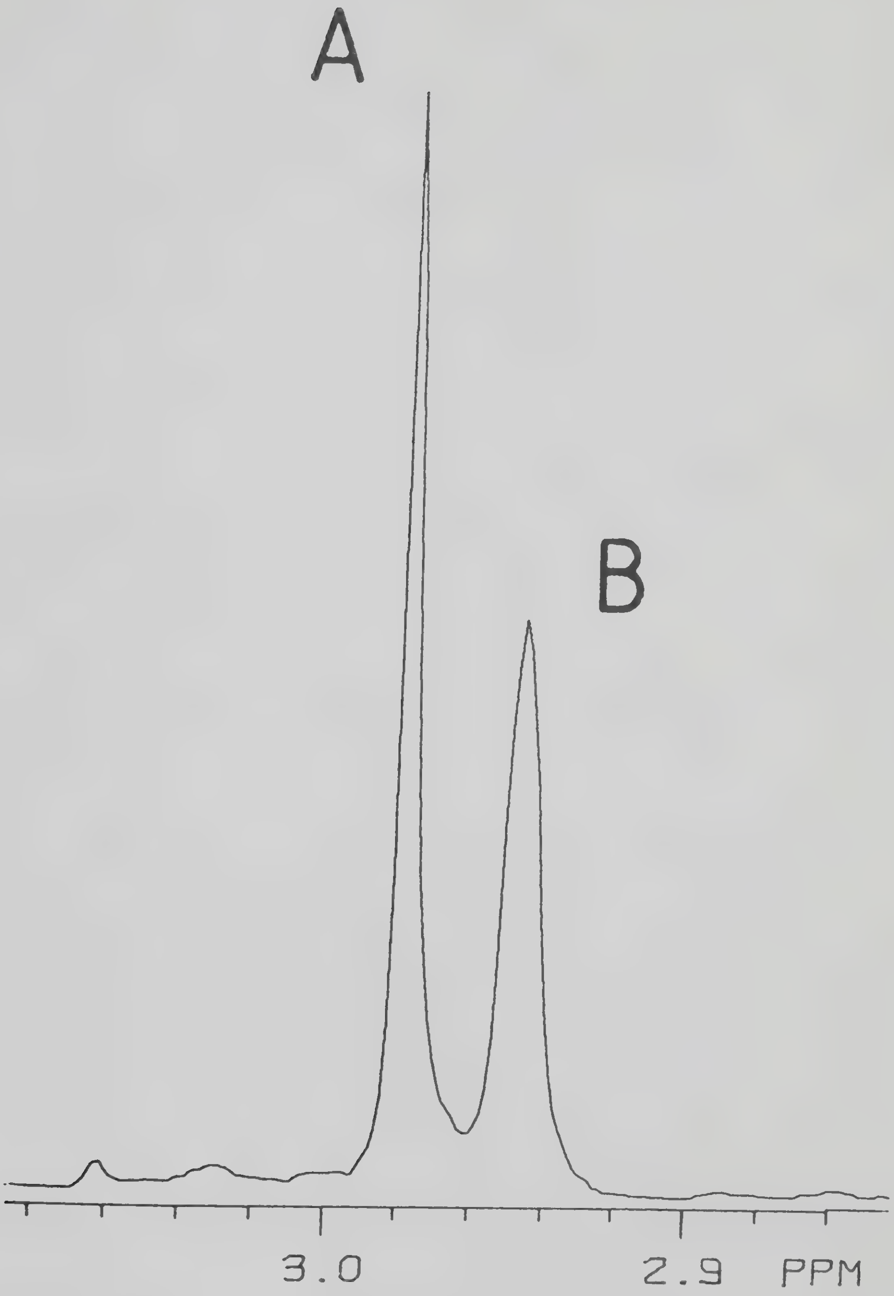

Figure III-8 The proton NMR of H_2O and HDO in acetone-d_6. The sample contained 4 µl each of H_2O and 99.98 % D_2O and less than 1 µl of TMS in 0.5 ml acetone-d_6. Resonance A is from H_2O while resonance B is from HDO. The spectrum is the result of 4 scans, acquired at 299°K using 2 µsec (18°) pulse, ±800 Hz sweepwidth, 8K data and no delay between transients. 0.2 Hz line-broadening was used.

-0.030±0.005 ppm. This is in good agreement with Holmes *et al.* (1962), who obtained a shift of -0.030±0.003 ppm.

Knowing that the H_2O signal shifts upfield by 0.030 ppm when it is deuterated, its proton chemical shift was monitored throughout a range of 12.5 to 100% D_2O in a sample containing water and/or deuterium oxide, DOC, and bicarbonate buffer (pH 9.0) (Figure III-9). In this case, the H_2O and HDO are in fast exchange, hence one would expect to see only a single resonance whose chemical shift (~100% D_2O) would be 0.030 ppm upfield of that of the H_2O. Figure III-9, though, shows that the water signal does not shift significantly; the H_2O signal (in 12.5% D_2O [Figure III-9(i)]) is at 4.745 ppm relative to DSS while the HDO signal (~100% D_2O [Figure III-9(v)]) is at 4.749 ppm. (This chemical shift difference is within the error of the measurements). These samples were obtained using the deuterium signals from the DHO and/or D_2O for the frequency lock so that not being able to detect the 0.030 ppm shift of the H_2O to HDO substitution means that the same shift was occurring for the deuterium signal as DHO was replaced with D_2O. Thus, the change in chemical shift of a fluoro-compound as a function of % D_2O is the result of the SIIS effects on both the fluoro-compound and the lock compound (D_2O). (SIIS is herein defined as the difference between the chemical shift of a compound in 100% D_2O minus the chemical shift of the compound in 100% H_2O (0% D_2O), ($= \delta_{d_2o} - \delta_{h_2o}$).)

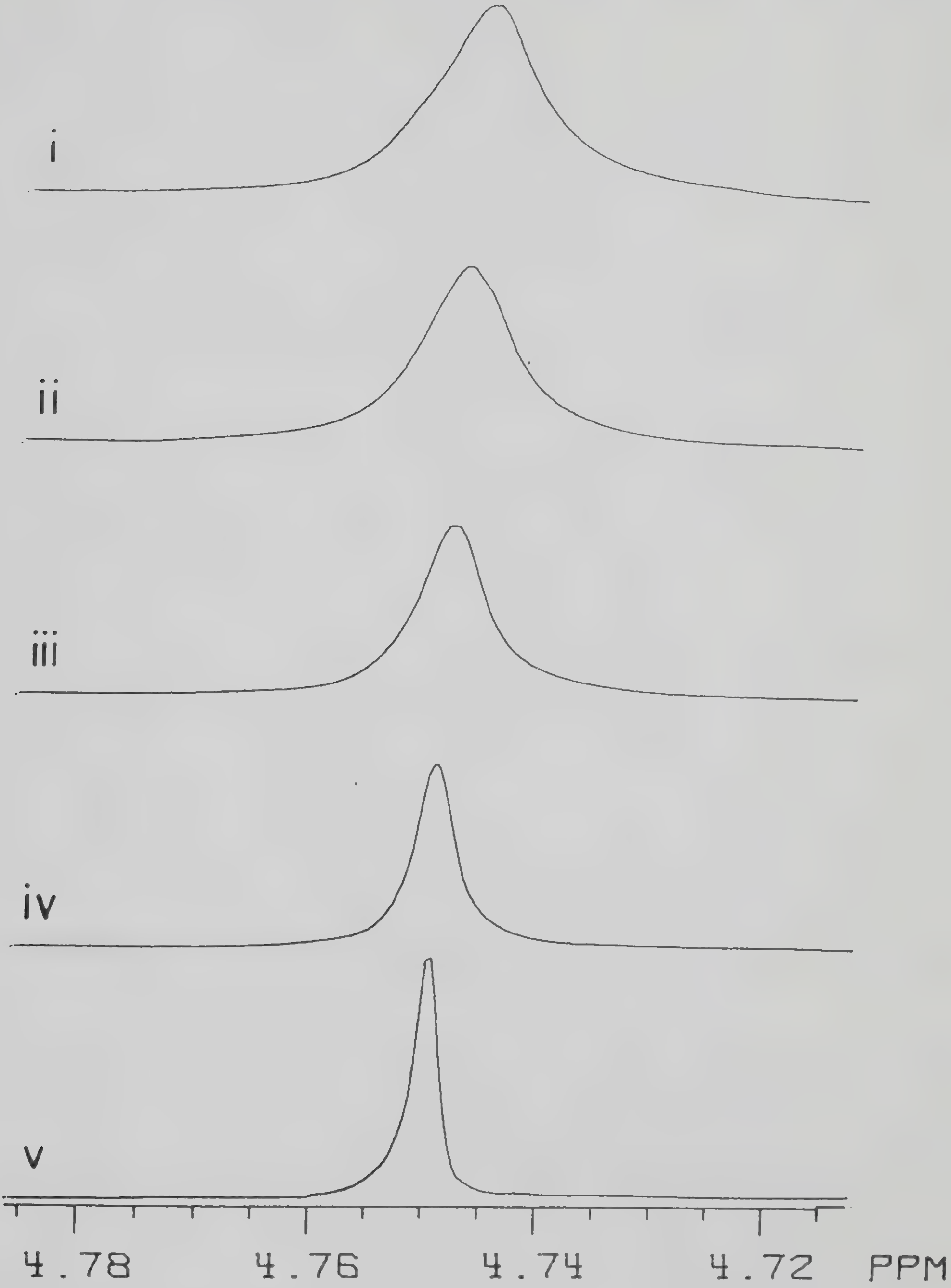

Figure III-9 The ^1H NMR spectra at 300°K of mixtures of H_2O and 99.9% D_2O. The solutions contained 0.1M $NaHCO_3$ (pH 9), 8 mM DOC and varying % D_2O content: i) 12.5; ii) 25; iii) 50; iv) 75; v) 100%. The spectra resulted from 16 scans using a 1 μsec (9°) pulsewidth, a ±250 Hz sweepwidth, 8K data points and no delay between transients. The linebroadening was 0.2 Hz.

The ^{19}F resonances at 298°K of Fphe and Ftyr in samples containing DOC, ammonium bicarbonate buffer (pH 9.0), and varying % D_2O are shown in Figure III-10: spectra A are from Fphe; spectra B are from Ftyr. As the % D_2O is increased, the fluorine chemical shifts of both amino acids move upfield (i-v). The total SIIS [=SIIS(amino acid) + SIIS(lock)] of replacing H_2O with D_2O are obtained from the graphs of the fluorine chemical shifts as functions of % D_2O, shown in Figure III-11. The true SIIS effects of each of the amino acids are those obtained from Figure III-11 minus the SIIS of the HDO (-0.030 ppm) and are given in Table III-4. Although the chemical shifts of both Fphe and Ftyr move upfield with increasing % D_2O, the SIIS of the Ftyr resonance is significantly larger than that of the Fphe. [The resonances upfield of the major resonances in Figure III-10(i) at ~-38.8 and ~-62.0 ppm are from the carbamate species of each of Fphe and Ftyr (see Chapter III-A)].

Figure III-11 shows the chemical shift behaviours of Fphe and Ftyr with changing D_2O, when DOC is either included or excluded from the sample. Figure III-11(A) shows that the chemical shift of Fphe moves downfield when DOC is added while Ftyr (graph B) does not change. The chemical shift of Fphe in $NaHCO_3$ buffer (i) (0% D_2O) is -38.02 ppm, in $NaHCO_3$ buffer and 8 mM DOC (ii) (0% D_2O), it is -37.98 ppm[27] while

---

[27] The data were collected at 302°K rather than ~298°K. As well, the samples were allowed only 15 minutes to equilibrate (see Chapter II-F), thus the chemical shifts actually have more error than shown. That the points fit the line as

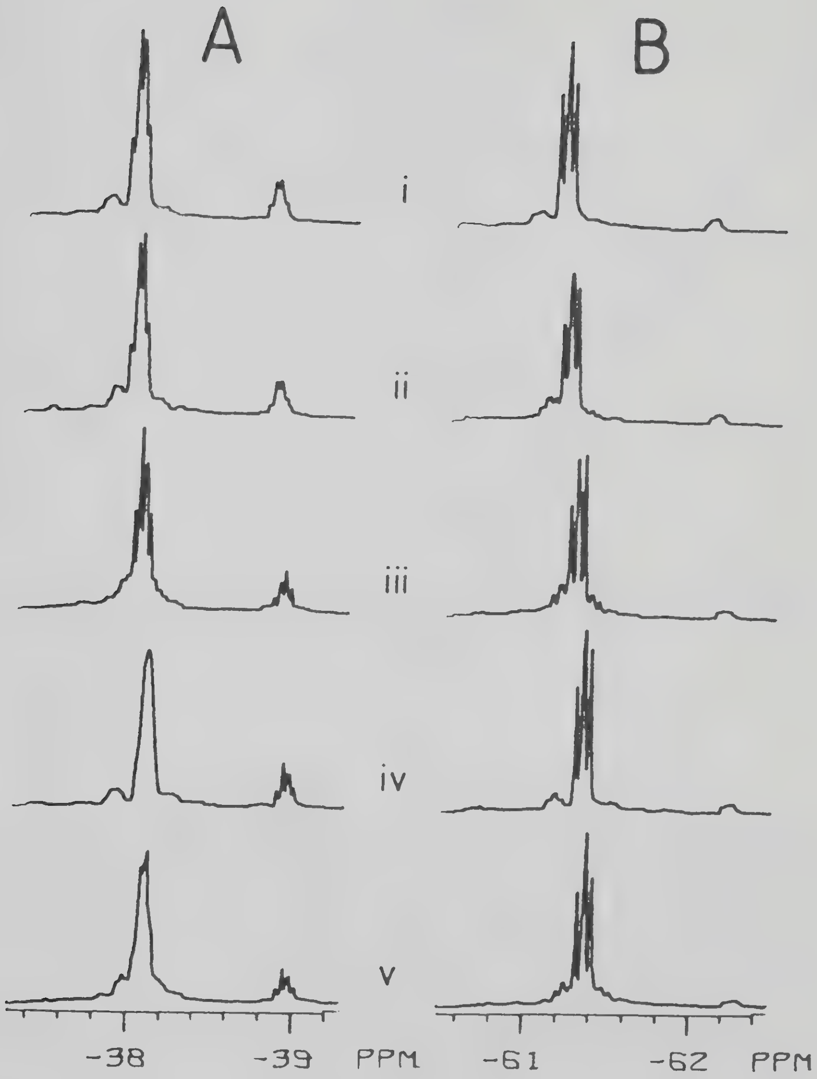

Figure III-10 The ^{19}F NMR spectra of Fphe and Ftyr as functions of % D_2O. The solutions contained ~4mM of each amino acid, 0.1M NH_4HCO_3 (pH9) and 8mM DOC. Spectra A are from Fphe, while spectra B from Ftyr. The D_2O content was: i)20 ii)40 iii)66 iv)86 v)99%. The spectra were acquired at 297°K with a 15 μsec (75°) pulsewidth, ±5000 Hz sweepwidth and 8K data. 500 scans were collected with a 1 sec delay between transients. 1 Hz linebroadening was used.

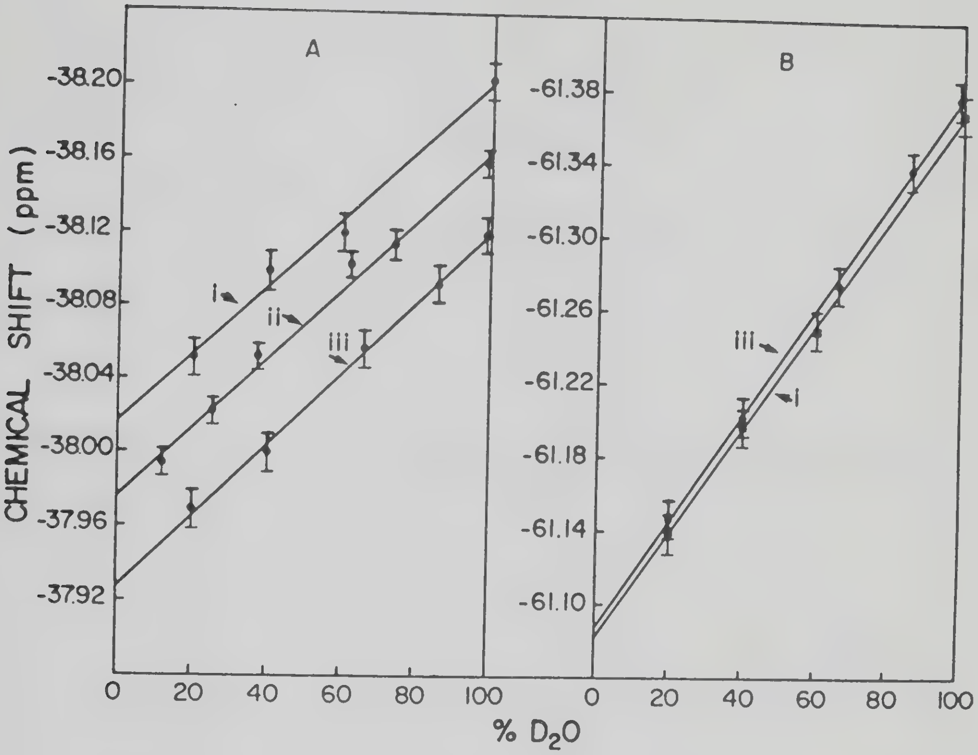

Figure III-11 The graphs of the ^{19}F NMR chemical shifts of Fphe and Ftyr as functions of % D_2O, with and without DOC. The solutions without DOC at 299°K (i) contained 0.1M NaHCO3 (pH9), and 3mM concentrations of each amino acid, while the solutions with DOC contained either 0.1M NaHCO3 (pH9), 8mM DOC, and 5mM Fphe (at 302°K) (ii) or 0.1M NH_4HCO_3 (pH9), 8mM DOC, and 4mM concentrations of the amino acids at (297°K) (iii). The lines in A are from the Fphe data, while those in B are from the Ftyr. The ^{19}F NMR spectra from which the data of lines (i) and (iii) were obtained were run as outlined in Figure III-10. The Fphe spectral data of line (ii) used 4K data, ±1000 Hz sweepwidth, and a pulsewidth of 8 μsec (72°). 100 scans were collected per spectrum and 1 Hz linebroadening was used. The lines were drawn using the fit obtained by a linear regression calculator program, from which the 0% and 100% D_2O concentration chemical shifts were determined.

Table III-4

The SIIS values of Fphe, 4-Fphe, and Ftyr as functions of pH

		Fphe[1]		Ftyr[1]	
pH	[DOC](mM)	Free	N-/C-Blocked	Free	N-/C-Blocked
7	0	(-0.12)[2]	-0.17	-0.21	-0.24
9	0	-0.16	-0.17	-0.26	-0.27
9	8	-0.16[3]	-	-0.26[3]	-
9	8	-0.16	-	-	-
11	0	(-0.21)	-	-0.31	-

[1] the error in the SIIS values is ±0.01 ppm.
[2] the data in brackets are the SIIS's of 4-fluoro-phenylalanine.
[3] all samples contained 0.1M $NaHCO_3$ except for these which had 0.1M NH_4HCO_3.

in NH_4HCO_3 buffer and 8 mM DOC (iii) (0% D_2O), the Fphe chemical shift is -37.93 ppm. The Ftyr resonance, without DOC, is at -61.08 ppm while with DOC, is at -61.09 ppm (both at 0% D_2O). These shifts are the same within the error of the data (±0.01ppm). The DOC (and whether the buffer is $NaHCO_3$ or NH_4HCO_3) has negligible effects on the SIIS's of the amino acids (see Table III-4).

Figure III-12 shows the effects of pH on the chemical shifts (and SIIS's) of 4-fluoro-phenylalanine (4-Fphe) and Ftyr in $NaHCO_3$ solutions. (The pH dependence of the chemical shift annd SIIS of Fphe, which has the fluorine at the 3 position of the ring, was not measured.) Graph A shows that increasing the pH causes a dramatic upfield shift of the 4-Fphe fluorine resonance: from -40.05 ppm at pH 7 (0% D_2O) to -41.60 ppm at pH 11 (0% D_2O). The same trend is seen for Ftyr (graph B), though not so large. The Ftyr resonance shifts from -60.92 ppm at pH 7 to -61.08 ppm at pH 9 to -61.60 ppm at pH 11 (all with 0% D_2O). As well, the SIIS's of 4-Fphe and Ftyr increase with pH, the values of which are given in Table III-4.

The N- and C-termini of the Fphe and Ftyr amino acids were then chemically blocked: the N-termini were acetylated; methyl esters were made of the C-termini (see Chapter II-B). The ^{19}F NMR spectra at 299°K of N- and C-blocked Fphe and Ftyr in sodium bicarbonate buffer (pH 9), are shown in

---

[27](cont'd) well as they do suggests that the drifts of the resonances are the same in the 15 min given them, hence the slope (and the SIIS) should be representative.

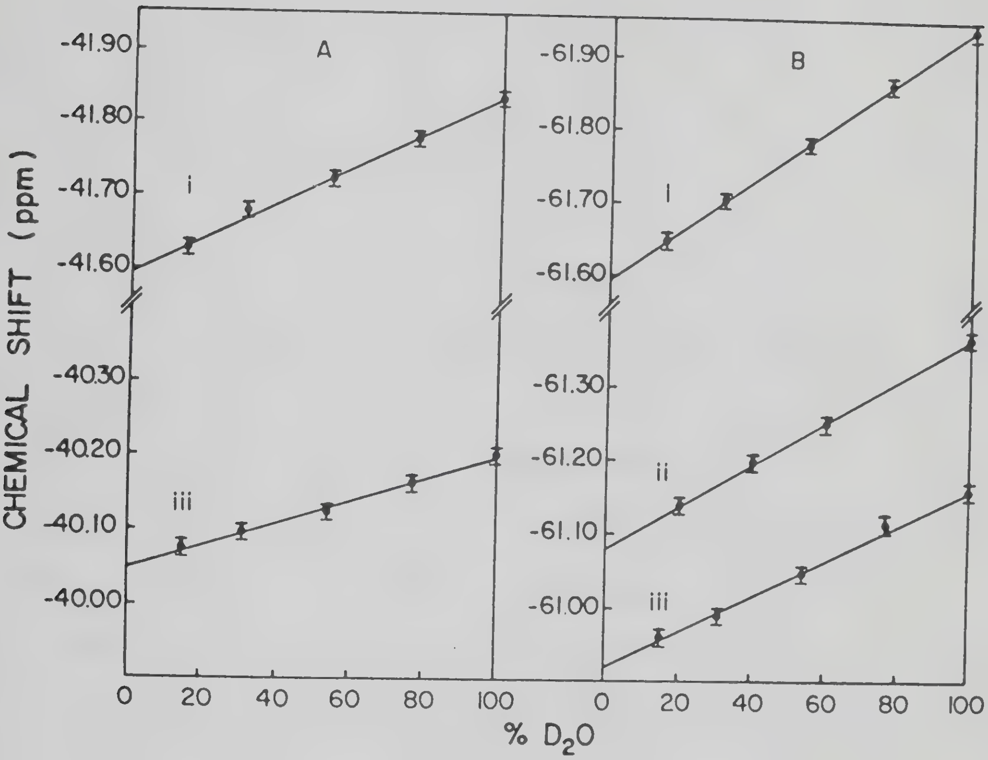

Figure III-12 The graphs of the ^{19}F NMR chemical shifts of 4-Fphe and Ftyr as functions of % D_2O and pH. The samples contained 4-Fphe and Ftyr (3mM) and $NaHCO_3$ (0.1 M). The lines in A are from 4-Fphe, while those in B are from Ftyr. The pH of the samples were: i) 11 ii) 9 iii) 7. The chemical shift data were taken from spectra obtained as outlined in Figure III-10 and were analyzed using a linear regression program.

Figure III-13(A) and (B), respectively. Both the Fphe and Ftyr analogs shift upfield during the replacement of H_2O with D_2O, the Ftyr analog shifting the most. The fluorine chemical shifts as a functions of % D_2O are plotted in Figure III-14(A) and (B) and the SIIS's of the N- and C-blocked fluoro-amino acids at pH 9 are given in Table III-4.

Table III-4 contains not only the SIIS's of the fluoro-amino acids (with and without DOC) and their analogs (without DOC) at pH 9, but, as well, shows the data obtained at pH 7 and 11. The SIIS's of both Ftyr and its analog are seen to increase as the pH increases. The pH dependence of the SIIS of 4-Fphe was also found to increase. Only the SIIS of the blocked Fphe was not pH dependent. (The pH was not taken above pH 9 for the N- and C-blocked fluoro-amino acids as the methyl ester is removed at alkaline pH. Proton NMR spectra of a sample containing blocked Fphe were collected at pH 9.0 to monitor the appearance of methanol due to saponification of the methyl esters; less than 10% of the ester was lost in the time taken for the acquisition of the ^{19}F NMR SIIS spectra.)

Discussion

The results given have been obtained either using $NaHCO_3$ or NH_4HCO_3 buffer, including DOC or not including DOC and at temperatures between 297°K to 302°K. The effect of increasing the temperature of a Fphe sample was to shift its

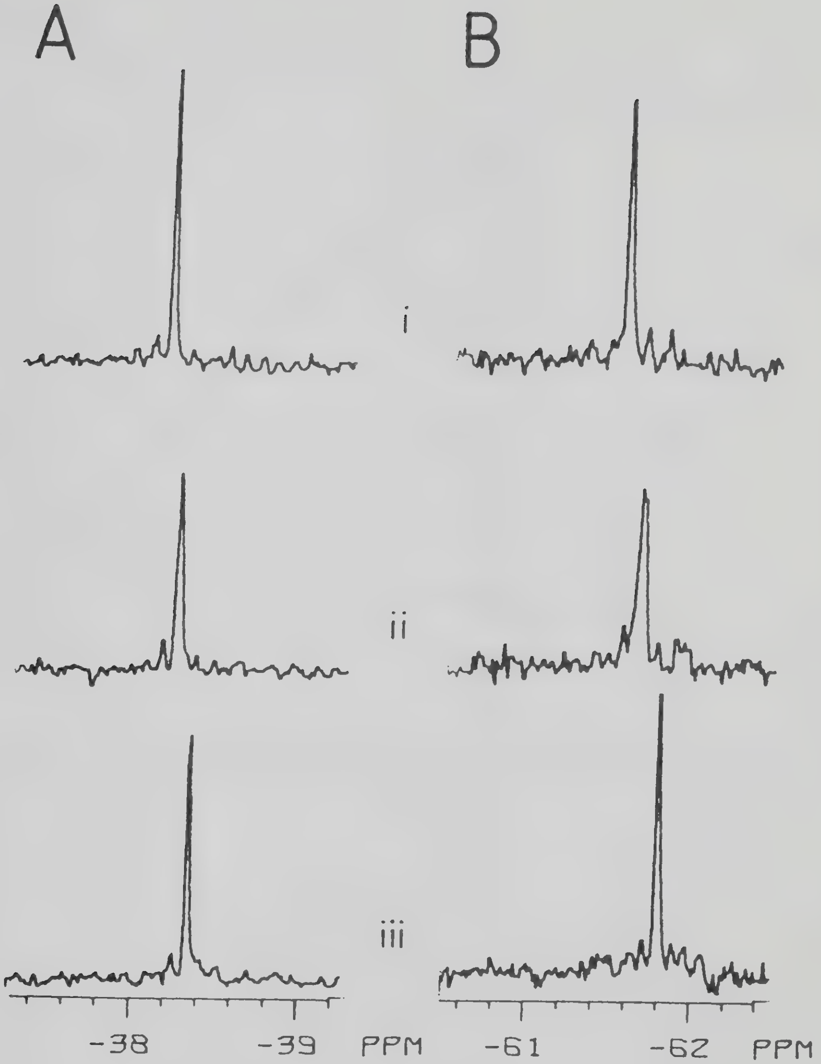

Figure III-13 The ^{19}F NMR spectra of N- and C-blocked Fphe and Ftyr as functions of % D_2O. The samples consisted of both blocked amino acids (3 mM each) and 0.1 M $NaHCO_3$ (pH9). Spectra A are Fphe-analog resonances, while spectra B are from the Ftyr-analog. The D_2O content was: i) 15% ii) 54 iii) 100. The spectra were aquired at 299°K with a pulsewidth of 18 μsec (90°), a sweepwidth of ±5000 Hz, 8K data, and decoupling of the aromatic protons. 600 scans were collected with 500 msec delays between scans. 2 Hz linebroadening was used.

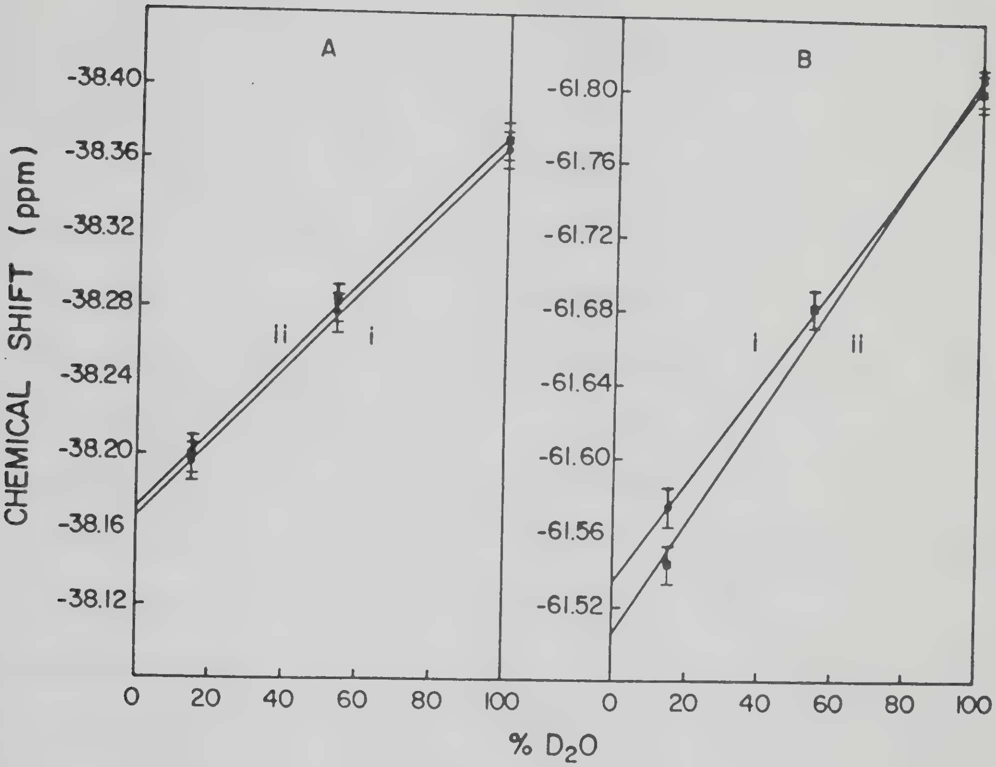

Figure III-14 The graphs of the ^{19}F NMR chemical shifts of N- and C-blocked Fphe and Ftyr as functions of % D_2O and pH. The samples contain both amino acid analogs (3 mM each) and 0.1M $NaHCO_3$. Graph A is the blocked Fphe data, while graph B contains the blocked Ftyr data. The pH values of the experiments were: i) 7 ii) 9. The chemical shift data were taken from spectra obtained as outlined in Figure III-13 and were analyzed using a linear regression program.

resonance downfield (data not shown). The $NaHCO_3$/DOC sample resonances at 302°K [Figure III-11(ii)] were upfield of the resonances of the NH_4HCO_3/DOC sample at 297°K. Thus, the differences in their chemical shifts could not be due to their difference in temperature but, rather, due to some effect of the sodium or ammonium ions; the exact size of the effect is not certain, as outlined in the Results. The SIIS was not affected by the choice of buffer (Table III-4).

The effect of DOC on the Fphe chemical shift was to move it downfield (Figure III-11), suggesting that there was interaction between the DOC and the Fphe. Whatever the nature of the interaction, it did not inhibit the interaction of the fluorine with the solvent; the SIIS was not changed within the experimental error, thus the Fphe was not bound by the DOC micelles. [Prof. Poul Hansen, Roskilde, Denmark, working in this lab, had found that even uncharged solutes such as ρ-fluoro-nitrobenzene, were not bound by DOC, hence it was unlikely that even the N- and C-blocked Fphe was bound (results to be published)]. Those results showed that although one must be careful in comparing the chemical shifts of Fphe in solutions containing the different compounds given above, it was reasonable to compare their SIIS's.

The Ftyr resonances appeared to be indifferent to whether the buffer was $NaHCO_3$ or NH_4HCO_3 or whether DOC was present or not. Figure III-11(B) showed that there was little change in the chemical shifts of the Ftyr in a sample

at 297°K containing NH_4HCO_3 and DOC to that at 299°K containing only $NaHCO_3$. The slight downfield shift may have been due to the difference in temperature between the two; the changes, however, were within the errors of the measurements. As well, the SIIS's were essentially the same (Table III-4), so the Ftyr SIIS's may also be compared to each other, regardless of whether the buffer was $NaHCO_3$ or NH_4HCO_3, the DOC was present or not, or whether the temperature was 297 or 299°K.

Table III-4 summarized the data from the fluoro-amino acids and their N- and C-blocked analogs. Regardless of the pH or whether or not their N- and C-groups are blocked, the SIIS of Ftyr was always greater than that of Fphe. Greater Ftyr SIIS meant that there was greater interaction between the Ftyr ring fluorine and the solvent molecules. As the dominant contributor to fluorine chemical shift SIS effects was from van der Waal's forces (see the σ_w term in the Theory) and since van der Waal's forces have an r^{-6}-distance dependence between the fluorine and the ^1H or ^2H of the solvent, (Hull and Sykes, 1976) then that the Ftyr SIIS was larger than the Fphe SIIS suggests that the solvent molecules were, on the average, closer to the Ftyr fluorine than the fluorine of the Fphe. The explanation for this resides in the Ftyr hydroxyl group. Below its pK_a (~8.62[28], the

---

[28] The hydroxyl and amino group dissociation constants are given in Chapter III-A for D_2O and the ionic strength of the 0.1M NH_4HCO_3 buffer at the pK_a. The constants given here are calculated for H_2O using the relationship given by Marshall (1978) (Chapter III-A).

hydroxyl-oxygen would be bonded to either a proton or a deuteron. Rotation about the carbon-oxygen bond would place the proton (deuteron) close to the fluorine, hence the possiblity of van der Waal's interactions would be greater than in the Fphe case where there is no particular reason for the water to be close to the fluorine nucleus other than for the electronegativity of the fluorine. (As well, hydrogen bonding to the oxygen of the Ftyr hydroxyl would contribute, hence a σ_c term contribution.) Above the pK_a of the hydroxyl, the oxygen would no longer be binding a proton or deuteron but its negative charge would be effective at drawing water molecules into the vicinity of the fluorine (again, through hydrogen bonding).

Table III-4 also showed that the SIIS's of Fphe, Ftyr and the N- and C-blocked Ftyr all increase with increasing pH; the N- and C-blocked Fphe SIIS did not. The pH dependences of the SIIS values of the unblocked amino acids were the result of the titration of their amino groups (and for Ftyr, its ring-hydroxyl). In Chapter III-A, the dissociation constant in D_2O, for the Fphe amino group was found to be 2.29×10^{-10} ($pK_z{}^d=9.64$), while for Ftyr, the amino dissociation constant was 5.89×10^{-11} ($pK_z{}^d=10.23$) and the ring hydroxyl, 6.17×10^{-10} ($pK_{OH}{}^d=9.21$), in 0.1 M bicarbonate buffer, ~100% D_2O. These pK_a's are all in the pH region of the SIIS measurements. As well, that the SIIS of N- and C-blocked Fphe was not dependent upon pH while the SIIS of N- and C-blocked Ftyr was, reinforces the suggestion

that the effects of pH on the SIIS's of the fluoro-amino acids containing titratable groups were due to the titration of those groups; blocked Fphe did not contain any titratable groups while blocked Ftyr still had its ring hydroxyl to be deprotonated.

The molecular details by which the titrations cause the SIIS's of the fluoro-amino acids to increase is not totally clear. The increase in SIIS with pH suggests that as the pH increases, the solvent molecules draw closer, on average, to the fluorine. This is easily justified in the case of the deprotonation of the hydroxyl group; the water would form hydrogen bonds with the negative charge on deprotonated hydroxyl group. This, in turn, would localize the water in the vicinity of the neighbouring fluorine. (This was the same reasoning used to explain the Ftyr SIIS being consistently larger than the SIIS of the Fphe.) The reason for the increase of the fluoro-amino acids as their amino termini are deprotonated is more subtle. The chemical shifts of the ring fluorines of both Fphe and Ftyr are sensitive to the protonation state of their amino groups. It was seen in Chapter III-A that the fluorine resonance of Fphe shifts upfield ~1 ppm while the Ftyr resonance shifts upfield ~0.8 ppm, as the amino groups were deprotonated. The mechanism by which the chemical shifts are affected, also seems to affect the extent to which the ring fluorines interact with the solvent; the SIIS's of both Fphe and Ftyr increase as the pH is increased above their amino pK_a's. An

explanation of the Fphe and Ftyr sensitivities to the amino groups is not clear: it may simply be an electrostatic interaction between the positive charge of the amino group and the ring electrons thus affecting the electronegativities of the fluorines on the far sides of the rings; or it may be a complex effect due to the electric field produced by the amino group dipole and its average orientation to the ring. The explanation of the results requires additional studies to be done.

IV. Studies of Fphe and Ftyr Labelled M13 Coat Protein in DOC Micelles

A. Assignments of the Resonances of the ^{19}F NMR Spectrum

Introduction

It was shown in Chapter I-B that ^{19}F NMR of fluoro-amino acid residues in proteins can give useful information about the environment of the fluorine labelled amino acid. The analyses of the ^{19}F spectrum of a fluoro- amino acid residue in the presence of substrates or with changes in temperature, pH, or solvent can give useful information as to the role of the particular residue in maintaining the protein's structure and/or function. The full appreciation of the information obtained from the spectra though, requires that the fluoro-resonances be assigned to particular fluoro-residues in the protein. Thus the first step in the analysis of any protein spectrum is to obtain assignments of the resonances.

The methods of assignments are certainly as varied as there are proteins. A common requirement to all, of course, is that the amino acid sequence of the protein be known. If the x-ray structure is known, correlation of the behavior of the protein's ^{19}F NMR spectrum with, for example, binding substrate or changing pH might allow the assignment of the resonance from the fluoro-residue at the binding site or on the surface of the protein. Barring such methods of

assignment, it is necessary to induce specific changes in the spectrum. To this end, site-specific proteases and/or chemical cleavage may be used to remove one or more fluoro-residues from the protein. Monitoring the reactions using ^{19}F NMR correlates the processes with changes in the resonances of the spectrum, thus aiding their assignments. Similarly, chemical labelling experiments may be used to specifically modify a certain residue thereby inducing a corresponding change in the NMR spectrum. An alternative approach to assignments was done by P. Lu and coworkers, making use of the available molecular genetic techniques (Jarema *et al.*, 1981). They have introduced a series of point (nonsense) mutations at the tyrosine codons in the *lacI*gene (lac repressor protein) of *E. coli*. Using suppressor positive *E. coli* strains and including Ftyr in the growth medium, they obtained a series of Ftyr-labelled repressor proteins lacking Ftyr at the mutant sites. The ^{19}F NMR spectra of those proteins were correspondingly missing one or the other of the Ftyr resonances, hence their assignments were obtained.

Experiments to study the structure of Fphe- and Ftyr-labelled M13 coat protein when bound by sodium deoxycholate (DOC) micelles are outlined in this Chapter. The structure of DOC, in the acid form, is shown in Figure IV-1. This bile acid forms micelles at a critical micellar concentration (CMC) of ~1 mM when in a 0.1 M ionic strength aqueous solution (Small, 1971). At concentrations close to

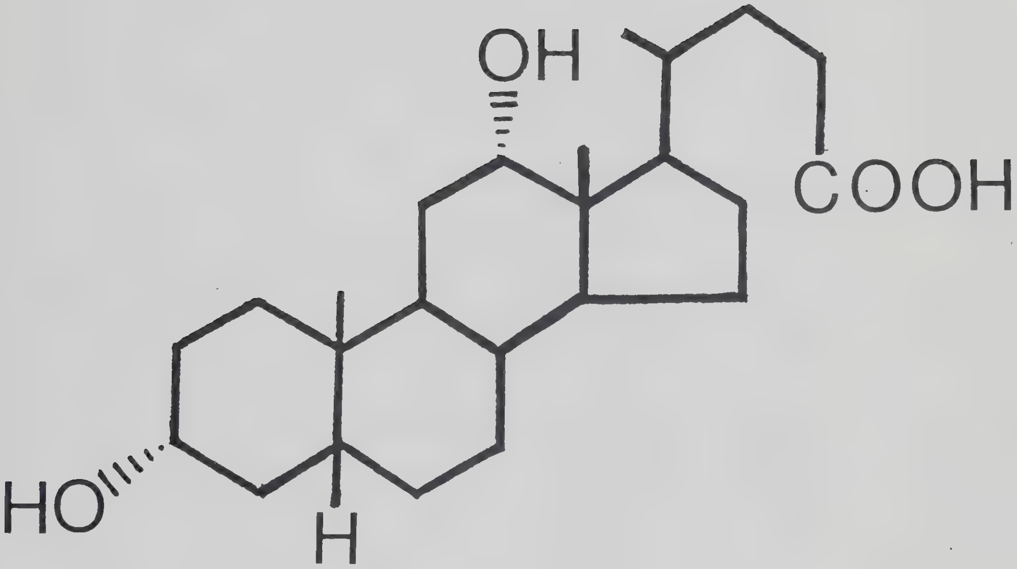

Figure IV-1 The chemical structure of deoxycholic acid.

its CMC (for example 8 mM), there are 16 deoxycholate molecules per micelle; Webster and co-workers found that the DOC micelles containing coat protein also consist of 16 (±2) DOC molecules per micelle at an ionic strength of ~0.1 M; there are two coat proteins per micelle [Makino *et al*. (1975)]. If the DOC binds the coat protein dimer as cholate solubilizes lecithin (Small, 1971), the DOC molecules would be arranged in a double-layered ring about the hydrophobic region of the protein with 8 DOC molecules per ring.

The ^{19}F NMR spectrum of Fphe- and Ftyr-containing M13 coat protein in DOC micelles is shown in Figure IV-2. The fluoro-resonances of this spectrum result from three Fphe and two Ftyr residues in the protein (Figure IV-3). The comparison of this spectrum to that of the Fphe and Ftyr amino acids (see Figure III-1), immediately assigns the asymmetrical resonance at -37.76 ppm to the Fphe residue(s) and the doublet at -61.03 ppm to the Ftyr residues. The further assignment of individual resonances to particular protein residues has been done by temperature and proteolysis experiments. The results are presented herein.

Results

Figure IV-4 shows the ^{19}F NMR spectra of DOC-bound Fphe- and Ftyr-labelled coat protein as a function of temperature. The pH of the sample was adjusted at room temperature so that at least part of the chemical shift change with temperature is due to the change in pH. Figure IV-4(A) shows

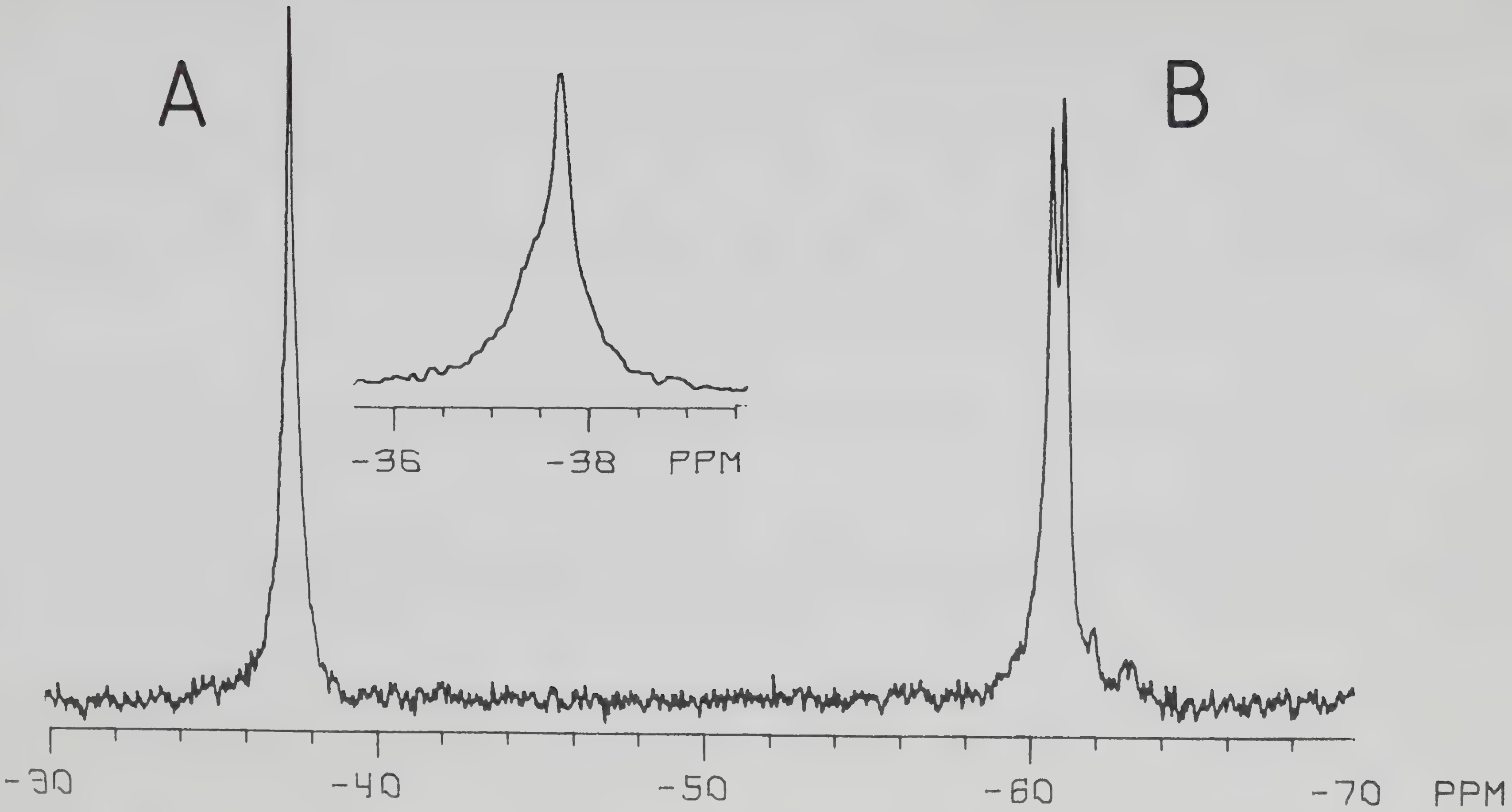

Figure IV-2 The ^{19}F NMR spectrum at 297°K of Fphe and Ftyr labelled M13 coat protein in DOC micelles. The sample was prepared starting with 20 mg's of each of the labelled phage and using 0.1M NH_4HCO_3(pH9.0), 8mM DOC as the sample buffer (the final D_2O content was ~68 %.). The resonance(s) of A are from Fphe labelled coat protein, while those of B are from Ftyr labelled coat protein. The spectrum has 10 Hz linebroadening and results from 5,000 scans using a pulsewidth of 16 usec (80°), a sweepwidth of ±6300 Hz and 4K data. There was a delay of 200 msec between transients.

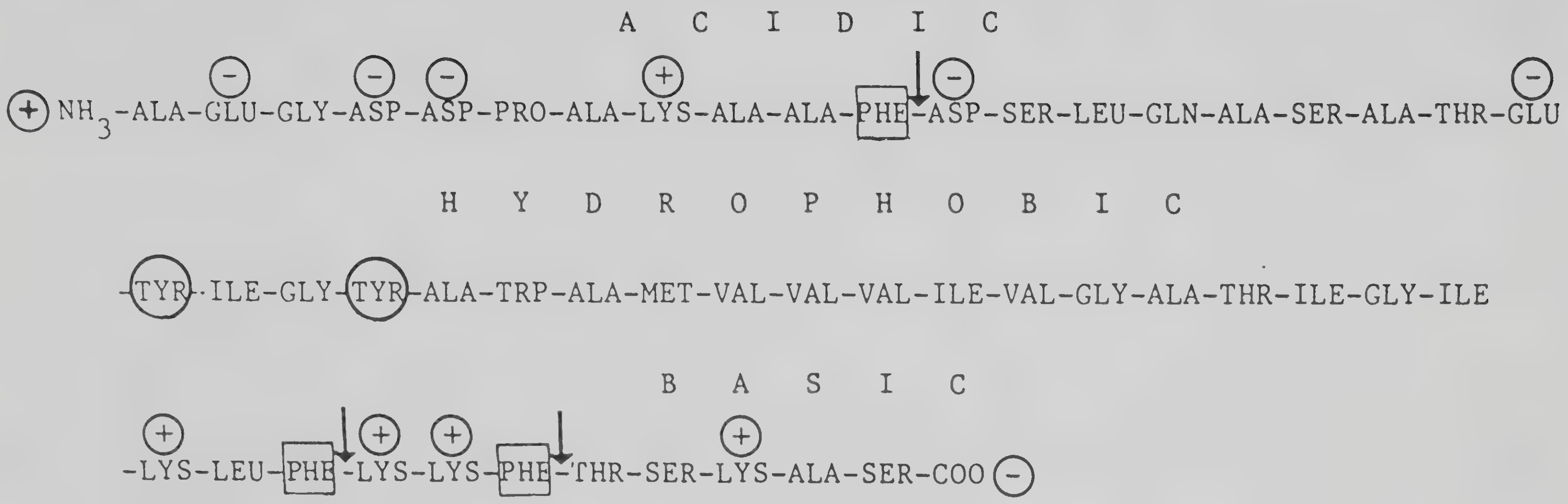

A C I D I C
+ NH3-ALA-GLU-GLY-ASP-ASP-PRO-ALA-LYS-ALA-ALA-PHE-ASP-SER-LEU-GLN-ALA-SER-ALA-THR-GLU
H Y D R O P H O B I C
-TYR-ILE-GLY-TYR-ALA-TRP-ALA-MET-VAL-VAL-VAL-ILE-VAL-GLY-ALA-THR-ILE-GLY-ILE
B A S I C
-LYS-LEU-PHE-LYS-LYS-PHE-THR-SER-LYS-ALA-SER-COO −
−
+

Figure IV-3 The amino acid sequence of the coat protein of the bacteriophage M13. Fphe and Ftyr have been biosynthetically incorporated into the protein at the boxes and circles, respectively. The arrows indicate the chymotryptic cleavage sites of DOC micelle-bound coat protein.

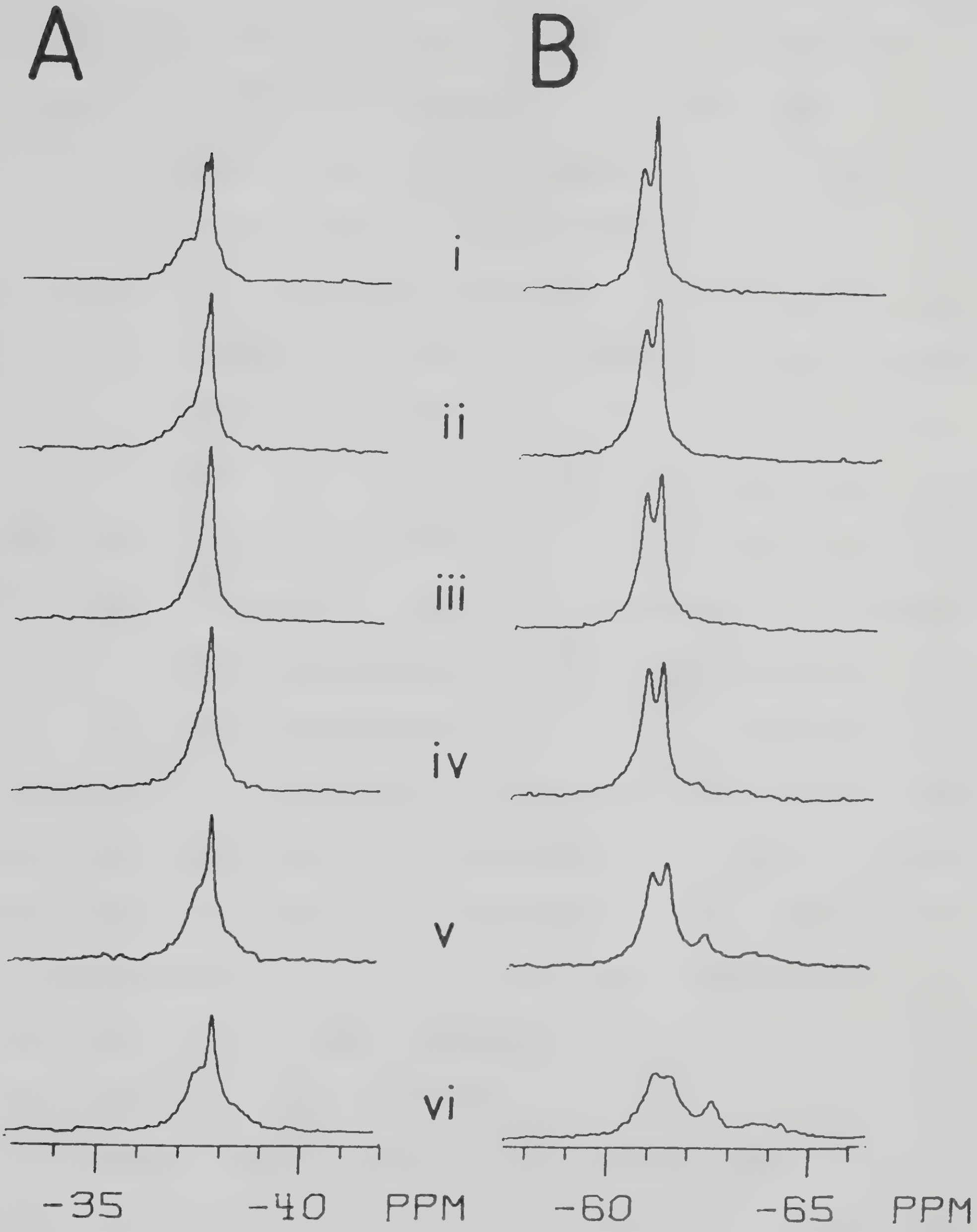

Figure IV-4 The ^{19}F NMR spectrum of Fphe- and Ftyr-labelled M13 coat proteins in DOC micelles with varying temperature. The sample and acquisition parameters were the same as given in the legend of Figure IV-2. The resonances in A are from Fphe labelled protein while those in B are the Ftyr resonances. The spectra were collected at: i) 327°K; ii) 317; iii) 307; iv) 297; v) 287; vi) 277.

the Fphe spectra. At 277°K (Figure IV-4[A(vi)]), the resonance appeared to contain at least three overlapping resonances: a broad one (~154 Hz) centered at -37.59 ppm and a narrower one (~58 Hz) at -38.01 ppm and a very broad one (~216 Hz) at -38.54 ppm. The relative areas, determined by computer simulation of the spectrum, were approximately 44:34:21. As the temperature was increased, the peak shape changed until at 327°K (Figure IV-4[A(i)]), there were three resonances resolved: a broad resonance (~163 Hz) at -36.92 ppm and two narrower peaks (35 and 33 Hz) at -37.37 and -37.53 ppm. Computer simulation showed that their relative areas were approximately 44:26:30. There were two major Ftyr protein resonances at all temperatures (Figure IV-4[B(i-vi)]). The downfield resonance at 327°K (at -60.41 ppm) was 76 Hz wide while the upfield resonance (at -60.75 ppm) was 51 Hz. At lower temperatures, two additional resonances appeared. At 277°K, the two resonances at -61.17 ppm and -61.63 ppm broadened to 142 and 134 Hz, respectively. The two new resonances, which appeared at -62.63 and -63.92 ppm, were 100 and 383 Hz wide, respectively. The relative area of the four resonances, determined by computer simulation, were approximately 35:38:14:23, in order from the downfield resonance at -61.17 ppm to the upfield resonance at -63.92 ppm.

The assignments of the Fphe resonances were obtained by monitoring the chymotryptic digestion of DOC micelle-bound fluoro-labelled coat protein. Chymotrypsin specifically

cleaves at phe, tyr and trp (and, more slowly, leucine). The ^{19}F NMR spectra of the digestion are shown in Figure IV-5. The digestion of Fphe is shown in the spectra in (A). Figure IV-5[A(i)] was collected before the addition of chymotrypsin. Figure IV-5[A(ii-vi)] show the decrease in intensity of the narrower central component of the composite Fphe protein peak after the addition of the enzyme, and the concommitant appearance of a narrow peak upfield at -38.84 ppm. The time-course of the digestion is shown more clearly in Figure IV-6. The curve shows that the release of Fphe from the protein is biphasic; the intensity of the narrow resonance rises quickly for the first 100 min, then more slowly until the completion of the digestion (~24 hrs later). To determine what fraction of the total Fphe's are released in the initial burst phase, the area of the broad component of the spectrum in Figure IV-5[A(iv)] at 1.29 hr was compared to the total area of the spectrum in Figure IV-5[A(i)]. It was found that 1/3 of the m-Fphe's were initially cleaved. At longer times (Figure IV-5 [A(vi)]), the broad protein resonance slowly disappears to a minimum. The area of the broad component of Figure IV-5 [A(vi)] was 22% of the total area of Figure IV-5[A(i)].

Figure IV-5(B) shows the Ftyr resonances throughout the chymotrypsin digestion. There does not appear to be any release of Ftyr from the micelles as there is no appearance of a narrow peak corresponding to free Ftyr-containing peptides (Figure IV-5[B(i-vi)]). The intensity of the bound

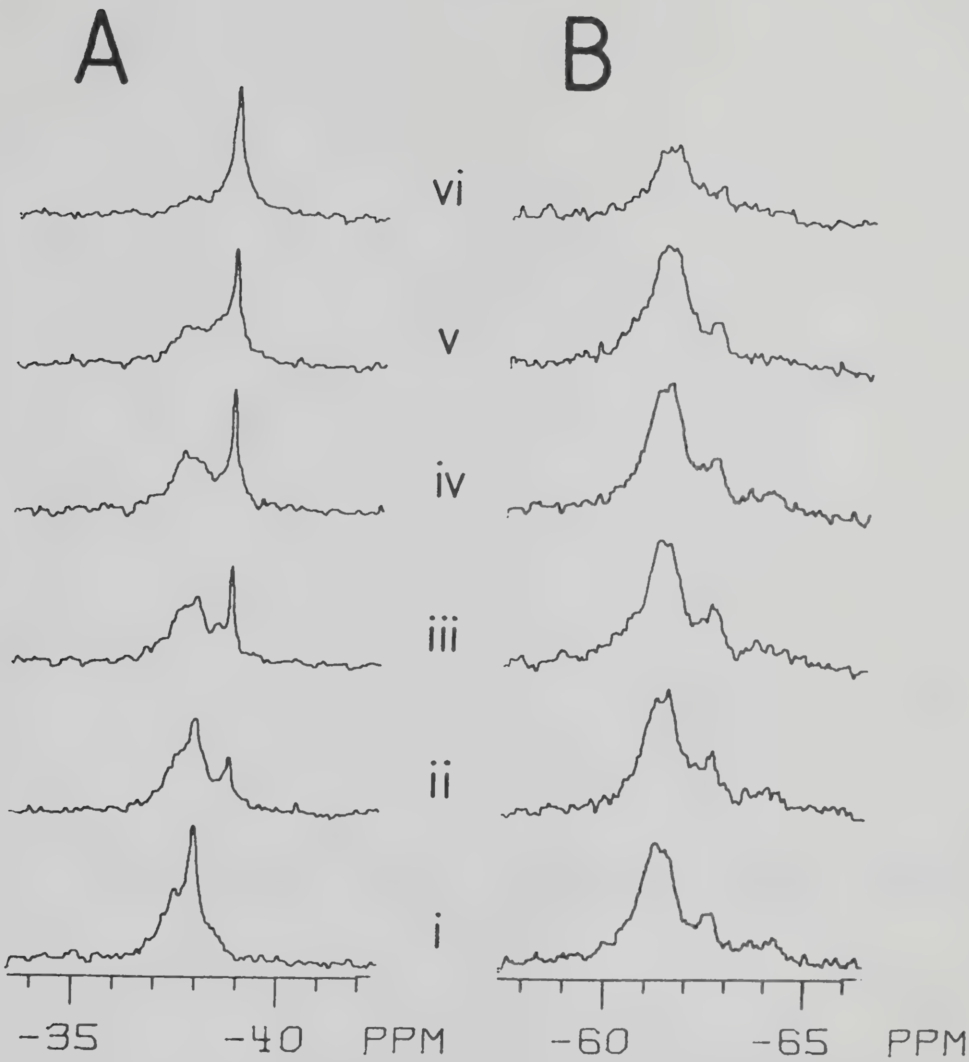

Figure IV-5 The ^{19}F NMR spectra of the chymotryptic digestion at 277°K of Fphe- and Ftyr-labelled M13 coat proteins in DOC micelles. The micelle-bound coat protein sample was prepared using 26.5 mg of each of the Fphe and Ftyr labelled M13 phage (see Chapter II-D) and 0.1M NH_4HCO_3(pH 9.0), 8mM DOC buffer (the final D_2O content was 89 %). The resonances in A are from the Fphe regions of the spectra while those in B are from the Ftyr. The spectra were collected at the following times after the addition of chymotrypsin: i) 0 hr; ii) 0.16; iii) 0.72; iv) 1.29; v) 7.72; vi) 21.14. The spectra each resulted from 2500 scans with 10 Hz linebroadening. They were collected using a 16 µsec (80°) pulsewidth, ±5000 Hz sweepwidth, 4K data and a delay of 200 msec between transients.

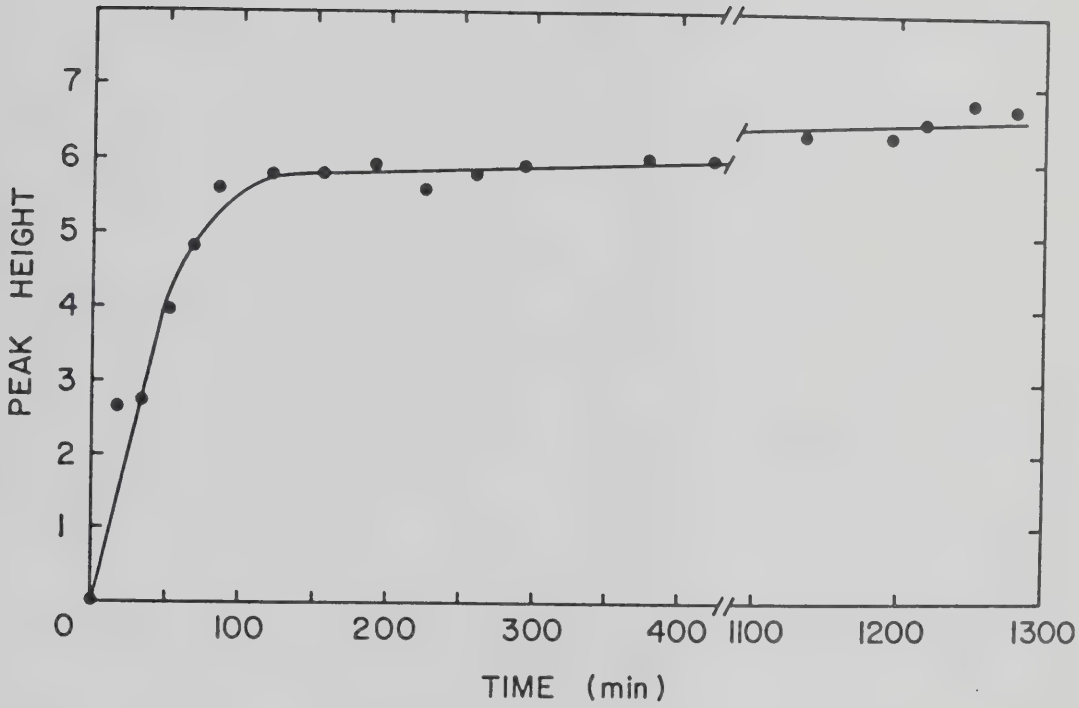

Figure IV-6 The graph of the increase of intensity of the Fphe chymotryptic fragment resonance with digestion time. The data points were obtained from the complete set of chymotryptic digestion spectra,a few of which are shown in Figure IV-5.

Ftyr peak does, however, decrease after a long time (Figure IV-5[B(vi)]). This is due to linewidth and T_1 changes caused by aggregation (see Chapter II-D) after extensive cleavage of the protein at the phe residues.

To correlate the observed chymotryptic digestion pattern with the release of specific fluoro-residues from the protein, the chymotryptic digestion of the coat protein in DOC micelles was monitored using paper electrophoresis. Figure IV-7 shows the appearance of the hydrophilic fragments as a function of digestion time: cleavage at phe 11 results in an acidic fragment, while the cleavage at phe 42 and phe 45 both result in basic fragments (fragment 43-45 being more basic than 46-50 (see Figure IV-7). Lanes i, ii, xvi and xvii contain free amino acids used as references; in particular, lanes ii and xvi contain aspartic acid for an internal standard. Lane iii is an aliquot of sample withdrawn before chymotrypsin was added while lanes iv-xv are of aliquots withdrawn at various times throughout the digestion. Amino acid analysis of the separated fragments from another chymotryptic digestion of the coat protein in micelles resulted in the assignments of fragments given in Table IV-1. Figure IV-7 shows, then, that fragment 1-11 is released first, followed by 46-50. Fragment 43-45 is the most slowly released fragment.

The assignment of the two major resonances of the Ftyr region of the spectrum requires an alternative technique other than chymotrypsin as the Ftyr residues are apparently

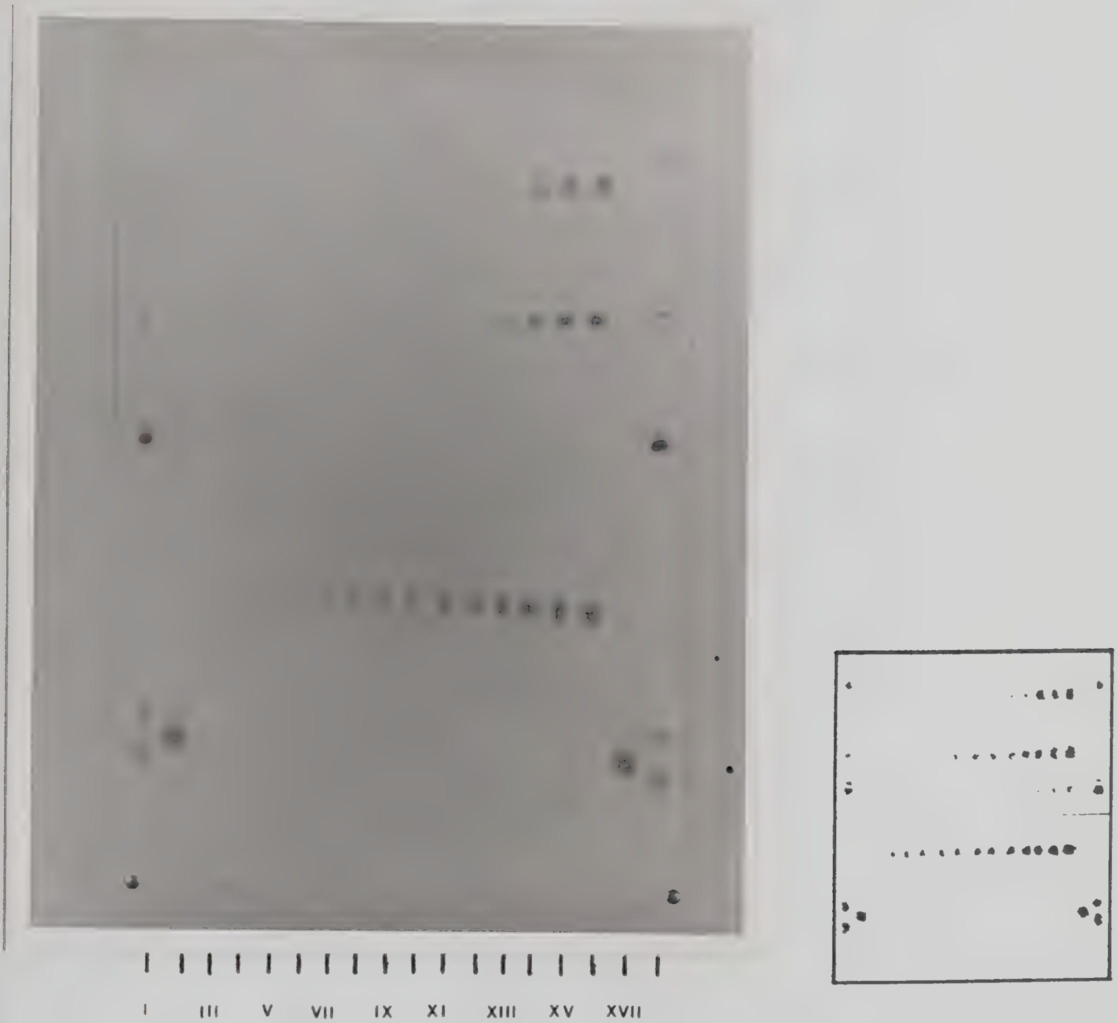

Figure IV-7 The paper electrophoresis of the fragments released from the chymotryptic digestion at 277°K of Fphe- and Ftyr-labelled M13 coat proteins in DOC micelles. Aliquots were withdrawn from the digestion mixture and the digestion stopped at the following times: Lane iii) 0 min; iv) 5; v) 10; vi) 15; vii) 30; viii) 45; ix) 60; x) 90; xi) 120; xii) 180; xiii) 420; xiv) 24 hr; xv) 51; xvi) 72. Lanes i and xviii contained control mixtures of amino acids while lanes ii and xvii contained the aspartic acid standard.

Table IV-1

Paper electrophoresis mobilities at pH6.5 of the chymotryptic fragments of M13 coat protein

Fragment	Rf
1 - 11	0.48
46 - 50	-0.59
43 - 45	-1.07
Asp	1.00

protected from that protease. Hagen *et al.* (1979) had found that the Ftyr residues could be digested when the non-specific protease, pronase, was used. The experiment was repeated, using both Fphe- and Ftyr-labelled M13 coat protein to make the DOC micelle sample; the ^{19}F NMR spectra of the digestion are shown in Figure IV-8. The ^{19}F NMR spectra of the Fphe- and Ftyr-labelled coat proteins, prior to the addition of the pronase, are shown in Figure IV-8, A and B, respectively. A Fphe fragment resonance at -37.91 ppm was detected within the first half hour of digestion (Figure IV-8[A(ii)]); Ftyr fragments at -61.89 ppm were not seen until approximately one hour after the addition of the pronase (Figure IV-8[B(iii)]). The Ftyr protein resonances show that the protein structure in the vicinity of the tyrosines changes before the Ftyr residues become digestible (compare Figure IV-8[B(i)] to B(ii). It appears, from the Ftyr spectra shown in Figure IV-8, B(ii) to B(v), that the Ftyr residue responsible for the downfield resonance is cleaved first. After 48 hours of digestion, only Fphe and Ftyr fragment resonances are seen [Figure IV-8(vii)]. The fragment intensities are much less than those of the initial protein resonances due to their longer T_1's. The resonances from the Fphe and Ftyr residues remaining with the DOC micelle are no longer seen due to the T_1 and linewidth changes that occur upon protein aggregation (as seen for the chymotryptic digestion).

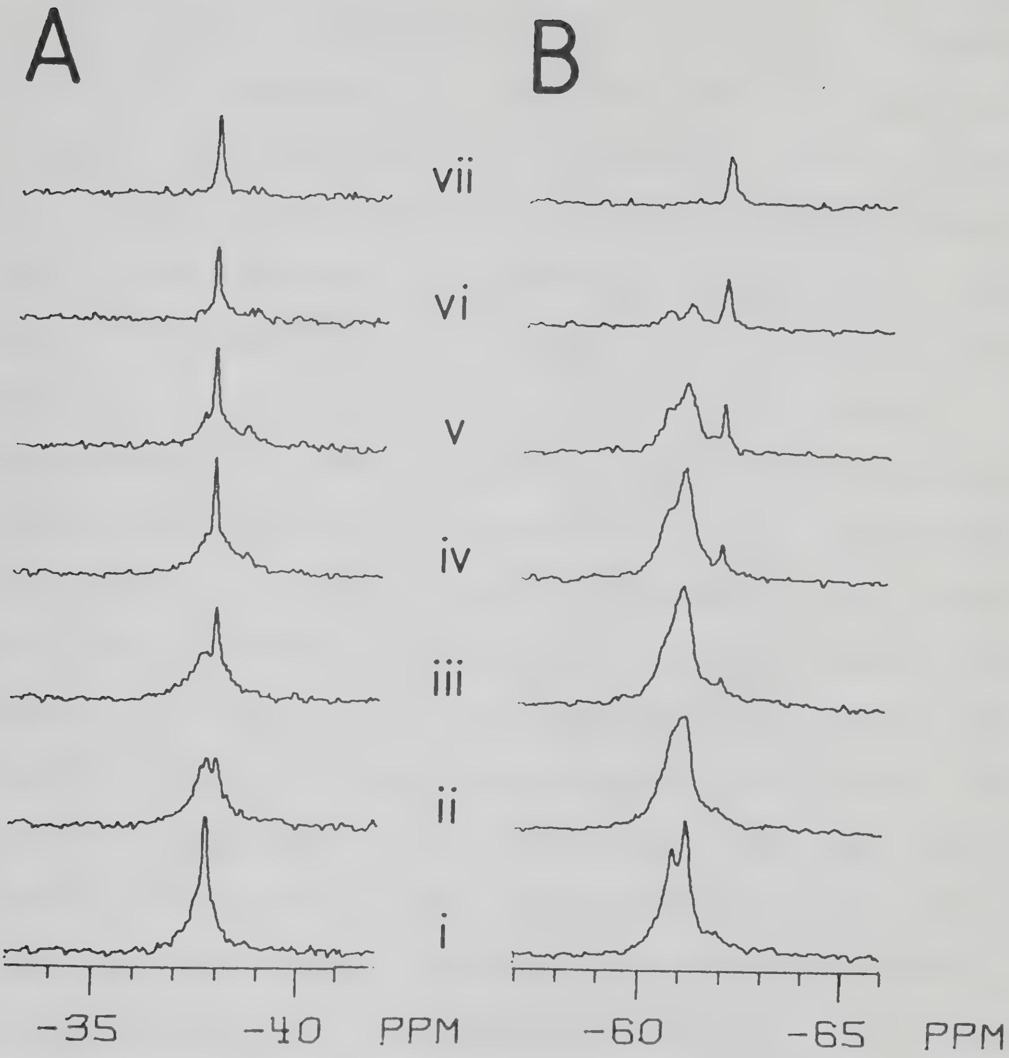

Figure IV-8 The ^{19}F NMR spectra of the pronase digestion at 300°K of Fphe- and Ftyr-labelled M13 coat proteins in DOC micelles. 20 mg of each of the labelled coat proteins was used to prepare the coat protein in DOC micelles sample; the final sample contained 0.1M $NaHCO_3$(pH 9.0), 8mM DOC buffer (~ 85 % D_2O). The resonances in A are from the Fphe region of the spectrum while those in B are from the Ftyr. The spectra were collected at the following times after the addition of the pronase: i) 0 hr;ii) 0.42; iii) 0.98; iv) 2.67; v) 6.60; vi) 21.17; vii) 48.16. The spectral acquisition and line-broadening parameters were as those given in Figure IV-5 except that the pulsewidth was 13 μsec (58°).

Discussion

In this section experiments have been done to assign the fluorine resonances in the spectrum of the Fphe- and Ftyr-labelled coat protein in DOC micelles to particular residues in the protein. From the sequence of the protein one expects that there will be resonances from three Fphe residues (at positions 11, 42 and 45) and from two Ftyr residues (at positions 21 and 24). The spectra of Fphe-/Ftyr-labelled coat protein in DOC micelles contain only three distinguishable resonances at 297°K; the two resonances from the Ftyr residues are resolved, but only a composite Fphe resonance is observed. At 327°K three Fphe resonances are seen, which have approximately equal areas, considering the error in the measurements of the broad resonances. As the temperature is decreased, the three resonances shift and broaden so that at 277°K the broad resonance and the upfield narrow resonance from the 327°K spectrum remain, and a new, broad resonance, upfield of the narrow resonance, appears. Again, the relative areas of these three resonances are approximately equal. Therefore, although the room temperature spectrum might lead one to think that there is only a single Fphe label incorporated into the protein (see Figure IV-4), at other temperatures three resonances are detected. (The significance of the varying linewidths with regards to structure will be discussed in Chapter IV-B.)

Although the Fphe spectrum appears to not have enough resonances at 297°K, the Ftyr region of the spectrum appears to have too many (Figure IV-4). The extra resonances upfield of the doublet appear most clearly in the 277°K and 287°K spectra in Figure IV-4(B)[(v) and (vi), respectively]. Their origin is not completely understood, but a number of experiments have been carried out to characterize their behavior (see Chapter IV-B).

The assignments of the Fphe resonances were obtained by comparing the spectral data of the chymotryptic digestion of the fluoro-labelled coat proteins bound by DOC micelles, in Figures IV-5 and IV-6, to the analyses of the digestion fragments shown in Figure IV-7. The first fragment released, as shown by its appearance on the electrophoresis paper, was 1-11. This was followed by fragment 46-50 and then, most slowly, by 43-45. Comparing this data to the changes in the ^{19}F NMR spectrum with digestion assigns the narrow, quickly disappearing, resonance to Fphe11 and the resonances from Fphe42 and 45 to the broad resonances. The spectrum around the free resonance becomes too complicated to determine whether the broad upfield resonance is from Fphe42 or Fphe45. One might speculate that the broad resonance that narrows at higher temperatures (Figure IV-4(A) is from Fphe45, since it is further than Fphe42 from the DOC-solubilized hydrophobic region of the protein, but this is not proven conclusively by the present data.

A possible assignment of the Ftyr resonances is suggested by the pronase digestion results (see Figure IV-8). Ftyr21 is on the edge of the hydrophobic domain of the protein, while Ftyr24 is three amino acids deeper into the hydrophobic core. The Ftyr residues are not susceptible to chymotryptic cleavage suggesting that both Ftyr's are protected by the DOC. When treated with pronase, however, the residue responsible for the downfield resonance appears to be removed more rapidly than the residue responsible for the upfield resonance. Pronase can only digest residues that are in the aqueous medium so it seems that with the removal of the hydrophilic ends, the Ftyr residues become exposed (compare the Fphe spectra to those of the Ftyr in Figure IV-8). This suggests that the downfield resonance affected first by the digestion is from Ftyr21, leaving the upfield resonance to be from Ftyr24, although, possible structural changes occurring before cleavage make this conclusion tentative. (Additional evidence for these assignments is given in Chapter IV-B.)

B. The Exposure of Fphe and Ftyr Amino Acid Residues of M13 Coat Protein in DOC Micelles

Introduction

To fully understand the mechanism by which a protein performs its function, it is necessary to determine its structure and the conformational changes that occur during

function. Ideally, this is achieved through comparison of the x-ray crystal structure of the protein with dynamic structural studies (such as chemical labelling and/or NMR experiments). An example of a water-soluble protein for which this has been done is bovine pancreatic trypsin inhibitor (BPTI) (for a short review, see Wuthrich and Wagner, 1984; Simon *et al*., 1984). If, however, the x-ray structure of the protein is not known, then one must rely on the interpretation of the dynamic structural studies.

Two types of information that can be obtained from dynamic studies are protein residue exposure and mobility. These may be correlated with the structure of the protein in the vicinity of the residue: if a chemical modification is easily achieved and/or analysis of the NMR spectrum shows the residue to be very mobile, then chances are it is on the surface of the protein; conversely, if it cannot be chemically labelled and/or is found to be immobile, then it is probably buried within the hydrophobic core of the protein.

One must be careful, though, in applying this simple rule of thumb, especially in defining exposure. One method of measuring exposure is to monitor the permeability of water and/or deuterium oxide into a protein through measurement of the rates of exchange of the amide protons of the protein backbone (Simon *et al*., 1984). Most protein amide protons are exchangeable within seconds. This shows that, regardless of where they are within a protein, the amide is exposed to water (whether by local unfolding or through

penetration of the protein (Kossiakoff, 1982)). Thus, amide protons within the core of the protein are exposed. On the other hand, some amide protons do not exchange, even on the timescale of a year (Kossiakoff, 1982). These slow rates were found to be independent of the distance of the proton from the surface of the protein, but rather to be part of β-sheet structures. Therefore, an amide proton that is close to the surface of the protein may appear to be buried. Clearly, other experiments would be necessary to obtain the complete information desired.

The application of structural techniques to the study of membrane proteins is more complex, yet potentially extremely informative. Measurements of exposure and mobility give information not only of protein structure, but as well, of the topology of the protein in the lipid bilayer or detergent micelle: one can determine which protein residues are within the bilayer or micelle (the hydrophobic domain) and which residues are in the region of the protein outside the lipid bilayer or detergent micelle (the hydrophilic domain). The degree of protection of the protein residues of the hydrophobic domain by the lipids or detergent molecules is also of interest. With these goals in mind, experiments to determine the exposure and mobility of the Fphe and Ftyr residues of labelled M13 coat protein in DOC have been done. The results are described herein.

Theory

The experiments used to study the exposure and mobility of the Fphe- and Ftyr-labelled coat proteins in DOC micelles include SIIS, fluorine photo-chemically induced dynamic nuclear polarization (CIDNP), proteolysis with pronase at 277°K, circular dichroism (CD), pH titration and quantitation of internal motion of the Fphe and Ftyr rings by the analysis of fluorine NMR relaxation data. The theory for the SIIS studies was decribed in Chapter III-B and the formulae necessary for the motion analyses are given in Chapter V-B. The two other techniques requiring introductory explanations are fluorine photo-CIDNP and CD. Their definitions are given below.

Chemically induced dynamic nuclear polarization

CIDNP is an NMR technique that requires a laser, a photo-excitable dye [such as flavin mononucleotide (FMN), see Figure IV-11] and an available tyrosine, tryptophan, and/or histidine residue to interact with the dye (see Kaptein *et al.*, 1978). The reactions of interest occur as follows:

$$F \xrightarrow{h\nu} {}^{1}F \rightarrow {}^{3}F$$

$${}^{3}F + TyrOH \rightarrow FH\cdot + TyrO\cdot$$

$$FH\cdot + TyrO\cdot \rightarrow F + TyrOH*$$

where F is the flavin dye, ^{1}F and ^{3}F is the dye in the singlet and triplet energy states, $FH\cdot$ and $TyrO\cdot$ are the radicals of the dye and a tyrosine molecule and TyrOH*

is the polarized tyrosine. The result of the polarization is that the tyrosine proton resonances, in particular from the 3-5 protons, are enhanced and are either positive or negative. The direction of the enhancement, whether an absorption or an emission, can be predicted (Kaptein, 1971) [with certain limitations (Hutton *et al.*, 1983)]. CIDNP of fluorine resonances have also been seen with 3-fluoro-tyrosine (Sykes and Weiner, 1980). The application of this technique to study protein structure is due to the dependence of the enhancement on the direct interaction of the dye with the residue; it provides a method of measuring the exposure of the residue to the medium in which the dye is dissolved.

Circular dichroism

CD is a spectrophotometric technique which measures the ellipticity of circularly polarized light after passing through an optically active molecule (see Friefelder, 1976). The correlation of the circular dichroism (the difference between the extinction coefficients of the left and right components of the polarized light ($\Delta\epsilon$) with α-helical, β-sheet and random structure in proteins is empirical; the CD data of poly-L-lysine in α-helix, β-sheet or random coil conformations (Greenfield and Fasman, 1969) have been used to interpret the CD spectra of proteins. The solution of protein x-ray structures has allowed a more

precise analysis of CD data. Chen *et al.* (1974) have suggested a multiparameter method, the coefficients of which have been determined through correlating known protein structures with their CD spectra. This method has been used to analyse the data in this Chapter.

The data obtained from a CD spectrum is the ellipticity (θ) ($=3300\Delta\epsilon$) as a function of wavelength. [For the CD of protein backbone structure, hence, the CD of peptide amides, the spectrum is run from 200 nm (or less) to 250 nm]. The mean residue ellipticity at a particular wavelength is given by:

$$[\theta] = \frac{m_r \theta}{10\ lc}$$

where m_r is the average residue molecular weight, l is the pathlength in dm, c is the protein concentration in g/ml and θ is the observed ellipticity in degrees. [For the CD experiments described herein, $m = 105$ g/mole, $l = 5 \times 10^{-3}$ dm and $c = 2.90 \times 10^{-4}$ g/ml (see Chapter II-D).] The % α-helix, β-sheet and random coil are then calculated by using the ratios of the multiparameter equations at different wavelengths throughout the sensitive region of the spectrum (α-helix negative maxima are at ~209 and 222 nm while β-sheet structure has a negative maximum at ~216 nm and random structure has a small positive maximum at ~218 nm. The coefficients were those given in the

Handbook of Biochemistry and Molecular Biology[29].

$$\alpha(220/225) = \frac{(\theta_{220}+1800)1276+(\theta_{225}+264)7860}{267595840}$$

$$\beta(220/225) = \frac{(\theta_{220}+1800)-31300(\alpha)}{7870}$$

$$\alpha(215/225) = \frac{(\theta_{215}+669)1276+(\theta_{225}+264)10009}{323547520}$$

$$\beta(215/225) = \frac{(\theta_{215}+669)-26369(\alpha)}{10009}$$

$$\alpha(210/225) = \frac{(\theta_{210}-2200)1276+(\theta_{225}+264)5990}{204373560}$$

$$\beta(210/225) = \frac{(\theta_{210}+2200)-24200(\alpha)}{5990}$$

$$\%\alpha = \frac{[\alpha(220/225) + \alpha(215/225) + \alpha(210/225)]}{3} \times 100$$

$$\%\beta = \frac{[\beta(220/225) + \beta(215/225) + \beta(210/225)]}{3} \times 100$$

$$\%\text{random} = 100 - \%\alpha - \%\beta$$

Results

SIIS studies

The exposure of the Fphe and Ftyr residues of the labelled coat protein in micelles was first probed by solvent isotope induced shift (SIIS) experiments (see Chapter III-B for an explanation of the theory). Figure IV-9 shows the ^{19}F NMR spectra of samples containing Fphe/Ftyr-labelled M13 coat proteins in DOC

---

[29] Handbook of Biochemistry and Molecular Biology: Proteins (Volume 3) 1976, ed. Fasman, G.D. (CRC Press, Cleveland, Ohio) pp138-139.

micelles at 297°K as the H_2O of the solvent is replaced with D_2O. At this temperature, only Fphe11 [the narrow resonance at -37.76 ppm in the 87% D_2O spectrum of Figure IV-9(A(i)] is resolved and can be accurately monitored. The resonances from Ftyr21 and 24 are clearly resolved from each other at -60.87 ppm and -61.16 ppm, respectively, in the 87% D_2O spectrum of Figure IV-9(B) (see Chapter IV-A). The amount of D_2O in the sample affects the chemical shifts of these three resonances differently; the position of the resonance for Ftyr21 has greater dependence upon the D_2O content of the medium than that of Ftyr24, while Fphe11 has an intermediate dependence. The changes in chemical shifts seen in these spectra are illustrated in Figure IV-10. Graph A is a plot of the Fphe11 chemical shifts as a function of % D_2O while the lines in graph B show the behavior of the Ftyr21 and Ftyr24 chemical shifts. The SIIS's of the residues (= $\delta_{d_2o} - \delta_{h_2o} - SIIS_{lock}$, see Chapter III-B) were obtained using the data shown in the graphs and are listed in Table IV-2.

The coat protein Fphe and Ftyr residue SIIS's were then compared to those obtained for the respective free amino acids and N- and C-terminal blocked amino acids (Chapter III-B).

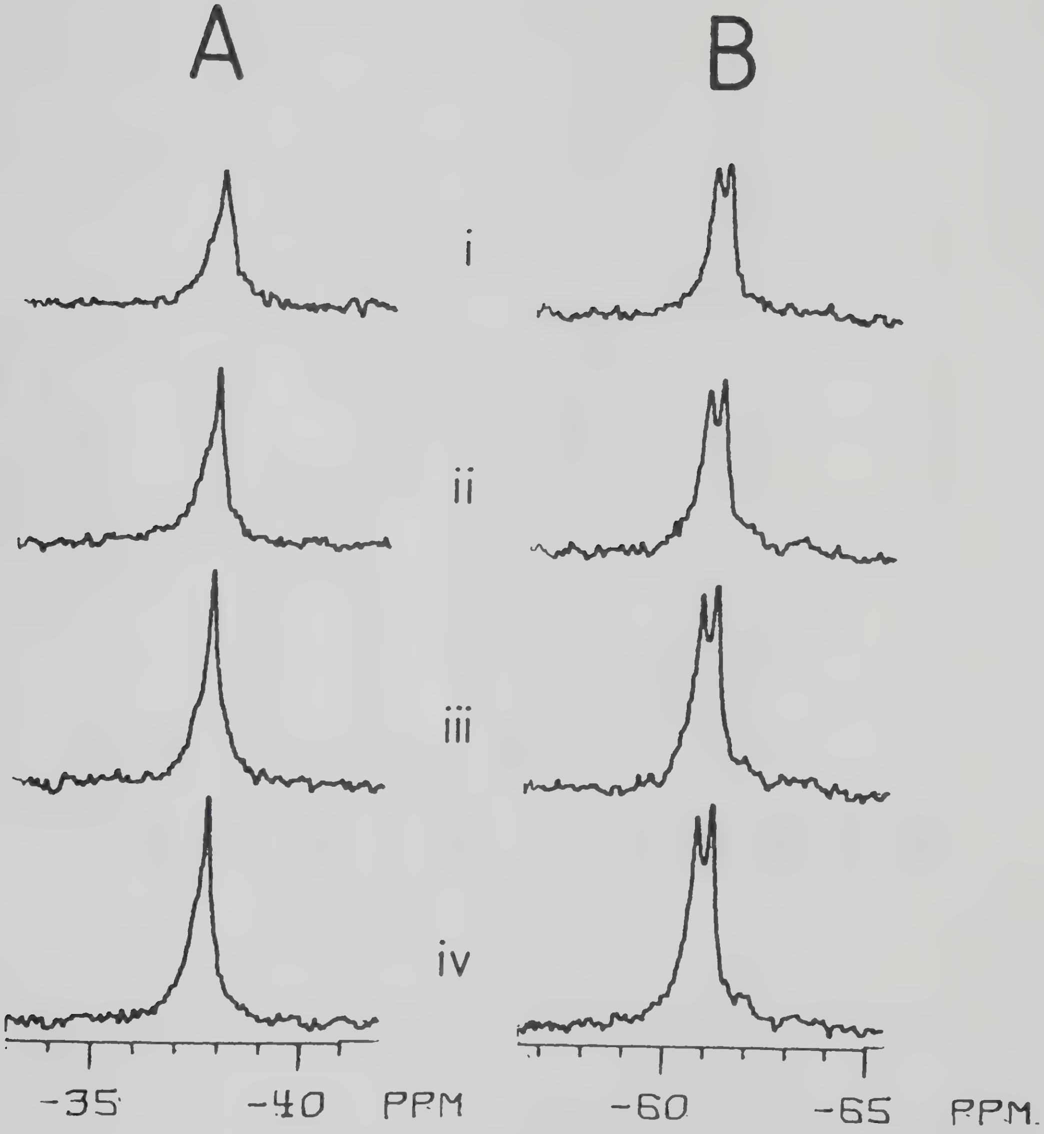

Figure IV-9 The ^{19}F NMR spectra of Fphe- and Ftyr-labelled coat protein in DOC micelles with varying D_2O content. The micelle-bound protein sample was prepared using 20 mg of each labelled phage (see Chapter II-D) and contained 0.1M NH_4HCO_3 (pH 9.0) and 8 mM DOC. The resonances in A are from Fphe while those in B are from Ftyr. The D_2O concentrations are: i) 87%; ii) 70; iii) 50; iv) 33. The spectra resulted from 5000 scans at 297°K using a 16 μsec (72°) pulse, 4K data, ±6300 Hz sweepwidth and a delay of 200 msec between transients. 10 Hz linebroadening was used.

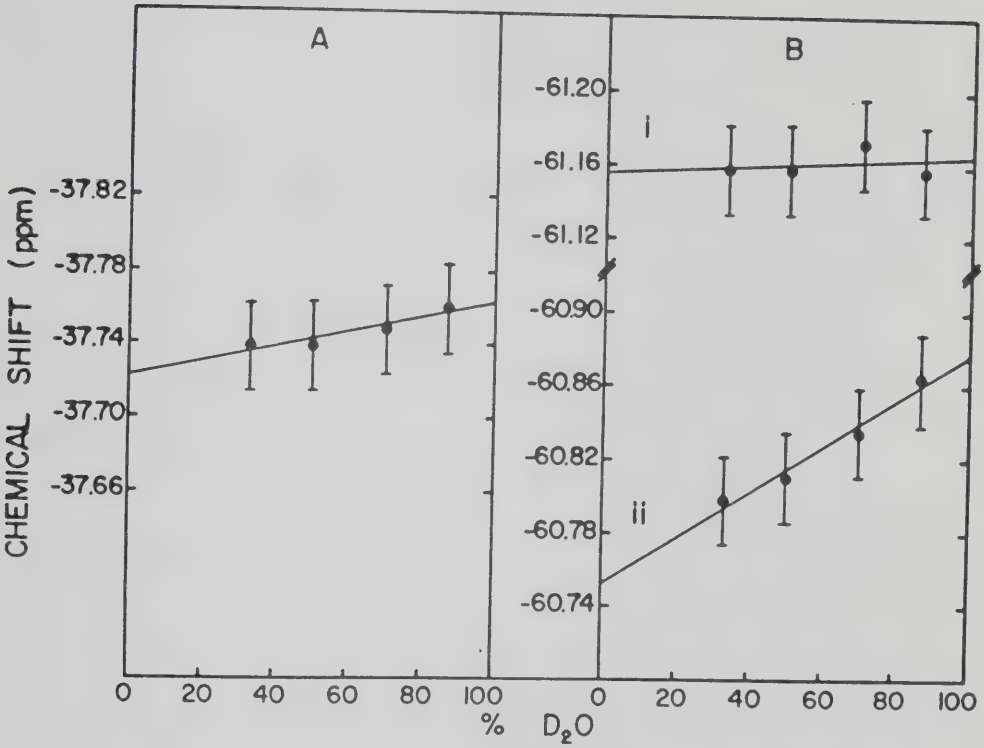

Figure IV-10 The graphs of the ^{19}F NMR chemical shifts of Fphe- and Ftyr-labelled M13 coat proteins in DOC micelles as functions of %D_2O. The data were obtained from the spectra shown in Figure IV-9. Graph A is the Fphe data, while Graph B is the Ftyr data: i) Ftyr24; ii) Ftyr21.

Table IV-2

The SIIS data for the Fphe and Ftyr resonances of labelled coat protein in DOC micelles

	Amino Acid	SIIS[1]
Free[2]:	Fphe	-0.16 (-0.17)[3]
	Ftyr	-0.26 (-0.27)
Protein[4]:	Fphe11	-0.01
	Ftyr21	-0.10
	Ftyr24	-0.02

[1] The SIIS units are ppm.

[2] The data were taken from Table III-4 (pH 9.0); the error was ±0.01 ppm.

[3] The data (pH 9.0) for the Fphe and Ftyr amino acids that were N-acetylated and methyl esterified are given in paretheses.

[4] The data were taken from Figure IV-10 and corrected for the SIIS of the lock resonance (Chapter III-B); the error was ±0.03 ppm.

The exposure of the fluorine on the ring of the residues in the protein relative to its exposure in the free amino acids was quantitated as follows:

$$\%\text{exposure} = \frac{SIIS_{p} \times 100}{SIIS_{aa}}$$

where $SIIS_{p}$ and $SIIS_{aa}$ are the SIIS values of the protein residue and the amino acid, respectively. The results are shown in Table IV-3.

CIDNP experiments

Ftyr residue exposure in the Ftyr-labelled coat protein in DOC micelles was also determined using laser photo CIDNP measurements (see Theory). The CIDNP experiments were done by a summer student, Mr. Meyer Aaron, using one of two dyes: flavin mononucleotide (FMN) or 3-N-carboxymethyl-lumiflavine (CM-LUM); the structures are shown in Figure IV-11. While both dyes were chosen/ designed to be hydrophilic and water soluble, FMN, having the mononucleotide attached to the flavin ring, might be much less able to penetrate the micelle than CM-LUM. Thus, FMN could interact with tyr residues outside the micelle, while CM-LUM, could partition into the micelle and interact with Ftyr (or tyr) residues either at the micelle/water interface or within the micelle. Figure IV-12 shows the results of the FMN and CM-LUM experiments (spectra A and B, respectively). The dark spectra [Figure IV-12(iii)] were collected with the

Table IV-3

The % exposure of the Fphe and Ftyr residues of the labelled coat proteins in DOC micelles as determined by SIIS

	% Exposure relative to:	
Residue	Amino Acid	Blocked[1] Amino Acid
Fphe11	7±22	6±19
Ftyr21	36±13	35±13
Ftyr24	-8±14	-7±12

[1] The "blocked amino acids" refers to Fphe and Ftyr amino acids that had been N-acetylated and methyl esterified (see Chapter III-B).

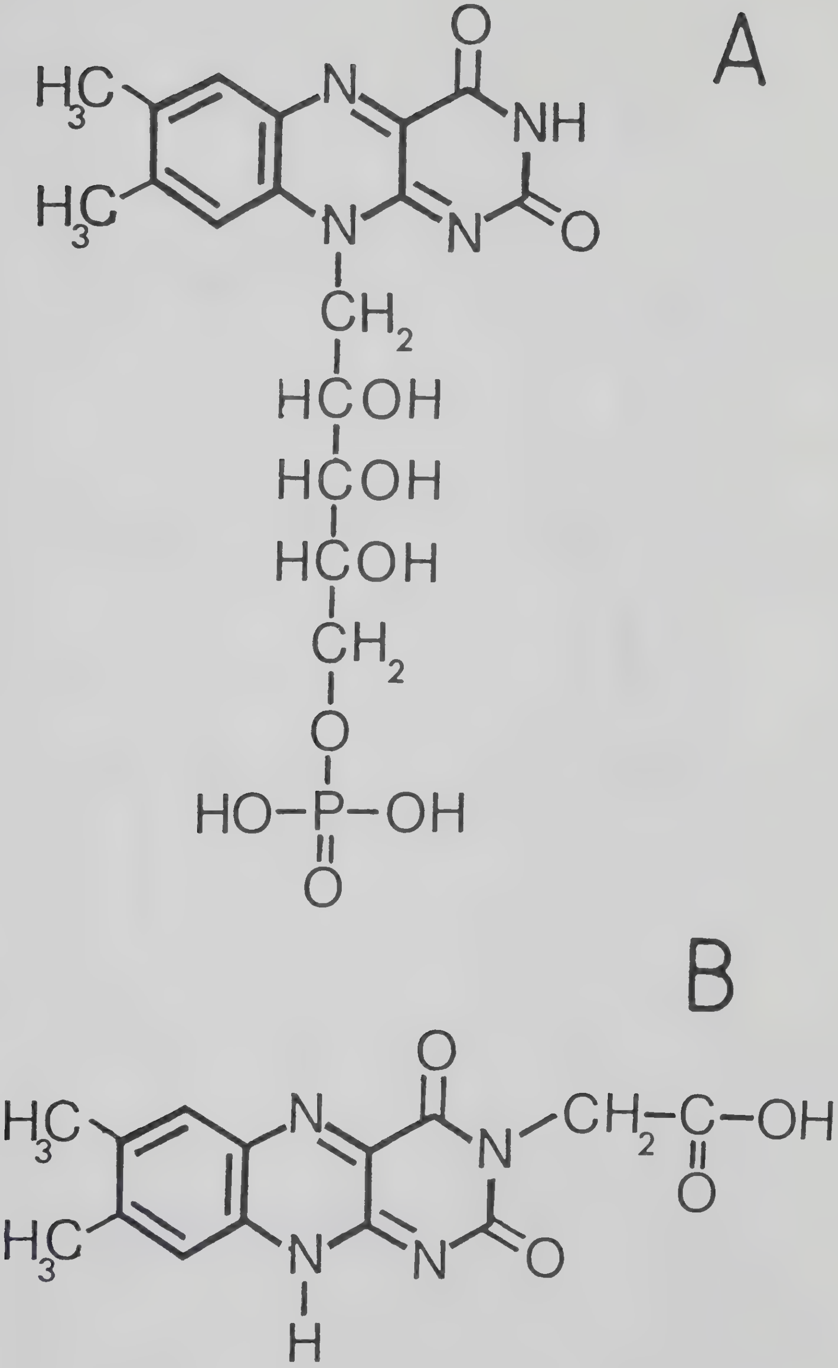

Figure IV-11 The chemical structures of the dyes used in the photo-CIDNP experiments on Ftyr-labelled coat protein in DOC micelles. Structure A is flavin mononucleotide, while B is 3-N-carboxy-methyl-lumiflavine.

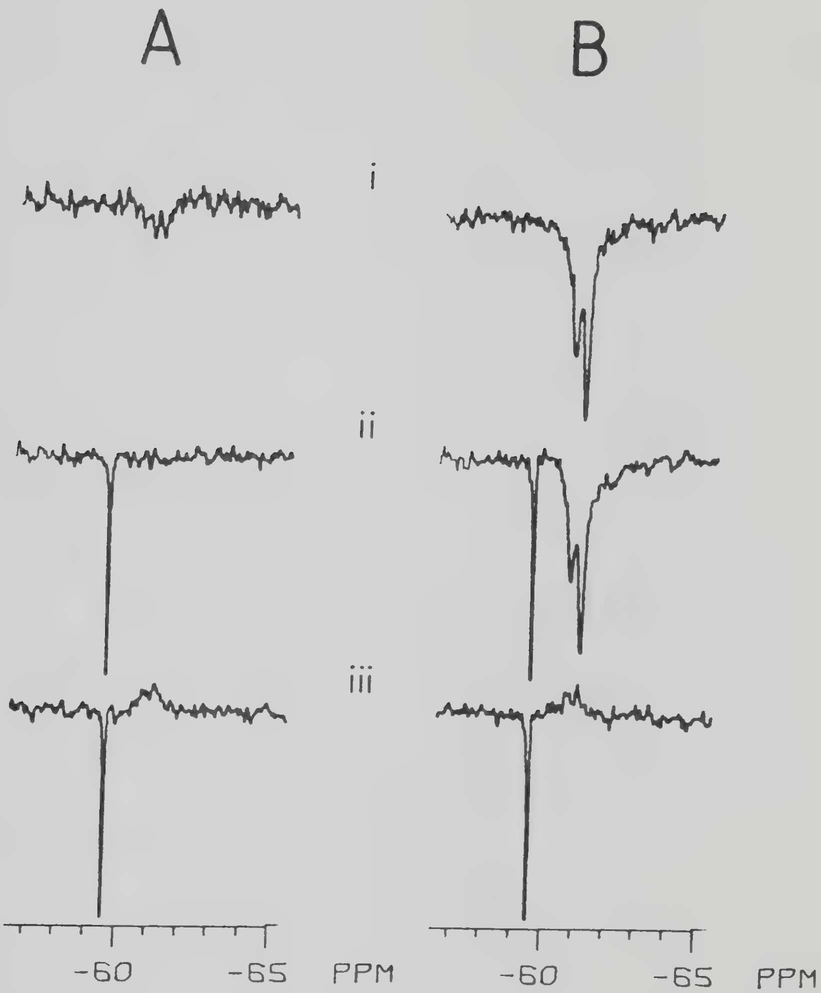

Figure IV-12 The ^{19}F NMR CIDNP spectra of Ftyr labelled M13 coat protein in DOC micelles. The coat protein in micelles sample was prepared using 15 mg of Ftyr-labelled phage (see Chapter II-D) and contained 0.1M NH_4HCO_3 (pH9), 8mM DOC (85% D_2O). The resonances in A were taken using FMN as the dye, while the resonances in B were using CM-LUM; the final concentration of dye was 0.2 µmole/ml. The spectra were taken as follows: i) light-dark; ii) light; iii) dark. The spectral parameters are given in Chapter II-F, with only 72 scans/spectrum. The resonance at ~-59.95 ppm, which is present in all but the difference spectra, is a spectrometer artifact.

laser shutter in place so that no light was allowed into the sample while the light spectra [Figure IV-12(ii)] were collected after irradiation for 1 sec. The dark spectra show the normal Ftyr resonances from the coat protein in micelles: an absorption spectrum. The photoactivation of the dye and its subsequent interaction with the Ftyr residues, results in the perturbation of the ^{19}F spin state populations so that the resulting spectrum may be an absorption or an emission. In the experiment using FMN, the result was the equilization of the ^{19}F spin state populations so that no resonance was observed. In the experiment with the CM-LUM, an enhanced emission was obtained; the enhancement was 6-fold. Both of these results are different from the ^{19}F NMR CIDNP effect found for the free Ftyr amino acid, which is an enhanced absorption (Sykes and Weiner, 1980).

Pronase digestion

The pronase digestion of the Fphe- and Ftyr-labelled protein in DOC micelles at 300°K resulted in the release of both Fphe and Ftyr containing fragments (Chapter IV-A). Since the spectra in Figure IV-4 showed that additional Ftyr resonances were present at lower temperatures, the digestion was repeated at 277°K to determine the exposure of the Ftyr residues corresponding to the new upfield Ftyr resonances (see Figure IV-13). The same amount of pronase was used as in Figure IV-8, hence the progress of the digestion was

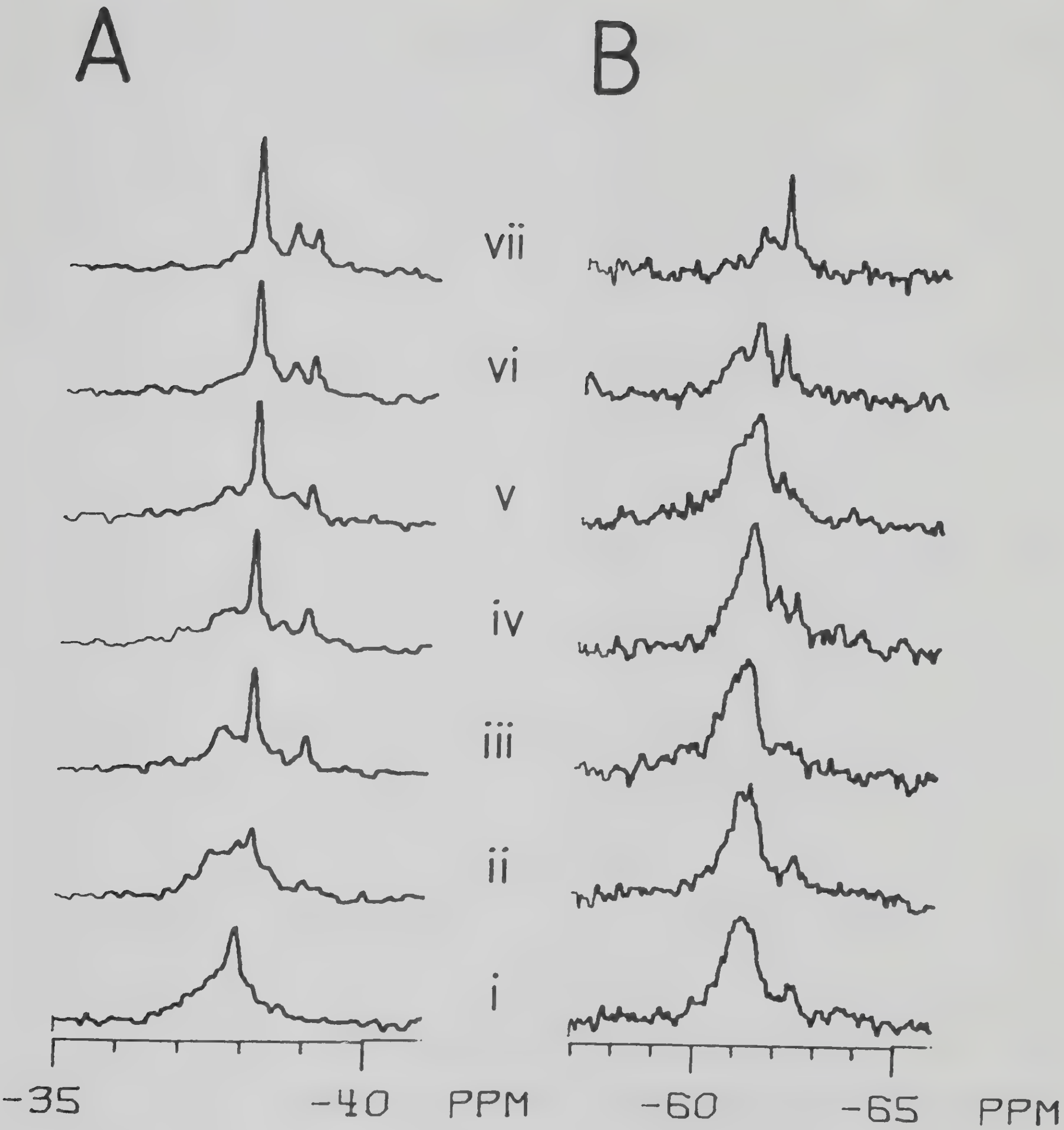

Figure IV-13 The ^{19}F NMR spectra of the pronase digestion of Fphe and Ftyr labelled M13 coat protein in DOC micelles at 277°K. The micelle-bound coat protein sample was prepared using 10 mg of each labelled phage (see Chapter II-D) and contained 0.1M NH_4HCO_3 (pH9) and 8 mM DOC (61% D_2O). The Fphe resonances are shown in A, while B are from Ftyr. The spectra were collected at the following times after the addition of pronase (final concentration 58 µg/ml): i) 0 hr; ii) 0.27; iii) 2.79; iv) 6.00; v) 8.50; vi) 19.5; vii) 35.7 There are 10,000 scans/spectrum, which were collected using 6 µsec (30°) pulsewidth, ±6300 Hz sweepwidth, 4K data and a 20 msec delay between transients. 15 Hz linebroadening was used.

much slower due to the lower temperature. The comparison of the spectra of Figure IV-13(A) with those in Figure IV-13(B) shows that, in agreement with the results at 300°K, the Fphe residues are cleaved faster than the Ftyr residues. Resonances corresponding to three Fphe fragments can be resolved during the digestion: one, released quickly, whose resonance was first detected after a quarter of an hour (Figure IV-13[A(ii)] at -38.11 ppm); a second fragment, whose release was almost as fast as the first, was also detected after the first quarter of an hour (at -38.95 ppm); and a slowly released fragment, the resonance from which did not appear until two and three-quarter hours after the addition of the pronase (Figure IV-13[A(iii)] at -38.52 ppm). The appearance of a ^{19}F NMR resonance from Ftyr fragments at -61.92 ppm in Figure IV-13(B) followed a similar time-course to that of the appearance of the most slowly digesting Fphe fragment; it only became detectable after two and three-quarter hours of digestion (Figure IV-13[B(iii)]). The upfield Ftyr resonance at -62.43 ppm in Figure IV-13(B(i)) was present in the spectra until the Ftyr fragment resonance (at -61.92 ppm) became well-resolved (Figure IV-13[B(iv)]). The upfield Ftyr resonance, then disappeared with continued digestion (Figure IV-13[B(v-vii)]).

CD experiments

To determine whether the upfield Ftyr resonances present in the low temperature spectra were the result of extensive changes in the structure of the protein, CD spectra of the protein in DOC micelles were recorded at temperatures between 279°K and 323°K. Sample spectra of the ellipticity as a function of wavelength are shown in Figure IV-14. The spectra were used to calculate % α-helix, % β-sheet and % random coil content of the protein using the formulae given in the Theory Section[30]; a graph of the results as a function of temperature is shown in Figure IV-15. The errors were calculated as shown in Chapter II-D. The only effect seen over the temperature range studied was a small decrease in the content of α-helix and β-sheet with concommitant rise in the % random coil (from 0 to 10% as the temperature was raised from 284°K to 323°K). ^{19}F NMR spectra as a function of temperature were run using the same sample. The results were the same as shown in Figure IV-4.

pH titration

The behavior of the fluoro-resonances with pH was also monitored. The experiment was done using 25 mM sodium borate rather than 0.1 M NH_4HCO_3 to prevent anomalies due to the carbamate formation of lysine amino

---

[30] The coefficients used in the calculations were determined at room temperature so they are not completely accurate over the temperature range at which the measurements were made. The error introduced, however, was small.

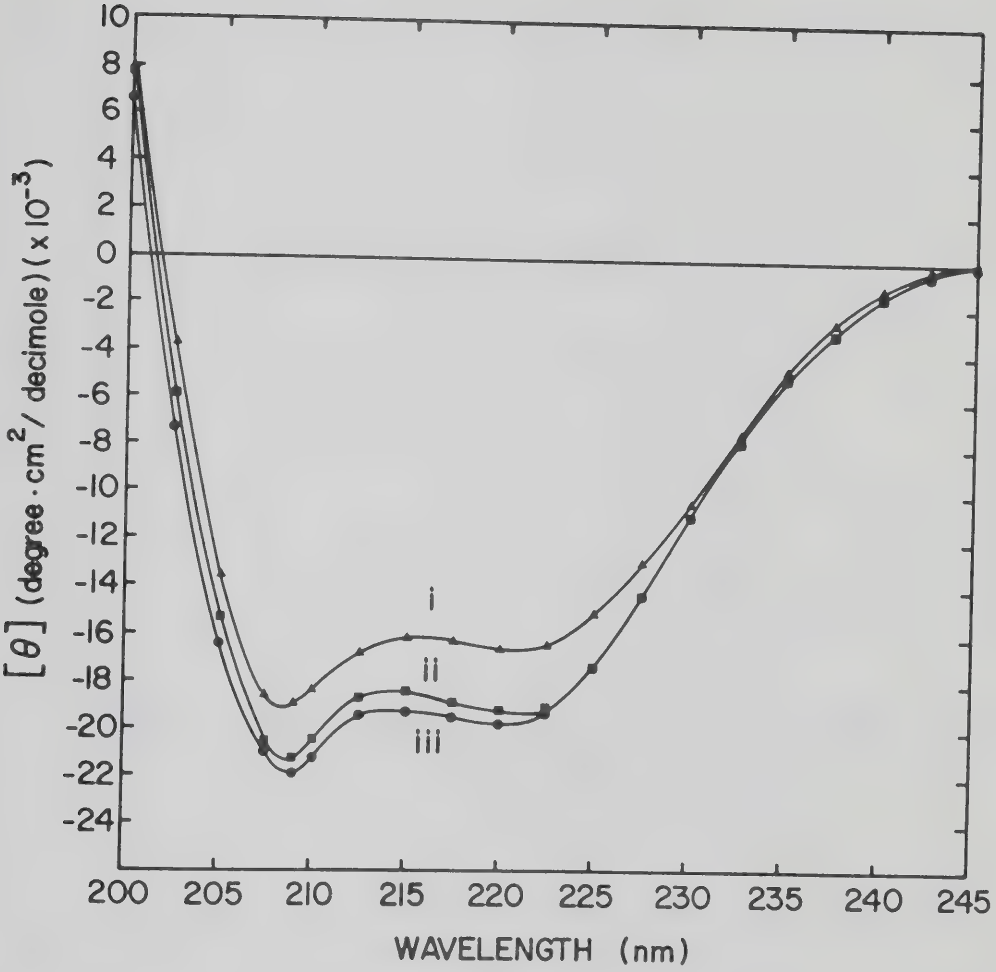

Figure IV-14 The CD spectra of Fphe- and Ftyr-labelled M13 coat proteins in DOC micelles as a function of temperature. The coat protein in micelles sample was made using 11 mg each of Fphe and Ftyr labelled phage (see Chapter II-D) and contained 0.1M NH_4HCO_3 (pH9.0) and 8mM DOC. The temperatures shown are: i) 323°K; ii) 294; iii) 280.

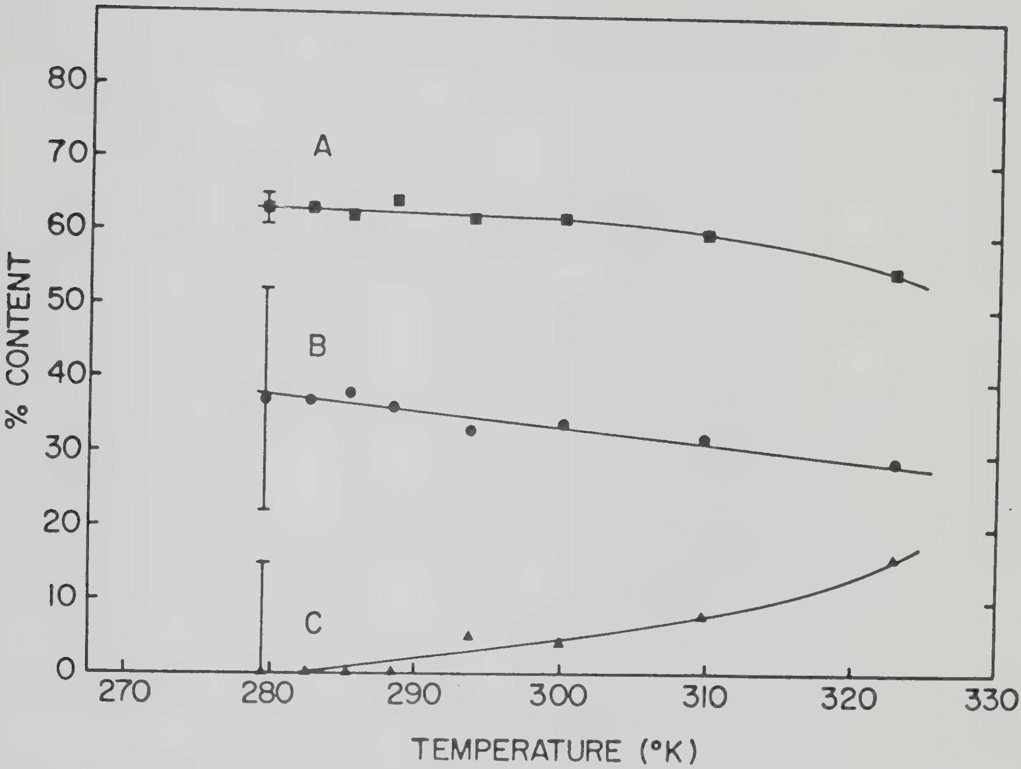

Figure IV-15 The graphs of the % α-helix, β-sheet and random coil in the labelled M13 coat protein in DOC micelles as a function of temperature. The data were obtained from the analyses of the CD spectra in Figure IV-14 (where only three spectra of the series were shown). The curves are: A) α-helix; B) β-sheet; C) random coil.

groups (see Chapter III-A). The pH was adjusted at 287°K. Figure IV-16 shows the Fphe (A) and Ftyr (B) spectra as the pH was increased from 7.73 to 11.85 at 287°K. The Fphe resonance did not have much dependence on pH, but the behavior of the Ftyr resonances was interesting. The upfield Ftyr resonances were observable at pH 10 and less (Figure IV-16[B(iii-v)]). As the pH was increased above 10, however, the intensities of the upfield resonances decreased. As well, the Ftyr intensity of the major Ftyr resonance increased until, at pH 11.85, partial resolution of the Ftyr21 and Ftyr24 resonances is obtained; an increase in pH causes similar effects to those seen when the temperature was increased.

The behavior of the Fphe11 and Ftyr21/24 chemical shifts and the upfield Ftyr resonance intensity with pH is shown in Figure IV-17. There is little change in chemical shift for the Fphe resonance (curve (C)). The chemical shift Ftyr21/24 resonance moves upfield with increasing pH and is shown in curve (B); the simultaneous decrease of intensity of the upfield resonances relative to the total Ftyr resonance intensity is shown in curve (A). Analyses of the two Ftyr curves using a non-linear least mean squares program gave a pKa for the Ftyr chemical shift titration of 10.25±0.07 while the "pKa" of the decrease in intensity of the upfield resonances was 10.10±0.10.

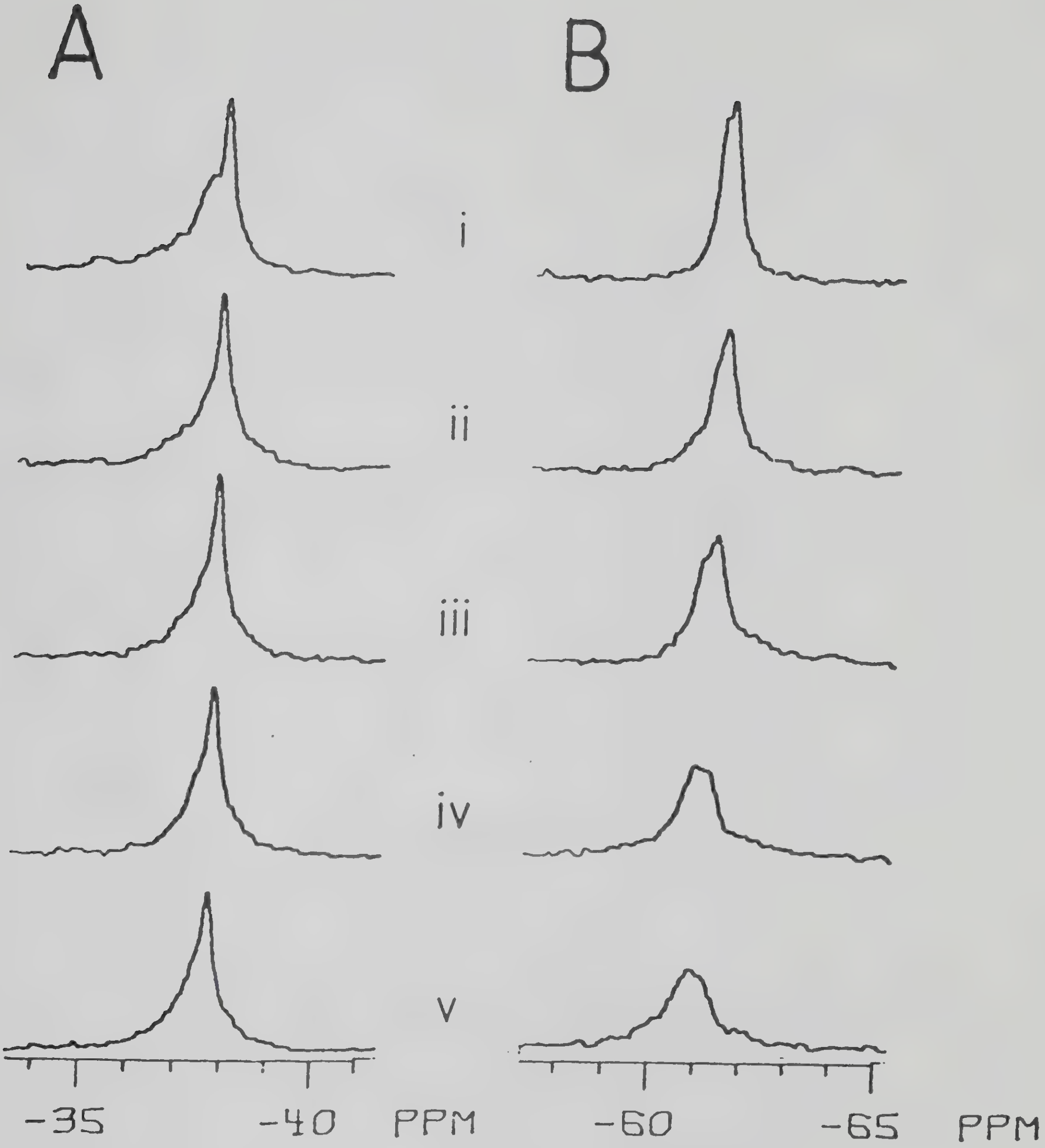

Figure IV-16 The ''F NMR spectra of the pH titration of Fphe- and Ftyr-labelled M13 coat proteins in DOC micelles. The coat protein in micelles sample was prepared using 14 mg Ftyr and 16 mg Fphe phage (see Chapter II-D) and contained 25 mM sodium borate (pH 9.0) and 8 mM DOC (final D_2O content was 43%). The spectra in A are from the Fphe residues, while those in B are from the Ftyr. The pH values are: i) 11.85; ii) 10.82; iii) 9.96; iv) 9.00; v) 7.73. The spectra were acquired at 283°K using the same parameters as in Figure IV-13, except that a 7 μsec (45°) pulsewidth and no delay between transients were used.

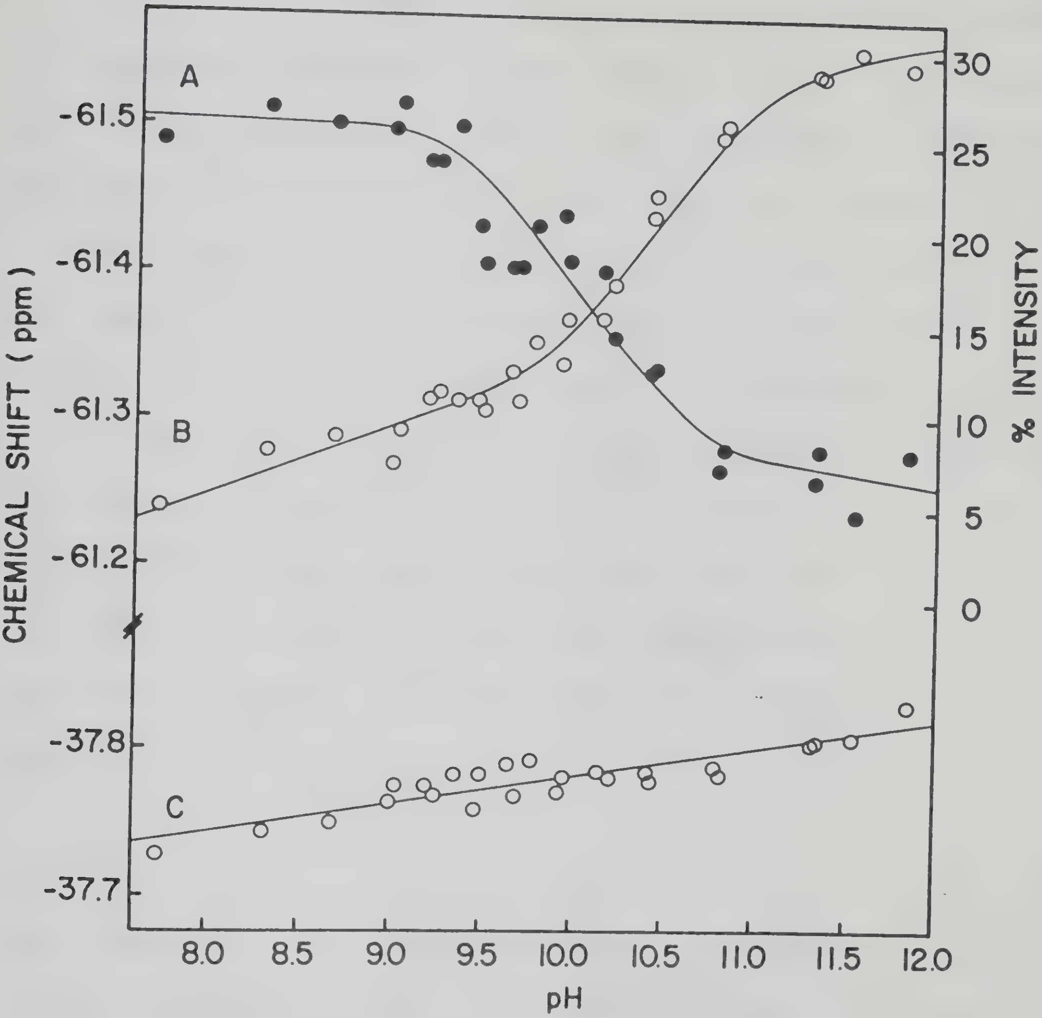

Figure IV-17 The graphs of the ¹⁹F NMR chemical shifts of the Fphe11 and Ftyr21/24 resonances and of the intensity of the Ftyr upfield resonances (relative to the total Ftyr resonance intensity) as functions of pH. The data were obtained from the spectra shown in Figure IV-16 (where only five spectra were shown). The curves are as follows: A) the upfield Ftyr resonances relative intensity; B) the major Ftyr resonances chemical shift; C) the Fphe11 resonance chemical shift.

^{19}F NMR relaxation data

Table IV-4 shows the spin lattice relaxation times (T_1) and the linewidths of the Fphe11, Ftyr21 and Ftyr24 resonances at 299°K. The T_1's were measured at 254 MHz using an inversion recovery technique (see Chapter II-F) and analysed using a three parameter-fit program (Levy and Peat, 1975). The linewidths were measured using a curve-fitting program and have been corrected for contributions from both the linebroadening used to improve the spectral signal to noise ratio and the width of the Fphe and Ftyr amino acid J-coupling. This data will be analysed to quantitate the ring mobilities of the Fphe and Ftyr residues of the labelled coat protein in DOC micelles.

Discussion

As suggested in the Introduction, structural information can be obtained from the determination of residue exposure and/or mobility. For membrane proteins, the topology of the protein relative to the hydrophobic bilayer or micelle can also be determined. The chymotryptic and pronase digestions described in Chapter IV-A have suggested the relative positions of the Fphe and Ftyr residues relative to the micelle: Fphe11, 42, and 45 are "exposed" to both proteases while Ftyr21 and Ftyr24 only become exposed to pronase after significant digestion of the protein. The differences in rates of cleavage between the Fphe residues

Table IV-4

The chemical shift, T_1, and linewidth data of the ^{19}F NMR resonances of Fphe- and Ftyr-labelled M13 coat protein in DOC micelles

Residue	Chemical shift(ppm)[1]	T_1(sec)	Linewidth(Hz)
Fphe11	-37.79	0.38[2]	21±5
Fphe(?)[4]	-37.45	-	230±50
Ftyr21	-60.86	0.40	36±5
Ftyr24	-61.19	0.43	47±5
Ftyr(?)	-61.97	0.24[3]	81±10
Ftyr(?)	-63.66	-	330±50

[1] All measurements were made at 299°K.

[2] The error in the T_1 values were ± 0.02 sec.

[3] The error in this T_1 value was ± 0.03 sec.

[4] The residues denoted by (?) are Fphe and Ftyr resonances that have not been assigned to a particular residue.

may be due to either primary sequence specificities and/or secondary and tertiary structure. The lack of exposure of the Ftyr residues to the chymotrypsin indicates that the micelle protects those residues; they only become exposed to pronase after release of the hydrophilic ends, suggesting that there was disruption of protein structure in the vicinity of the Ftyr residues.

It was also suggested in the Introduction that one must be cautious when talking about exposure of residues; a residue which may be exposed by one technique, may seem buried by another. This is exemplified by the SIIS results. Table IV-3 shows that Ftyr24 is less exposed to water compared to Ftyr21. This agrees with the pronase digestion results (which prompted the assignments of the two resonances). The sequence position of Ftyr24 is further into the hydrophobic domain of the protein (see Chapter I-C), hence would be expected to be further buried in the micelle and less exposed to water than Ftyr21. The anomaly occurs when the exposure of Ftyr21 is compared to that of Fphe11 and, indeed, when the exposure of Fphe11 is compared to that of free Fphe. The Fphe11 appears exposed to enzymes for digestion, but buried from solvents. SIIS is predominantly due to van der Waals and H-bonding interactions (Chapter III-B). Thus, direct contact between the ring fluorine and water molecules are necessary. The position of Ftyr21 in the amino acid sequence and micelle structure suggests that carboxyl groups in its immediate vicinity (from either glu 20 or the

DOC itself) may be involved. These would hydrogen bond to water creating an artificially high concentration of water close to the Ftyr fluorine. This might explain why the Ftyr21 SIIS is high, even though it is not readily susceptible to proteases. The explanation for the low value of the Fphe residue is not so easily found. One question is whether the free amino acids are good controls for 100% exposure of SIIS as they have both charged amino and carboxyl groups. Chapter III-B showed that there was no significant difference between the SIIS of the charged and N- and C-blocked amino acids. As well, Table IV-3 gives the % exposures obtained using the pH 9.0 SIIS's of the N- and C-blocked amino acids; the % exposures are the same regardless of the control used. Another question is whether the denatured coat protein would be a better control for the 100% exposed residue. Six molar guanidine-HCl was found to cause the DOC and/or protein to polymerize[31]; 8M urea solubilized the protein but caused a decrease in SIIS compared to the native state. It appeared to be forming a complex with the protein thus limiting water-access. A final test of the use of the free amino acids as 100%-exposure controls was done by Dr. Poul Hansen (visiting Professor in this laboratory from the University of Roskilde, Denmark). He determined the SIIS of the Fphe11 resonance of the chymotryptic fragment 1-11. He obtained a value of -0.16 ppm;

---

[31] Tanford and coworkers obtained the same result but also found that if the concentration of the guanidine-HCl was greater than 7.3 M, denaturation could be achieved (Nozaki *et al.*, 1978).

this is the same as the SIIS of the free Fphe (Chapter III-B). Hence, the low SIIS of the Fphe11 fluorine of the micelle-bound coat protein appears to be due to the structure about the Fphe11 residue and not due to a poor choice of control; it seems that the Fphe ring fluorine resides, at least partially, in a hydrophobic pocket (it must have some exposure to the solution, however, to allow the chymotrypsin to recognize, bind and cleave the Fphe residue at the observed rate.)

One other technique was used to measure exposure of the Ftyr residues: laser photo CIDNP-measurements. Figure IV-12 shows that CM-LUM interacts with the Ftyr residues much more than FMN. As CM-LUM is lipophilic and is similar in structure to the DOC (compare Figures IV-1 and IV-11), it would be expected to intercalate into the micelle and react with residues within the micelle. The relative area of the Ftyr21 resonance to the Ftyr24 resonance is approximately 1 prior to irradiation (found in the usual NMR spectra), while it is 0.70 after irradiation. Hence Ftyr21 interacts less with the dye than Ftyr24, possibly indicating it is less buried than Ftyr24. This datum, as well, agrees with the initial assignments of the resonances corresponding to Ftyr21 and Ftyr24, using the logic outlined previously.

The experiments discussed so far demonstrate that the coat protein in DOC micelles is not a random coil, but contains secondary, if not tertiary, structure. Further evidence for structure was seen in the spectra of Fphe- and

Ftyr-labelled coat protein in DOC micelles at different temperatures (Figure IV-4). At 327°K the Fphe resonances could be fit with three Lorentzian lineshapes: two narrow and one broad; this changed as the temperature was decreased until at 277°K, a fit required two broad and one narrow. The temperature behavior of the Ftyr resonances was even more dramatic. At 327°K, there were two narrow Lorentzian resonances seen, while by 277°K, there were two narrow and two broad resonances present. Chemical shift changes result from changes in the magnetic environments about the nuclei and resonance linebroadening results from decreasing internal motions (assuming that the broadening is not due to exchange processes and that the population of micelles is homogeneous.) There were changes in both the chemical shifts and linewidths of the Fphe and Ftyr residue resonances with temperature thus suggesting that there are structural differences between the proteins at high temperature compared to the proteins at low temperature.

CD spectra were collected over the temperature range of 280-323°K to determine whether gross structural changes in the DOC micelle-bound coat protein occurred. The shapes of the curves in Figure IV-14 showed that there was considerable α-helical content at all temperatures measured. [As well, that the ellipticity values returned to zero outside of the absorption band (>240 nm) indicates that the contributions to the spectrum due to lightscattering are negligible (Dorman *et al.*, 1973).] The analysis of the CD

spectrum collected at 280°K shows that there is 63±2 % α-helix, 37±15 % β-sheet and 0±15 % random coil structure present in the DOC micelle-bound Fphe- and Ftyr- labelled M13 coat proteins (see Figure IV-15). This agrees fairly well with the results of others (Makino *et al.*, 1975; Nozaki *et al.*, 1976; Williams and Dunker, 1977; Chamberlain *et al.*, 1978) Figure IV-15 also shows that, within experimental error, the relative contents of α-helix, β-sheet and random coil do not change dramatically over the temperature range. Above 300°K, the increase in % random coil may be indicative of a loosening of the protein structure at the hydrophilic ends, resulting in the resolution of the three Fphe resonances; below 300°K, there was little change in structural content. Thus, the development of the broad upfield Ftyr resonances at temperatures below 298°K as well as the changes in the Fphe spectra over the temperature range, are not the result of gross conformational changes of the entire protein but rather appear to be local. The lack of resolution of the Fphe resonances at most temperatures made their study difficult. The Ftyr resonances are resolved enough to allow further analysis. To study the relationship between the Ftyr residues corresponding to the resonances of the two major peaks to those responsible for the upfield Ftyr resonances, two experiments were done: 1) a pronase digestion at 277°K; and 2) pH titration at 287°K.

The pronase digestion (at 277°K) showed clearly the order of release of the Fphe and Ftyr residues.

The narrow resonance from Fphe11 of the protein spectrum is the first to disappear, hence the fragment resonance at -38.11 ppm, that appears at the same rate, contains Fphe11. The relative rates of appearances of the other fragment resonances combined with the observation that the last Fphe fragment resonance appears with a similar rate as the Ftyr21 fragment resonance (Figure IV-13), suggest that the Fphe fragment resonance at -38.95 ppm is from a fragment containing Fphe45, while the most slowly appearing fragment resonance at -38.52 ppm is from a Fphe42-containing peptide. Confirmation of these assignments requires the correlation of the spectral data with the characterization of the fragments released (as was done for the chymotrypsin digestion.) The Ftyr resonance assigned to Ftyr21 is seen to decrease in intensity at the same time as the last protein-bound Fphe resonance. As well, the upfield Ftyr resonance at -62.43 is present through the spectra (i) to (iv), but disappears with continued digestion. This indicates that removal of a certain number of Ftyr21 residues (or other residues before and including Ftyr21) disrupts the interaction causing the upfield resonance. Little of Ftyr24 is removed by this time. Thus, at least Ftyr21, if not Ftyr24, is responsible for maintaining a structure of the protein which exhibits the upfield Ftyr resonance at -62.43 ppm.

The pH titration of Fphe and Ftyr labelled coat proteins in DOC micelles at 287°K showed interesting behavior. Increasing the pH from 7.73 to 11.85 had similar effects as

increasing the temperature on the ^{19}F NMR spectra, particularly for the Ftyr resonances (compare Figure lV-16 to Figure lV-4). Further, the pKa determined from the loss of the upfield resonance intensity was the same as the pKa determined from the change in the Ftyr chemical shift (see Figure lV-17). Thus, ionizations and/or deionizations of some, as yet, unidentified residues appear to disrupt the interactions causing the upfield Ftyr resonances.

Amino and tyr-hydroxyl groups both have pKa's in the region of pH 10; this presents a number of possibilities for the origin of the upfield resonances. The protein is a dimer when bound by DOC micelles (Chapter I-C). Thus, if they are in a head to tail orientation, there may be inter-chain interactions between glutamic acid 20 and lysine 40. An alternate possibility is that Ftyr21 (or tyr21) may stack on Ftyr24 (or tyr24) resulting in an intra-chain interaction. This would suggest that the protein is α-helical in the region of the tyr residues. Additional experiments, including the determination of the relative orientations of the proteins in the micelles and the titrations of tyr and lys residues by proton and/or carbon NMR are necessary to determine all of the residues involved.

The last type of experiment performed to give structural information of Fphe- and Ftyr-labelled M13 coat proteins in DOC micelles was the motion analysis of the ^{19}F NMR relaxation data. Qualitatively, one can observe that there are both mobile and motionally-restricted regions in the

micelle-bound coat protein; there are always both narrow and broad components in the Fphe and Ftyr resonances. The width of a resonance reflects the overall motion of the nucleus in solution: the faster the nucleus tumbles in solution, the narrower will be its linewidth (thus, the amino acids have narrower lines than the micelle-bound protein residues, which are narrower, in turn, than the resonances for the coat protein in vesicles). The presence of internal motions faster than the overall tumbling time (for example, about the $\alpha\beta$- and $\beta\gamma$-bonds in Fphe and Ftyr) causes additional narrowing of the resonances. If the micelles in the samples are predominantly of one size, the distribution of linewidths seen in any one spectrum reflect a distribution of internal motions: the narrow resonances are from residues having rapid internal motions, while the broad resonances are from residues that are essentially restricted to moving with the micelle as a whole. The variation in the frequencies of internal motion suggests that there are structured regions in the coat protein, whether as a result of intra- or inter-protein interactions or interactions with the DOC.

The motions of the Fphe and Ftyr rings in DOC micelle-bound labelled coat protein have been quantitated. The analysis used the model-dependant approach that is outlined in detail in Chapter V-B. The calculated results were compared with the linewidth ($\Delta\nu$) and spin lattice relaxation time measurements of the micelle-bound protein resonances.

Briefly, the model for the Fphe/Ftyr ring motions (shown in Figure V-8) allows free rotation about the $\beta\gamma$-bond with a diffusion constant D_2, wobble through an angle γ_0 about the $\alpha\beta$-bond with a diffusion constant D_1, and overall spherical symmetry for vesicle (or in this case, micelle) rotation in solution, with a correlation time τ_c (= 1/(6D). The assumption that the micelles are spherical, will be discussed further. Both dipole-dipole and chemical shift anisotropy relaxation mechanisms were included; dipolar interactions were assumed to only occur between the fluorine and neighbouring ring protons. Computer programs were written (given in Appendix B) which calculate the T_1, $\Delta\nu$ and nuclear Overhauser effects (nOe) when given τ_c, D_1, D_2 and γ_0. The best-fit values for both the Fphe and Ftyr residues are given in Table lV -5. The comparison of the results for the resonances assigned to Fphe11, Ftyr21, and Ftyr24 shows that there was not much difference in the wobble frequencies about the $\alpha\beta$-bonds, nor in the rotation frequencies about the $\beta\gamma$-bonds. The key differences were in the γ_0 angles, 140° for Fphe11, 80° for Ftyr21 and 70° for Ftyr24. In all cases, the linewidths fit well but the T_1's were too long. Inspection of the sample results in Appendix B show that at each γ_0 value, the linewidths do not change much with increasing D_1 and D_2, while the T_1's have definite minima at the D_1 and D_2 values given above; hence they were chosen. That the values of T_1 at the minima were too long, suggests that there are more interactions present than the model

Table IV-5

The T_1 and linewidth results calculated using the best-fit values of D_1, D_2 and γ_0

Residue	T_1(sec)	linewidth(Hz)
Fphe11[1]	0.68 (0.38)	22 (21)
Fphe(?)[2]	-	258 (232)
Ftyr21[3]	0.70 (0.40)	37 (36)
Ftyr24[4]	0.72 (0.43)	45 (47)
Ftyr(?)[5]	0.89 (0.24)	81 (81)
Ftyr(?)[2]	-	305 (335)

All results were calculated using $\tau_c = 3\text{x}10^{-7}$ sec. The values in parentheses are the experimentally measured data, shown in Table IV-4.

[1] $D_1=1\text{x}10^8$ sec^{-1}, $D_2=5\text{x}10^8$ sec^{-1}, $\gamma_0=140°$

[2] D_1 and D_2 >> τ_c

[3] $D_1=1\text{x}10^8$ sec^{-1}, $D_2=5\text{x}10^8$ sec^{-1}, $\gamma_0=80°$

[4] $D_1=5\text{x}10^7$ sec^{-1}, $D_2=5\text{x}10^8$ sec^{-1}, $\gamma_0=70°$

[5] $D_1=1\text{x}10^7$ sec^{-1}, $D_2=5\text{x}10^8$ sec^{-1}, $\gamma_0=45°$

takes into account. Rapid interactions with neighbouring residues and/or DOC molecules are implicated.

These values were obtained using a correlation time, τ_c, of 3×10^{-7} sec for the micelle rotation. This value was chosen as the correlation time which allowed the calculated linewidth for motions with D_1 and $D_2 << \tau_c$ to be comparable to the broad lines measured in the Fphe and Ftyr spectra as well as giving the shortest T_1 values (see Table IV-5 and the sample results in Appendix B; the T_1's decrease slightly with decreasing τ_c, while the linewidths decrease proportionally.) An approximation of the correlation time of a protein in solution may be obtained by knowing the molecular weight of the protein (Marshall, 1978; Brauer and Sykes, 1984). The volume of the protein (Vp) may be calculated using the protein's molecular weight (Mp) by the following:

$$Vp \cong \frac{Mp[\bar{\nu}_p + \delta'\bar{\nu}_w]}{N_0}$$

where $\bar{\nu}_p$ is the partial specific volume of the protein (~$0.72 cm^3/g$), δ' is the amount of water bound to the protein (~0.35g (H2O)/g(protein)), $\bar{\nu}_w$ is the partial specific volume of water (~$1 cm^3/g$), and N_0 is Avogadro's number. Once Vp is determined, it may be substituted into Stokes- Einstein equation to obtain τ_c:

$$\tau_c = \frac{Vp\ \eta}{kT}$$

where η is the solution viscosity, k is the Boltzman constant and T is the temperature. When the protein is in a detergent micelle, a third component is added: the detergent. Hence, a third term in the equation must be added:

$$Vm \cong \frac{Mp[\bar{\nu}_p + \delta'\bar{\nu}_w + \kappa\bar{\nu}_d]}{N_0}$$

where Vm is the volume of the micelle, Mp is now the molecular weight of the protein per micelle, κ is the amount of detergent bound per protein (=˜0.63g DOC/g coat protein, Makino *et al.*, 1975) and $\bar{\nu}_d$ is the apparent partial specific volume of the detergent (= 0.765 cm^3/g, Small (1971)). Solving for Vm, using a Mp of 10,480 g/mole for the coat protein dimer (see Chapter IV-A), one obtains a Vm of $2.7x10^{-20}$ cm^3, which results in a τ_c of ˜$6x10^{-9}$ sec (6 nsec). This is significantly smaller that the best-fit correlation time of $3x10^{-7}$ sec (300 nsec).

The explanation for the discrepancy may be in one of the three assumptions made in using the equation for Vm: 1) there may be more water bound to the micelle-protein complex than is included in the relationship; 2) the micelle-protein complex is probably non-spherical; and 3) the solution viscosity is higher than that of water alone. The calculation allows for 0.35 g water per gram of protein. This value is probably high for the coat protein as it is extremely hydrophobic. The relationship, however, did not include the water that would be bound by the DOC so that it

was assumed that the over- estimation for the protein would approximately cancel the under-estimation for the bile acid. This may not have been a good assumption; more water may actually be bound by the DOC, thus the effective micelle volume may be larger than calculated. The second possibility would contribute little to τ_c. From Small (1971), DOC is 8 Å across the plane of the rings, 15 Å long, and 6 Å thick. In Chapter IV-A, the coat protein-micelle complex was described: the hydrophobic domains of the coat protein dimer are surrounded by two rings of DOC molecules (8 per ring). Given the dimensions of the DOC, the diameter of the hydrophobic domain of each coat protein would be ~10 Å. This results in an estimate of the micelle width of 32 Å. The DOC molecules are ~15 Å long thus the micelle length would be ~30 Å. If the total length of the protein outside of the micelle is estimated to be 45 Å, then the total length of the complex would be ~75 Å. The axial ratio would then be 75/32= 2.3. In Figure 7-23 of Marshall, (1978) it is shown that an axial ratio of ~4 is necessary to cause the frictional ratio f/f_0 to vary from 1, when the molecule is a sphere (a/b = 1), to 1.25. Thus, even if the axial ratio estimated above was wrong to the limit of a/b = 4, the correlation time, τ_c, would only increase by 1.25 times (τ_c and f are proportional). The third assumption, that η can be taken as the viscosity of water at 300°K, is likely a source of error. The addition of solutes, particularly macromolecules, causes η to increase (Marshall, 1978; Freifelder,

1976). Whether the viscosity of a sample containing 0.1M $NaHCO_3$, 8mM DOC and ~1mM M13 coat protein is fifty times more viscous than water, would have to be determined.

One other possibility for the difference between the calculated correlation time and the τ_c determined from the linewidths of the resonances is that the resonances for Fphe 11, Ftyr 21 and Ftyr 24 are not single resonances but are actually composite resonances having similar linewidths but slightly different chemical shifts. This situation could be tested by measuring the T_2 relaxation times of the resonances, for example, a Meiboom-Gill technique (see Farrar and Becker, 1971).

The experiments in this Chapter have given some insight as to the structure of the M13 coat protein in DOC micelles. The exposure studies showed that although Fphe11 is very susceptible to proteases, water does not have easy access to the ring fluorine. This suggests that the Fphe is not out in solution, but spends some of its time in a hydrophobic pocket. This is supported by the motion analyses in that Fphe11 is not significantly more mobile than either of the Ftyr residues. Ftyr21 and Ftyr24 were found to be protected from chymotrypsin and interaction with the hydrophilic dye, FMN. In particular, Ftyr24 is not accessible by water, as indicated by the SIIS experiments, and interacts with the lipophilic dye, CM-LUM, thus Ftyr24 seems to be well within the micelle. Ftyr21, on the other hand, appears to be at the water/micelle interface as it is exposed to water, is the

first Ftyr to be released by pronase, and interacts less than Ftyr24 with CM-LUM. Structural changes appear to occur in the vicinities of the Ftyr and Fphe rings with temperature. The Ftyr temperature dependence is partially reversible by increasing the pH to greater than 11, hence the interaction involves either an ionic bond, or ring stacking. Finally, the presence of both broad and narrow resonances at all temperatures studied indicate that the protein dimer contains regions of both immobile and mobile protein residues, suggesting the presence of structure.

V. Fphe and Ftyr Labelled M13 Coat Protein Reconstituted into Phospholipid Vesicles

A. The Exposure of the Fphe and Ftyr Residues

Introduction

The study of an intrinsic membrane protein can be no more complete than to characterize its behavior in its native environment: a membrane. This, however, has been difficult with regards to most physical and biochemical approaches to the study of the protein due to the reasons discussed in Chapter I. Hence, physical biochemists, including NMR spectroscopists, tend to prefer detergent micelle-bound membrane proteins.

Experiments with membrane proteins in micelles can certainly give useful information. Their smaller size compared to lipid vesicles (hence narrower linewidths) may allow the resolution of individual residue resonances; detailed analyses of structural and mobility changes can be monitored (see Chapter IV). Micelles, however, cannot imitate membranes completely. Some types of detergents form small micelles, so that no more than one or two proteins may be bound per micelle. Thus, the communication, if present, between proteins in a membrane is not allowed between proteins in micelles. The cooperativity present between the lipids of a membrane bilayer (as exhibited by the gel to liquid crystal phase transition) may also have effects on

the structure or motions of a protein surrounded by them. For membrane proteins possessing measurable activities, the presence of specific lipids and the orientation of these proteins across the bilayer have been found important. Thus studies with lipid-bound proteins, although they may seem less spectroscopically and biochemically satisfying, are necessary to complete the picture of a membrane protein's biological dynamic behavior.

The coat protein from M13 coliphage is a cytoplasmic membrane protein during infection (see Chapter I-C). It is found oriented with its N-terminus in the periplasmic space and its C-terminus in the bacterial cytoplasm. Its function, during infection, is to aid the phage DNA through the lipid bilayer to both enter and leave the cell. Clearly, the orientation of the protein across the cell membrane and (perhaps) communication between protein monomers (to allow smooth entries and exits) are necessary for its biological function in the membrane. As well, it has been found to cause an increase of synthesis of cardiolipin in the *E. coli* (Chamberlain and Webster, 1976). Although cardiolipin is not essential for M13 (or fd) infection (Pluschke *et al.*, 1978), it may enhance some aspect of the coat protein's activity. Its activity (of phage DNA transport), is difficult to quantify, hence the differences between its structure and internal motions in the micelles compared to the membrane-bound form are not readily measurable. The best that one can do is to compare the results of dynamic experiments done on

the micelle-bound protein to data obtained from experiments done on lipid-bound protein; NMR studies of the behavior of Fphe and Ftyr residues of labelled M13 coat protein in synthetic lipid vesicles are described herein.

Results

Figure V-1 shows the ^{19}F NMR spectrum of Fphe- and Ftyr-labelled M13 coat protein reconstituted into synthetic lipid vesicles, consisting of 80% dimyristoylphosphatidylcholine(DMPC), 10% cardiolipin (CL)[32], and 10% dipalmitoylphosphatidic acid (DPPA); the structures of these lipids are shown in Figure V-2. The lipid to protein ratio of these vesicles was 54 ± 8 (see Chapter II-E). From comparing the spectrum in Figure V-1 to those of the coat protein in micelles (Figure IV-2) and of the free amino acids (Figure III-1), one can immediately assign the resonance at -38.0 ppm to the Fphe residues and resonance at -61.0 ppm, to the Ftyr residues. Neither the J-coupling of the ring protons to the fluorine (seen in Figure III-2) nor the partial resolution of the fluoro-resonances from Ftyr21 and 24 (Figure IV-2) are seen in the spectrum of Figure V-1 due to the width of the lines.

Figures V-3, 4 and 5 show the effect of temperature on the Fphe and Ftyr resonances. In these vesicles, the monofluorinated lipid, 8-fluoro-dipalmitoyl phosphatidylcholine (8-FDPPC) was also included in the preparation to allow the

---

[32] The CL is from beef heart thus the fatty acyl chains will be a mixture of stearic and oleic acids.

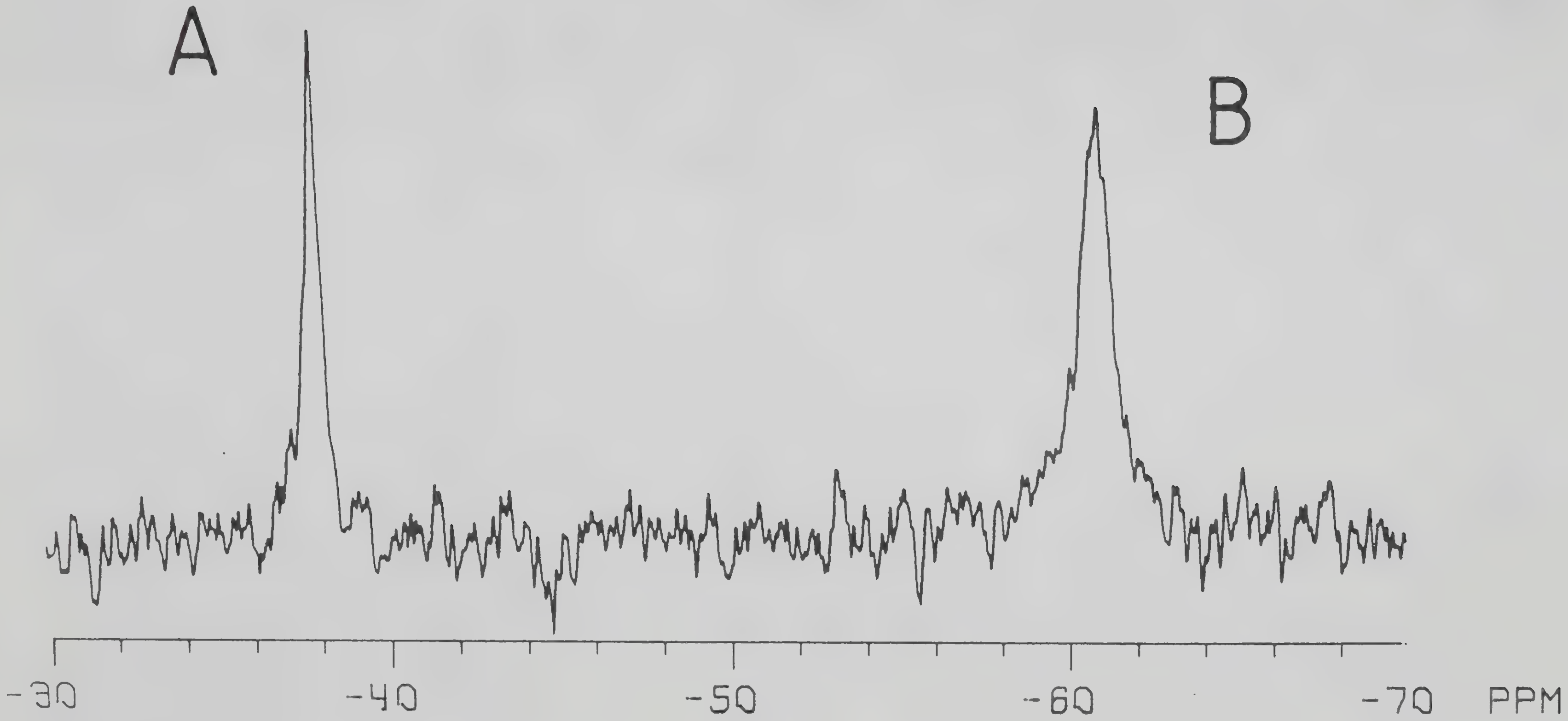

Figure V-1 The ^{19}F NMR spectrum of Fphe- and Ftyr-labelled M13 coat proteins reconstituted into small unilamellar vesicles. The sample was prepared using 17 mg each of Fphe- and Ftyr- labelled, lyophilized, coat proteins, by the urea-cholate procedure (see Chapter II-E) and contained 60mM Tris-HCl (pH8.0) and 1mM EDTA. The final D_2O content was 67%. Resonance A is from the Fphe residues while resonance B is from the Ftyr residues. The spectrum was collected at 303°K using a pulsewidth of 13 usec (69°), a sweepwidth of ± 6300 Hz and 4K data points, with a delay of 200 msec between transients. It was the result of 30,000 scans using 25 Hz linebroadening.

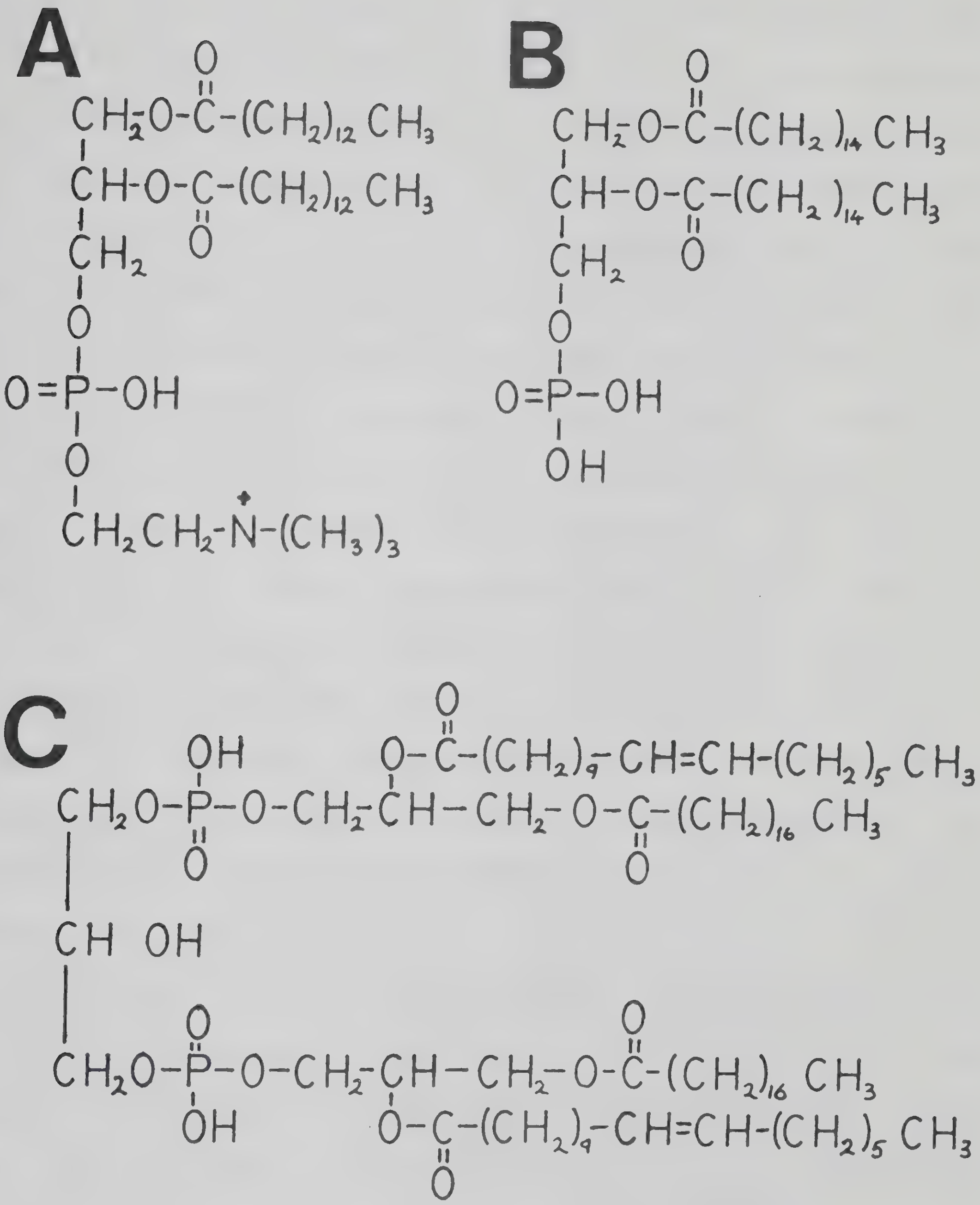

Figure V-2 The chemical structures of dimyristoylphosphatidylcholine (DMPC), dipalmitoyl phosphatidic acid (DPPA) and cardiolipin (CL). Structure A is DMPC, structure B is DPPA and structure C is CL. The CL structure shows two stearic and two oleic fatty acid chains per molecule. The CL is from beef heart, which actually contains a heterogeneous mixture of stearate and oleate chain content.

fluidity of the lipids to be monitored simultaneously. Figure V-3 shows the spectra obtained at two temperatures, the 8-FDPPC resonance appearing at -104.7 ppm. Comparison of the spectrum obtained at 317°K [Figure V-3(ii)] with that obtained at 292°K [Figure V-3(i)] indicates that all three resonances, but particularly, the Ftyr and the 8-FDPPC resonances are broader at the lower temperature. In addition to the linebroadening at the lower temperatures a change in lineshape was observed. With the signal to noise of the spectra shown, the resonances at 317°K may be fit approximately with a single Lorentzian curve. At 292°K, however, this is not possible; there is a "broad" component underneath the "narrow" component. To improve the signal to noise of the 8-FDPPC resonance to allow a quantitative analysis of the spectra, vesicles were prepared with a higher concentration of the 8-FDPPC. The resulting 8-FDPPC spectra at 292°K and 317°K are shown in the insets of Figure V-3. All of the 8-FDPPC spectra in the temperature series were analysed as the sum of two Lorentzians and the relative contribution of the broader component to the total area of the 8-FDPPC resonance as a function of temperature is shown in Figure V-4(A). As well, the linewidth of the broad component of the 8-FDPPC resonance as a function of inverse temperature is shown in Figure V-4(B). There is a certain amount of error in the measurements but the trend is readily apparent: as the temperature is lowered through the phase transition of the DMPC (24°C), there is a trend

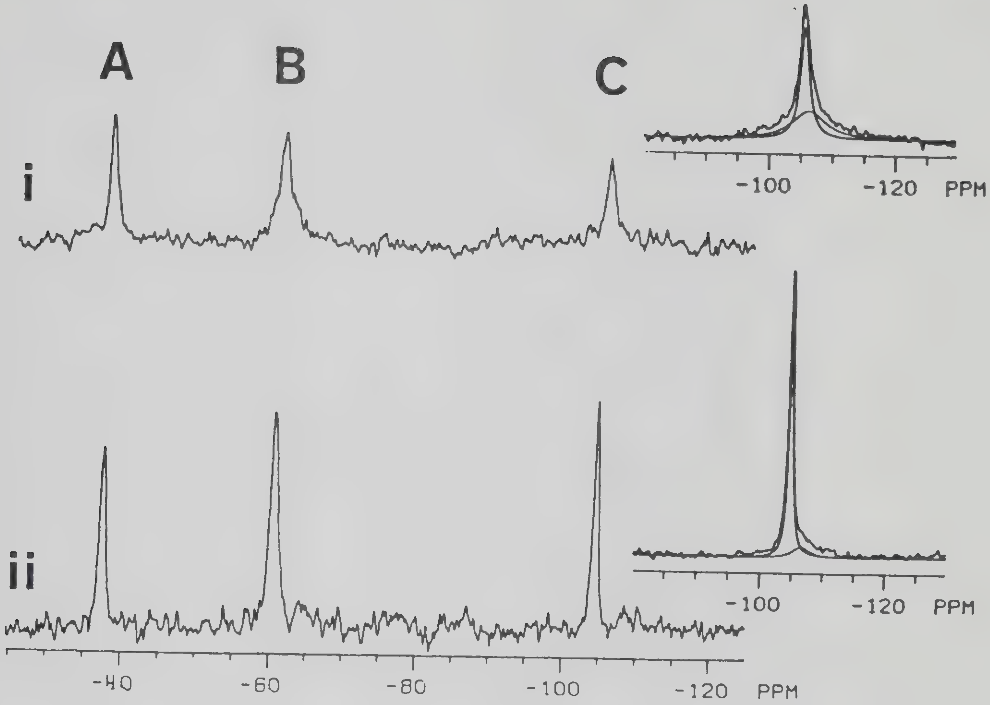

Figure V-3 The ^{19}F NMR spectra of Fphe- and Ftyr-labelled M13 coat proteins reconstituted into 8-FDPPC-labelled vesicles at two temperatures. The sample was prepared by the cholate procedure using 15 mg each of Fphe- and Ftyr-labelled , lyophilized, coat protein and 0.8 % 8-FDPPC (by weight), and contained 60 mM NH_4CO_3 (pH 8.0); the final D_2O content was 37%. The spectral resonances are: A) Fphe; B) Ftyr; C) 8-FDPPC. The spectra were acquired at: i) 292°K (40,000 scans); ii) 317°K (20,000 scans). The spectra were collected using a pulsewidth of 12 μsec (64°), a sweepwidth of ±50,000 Hz, 8K data points, and a delay of 300 msec between transients. The inset 8-FDPPC resonances were from vesicles made with 2.4% 8-FDPPC (by weight). The upper inset resulted from 30,000 scans while the lower, from 15,000. The broad and narrow spectral components of these resonances (from computer simulations) are shown by the smooth curves.

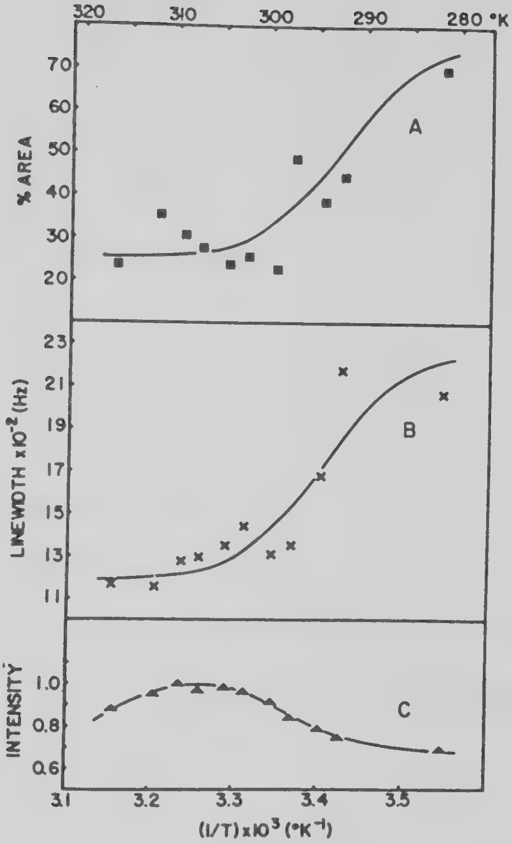

Figure V-4 The analyses of the broad spectral component of the 8-FDPPC resonance from 8-FDPPC-labelled vesicles containing Fphe- and Ftyr-labelled M13 coat proteins with temperature. (A) The increase in percent area of the broad spectral component of the 8-FDPPC resonance as a function of the inverse temperature. The data were obtained by simulating the 8-FDPPC lineshape using two Lorentzians (see Figure V-3). The computer then calculated the relative areas of the simulated peaks. The curve through the points is the same as that drawn through the points in (B). (B) The ^{19}F-NMR linewidths of the broad components of the 8-FDPPC spectra (see Figure V-3) plotted as a function of inverse temperature. (C) The relative total intensities of the 8-FDPPC peak as a function of temperature. The 8-FDPPC resonances were integrated, then normalized to the maximum intensity, at 310°K. The curves through the data points in Figures V-4 and V-5 were drawn to indicate a levelling off at low temperature to be consistent with the data for 8-FDPPC [Figure V-5(C)] which had the highest signal-to-noise ratio.

towards the broad component. This trend is reversible as the temperature was varied pseudo-randomly. The behavior of the linewidth of the broad component of the 8-FDPPC resonance with temperature also reflects the phase transition temperature of the DMPC [as does the linewidth of the narrow component (see below)].

To determine whether we were seeing all of the 8-FDPPC signal, the area of the 8-FDPPC resonance was measured as a function of temperature. The results are shown in Figure V-4(C). The spectral parameters were the same for all the spectra collected. A significant decrease in intensity is observed below, and a slight decrease above, 310°K. The decrease in intensity below 310°K is interesting as the inflection point of the curve is near the T_m of the DMPC, 297°K. Again, this behavior is reversible as the points were obtained pseudo-randomly.

To study the correlation between temperature and the linewidth of the narrow components for Fphe, Ftyr and 8-FDPPC, the linewidths of the narrow components were plotted as a function of the inverse temperature in Figure V-5. The melting temperature (T_m) of the DMPC is 3.376×10^{-3}°K^{-1} on these graphs. Curves A and B show the effect of temperature on Ftyr and Fphe resonances, respectively, of labelled protein in vesicles while curve C shows the simultaneous effect of temperature on the 8-FDPPC. As the temperature is lowered from 317°K (3.155×10^{-3}°K^{-1}), the linewidths of all three resonances initially broadened

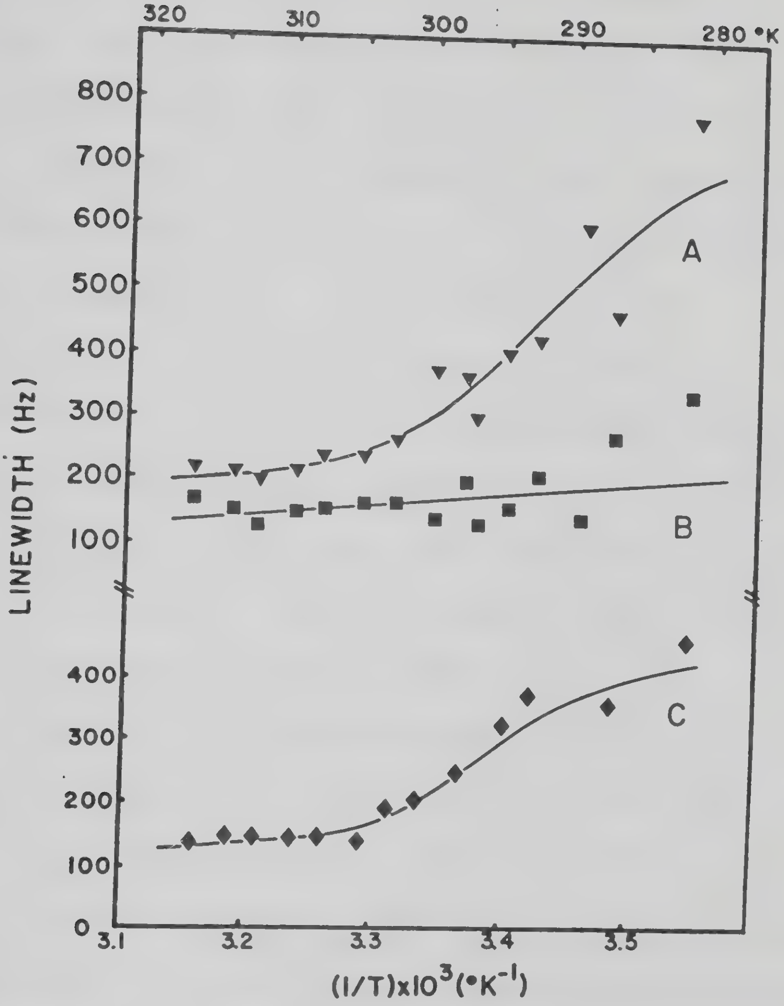

Figure V-5 The plots of the linewidths of the narrow components of the ¹⁹F resonances of Fphe- and Ftyr-labelled M13 coat proteins reconstituted into 8-FDPPC-labelled vesicles as a function of the inverse temperature. The linewidth data were obtained (see Figure V-3) from the following resonances: A) Ftyr; B) Fphe; C) 8-FDPPC. The curves through the data points in Figures V-4 and V-5 were drawn to indicate levelling off at low temperature to be consistent with the data for 8-FDPPC [Figure V-5(C)] which had the highest signal-to-noise ratio.

linearly with reciprocal temperature. As the Tm of the DMPC is approached, the increase in the linewidths of the Ftyr and 8-FDPPC resonances becomes nonlinear and the linewidths increase dramatically. The increase in linewidth of the Fphe resonance remains linear throughout the temperature range until ~292°K, where it, as well, increases nonlinearly.

The chymotryptic digestion of the Fphe- and Ftyr-labelled coat protein in vesicles was done to determine both the relative exposures of the residues to the enzyme and the orientation of the protein across the bilayer. The results of this digestion are shown in Figure V-6. Figure V-6(A) shows the decrease of the area of the Fphe protein resonance at -38.0 ppm with the concomitant appearance of a free Fphe peptide resonance at -38.5 ppm. The relative areas of the protein and peptide resonances cannot be compared as care was not taken to prevent saturation of the peptide resonance; spectral parameters were optimized for collection of the protein resonance which has a shorter T_1 than the peptide resonance. Comparison of either resonance as a function of time is, however, valid. Comparison of the area under the Fphe protein resonance before the addition of chymotrypsin, to that of the protein resonance after 3.5 hours of digestion, indicates that 1/3 of the Fphe's have been cleaved. Chymotrypsin predominantly cleaves at the C-terminal side of exposed phenylalanine, tyrosine, and tryptophan residues. The phe (Fphe) cleavage sites of the coat protein were available when it is in DOC

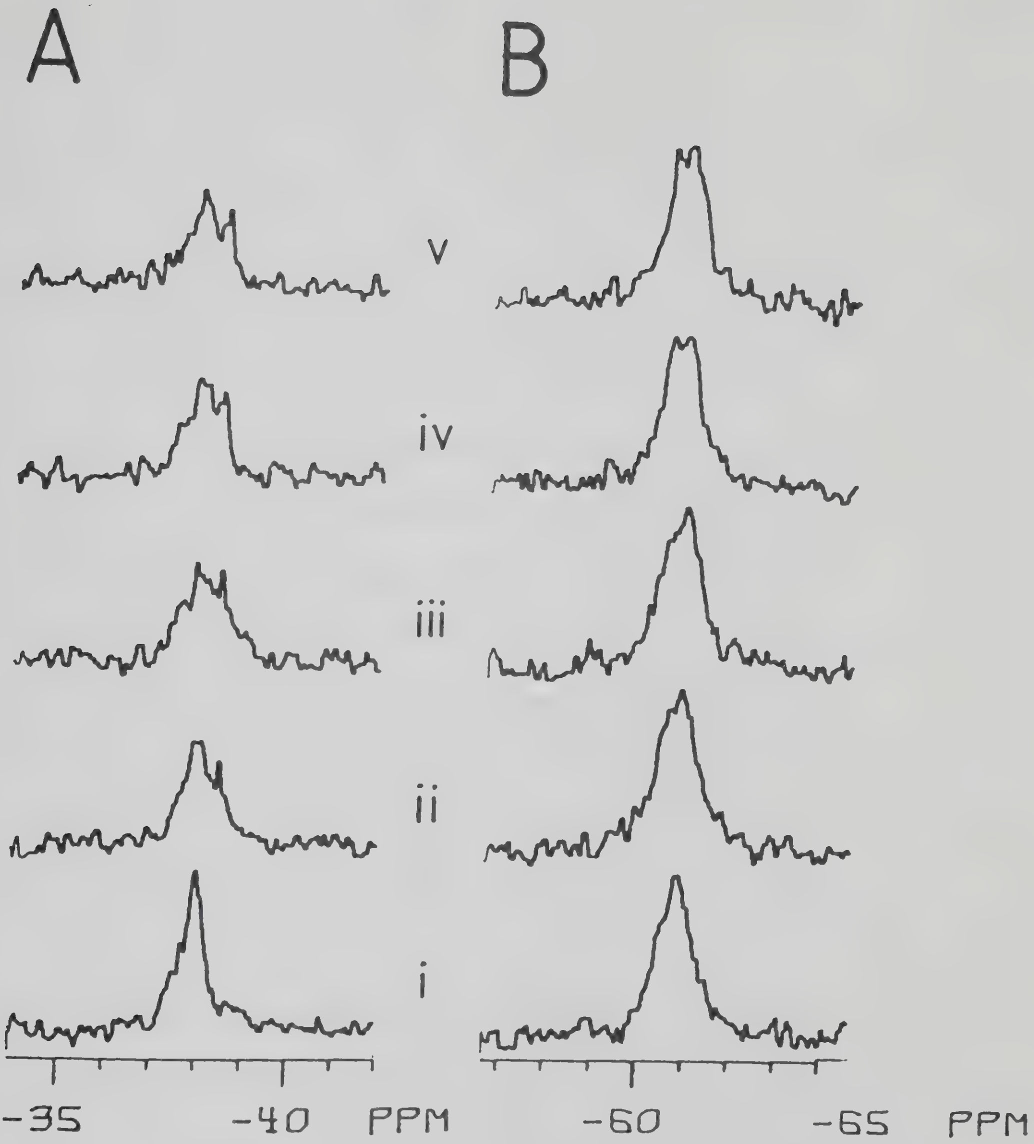

Figure V-6 The ^{19}F NMR spectra of the chymotryptic digestion of the Fphe- and Ftyr-labelled M13 coat proteins reconstituted into vesicles. The sample was prepared as outlined in Figure V-3 (the final D_2O content was 50%). The resonances in A are from Fphe residues, while the resonances in B are from Ftyr residues. The spectra were collected at the following times after the addition of the enzyme (the final concentration was 67 μg/ml): i) 0 hr; ii) 0.5; iii) 1.5; iv) 2.5; v) 3.5. The spectra contained 10,000 scans each and were collected at 309°K with a pulsewidth of 14 μs (74°), a sweepwidth of ±6300 Hz ,4K data, and a delay between transients of 200 ms. The linebroadening was 20 Hz.

micelles; the tyr (Ftyr) sites were not exposed (Chapter IV-A). When the protein is in lipid vesicles only half of the protein termini are exposed; the other half are protected inside the vesicle. Thus 1/3 of the Fphe residues would be released, regardless of the orientation of the protein in the membrane: exposed N-termini would be cleaved at Fphe11 releasing Fphe11, while exposed C-termini would be cleaved at Fphe42 and Fphe45, releasing Fphe45. In both orientations, two phenylalanines would be left with the vesicle-bound protein. Paper electrophoresis of the released peptide fragments showed that fragments were obtained from both the N- and C-termini (data not shown).

Figure V-6B shows the Ftyr region of the spectra during digestion. There is no release of Ftyr-containing peptides seen in these spectra (these would have been seen at ~-61.8 ppm); nor is tyrosine found in the amino acid analysis of the fragments. It is apparent, however, that the release of the Fphe peptides causes a change in the environment of the Ftyr residues as indicated by the change in lineshape with digestion.

Discussion

The temperature and chymotryptic digestion studies have given information on the location of the Fphe and Ftyr residues of the coat protein with respect to the membrane. (Although the Fphe and Ftyr resonances from the vesicle-bound coat protein are too wide to detect individual residue

behavior, the information obtained shows whether or not they are within the membrane bilayer.) At temperatures above the phase transition temperature of the major lipid (DMPC), the linewidths of the "narrow" components of the Fphe, Ftyr and 8-FDPPC have a linear dependence upon the reciprocal temperature (Figure V-5). This is the expected dependence if the linewidth ($\Delta\nu$) is dominated by τ_c, the overall correlation time of the particle: the "particle", in this case, is the vesicle which has been assumed to be spherical, thus, the Stokes-Einstein relationship will apply:

$$\tau_c = \frac{4}{3} \frac{\pi r^3 \eta}{kT} \cong \frac{K'}{T}$$

$$\Delta\nu \;\alpha\; \tau_c \text{, therefore } \Delta\nu \;\alpha\; 1/T$$

where r is the radius of the vesicle, η is the viscosity of the medium, k is Boltzman's constant and T is the temperature.

As the temperature is lowered through the phase transition temperature, the Ftyr and 8-FDPPC resonances broaden dramatically. Qualitatively, this suggests that their internal motions are being severely restricted; the transition of the DMPC lipids to the gel state is inhibiting the Ftyr ring and 8-FDPPC methylene chain mobilities. (η is no longer a constant but increases as the lipids become rigid.) The Fphe is not affected at the transition temperature but appears to broaden nonlinearly below ~19°C. This possibly reflects an increase in the viscosity of the

solution as the particles in it have become "rigid". It is clear, though, that the Fphe linewidths do not reflect the T_m of the DMPC as the Ftyr and 8-FDPPC linewidths do, thus showing that the Fphe residues are outside the lipid bilayer.

The topology of the Fphe and Ftyr residues with respect to lipid bilayer suggested by the temperature studies was confirmed by the chymotryptic digestion results. Previous, studies have shown that the chymotryptic digestion of the protein in DOC micelles resulted in cleavage at the three phenylalanines but not at either of the two tyrosines (Chapter IV-A). It was concluded that the Ftyr residues were within the hydrophobic core of the micelle and consequently were protected from the protease, while the Fphe residues were outside the micelle and therefore exposed. The situation for the vesicle-bound protein has been found to be similar in that the protein Fphe residues are susceptible to chymotryptic cleavage while the Ftyr residues are not. In this case, however, only half of the termini are exposed; the other half are in the internal space of the vesicle. This raises the question of protein orientation: is the protein oriented with the N-termini on only one side of the membrane (asymmetrical orientation) or are the N- and C-termini distributed randomly on both sides of the bilayer (symmetrical orientation). Paper electrophoresis of the hydrophilic fragments released show that there is digestion of both the N- and C-termini. This indicates that the

protein is symmetrically incorporated into the vesicle. Wickner (1976) has suggested that symmetrical orientation may also result from the protein being incorporated not transmembranously, but in a "U" conformation.

The curve-fitting analyses of the spectra of the Fphe/Ftyr-labelled coat protein in vesicles not only showed the sensitivity of their linewidths to temperature (dicussed above) but as well, showed that their lineshapes changed with temperature (Figure IV-4): as the temperature was decreased, a broad component developed. Two possible explanations for the two (multi-)state nature of the system are discussed herein: vesicle aggregation (without fusion), or phase separation due to the mixed lipid composition.

Evidence for the existence of reversible vesicle aggregation is found in two observations. Firstly, it was qualitatively observed that as the temperature was lowered, the NMR sample became turbid, indicative of "larger-particle" formation. [If the sample was placed in the refrigerator (4°C) overnight, the vesicles would settle to the bottom of the tube.] Secondly, the comparison of the linewidths of the broad components with those of the narrow components showed they were approximately eight times larger at all temperatures. In the limit where the internal motions of the protein amino acid sidechains are faster than the overall rotational correlation time for vesicle rotation, which certainly pertains to this situation, the linewidth of the resonance is directly proportional to the correlation

time (Marshall *et al.*, 1972), and hence, to r^3 (see the Stokes-Einstein equation, given above.) This predicts that, if the broad component results from an aggregate of the monomeric vesicles, the ratio of the radii of the aggregates to that of the monomer should be given by:

$$\sqrt[3]{\frac{\Delta\nu_b}{\Delta\nu_n}} = \frac{r_b}{r_n}$$

where $\Delta\nu_b$ and r_b are the linewidths and radii of the broad components and $\Delta\nu_n$ and r_n are the linewidths and radii of the narrow components. From the data at all temperatures, the radius of the vesicles giving the broad component of the spectrum is calculated to be 1.94 ±0.17 times that of the vesicles giving the narrow component.

In terms of this model the decrease in intensity of the 8-FDPPC resonance below 310°K, shown in Figure V-4(C), is taken as evidence for higher orders of aggregation. If tetramers were formed, for example, their linewidth would be 64 times that of the narrow monomer component and they would be too broad to be observed. The decrease in intensity seen above 310°K where only the narrow component exists is most likely due to the expected change in T_1 with increasing temperature. As the temperature increases, the T_1 becomes longer. The spectral acquisition parameters were constant throughout the entire temperature study so that as the T_1 increased, the resonances became more saturated.

Although the above discussion offers an explanation for the linewidth data, Figure V-4(A) shows that in the temperature range (282-317°K), there is never less than ~20% of the broad component present at the highest temperature. If the two-component phenomenon was purely a DMPC-phase-transition-modulated aggregation, one would expect the curve to show all monomer above the T_m. That there is ~25% of the broad component present at 317°K raises the suspicion that the non-DMPC lipids (20% of the total lipid), whose T_m's are higher than 317°K, may actually be in pseudo-gel state patches. This would result in two commponent spectra. The presence of the narrow component at 282°K may be explained by typical behavior of small unilamellar vesicles (SUV's)(see Evans and Parsegian, 1983). SUV's are strained spheres with high radii of curvature above the T_m of their lipids. As the temperature is lowered through the phase transition, the strain causes the spheres to become polygonal, to relieve the tension. The lipids in the interspace between the polygonal faces would have greater methylene chain mobility than those in the gel state faces and consequently ^{19}F-labelled lipid (or protein) in these regions would result in the narrow components seen.

From the above discussion, it is not clear which model, either reversible vesicle aggregation or lipid phase separation, is the best explanation of the results. However, it does not affect the validity of the motion analysis to be presented in Chapter V-B, as the data used was obtained from

the narrow component at 303°K (above the DMPC phase transition temperature) and therefore pertains to the protein in liquid-crystalline lipids in monomeric vesicles.

The results of this Chapter have shown that the topology of vesicle-bound coat protein is the same as that of DOC micelle-bound coat protein: namely, the Fphe residues are outside the bilayer and the Ftyr residues are either at the interface or inside the bilayer. As well, the coat protein in vesicles were found to be symmetrically oriented, with both the N- and C-termini accessible from the outside of the vesicle. This observation, combined with a preliminary result that asymmetric incorporation of the coat protein (the N-terminus on the outside of the vesicle) can be obtained when the vesicles are prepared using higher concentrations of cholate (the "modified cholate procedure"), leads one to wonder whether the vesicle-bound coat proteins are dimers or higher aggregates and whether the DOC micelle-bound dimers are in head to tail or head to head conformations. These questions, along with determining whether the absence of cardiolipin has any effect on the coat protein structure, remain to be answered by further experiments.

B. The Analyses of Fphe and Ftyr Ring Motions

Introduction

There has been considerable interest in the internal motions of amino acids of proteins. Results of residue mobility studies give information as to the structure around the residue in the protein; the more "structured", the less mobile the residue. Most work has been done on water-soluble proteins which tend to be the best characterized, the most available, and the easiest to study (for a recent review,, see Jardetzky and Roberts, 1981). Membrane-bound proteins have been studied much less (Kinsey *et al.*, 1981). For these proteins the mobility of individual residues is not only influenced by the secondary and tertiary structure of the protein, but, as well, by the structure of, and interaction with, the surrounding lipids. The extent of the influence of the lipids is not well documented.

Motion analyses will also give another criterion to determine whether DOC micelle-bound coat protein structure is the same as that of phospholipid vesicle-bound coat protein. Qualitative and quantitative discussions have been presented in Chapter IV-B of the Fphe and Ftyr ring mobilities of DOC micelle-bound coat protein. The results of the motion analyses of Fphe and Ftyr relaxation data from vesicle-bound coat protein will be presented in this Chapter.

Theory

The overall goal of this Chapter is to quantitate the internal mobility of the side chain residues of a membrane-bound protein from an analysis of NMR relaxation parameters measured as a function of resonance frequency. The relaxation parameters include the spin lattice relaxation time (T_1), the transverse relaxation time (T_2), and the nuclear Overhauser effect (nOe). A brief description of each of these follows: (more detailed explanations are available in, for example, Slichter, 1978.)

Spin Lattice and Transverse Relaxation Times, T_1 and T_2

In a one-pulse Fourier transform NMR experiment, the net magnetization (M_0) of a diamagnetic sample starts aligned against the field (B_0) as shown in Figure V-7(i). (This is arbitrarily called the z-axis of the Cartesian coordinate system). A second field (H_1) is applied along the x-axis in the form of a radiofrequency pulse, the result being that the magnetization is moved away from the z-axis in Figure V-7(ii). (The diagram is assuming that there is only a single type of spin nucleus in the sample and that the viewer is in a reference frame that is rotating at the resonant frequency of that nucleus, so that the magnetization vector follows the simple pathway from the z-axis as shown.)

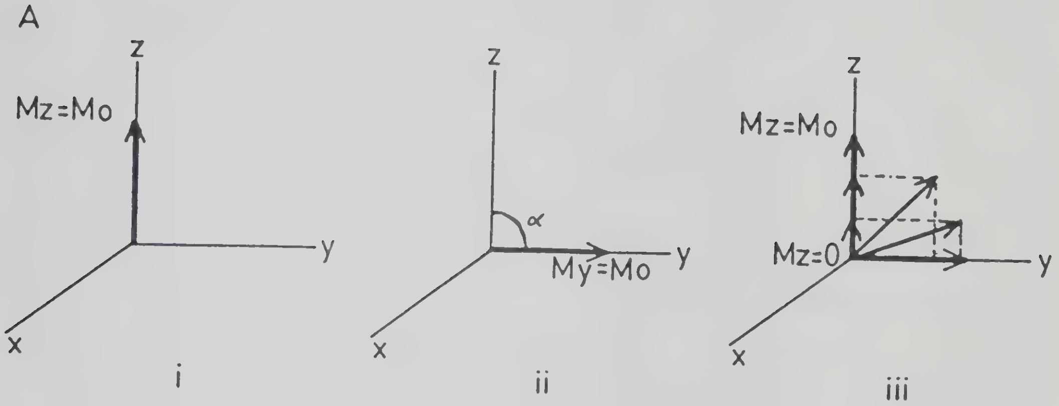

Figure V-7 Diagrammatic representations of the behavior of the net magnetization of spin 1/2 nuclei in a reference frame rotating at the resonance frequency of the nuclei. The 3-dimensional axes show the net magnetization of the nuclei: i) after the sample has been placed in the magnet ($M_z = M_0$, M = 0); ii) after the H_1 field has been applied along the x-axis for a time, t , to cause the net magnetization to rotate through an angle, α radians [in this case $\pi/2$ radians (or a 90° pulse)]; iii) as the net magnetization relaxes along the z-axis from $M_z = 0$ to $M_z = M_0$, with a time constant T_1. (The component of the net magnetization along the y-axis relaxes with a time constant T_2.)

The longer the pulse, the further the magnetization is moved such that

$$\alpha = \gamma H_1 t_p$$

where α is the angle to the z-axis in radians, γ is the gyromagnetic ratio of the nucleus, and t_p is the length of the pulse. Thus, a $\pi/2$ radian pulse (90° pulse) is one that is on long enough to move the magnetization to the y-axis. Once H_1 is shut off, the magnetization slowly (or quickly) returns to equilibrium by realigning with B_0. T_1 is defined as the time constant for the exponential recovery of the magnetization along the z-axis to return to its M_0 value:

$$M_z(t) = M_0\ (1-(1-\cos(\alpha))\ \exp(-t/T_1))$$

T_1 can vary from less than a second to hours, depending upon the nucleus and its environment (spin lattice).

Figure V-7 also shows the behavior of the net magnetization along the y-axis after a 90°pulse. As the net magnetization increases along the z-axis to $M_z = M_0$, the magnetization along the y-axis decreases from $M = M_0$ to $M = 0$. The time constant for the exponential decrease of the magnetization along the y-axis is T_2. T_2 is visualized by the decay of the FID during acquisition (which is directly proportional to $\exp(-t/T_2)$ where t is the time after the 90° pulse) and, hence, by the width ($\Delta\nu$)

of the Fourier transformed signal [$\Delta\nu = 1/(\pi T_2)$].

The T_2 (observed) that is obtained from the measurement of the resonance linewidth is caused by two types of mechanisms. The first, is due to the natural T_2 processes of the spins; the second is due to field inhomogeneity ($T_2\dagger$). Thus,

$$\frac{1}{T_2\text{(observed)}} = \frac{1}{T_2} + \frac{1}{T_2\dagger}$$

For narrow linewidths (<5 Hz), field inhomogeneity contributes significantly to the width of the line, so that elaborate pulse sequences are required to determine the true T_2 (Farrar and Becker, 1971). For broad lines (>20 Hz), the contribution to the linewidth from field inhomogeneity is small, therefore linewidth measurements may be used (providing that broadening due to other processes like chemical exchange is not present). The maximum that T_2 can be is $T_2 = T_1$, when $\omega_0\tau_c \ll 1$ (ω_0 is the spectrometer frequency and τ_c is the overall correlation time of the tumbling of the molecule in solution). For proteins, $\omega_0\tau_c$ is usually $\gg 1$, thus protein T_2 values tend to be much smaller than T_1.

Nuclear Overhauser Effect

The nOe is a method to determine "through-space" interactions. It involves the irradiation (and saturation) of the nuclei to which the observed nuclei

are dipolar coupled, prior to the pulse and acquisition of the observed nuclei (see Chapter II-F). The effect is to either increase, to have no effect or to decrease the observed nuclei signal intensities. The mechanism by which the effect takes place is complex (see Noggle and Schirmer, 1971) but involves alterations of the equilibrium populations of the energy states of the observed and coupled nuclei, and the mechanisms by which they are relaxed. The resulting "enhancement" can range from $0.5(\gamma_s/\gamma_i)$, where γ_s is the gyromagnetic ratio of the coupled nuclei and γ_i is the gyromagnetic ratio of the observed nuclei, to $-(\gamma_s/\gamma_i)$, depending upon the correlation time of the molecule and the nuclei involved. For observing ^{19}F and irradiating ^{1}H, the enhancement ranges from 0.53 to -1.06.

The Model

In the derivation of the equations which relate the experimentally measured variables to the parameters which characterize the motions within the system, two approaches are possible (for recent reviews see London, 1980; Jardetzky annd Roberts, 1981). The first approach is to make no assumptions about what kinds of motion are present; the second is to assume a particular physical model for the motions. We have chosen the second approach for two reasons. Firstly, it limits the number of variable parameters by fixing the bond angles around which motions are allowed and only letting the

timescales of the motions be unknowns. This is necessary in our case given that only a limited number of measurements are possible and two relaxation mechanisms are present. The second reason for choosing the model dependent approach is that the contributions of the various time scales determined with the model independent approach are invariably rationalized in retrospect in terms of the physically most meaningful model for the motions. Time scales of the same orders of magnitude are extracted from the data in either case.

The model we have used for the possible motions is shown in Figure V-8. This model allows restricted rotation (or wobble) about the $\alpha\beta$-bond of the aromatic ring of the amino acid side chain, free rotation about the $\beta\gamma$-bond, and overall spherical symmetry for vesicle rotation. Other motions of the α-carbon backbone of the protein with the vesicle such as lateral diffusion are, of course, possible and can be incorporated into this model by reducing the effective overall rotational correlation time for the protein. Further, experimental evidence from solid state NMR (Gall *et al.*, 1982) indicates that rapid vibration of the aromatic ring, coupled with rarer 180° flips may be a better model than free diffusion for rotation about the $\beta\gamma$-bond.

The derivations of the equations of motion are outlined by Wittebort and Szabo (1978). We have extended their equations to include chemical shift anisotropy as

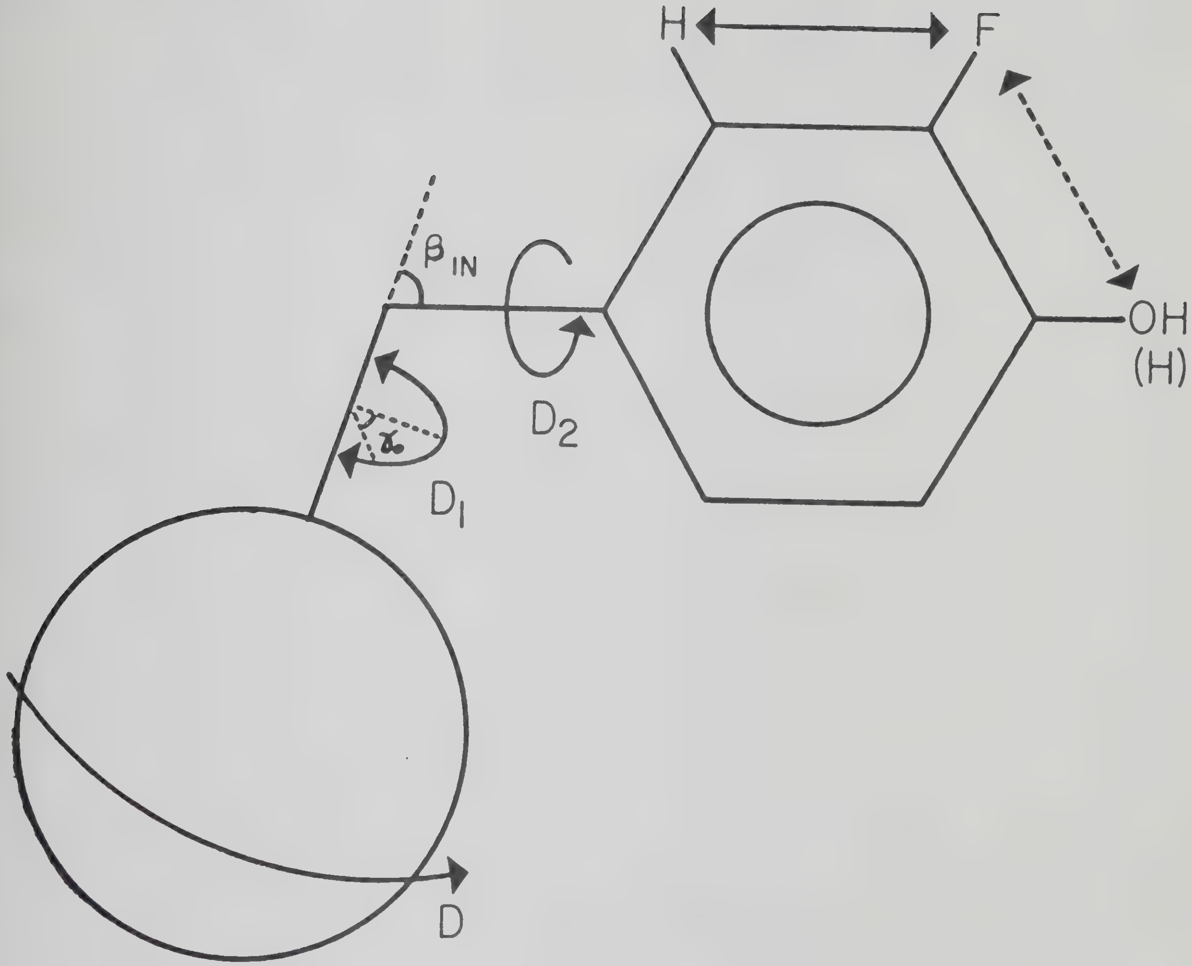
H
F
β_{IN}
OH
(H)
D_2
α_0
D_1
D

Figure V-8 A diagram of the rotations, angles, and possible dipolar interactions of the model assumed for the analysis of the Fphe and Ftyr relaxation data.

a relaxation mechanism. Dipolar interactions are calculated between the fluorine nuclei and the adjacent ring protons only. The dipole-dipole contribution to the spin lattice and transverse relaxation rates is given by:

$$1/T_1^{dd} = K \cdot F_1$$

$$1/T_2^{dd} = (K/2) \cdot F_2$$

where

$$K = (1/10)\gamma_F^2 \gamma_H^2 \hbar^2 / r_{F-H}^6$$

$$F_1 = J(\omega_F - \omega_H) + 3J(\omega_F) + 6J(\omega_F + \omega_H)$$

$$F_2 = F_1 + 4J(0) + 6J(\omega_H)$$

$$J(\omega) = \sum_{n=0}^{9} \sum_{b_1 b_2 = -2}^{2} (f_{nb_2}/(f_{nb_2}^2 + \omega^2)) \tilde{\Gamma}_{b_1 b_1 n}(\gamma_o) \times [d_{b_1 b_2}(\beta_{IN})]^2 [d_{b_2 0}(\beta_{NF})]^2$$

$$f_{nb_2} = 6D + \frac{D_1 n^2 \pi^2}{4\gamma_o^2} + b_2^2 D_2$$

$$n = 0 : \quad \tilde{\Gamma}_{b_1 b_1 n}(\gamma_o) = \sin^2(b_1\gamma_o)/(b_1\gamma_o)^2$$

$$n \geqq 1 : \quad \tilde{\Gamma}_{b_1 b_1 n}(\gamma_o) = \frac{b_1^2\gamma_o^2\,[\cos^2(b_1\gamma_o)(1-(-1)^n) + \sin^2(b_1\gamma_o)(1+(-1)^n)]}{[b_1^2\gamma_o^2 - (n\pi/2)^2]^2}$$

The chemical shift anistropy contributions to the relaxation rate is given by:

$$1/T_1^{CSA} = (6/40)\gamma_F^2 H_o^2 \delta_Z^2 \sum_{b_2=0}^{2} \sum_{n=0}^{9} C_{b_2n} J_{b_2n}(\omega_F)$$

$$1/T_2^{CSA} = (1/40) \gamma_F^2 H_o^2 \delta_Z^2 \sum_{b_2=0}^{2} \sum_{n=0}^{9} C_{b_2n} \times[3J_{b_2n}(\omega_F) + 4J_{b_2n}(0)]$$

where

$$J_{b_2n}(\omega) = 2f_{b_2n} / (f_{b_2n}^2 + \omega^2)$$

$$f_{b_2n} = 6D + \frac{n^2\pi^2 D_1}{4\gamma_o{}^2} + b_2^2 D_2$$

$$C_{b_2n} = \sum_{b_1=-2}^{2} \tilde{\Gamma}_{b_1b_1n}(\gamma_o) [d_{b_1b_2}(\beta_{IN})]^2 C_{b_2}$$

$$C_{b_2} : C_o = (1/4)[(3\cos^2\beta-1) + \eta\sin^2\beta\cos2\gamma]^2$$

$$C_1 = (1/3)\sin^2\beta[\cos^2\beta(3-\eta\cos2\gamma)^2 + \eta^2\sin^2 2\gamma]$$

$$C_2 = [\sqrt{3/4} \sin^2\beta + [\eta/(2\sqrt{3})] (1+\cos^2\beta)\cos2\gamma]^2 + (\eta^2/3)\sin^2 2\gamma \cos^2\beta$$

Neglecting cross-correlation between the two relaxation mechanisms, the total relaxation rates are given by:

$$1/T_1 = 1/T_1^{dd} + 1/T_1^{csa}$$

$$1/T_2 = 1/T_2^{dd} + 1/T_2^{csa}$$

and the nOe is given by:

$$\text{Fphe:} \quad \frac{\gamma_H}{\gamma_F} \; \frac{\sigma_{H_2F} + \sigma_{H_4F}}{\rho^{DD}_{H_2F} + \rho^{DD}_{H_4F} + \rho^{CSA}} = \frac{\gamma_H}{\gamma_F} \; \frac{\sigma_{H_2F} + \sigma_{H_4F}}{1/T_1{}^{Fphe}}$$

$$\text{Ftyr:} \quad \frac{\gamma_H}{\gamma_F} \; \frac{\sigma_{HF}}{\rho^{DD} + \rho^{CSA}} = \frac{\gamma_H}{\gamma_F} \; \frac{\sigma_{HF}}{1/T_1{}^{Ftyr}}$$

The nomenclature is that of Hull and Sykes (1974,1975b) and Wittebort and Szabo (1978), where γ_F and γ_H are the fluorine and proton gyromagnetic ratios, respectively, ω_F and ω_H are the fluorine and proton resonance frequencies, respectively, $D = 1/(6\tau_c)$ where τ_c is the overall rotational correlation time for the protein, D_1 is the wobble frequency about the $\alpha\beta$-bond, D_2 is the ring rotation frequency about the $\beta\gamma$-bond and γ_0 is the angle through which the ring "wobbles" (see Figure V-8).

Results

The NMR spectral data required for motion analysis include T_1, $\Delta\nu$, and nOe measurements. These data for Fphe- and Ftyr-labelled coat proteins reconstituted into vesicles are given in Figure V-9 and Table V-1. These measurements were taken at 303°K where the resonances are dominated by the narrower component (see Chapter V-A). The linewidths were measured at 141, 254 and 376 MHz, while the T_1's and nOe's were collected at 141 and 254 MHz. The T_1's were obtained by progressive saturation method in the absence of any ^1H irradiation (Hull & Sykes, 1975a)(see Chapter II-F). The nOe's resulted from irradiation of the entire proton spectrum (see Chapter II-F).

One other parameter that is required is the correlation time for the vesicle rotation, τ_c. This is related to the radius of the vesicles by Stokes-Einstein equation (see below). An electron micrograph was taken of vesicles from an NMR sample used for the above measurements. The sizes of 178 vesicles were measured; their size distribution is shown in Figure V-10. The mean radius was 159 ±63Å.

Discussion

Upon inspection of Figure V-10 showing the size distribution of the vesicles, it is obvious that the vesicles are a mixed population of sizes. As every size of vesicle will have its own characteristic correlation time and that the T_1, nOe, and particularly, linewidth results depend on the

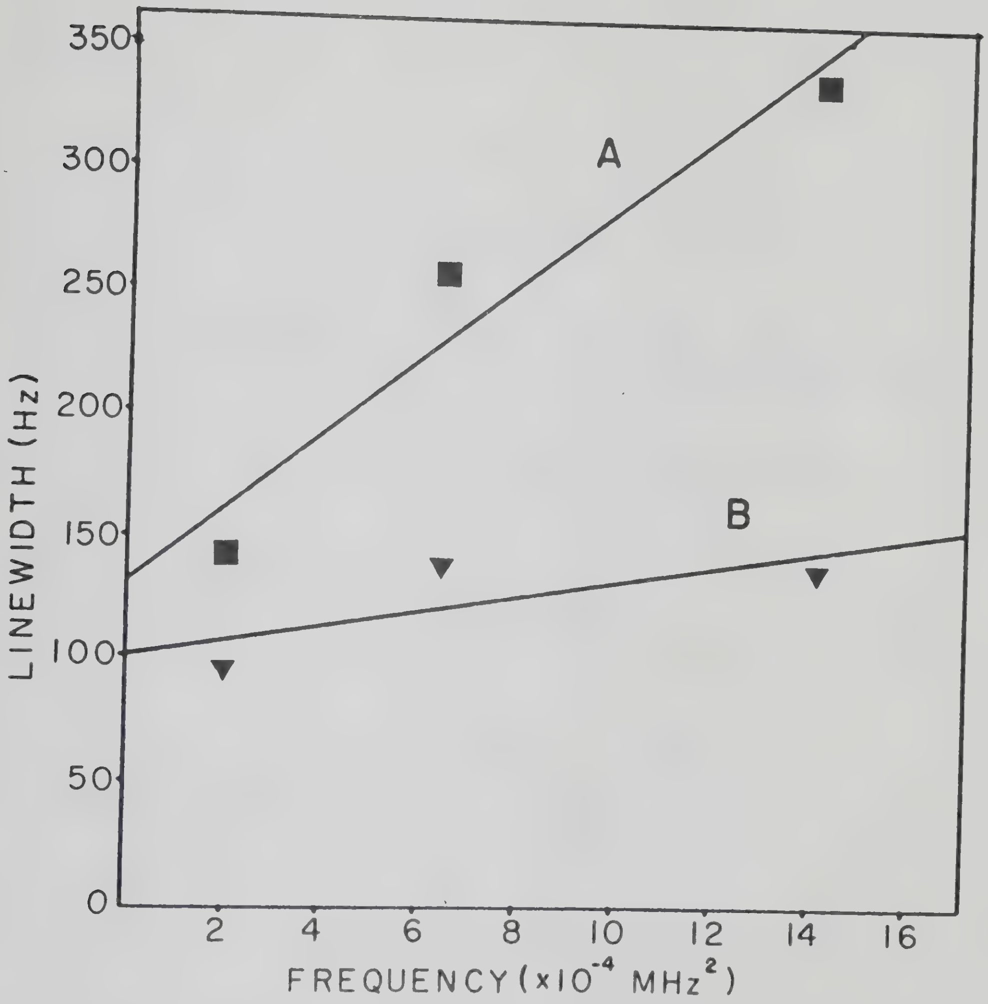

Figure V-9 The ^{19}F NMR linewidths for Fphe- and Ftyr-labelled M13 coat proteins in vesicles plotted as a function of the square of the spectrometer frequency. Line A is the Ftyr data while line B is the Fphe data. The spectral parameters for the measurements at 303°K were as follows: the 141 MHz (1.99×10^4 MHz^2) spectrum was the result of 15,000 scans using a 25 μs (78°) pulse, a ±10,000 Hz sweepwidth, 8K data and a 300 ms delay between transients; the 254 MHz (6.45×10^4MHz^2) spectral parameters were as listed in Figure V-1; the 376 MHz (14.17×10^4MHz^2) spectrum was obtained from 60,000 scans using a pulsewidth of 10 μs (75°), a sweepwidth of ±20,000 Hz, 8K data, and a delay of 300 ms between transients.

Table V-1

T_1 and nOe data[1] of Fphe- and Ftyr-labelled M13 coat proteins reconstituted into phospholipid vesicles

	T_1 (s)	
Frequency (MHz)	Fphe	Ftyr
141.178	0.43	0.52
254.025	0.50	0.52
	nOe	
Frequency (MHz)	Fphe	Ftyr
141.178	-0.51	-0.40
254.025	-0.28	-0.46

[1] The measurements were made at 303°K

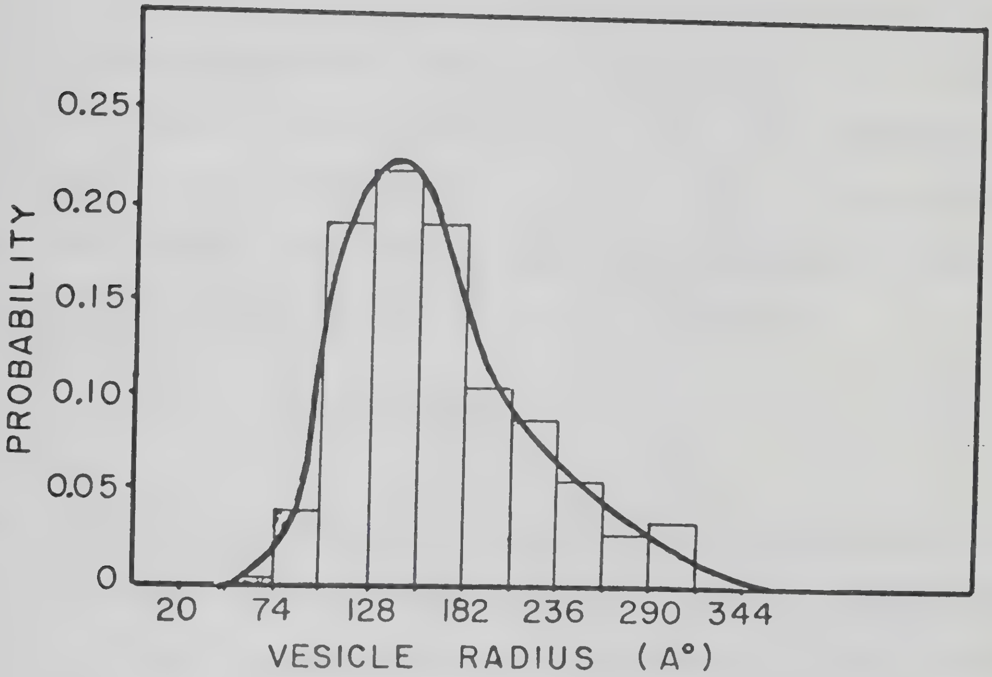

Figure V-10 A histogram of the size distribution of vesicles containing Fphe- and Ftyr-labelled M13 coat proteins. The vesicles were prepared using the cholate procedure (see Chapter II-E). A total of 178 vesicles were measured from an electron micrograph. From the distribution obtained, it was calculated that any vesicle in the preparation has a 95% probability of having a radius between 20Å and 327Å. The mean radius is 159 ±63Å.

overall correlation time (see Theory section), the measurements of these data are actually weighted averages according to the sizes of the vesicles and their relative probabilities in the vesicle population.

To determine the "weighted" effective overall correlation time corresponding to the observed data, the effect of the sample size heterogeneity on the linewidth was analyzed in the following manner. Correlation times at 303°K were calculated for each of the sizes of vesicles shown in Figure V-10, using the Stokes-Einstein equation:

$$\tau_c = \frac{4\pi r^3 \eta}{3kt}$$

These were used to calculate a Lorentzian lineshape for each size [with the assumption that the linewidth is proportional to the overall correlation time (Marshall *et al.*,1972)]. These linewidths were used in conjunction with their relative probabilities to simulate a "weighted" lineshape. The simulated lineshape was then measured in the same manner as the experimental data were analysed and a best fit linewidth was determined. This linewidth was used to calculate an effective "weighted" overall rotational correlation time of 1.9×10^{-6} sec. This effective correlation time derived from T_2 measurements has also been used for the analysis of the T_1 and NOE data since the T_1 calculations are not sensitive to the exact choice of the overall correlation time (see Table V-2).

Table V-2

The T_1, $\Delta\nu$, and nOe results obtained using the best-fit values of D_1, D_2, and γ_0 for the analyses of the Fphe and Ftyr residue ring motions in vesicle-bound coat protein

Parameter	Frequency (MHz)		
	141	254	376
Ftyr: $D_1 = 2x10^8$, $D_2 = 4x10^8$, $\gamma_0 = 75°$, $\tau_c = 1.9x10^{-6}$			
T_1	0.96(0.52)[1]	0.72(0.52)	0.59
$\Delta\nu$	115(143)	242(257)	461(336)
nOe	-0.18(-0.40)	-0.17(0.46)	-0.13
Fphe: $D_1 = 2x10^8$, $D_2 = 4x10^8$, $\gamma_0 = 90°$, $\tau_c = 1.9x10^{-6}$			
T_1	0.62(0.43)	0.69(0.50)	0.69
$\Delta\nu$	86(96)	173(139)	323(138)
nOe	-0.15(-0.51)	-0.26(-0.28)	-0.27
Fphe: $D_1 = 2x10^8$, $D_2 = 4x10^8$, $\gamma_0 = 90°$, $\tau_c = 1.5x10^{-6}$			
T_1	0.62	0.72	0.59
$\Delta\nu$	68(96)	137(139)	256(138)
nOe	-0.15(-0.40)	-0.26(0.46)	-0.27

[1] The experimentally determined data are given in parentheses.

With the evaluation of the effective overall rotational correlation time, we are now in a position to analyze the measured relaxation parameters determined for the Ftyr and Fphe residues of the vesicle-bound protein. Quantitation of the motions of the Fphe and Ftyr residues was done using a computer program based on the equations outlined in the Theory section. The rate of the diffusion about the $\alpha\beta$- and $\beta\gamma$-bonds (D_1 and D_2, respectively) and the wobble angle about the $\alpha\beta$-bond (γ_0) were varied to obtain the linewidth, T_1 and nOe values closest to the experimental data. The calculated values closest to the linewidth data at 254 MHz were chosen as these linewidths were measured in six individual experiments and so are known with greater accuracy than the data at the other two frequencies which were measured only once.

It was found that the calculated T_1, linewidth and nOe's for Ftyr were closest to those obtained experimentally when $D_1 = 2\times10^8$ sec^{-1}, $D_2 = 4\times10^8$ sec^{-1}, and $\gamma_0 = 75°$. The linewidth data agree quite well but the calculated T_1's are too long (see Table V-2). This indicates that some rapid intermolecular interactions must also be present. Such an interaction could be between the Ftyr and passing lipid chains (Hagen *et al.*, 1978). This would decrease the T_1 value but would have negligible effect on the linewidth.

The best fit values for the Fphe data were $D_1 = 2\times10^8$ sec^{-1}, $D_2 = 4\times10^8$ sec^{-1} and $\gamma_0 = 90°$ (Table V-2). In this case, however, neither the linewidths nor T_1's fit the data

very well. That the calculated linewidths are too large indicates additional motion is present that is not included in the model. This implies that the hydrophilic ends must have more backbone motion allowed than the hydrophobic domain. The effect of this would be to decrease the overall correlation time of the vesicle (as far as the Fphe are concerned). The results of a simulation with the overall correlation time reduced from 1.9×10^{-6} to 1.5×10^{-6} sec is shown in Table V-2. The linewidths now are closely simulated. The T_1's are still too long, however. Intermolecular interactions are again indicated. In this case, the fluorine could be experiencing dipolar interactions with either the phospholipid headgroups of the lipid or other protein residues (either intra- or inter-). The nOe's in both the Fphe and Ftyr cases do not fit very well. This is expected as the nOe calculations depend upon the T_1 values. Since the T_1 values do not fit well, then the nOe's will not either.

These studies have outlined an overall picture for the M13 coat protein's interaction with lipids when reconstituted into phospholipid vesicles. The rotations of the tyrosine residues in the hydrophobic domain of the protein, although not greatly restricted by the lipids, are still influenced by them. Above the T_m of the lipids the motional properties of the side chains of the Ftyr residues in the portion of the protein surrounded by lipids are very similar to those found for typical globular proteins in aqueous

solution (Hull and Sykes, 1975a). The Fphe residues, as markers of the hydrophilic regions of the protein, were found to be only slightly more mobile than the tyrosines. This finding indicates that the hydrophilic ends are not "waving" around in solution but must be either structured or associated with the phospholipid headgroups. Further experiments, as suggested in Chapter 5-A, are necessary to determine whether the structure of the coat protein in vesicles is the same as the structure of the coat protein in DOC micelles.

Concluding Discussion

A. Thesis Overview

This thesis has described structural studies of an intrinsic membrane protein, the coat protein of the coliphage, M13, when bound by either deoxycholate micelles or phospholipid vesicles. The hydrophilic and hydrophobic domains of the protein were biosynthetically labelled with the 3-fluoro-analogs of phenylalanine and tyrosine, respectively. The exposure and mobilities of the Fphe and Ftyr residues in those domains were monitored using ^{19}F NMR.

The first experiments described were performed with the Fphe and Ftyr amino acids, themselves: the effects of bicarbonate buffer and of the % D_2O present in the sample on the ^{19}F NMR spectra of these fluoro-amino acids were characterized. It was found that the spectra of Fphe and Ftyr in bicarbonate buffer contained extra resonances when compared to the spectra of Fphe and Ftyr in other buffers or just D_2O. The cause of the extra resonances was studied to determine if these resonances would be present in the spectra of the Fphe and Ftyr-labelled coat proteins. The results showed that the free amino groups of the fluoro-amino acids were interacting with the dissolved CO_2 from the bicarbonate buffer and that the carbamate species formed were the origin of the additional resonances. Neither Fphe nor Ftyr is the N-terminal amino acid of the M13 coat protein, thus, the direct interaction of the Fphe and Ftyr protein residues

with CO_2 was not possible. Therefore resonances in the ^{19}F NMR spectra of the labelled coat proteins due to the bicarbonate buffer should not be present. (The ^{19}F NMR spectra of the Fphe and Ftyr coat proteins in DOC micelles in sodium borate buffer were the same as the spectra of the fluoro-labelled coat proteins in DOC micelles in bicarbonate buffers, thus confirming this conclusion.) The second study involving the Fphe and Ftyr amino acids, was to determine the effects of changing the aqueous solvent from H_2O to D_2O on the ^{19}F chemical shifts. These experiments determined the solvent isotope induced shifts (SIIS's) of the Fphe and Ftyr chemical shifts when the amino acids were completely exposed to the solvent. These were then compared to the SIIS's of the fluoro-residues in the M13 coat protein when bound by DOC micelles; this provided a measure of the % exposure of the fluoro-residues in the DOC micelle-bound coat protein.

The incorporation of the Fphe and Ftyr amino acids into the M13 coat protein and the assignments of the resolved fluoro-resonances to specific residues in the protein in DOC micelles, has allowed a detailed study of the structure of the micelle-bound coat protein about those residues. Structural information was obtained by monitoring the exposure and motion of the Fphe and Fyr residues using ^{19}F NMR. The exposure of the fluoro-residues was judged by the results of proteolytic digestions, solvent isotope induced chemical shift measurements, fluorine photo-chemically induced dynamic nuclear polarization experiments and

pH titrations. The data showed that although Fphe 11 was exposed to proteolytic cleavage by chymotrypsin or pronase, water did not interact significantly with its fluorine. This indicated that the ring of the residue was outside the micelle but was, at least, partially buried in a hydrophobic pocket. Ftyr 21 and Ftyr 24 were protected from chymotrypsin and only became exposed to pronase after extensive removal of the hydrophilic ends. The fluorine of Ftyr 21 interacted with water significantly more than Ftyr 24 (and Fphe 11), while Ftyr 24 interacted with the lipophilic dye, 3-N-carboxymethyl-lumiflavine more than Ftyr 21. These data suggested that Ftyr 21 was at the water/micelle interface and Ftyr 24 was inside the micelle. These conclusions were supported by the ring motion analyses: Fphe 11 was more mobile than Ftyr 21; Ftyr 21 was more mobile than Ftyr 24. Fphe 11, however, was not much more mobile than Ftyr 21, suggesting that the protein sequence in the vicinity of the Fphe 11 residue was structured.

Changes in temperature induced changes in the structure about the Fphe and Ftyr residues of the labelled coat proteins in DOC micelles. The structure in the hydrophilic ends was found to be reversibly disrupted by increasing the temperature to 327°K: circular dichroism spectroscopy showed an increase in random coil structure as the ^{19}F NMR resonances of the three Fphe residues became resolved. Increasing the temperature had no effect on the Ftyr ^{19}F NMR resonances; rather, decreasing the temperature to 277°K appeared to

cause structural changes in the immediate vicinity of Ftyr 21 and Ftyr 24.

The exposure and mobility of the Fphe and Ftyr residues in the labelled coat proteins reconstituted into synthetic lipid vesicles were indicated from the results of chymotryptic digestion, temperature and ring motion analyses. The Fphe residues were susceptible to chymotrypsin: chymotryptic fragments from both the N- and C-termini were obtained showing that the protein was reconstituted symmetrically into the vesicles while the Ftyr residues were protected from the protease. Temperature studies showed that the mobilities of the Fphe residues were not affected by the lipid phase transition, hence they were outside the bilayer. The mobilities of the Ftyr residues were influenced by the phase state of the lipids, hence were inside the bilayer. Analyses of the ^{19}F NMR relaxation data gave Fphe and Ftyr ring motions comparable to those found for the DOC micelle-bound coat proteins: the Fphe residues were not much more mobile than the Ftyr residues; the Ftyr residues had comparable mobility to that found for tyr residues within the hydrophobic domain of a water-soluble protein. The lack of mobility of the Fphe residues compared to the mobility of the Ftyr residues suggested that the hydrophilic ends of the protein were not diffusing freely in solution but were structured.

B. Possible Future Studies

The motion and exposure of the Fphe and Ftyr residues of labelled M13 coat proteins when bound by either DOC micelles or phospholipid vesicles were studied in this thesis. The interpretation of the data allowed statements to be made as to the presence of structure in the vicinities of the Fphe and Ftyr amino acids. These labelled amino acids were only reporting on the surroundings of 5 protein residues out of a total of 50; clearly, more work is necessary to obtain a complete picture of the micelle- or vesicle-bound structure of M13 protein.

Amino acid residues in the coat protein, other than phenylalanine and tyrosine, are being monitored by two approaches. The first, taken by Dr. Gillian Henry, is to incorporate ^{13}C-enriched amino acids into the protein and follow the behavior of the residue(s) with ^{13}C NMR. The second, made feasible by the use of perdeuterated detergents (or lipids) and the forthcoming arrival of a 500 MHz NMR spectrometer, is to look at the proton resonances of the micelle-bound (or vesicle-bound) coat protein; this line of study will be undertaken by Dr. Joe O'Neil. The combined results from this thesis and their experiments will give a comprehensive view of the structure of the entire coat protein in either micelles or vesicles.

In the Discussion at the end of each Chapter, specific experiments to clarify or complement the results given in the Chapter, were suggested. Those experiments, although

immediately relevant to the work described in the Chapter, are only short term projects. In the long term, a number of pathways could be followed.

There is interest as to the effects of different detergents on the structure of intrinsic proteins: which detergent is the least perturbing to the protein's structure? A comparison of the structure of M13 coat protein in different detergents could be done to determine which one best maintains the structure found in vesicles (or membranes).

Vesicle studies, themselves, promise to be interesting. The modified cholate procedure appeared to produce reconstituted M13 coat protein in vesicles that were oriented with the N-terminus outside and the C-terminus inside. (This was determined by the analysis of the chymotryptic fragments released from the vesicles and the amino acid analyses of the protein left with the vesicles: only the fragment 1-11 was detected by paper electrophoresis and the protein left with the lipid was a mixture of the intact protein and fragment 12-50.) The ability to assymetrically incorporate the coat protein into lipid vesicles raises the possibility that placing a single label at each of the N-terminus, the C-terminus and in the hydrophobic core of the protein, would simultaneously result in three resolved resonances; one from each of the domains of the protein.

Vesicles could be prepared, varying the lipid composition. Infection of the *E. coli* with M13 phage causes an

increase in cardiolipin synthesis. An obvious study would be to compare the ease of reconstitution and the structure of the coat protein when cardiolipin is or is not present. The major lipid found in *E. coli* is phosphatidyethanolamine (PE). To see if the exposure and mobilities of the coat protein residues are different when PE is the major lipid would certainly be relevant. (Another possibility, of course, is to try to study the coat protein that actually is in the *E. coli* membrane. The coat protein obtains high concentrations in the inner membrane of *E. coli* bacterium during infection, hence one may be able to prepare vesicles of the host membrane that are suitable for NMR studies.) A third type of experiment would be to study the effect of cholesterol on the protein. Cholesterol is not normally found in *E. coli* membranes, but the coat protein could be used as a model intrinsic protein to see whether the cholesterol causes the protein to be "squeezed out" of the membrane, as suggested by Borochov and Shinitzky(1976).

Another area of research would be to study the mechanism of the coat protein's function: what interactions and structural changes occur as the coat protein helps the phage DNA into and out of the bacterium. Two approaches could be attempted. The first would be to monitor the structural changes present when the protein is reconstituted into vesicles in the presence or absence of single-stranded DNA fragments, with or without the gene V proteins bound to the DNA. The other would be to study the observations that

Griffith and coworkers made using electron microscopy (Manning *et al.*, 1982), that by treating a solution of M13 phage with chloroform, the coat protein arrangement on the DNA changed. When this "altered" phage was mixed with lipid vesicles, the phage particles disappeared: they concluded that the protein was leaving the DNA and going into the membrane. Preliminary ^{19}F NMR experiments using Fphe- and Ftyr-labelled M13 phage indicated that the coat protein does go into the vesicles. Further studies of the process, including analysis of the NMR tensor elements of the coat protein on the phage before and after the chloroform treatment, the study of where the DNA is after the coat protein leaves it (is the DNA inside the vesicle?), and the determination of the structural properties of the vesicle-bound protein, could give a great deal of information of the events that occur during the M13 infection of the *E. coli*.

Bibliography

Becconsall, J.K. and Hampson, P. (1965) *Mol. Phys.* **10**, 21-32.

Borochov, H. and Shinitzky, M. (1976) *Proc. Natl. Acad. Sci. USA* 73, 4526-4530.

Brauer, M. and Sykes, B.D. (1984) *Methods Enzymol.* **107**, 36-81.

Brenner, M. and Huber, W. (1953) *Helv. Chem. Acta.* **36**, 1109-1115.

Buckingham, A.D. (1960) *Can. J. Chem.* **38**, 300-307.

Buckingham, A.D., Schaefer, T. and Schneider, W.G. (1960) *J. Chem. Phys.* **32**, 1227-1233.

Castellan, G.W. (1971) in *Physical Chemistry*, ed. Bonner, F.T. (Addison-Wesley Publishing Company, Reading, Ma., U.S.A.), pp. 770-790.

Chamberlain, B.K. and Webster, R.E. (1976) *J. Biol. Chem.* **251**, 7739-7745.

Chamberlain, B.K., Nozaki, Y., Tanford, C. and Webster, R.E. (1978) *Biochim. Biophys. Acta.* **510**, 18-37.

Chen, Y.-H., Yang, J.T. and Chau, K.H. (1974) *Biochemistry* **13**, 3350-3359.

Coleman, J.E. and Armitage I.M. (1977) in *NMR in Biology*, eds. Dwek, R.A., Campbell, I.D., Richards, R.E. and Williams, R.J.P. (Academic Press, New York, N.Y., U.S.A), pp. 171-200.

Cross, T.A. and Opella, S.J. (1979) *J. Supramol. Struc.* 11, 139-145.

Cross, T.A. and Opella, S.J. (1980) *Biochem. Biophys. Res. Comm.* **92**, 478-484.

Cross, T.A. and Opella, S.J. (1981) *Biochemistry* **20**, 290-297.

Darszon, A. (1983) *J. Bioenerg. Biomem.* **15**, 321-334.

Dettman, H.D., Weiner, J.H. and Sykes, B.D. (1982) *Biophys. J.* 37, 243-251.

Dettman, H.D., Weiner, J.H. and Sykes, B.D. (1984) *Biochemistry* 23, 705-712.

Dorman, B.P., Hearst, J.E. and Maestre, M.F. (1973) *Methods Enzymol.* 27(D), 767-796.

Emsley, J.W. and Phillips, L. (1966) *Mol. Phys.* **11**, 437-456.

Emsley, J.W. and Phillips, L (1971) *Prog. NMR Spectrosc.* 7, 1-36.

Ernst, R.R. and Anderson, W.A. (1966) *Rev. Scientific Instrum.* 37, 93-102.

Evans, D.F. (1960) *J. Chem. Soc.* 877-880.

Evans, E.A. and Parsegian, V.A. (1983) *Ann. N.Y. Acad. Sci.* **419**, 13-33.

Farrar, T.C. and Becker, E.D. (1971) in *Pulse and Fourier Transform NMR: Introduction to Theory and Methods*, (Academic Press, New York, N.Y., U.S.A.) pp. 22-29.

Faurholt, C. (1924) *J. Chimie Physique* **21**, 400-455.

Freifelder, D. (1976) in *Physical Biochemistry: Applications to Biochemistry and Molecular Biology*, ed. Davern, C.I. (W.H. Freeman and Company, San Francisco, Ca., U.S.A.), pp. 444-474.

Gall, C.M., Cross, T.A., DiVerdi, J.A. and Opella, S.J. (1982) *Proc. Natl. Acad. Sci. USA* **79**, 101-105.

Isaacson, Y.A., Deroo, P.W., Rosenthal, A.F., Bittman, R., McIntyre, J.O., Bock, H.-G., Gazotti, P. and Fleischer, S. (1979) *J. Biol. Chem.* **254**, 117-126.

Gerig, J.T., Loehr, D.T., Luk, K.F.S. and Roe, D.C. (1979) *J. Amer. Chem. Soc.* 101, 7482-7487.

Greenfield, N. and Fasman, G.D. (1969) *Biochemistry* 8, 4108-4116.

Gurd, F.R.N., Matthew, J.B., Wittebort, R.J., Morrow, J.S. and Friend, S.H. (1980) in *Biophysics and Physiology of Carbon Dioxide*, eds. Bauer, C., Gross, G. and Bartels, H. (Springer-Verlag, Berlin, Germany), pp. 89-101.

Hagen, D.S., Weiner, J.H. and Sykes, B.D. (1978) *Biochemistry* 17, 3860-3866.

Hagen, D.S., Weiner, J.H. and Sykes, B.D. (1979a) in *NMR and Biochemistry*: A Symposium Honoring Mildred Cohn, eds. Opella, S.J. and Lu, P. (Marcel Dekker, Inc., New York, N.Y., U.S.A.), pp. 51-58.

Hagen, D.S., Weiner, J.H. and Sykes, B.D. (1979b) *Biochemistry* 18, 2007-2012.

Hall, N.P., Cornelius, M.J. and Keys, A.J. (1983) *Anal. Biochem.* 132, 152-157.

Hansen, P.E. (1983) *Ann. Reports NMR Spectrosc.* 115, 105.

Hartree, E.F. (1972) *Anal. Biochem.* 48, 422-427.

Holmes, J.R., Kivelson, D. and Drinkard, W.C. (1962) *J. Chem. Phys.* 37, 150-152.

Huang, H.J. and Niemann, C.J. (1951) *J. Amer. Chem. Soc.* 73, 1541-1548.

Hull, W.E. and Sykes, B.D. (1974) *Biochemistry* 13, 3431-3437.

Hull, W.E. and Sykes, B.D. (1975a) *J. Chem. Phys.* 63, 867-880.

Hull, W.E. and Sykes, B.D. (1975b) *J. Mol. Biol.* 98, 121-153.

Hull, W.E. and Sykes, B.D. (1976) *Biochemistry* 15, 1535-1546.

Hutton, R.S., Roth, H.D. and Bertz, S.H. (1983) *J. Amer. Chem. Soc.* 105, 6371-6377.

Imaizumi, K., Imai, K. and Tyuma, I. (1982) *J. Mol. Biol.* 159, 703-719.

Jardetzky, O. and Roberts, G.C.K. (1981) in *NMR in Molecular Biology* eds. Horecker, B., Kaplan, N.O., Marmur, J. and Scheraga, H.A. (Academic Press, New York, N.Y., U.S.A.), pp. 448-492.

Jarema, M.A.C., Lu, P., Miller, J.H. (1981) *Proc. Natl. Acad. Sci. USA* 78, 2707-2711.

Kaptein, R. (1971) *Chem. Commun.*, 732-733.

Kaptein, R., Dijkstra, K. and Nicolay, K. (1978) *Nature* **274**, 293-294.

Kauzmann, W. (1961) in *Quantum Chemstry* (Academic Press Inc., New York, N.Y., U.S.A.), pp. 503-517.

Keniry, M.A., Gutowsky, H.S. and Oldfield, E. (1984) *Nature* **307**, 383-386.

Kern, D.M. (1960) *J. Chem. Ed.* **37**, 14-23.

Kinsey, R.A., Kintanar, A. and Oldfield, E. (1981) *J. Biol. Chem.* **256**, 9028-9036.

Kinsey, R.A., Kintanar, A., Tsai, M-D., Smith, R.L., Janes, N. and Oldfield, E. (1981) *J. Biol. Chem.* **256**, 4146-4149.

Knowles, F.C. (1984) *Arch. Biochem. Biophys.* **230**, 327-334.

Kossiakoff, A.A. (1982) *Nature* **296**, 713-721.

Lauterbur, P.C., Kaufman, B.V. and Crawford, M.K. (1978), in *Biomolecular Structure and Function*, ed. Agris, P.F. (Academic Press Inc., New York, N.Y., U.S.A.), pp. 329-351.

Levy, G.C. and Peat, I.R. (1975) *J. Mag. Res.* **18**, 500-521.

London, R.E. (1980) in *Magnetic Resonance in Biology*, ed. Cohen, J.S. (John Wiley and Sons, New York, N.Y., U.S.A.), pp. 1-69.

Lorimer, G.H. (1983) *Trends in Biochem. Sci.* 8, 65-68.

Makino, S., Woolford, J.L., Tanford, C. and Webster, R.E. (1975) *J. Biol. Chem.* 250, 4327-4332.

Manning, M., Chrysogelos, S. and Griffith, J. (1982) *Biophys. J.* 37, 28-29.

Marshall, A.G. (1978) in *Biophysical Chemistry* (John Wiley and Sons, New York, N.Y., U.S.A.).

Marshall, A.G., Schmidt, P.G. and Sykes, B.D. (1972) *Biochemistry* 11, 3875-3879.

Morrow, J.S., Keim, P. and Gurd, F.R.N. (1974) *J. Biol. Chem.* **249**, 7484-7494.

Muller, N. (1976) *J. Mag. Res.* **23**, 327-334.

Muller, N. (1977a) *J. Mag. Res.* **25**, 111-121.

Muller, N. (1977b) *J. Mag. Res.* **28**, 203-216.

Murray-Rust, P., Stallings, W.C., Monti, C.T., Preston, R.K. and Glusker, J.P. (1983) *J. Amer. Chem. Soc.* **105**, 3206-3214.

Narahashi, Y. (1971) *Methods Enzymol.* **19**, 651-664.

Neuberger, A. (1937) *Prog. Roy. Soc. A* **158**, 68-96.

Noggle, J.H. and Schirmer, R.E. (1971) in *The Nuclear Overhauser Effect*, (Academic Press, New York, N.Y., U.S.A.).

Nozaki, Y., Chamberlain, B.K., Webster, R.E. and Tanford, C. (1976) *Nature* **259**, 335-337.

Nozaki, Y., Reynolds, J.A. and Tanford, C. (1978) *Biochemistry* **17**, 1239-1246.

O'Leary, M.H., Jaworski, R.J. and Hartman, F.C. (1979) *Biochemistry* **76**, 673-675.

Orrell, K.G. and Sik, V. (1980) *Anal. Chem.* **52**, 567-569.

Pluschke, G., Hirota, Y. and Overath, P. (1978) *J. Biol. Chem.* **253**, 5048-5055.

Post, J.F.M., Cottam, P.F., Simplaceanu, V. and Ho, C. (1984),*J. Mol. Biol.* (in press).

Putter, I., Baretto, A., Markley, J.L. and Jardetzky, O. (1969) *Proc. Natl. Acad. Sci. USA* **64**, 1396-1403.

Raheja, R.K., Kaur, C., Singh, A. and Bhatia, I.S. (1973) *J. Lipid Res.* **14**, 695-697.

Robinson, N.C., Strey, F. and Talbert, L. (1980) *Biochemistry* **19**, 3656-3661.

Roughton, F.J.W. (1970) *Biochem. J.* **117**, 801-812.

Roughton, F.J.W. and Rossi-Bernardi, L (1966) *Proc. Roy. Soc. B.* **164**, 381-400.

Simon, I., Tüchsen, E. and Woodward, C. (1984) *Biochemistry* **23**, 2064-2068.

Singer, S.J. (1971) in *Structure and Function of Biological Membranes*, ed. Rothman, L.I. (Academic Press, New York, N.Y., U.S.A.) p.145.

Singer, S.J. (1977) *J. Colloid Interface Sci.* **58**, 452-458.

Singer, S.J. and Nicolson, G.L. (1972) *Science* **175**, 720-731.

Slichter, C.P. (1978) in *Principles of Magnetic Resonance*, ed. Fulde, P. (Springer-Verlag, Berlin, Germany).

Small, D.M. (1971) in *The Bile Acids* (Volume 1), ed. Nair P.P. and Kritchevsky, D. (Plenum Press, New York, N.Y., U.S.A.),pp. 249-356.

Sykes, B.D. and Hull, W.E. (1978) *Methods Enzymol.* **49(G)**, 270-295.

Sykes, B.D. and Weiner, J.H. (1980) in *Magnetic Resonance in Biology* (Volume 1) ed. Cohen, J.S. (John Wiley and Sons, New York, N.Y., U.S.A.), pp. 171-196.

Tanford, C. (1976) *Nature* **259**, 335-337.

Unwin, P.N.T. and Henderson, R. (1975) *J. Mol. Biol.* **94**, 425-440.

Van Kempen, L.H.J., Breepoel, P.M. and Kreuzer, F. (1975) *Respir. Physiol.* **23**, 223-241.

Webster, R.E. (1978) *Biochim. Biophys. Acta.* **510**, 18-37.

Wickner, W. (1975) *Proc. Natl. Acad. Sci. USA* **72**, 4749-4753.

Wickner, W. (1976) *Proc. Natl. Acad. Sci. USA* **73**, 1159-1163.

Williams, R.W. and Dunker, A.K. (1977) *J. Biol. Chem.* **252**, 6253-6255.

Wittebort, R.J. and Szabo, A. (1978) *J. Chem. Phys.* **69**, 1722-1736.

Wüthrich, K. and Wagner, G. (1984) *Trends in Biochem. Sci.* **9**, 152-154.

Appendix A

This Appendix lists the recipes of the media, agar plates, and dilution buffer used for the growth and titer-determination of M13 bacteriophage. The procedures are given in Chapter II-C.

L Broth

Sodium chloride	5 g
Yeast extract	5 g
Tryptone	10 g
Sodium hydroxide	1.1 ml of 1.0 M

Add water to a volume of 1 liter. For plates, add 12.5 g agar.

M63 Minimum Medium

Potassium phosphate (dibasic)	7 g
Potassium phosphate (monobasic)	3 g
Ammonium Sulphate	2 g
Ferrous sulphate	0.5 mg

Add water to 1 liter. For plates, add 13 g agar.

After autoclaving, add:

Magnesium sulphate	0.8 ml of 1 M
Glucose	10 ml of 20%

As required:

Thymidine	10 ml of 0.5%
L-Amino acids	10 ml of 0.4%
D-,L-mixture of Amino acids	10 ml of 0.8%
Thiamine	0.5 ml of 1%

Sterile Saline (10x)

$Na_2HPO_4 \cdot 7H_2O$	26.8 g
$NaH_2PO_4 \cdot H_2O$	14.2 g
KH_2PO_4	13.6 g
Sodium chloride	5.0 g

Add water to 1 liter.

Phage Titer Media

Bottom Agar

Bactoagar	11 g
Bactotryptone	10 g
Sodium chloride	5 g

Add water to 1 liter. After autoclaving, add:

Sodium citrate	10 ml of 20%
Glucose	6.4 ml of 20%

Top Agar

Bactoagar	7 g
Bactotryptone	10 g
Sodium chloride	5 g

Add water to 1 liter. After autoclaving, add:

Sodium citrate	10 ml of 20%
Glucose	15 ml of 20%

Appendix B

The Fphe and Ftyr ^{19}F NMR relaxation data were analyzed using a model approach outlined by Szabo *et al*. (1978). The model allows restricted rotation about the $\alpha\beta$-bond (D_1) through an angle γ_0, free rotation around the $\beta\gamma$-bond (D_2) and overall spherical symmetry for micelle or vesicle rotation (D) (see Chapters IV-B and V-B).

The Basic computer programs to be given, allow the generation of linewidth, T_1, and nOe values for, first, a Fphe residue, then, a Ftyr residue, using the model described above. The programs allow for variation of τ (the overall correlation time for vesicle rotation), D_1, D_2 and γ_0. Sample results, calculated using the correlation times appropriate for the micelle-bound coat protein, are given.

```
!      ! F-PHE DIPOLE-CSA ANALYSIS       DDCSA_004
10     DIM D(-2:2,-2:2),B(2),Freq(5),G(9),D1(5),D2(5),Sum(5,2),E(-2:2,-2:2,2)
11     DIM R1(5,5,3),R2(5,5,3),C(5),Coef(3),R1csa(5,5),R2csa(5,5),Sumcsa(5)
12     DIM Both1(5,5),Both2(5,5),Sigma(5,5,2),Noe(5,5)
20     REAL X,Num,Den,Fnb2,Dall,Jw,Constant,Radius,Bet1,M1,Jcsa,Kcsa,Dz
30     INTEGER I,B1,B2,N,J,L,K,M
40     RAD
50     READ Bet1,B(1),B(2),Dall,Constant,Dz  ! ANGLES OF INTERNAL ROTATION: BETA(
IN) AND THE ANGLES BETWEEN THE H-F VECTORS AND THE BETA-GAMMA BOND.
55     ! 1/(6*TAUC ),DD CONSTANT,CSA TENSOR COORDINATE
60     FOR K=1 TO 4
61        READ C(K)  !GAMMA0 ANGLES
62     NEXT K
70     FOR J=1 TO 5
80        READ D1(J)  !WOBBLE FREQUENCY ABOUT ALPHA-BETA BOND
90     NEXT J
110    FOR L=1 TO 5
120       READ D2(L)  !ROTATION FREQUENCY ABOUT BETA-GAMMA BOND
130    NEXT L
140    READ Freq(2),Freq(5)  !OMEGA F AND OMEGA H
150    Freq(1)=Freq(2)-Freq(5)
160    Freq(3)=Freq(2)+Freq(5)
162    Freq(4)=0
165    !INTERNAL ROTATION TENSOR ELEMENTS****************************************
166       D(2,2)=COS(Bet1/2)^4
170       D(2,1)=-.5*SIN(Bet1)*(1+COS(Bet1))
180       D(2,0)=(3/8)^.5*SIN(Bet1)^2
190       D(2,-1)=.5*SIN(Bet1)*(COS(Bet1)-1)
200       D(2,-2)=SIN(Bet1/2)^4
210       D(1,2)=-D(2,1)
220       D(1,1)=.5*(2*COS(Bet1)-1)*(COS(Bet1)+1)
230       D(1,0)=-((3/2)^.5*SIN(Bet1)*COS(Bet1))
240       D(1,-1)=.5*(2*COS(Bet1)+1)*(1-COS(Bet1))
250       D(1,-2)=D(2,-1)
260       D(0,2)=D(2,0)
270       D(0,1)=-D(1,0)
280       D(0,0)=.5*(3*COS(Bet1)^2-1)
290       D(0,-1)=D(1,0)
300       D(0,-2)=D(2,0)
310       D(-1,2)=-D(2,-1)
320       D(-1,1)=D(1,-1)
330       D(-1,0)=-D(1,0)
340       D(-1,-1)=D(1,1)
350       D(-1,-2)=D(2,1)
360       D(-2,2)=D(2,-2)
370       D(-2,1)=-D(2,-1)
380       D(-2,0)=D(2,0)
390       D(-2,-1)=-D(2,1)
400       D(-2,-2)=D(2,2)
401          FOR M=1 TO 2
410       E(2,0,M)=(3/8)^.5*SIN(B(M))^2
420       E(1,0,M)=-((3/2)^.5*SIN(B(M))*COS(B(M)))
430       E(0,0,M)=.5*(3*COS(B(M))^2-1)
431       E(-1,0,M)=-E(1,0,M)
432       E(-2,0,M)=E(2,0,M)
442          NEXT M
452    FOR B2=0 TO 2
462       READ Coef(B2)   ! CSA TENSOR COEFFICIENTS
472    NEXT B2
473    Kcsa=(Freq(2)*Dz)^2/40   ! CSA CONSTANT
```

```
482   PRINT
483   PRINT "Tc= ";1/(6*Dall)."SF= ";INT(Freq(5)*!.E-6/(2*PI)+.5);"MHz","DDCSA_0
04","FPHE ANALYSIS"
490 FOR K=1 TO 4
500   PRINT
520   PRINT "WOBBLE ANGLE= ";INT(C(K)*360/(2*PI)+.5);"DEGREES"
530   PRINT
531   !SOLVING THE CORRELATION FUNCTION*****************************************
540   FOR J=1 TO 5
570      FOR L=1 TO 5
580         FOR I=1 TO 5
581            FOR M=1 TO 2
590              Sum(I,M)=0
591            NEXT M
593            Sumcsa(I)=0
594         NEXT I
600         FOR N=0 TO 9
620            FOR B1=-2 TO 2
630               X=B1*C(K)
540               IF N=0 THEN
642                  IF X=0 THEN
644                     G(N)=1
646                  ELSE
650                     G(N)=SIN(X)^2/X^2
652                  END IF
660               ELSE
670                  Num=COS(X)^2*(1-(-1)^N)+SIN(X)^2*(1+(-1)^N)
680                  Den=X^2-(N*PI/2)^2
690                  G(N)=X^2*Num/Den^2
700               END IF
720               FOR B2=-2 TO 2
730                  Fnb2=6*Dall+D1(J)*(N*PI)^2/(4*C(K)^2)+B2^2*D2(L)
750                  FOR I=1 TO 5
751                        FOR M=1 TO 2
760                     Jw=Fnb2/(Fnb2^2+Freq(I)^2)*G(N)*D(B1,B2)^2*E(B2,0,M)^2
770                     Sum(I,M)=Sum(I,M)+Jw
771                        NEXT M
780                  NEXT I
790               NEXT B2
791               GOTO 909
800            NEXT B1
810         NEXT N
813         !CALCULATING DIPOLAR 1/T1, 1/T2, AND THE NOE EQUATION NUMERATOR*****
814            FOR M=1 TO 2
820         R1(J,L,M)=Constant*(Sum(1,M)+3*Sum(2,M)+6*Sum(3,M))
830         R2(J,L,M)=Constant/2*(Sum(1,M)+3*Sum(2,M)+6*Sum(3,M)+4*Sum(4,M)+6*Su
m(5,M))
831         Sigma(J,L,M)=Constant*(6*Sum(3,M)-Sum(1,M))
840            NEXT M
870      NEXT L
880   NEXT J
892`  GOTO 931
894 NEXT K
895   DATA 1.239183769, 0,1.047197551, 5.55555555555555E5, 1.63312E8,5.12E-5
900   DATA 2.094395,2.268928,2.44346095,2.61799388
901   DATA 5E7,1E8,5E8,1E9,5E9
902   DATA 5E7,1E8,5E8,1E9,5E9
904   DATA 1.596086091E9,1.696460033E9
905   DATA .668,.403,.466
908   !CALCULATING CSA 1/T1 AND 1/T2********************************************
```

```
909   FOR B2=0 TO 2
910      Fnb2=6*Dail+D1(J)*(N*PI)^2/(4*C(K)^2)+B2^2*D2(L)
911      FOR I=2 TO 4 STEP 2
912         Jcsa=2*Fnb2/(Fnb2^2+Freq(I)^2)
913         M1=Coef(B2)*G(N)*D(B1,B2)^2*Jcsa
914         Sumcsa(I)=Sumcsa(I)+M1
915      NEXT I
916   NEXT B2
917   IF B1=2 THEN
918      IF N=9 THEN
919         R1csa(J,L)=6*Kcsa*Sumcsa(2)
920         R2csa(J,L)=Kcsa*(3*Sumcsa(2)+4*Sumcsa(4))
921         GOTO 810
922      ELSE
923         GOTO 810
924      END IF
925   ELSE
926      GOTO 800
927   END IF
930   !CALCULATING 1/T1 (= 1/T1(DD) + 1/T1(CSA)), 1/T2 (= 1/T2(DD) + 1/T2(CSA))
AND NOE (= CONSTANT * NOE EQUATION NUMERATOR / 1/T1)****************************
931   FOR J=1 TO 5
932      FOR L=1 TO 5
933         Both1(J,L)=R1(J,L,1)+R1(J,L,2)+R1csa(J,L)
934         Both2(J,L)=R2(J,L,1)+R2(J,L,2)+R2csa(J,L)
935         Noe(J,L)=26.7519/25.167*(Sigma(J,L,1)+Sigma(J,L,2))/Both1(J,L)
936      NEXT L
937   NEXT J
938   PRINT
939   PRINT USING "9A,5X,DE,9X,DE,9X,DE,9X,DE,9X,DE";" D1 // D2",D2(1),D2(2),D2(
3),D2(4),D2(5)
941   !PRINTING T1 VALUES*******************************************************
943   FOR J=1 TO 5
944      PRINT USING "DE,7X,3D.3D,7X,3D.3D,7X,3D.3D,7X,3D.3D,7X,3D.3D":D1(J),1/B
oth1(J,1),1/Both1(J,2),1/Both1(J,3),1/Both1(J,4),1/Both1(J,5)
945   NEXT J
946   PRINT
948   !PRINTING LINEWIDTH VALUES************************************************
950   FOR J=1 TO 5
951      PRINT USING "DE,5X,5D.3D,5X,5D.3D,5X,5D.3D,5X,5D.3D,5X,5D.3D":D1(J),Bot
h2(J,1)/PI,Both2(J,2)/PI,Both2(J,3)/PI,Both2(J,4)/PI,Both2(J,5)/PI
952   NEXT J
953   PRINT
955   !PRINTING NOE VALUES******************************************************
957   FOR J=1 TO 5
958      PRINT USING "DE,7X,MZ.4D,7X,MZ.4D,7X,MZ.4D,7X,MZ.4D,7X,MZ.4D":D1(J),Noe
(J,1),Noe(J,2),Noe(J,3),Noe(J,4),Noe(J,5)
959   NEXT J
960   IF K=4 THEN
961      GOTO 965
962   ELSE
963      GOTO 894
964   END IF
965   END
```

```
!       ! F-TYR DIPOLE-CSA ANALYSIS        DDCSA_002
10      DIM D(-2:2,-2:2),B(2),Freq(5),G(9),D1(5),D2(5),Sum(5),E(-2:2,-2:2),C(5)
11      DIM R1(5,5),R2(5,5),Coef(3),R1csa(5,5),R2csa(5,5),Sumcsa(5),Both1(5,5)
12      DIM Both2(5,5),Sigma(5,5),Noe(5,5)
20      REAL X,Num,Den,Fnb2,Dall,Jw,Constant,Radius,M,Jcsa,Kcsa,Dz
30      INTEGER I,B1,B2,N,J,L,K
40      RAD
50      READ B(1),B(2),Dall,Constant,Dz !ANGLES OF INTERNAL ROTATION: BETA(IN) AND
THE ANGLE BETWEEN THE H-F VECTOR AND THE BETA-GAMMA BOND, 1/(6*TAUC).
51      !DD CONSTANT,CSA Dz
60      FOR K=1 TO 4
61         READ C(K)        ! GAMMA0 ANGLES
62      NEXT K
70      FOR J=1 TO 5
80         READ D1(J)     ! WOBBLE FREQUENCY ABOUT THE ALPHA-BETA BOND
90      NEXT J
110     FOR L=1 TO 5
120        READ D2(L)  ! ROTATION FREQUENCY ABOUT BETA-GAMMA BOND
130     NEXT L
140     READ Freq(2),Freq(5)    ! OMEGA F AND OMEGA H
150     Freq(1)=Freq(2)-Freq(5)
160     Freq(3)=Freq(2)+Freq(5)
161     Freq(4)=0
162     ! INTERNAL ROTATION TENSOR ELEMENTS***************************************
165        D(2,2)=COS(B(1)/2)^4
170        D(2,1)=-.5*SIN(B(1))*(1+COS(B(1)))
180        D(2,0)=(3/8)^.5*SIN(B(1))^2
190        D(2,-1)=.5*SIN(B(1))*(COS(B(1))-1)
200        D(2,-2)=SIN(B(1)/2)^4
210        D(1,2)=-D(2,1)
220        D(1,1)=.5*(2*COS(B(1))-1)*(COS(B(1))+1)
230        D(1,0)=-((3/2)^.5*SIN(B(1))*COS(B(1)))
240        D(1,-1)=.5*(2*COS(B(1))+1)*(1-COS(B(1)))
250        D(1,-2)=D(2,-1)
260        D(0,2)=D(2,0)
270        D(0,1)=-D(1,0)
280        D(0,0)=.5*(3*COS(B(1))^2-1)
290        D(0,-1)=D(1,0)
300        D(0,-2)=D(2,0)
310        D(-1,2)=-D(2,-1)
320        D(-1,1)=D(1,-1)
330        D(-1,0)=-D(1,0)
340        D(-1,-1)=D(1,1)
350        D(-1,-2)=D(2,1)
360        D(-2,2)=D(2,-2)
370        D(-2,1)=-D(2,-1)
380        D(-2,0)=D(2,0)
390        D(-2,-1)=-D(2,1)
400        D(-2,-2)=D(2,2)
410        E(2,0)=(3/8)^.5*SIN(B(2))^2
420        E(1,0)=-((3/2)^.5*SIN(B(2))*COS(B(2)))
430        E(0,0)=.5*(3*COS(B(2))^2-1)
431        E(-1,0)=-E(1,0)
432        E(-2,0)=E(2,0)
433     FOR B2=0 TO 2
434        READ Coef(B2)      ! CSA TENSOR COEFFICIENTS
435     NEXT B2
436     Kcsa=(Freq(2)*Dz)^2/40  ! CSA CONSTANT
442     PRINT
452     PRINT
```

```
462   PRINT "Tc= ";1/6/Dall,"SF= ";INT(Freq(5)*1.E-6/2/PI+.5);"MHz":"   DDCSA_00
2","FTYR ANALYSIS"
490 FOR K=1 TO 4
500   PRINT
520   PRINT "WOBBLE ANGLE= ";INT(C(K)*360/(2*PI)+.5);"DEGREES"
530   PRINT
531   ! SOLVING THE CORRELATION FUNCTION****************************************
540   FOR J=1 TO 5
570     FOR L=1 TO 5
580       FOR I=1 TO 5
590         Sum(I)=0
591         Sumcsa(I)=0
592       NEXT I
600       FOR N=0 TO 9
620         FOR B1=-2 TO 2
630           X=B1*C(K)
640           IF N=0 THEN
642             IF X=0 THEN
644               G(N)=1
646             ELSE
650               G(N)=SIN(X)^2/X^2
652             END IF
660           ELSE
670             Num=COS(X)^2*(1-(-1)^N)+SIN(X)^2*(1+(-1)^N)
680             Den=X^2-(N*PI/2)^2
690             G(N)=X^2*Num/Den^2
700           END IF
720           FOR B2=-2 TO 2
730             Fnb2=6*Dall+D1(J)*(N*PI)^2/(4*C(K)^2)+B2^2*D2(L)
750             FOR I=1 TO 5
760               Jw=Fnb2/(Fnb2^2+Freq(I)^2)*G(N)*D(B1,B2)^2*E(B2.0)^2
770               Sum(I)=Sum(I)+Jw
780             NEXT I
790           NEXT B2
791           GOTO 1000
800         NEXT B1
810       NEXT N
811       ! CALCULATING THE DIPOLAR 1/T1, 1/T2, AND THE NOE EQUATION NUMERATOR
820       R1(J,L)=Constant*(Sum(1)+3*Sum(2)+6*Sum(3))
830       R2(J,L)=Constant/2*(Sum(1)+3*Sum(2)+6*Sum(3)+4*Sum(4)+6*Sum(5))
840       Sigma(J,L)=Constant*(6*Sum(3)-Sum(1))
870     NEXT L
880   NEXT J
892   GOTO 1321
894 NEXT K
895   DATA 1.239183769, 0, 5.55555555555555E5, 1.63312E8,7.24E-5
900   DATA 1.134464,1.396263,1.4835299,.000000000000001
901   DATA 5E7,1E8,5E8,1E9,5E9
905   DATA 5E7,1E8,5E8,1E9,5E9
910   DATA 1.596086091E9,1.696460033E9
920   DATA 0.386,0.059,0.634
930   ! CALCULATING THE CSA 1/T1 AND 1/T2*******************************************
1000  FOR B2=0 TO 2
1010    Fnb2=6*Dall+D1(J)*(N*PI)^2/(4*C(K)^2)+B2^2*D2(L)
1020    FOR I=2 TO 4 STEP 2
1030      Jcsa=2*Fnb2/(Fnb2^2+Freq(I)^2)
1040      M=Coef(B2)*G(N)*D(B1,B2)^2*Jcsa
1050      Sumcsa(I)=Sumcsa(I)+M
1060    NEXT I
1070  NEXT B2
1080  IF B1=2 THEN
```

```
1090       IF N=9 THEN
1100          R1csa(J,L)=6*Kcsa*Sumcsa(2)
1110          R2csa(J,L)=Kcsa*(3*Sumcsa(2)+4*Sumcsa(4))
1120          GOTO 810
1210       ELSE
1220          GOTO 810
1230       END IF
1240    ELSE
1250       GOTO 800
1260    END IF
1270    !  CALCULATING 1/T1 (= 1/T1(DD) + 1/T1(CSA)), 1/T2 (= 1/T2(DD) + 1/T2(CSA)
) AND NOE (= CONSTANT * NOE EQUATION NUMERATOR / 1/T1)****************************
1321    FOR J=1 TO 5
1322       FOR L=1 TO 5
1323          Both1(J,L)=R1(J,L)+R1csa(J,L)
1324          Both2(J,L)=R2(J,L)+R2csa(J,L)
1325          Noe(J,L)=26.7519/25.167*Sigma(J,L)/Both1(J,L)
1326       NEXT L
1327    NEXT J
1328    PRINT
1330    PRINT USING "9A,5X,DE,9X,DE,9X,DE,9X,DE,9X,DE":" D1 // D2",D2(1),D2(2),D2(
3),D2(4),D2(5)
1331    PRINT
1332    ! PRINTING T1 VALUES**********************************************************
1334    FOR J=1 TO 5
1335    PRINT USING "DE,7X,3D.3D,7X,3D.3D,7X,3D.3D,7X,3D.3D,7X,3D.3D";D1(J),1/Both
1(J,1),1/Both1(J,2),1/Both1(J,3),1/Both1(J,4),1/Both1(J,5)
1336    NEXT J
1337    PRINT
1338    ! PRINTING LINEWIDTH VALUES***************************************************
1340    FOR J=1 TO 5
1341    PRINT USING "DE,7X,3D.3D,7X,3D.3D,7X,3D.3D,7X,3D.3D,7X,3D.3D";D1(J),Both2(
J,1)/PI,Both2(J,2)/PI,Both2(J,3)/PI,Both2(J,4)/PI,Both2(J,5)/PI
1342    NEXT J
1343    PRINT
1344    ! PRINTING NOE VALUES*********************************************************
1346    FOR J=1 TO 5
1347    PRINT USING "DE,7X,MZ.4D,7X,MZ.4D,7X,MZ.4D,7X,MZ.4D,7X,MZ.4D";D1(J),Noe(J
1),Noe(J,2),Noe(J,3),Noe(J,4),Noe(J,5)
1348    NEXT J
1349    PRINT
1350    IF K=4 THEN
1351       GOTO 1380
1352    ELSE
1360       GOTO 894
1370    END IF
1380    END
```

```
     τc=  3.E-7          SF=  270 MHz          DDCSA_004 FPHE ANALYSIS
     WOBBLE ANGLE=  0 DEGREES

      D1 // D2       1E+03        1E+08        1E+10        1E+12
     1E+03           8.780        1.099        3.810       16.763
     1E+08           8.780        1.099        3.810       16.763
T1   1E+10           8.780        1.099        3.810       16.763
     1E+12           8.780        1.099        3.810       16.763

     1E+03         258.324      119.857      116.957      116.886
Δν   1E+08         258.324      119.857      116.957      116.886
     1E+10         258.324      119.857      116.957      116.886
     1E+12         258.324      119.857      116.957      116.886

     1E+03         -1.0021      -0.7623      -0.0220      -0.9616
     1E+08         -1.0021      -0.7623      -0.0220      -0.9616
nOe  1E+10         -1.0021      -0.7623      -0.0220      -0.9616
     1E+12         -1.0021      -0.7623      -0.0220      -0.9616
     WOBBLE ANGLE=  45 DEGREES

      D1 // D2       1E+03        1E+08        1E+10        1E+12
     1E+03           8.775        1.099        3.810       16.752
     1E+08           1.704         .869        1.900        3.062
     1E+10           8.153        1.478        4.694       15.801
     1E+12          13.529        1.592        5.851       27.961

     1E+03         258.136      119.753      116.853      116.782
     1E+08         170.434       71.578       69.402       69.332
     1E+10         169.696       70.930       68.985       68.932
     1E+12         169.679       70.913       68.970       68.923

     1E+03         -1.0021      -0.7624      -0.0222      -0.9616
     1E+08         -0.5052      -0.5658      -0.2134      -0.4996
     1E+10         -0.4876      -0.6622       0.0586      -0.4047
     1E+12         -0.9926      -0.7351       0.0032      -0.9412
     WOBBLE ANGLE=  90 DEGREES

      D1 // D2       1E+03        1E+08        1E+10        1E+12
     1E+03           8.777        1.100        3.811       16.757
     1E+08            .859         .694        1.204        1.585
     1E+10           3.415        1.700        3.767        6.919
     1E+12          26.693        2.981       11.932       62.816

     1E+03         258.077      119.721      116.822      116.751
     1E+08          86.996       30.714       28.939       28.869
     1E+10          83.362       28.148       27.147       27.105
     1E+12          83.272       28.060       27.084       27.060

     1E+03         -1.0021      -0.7623      -0.0222      -0.9616
     1E+08         -0.7296      -0.6243      -0.4842      -0.7177
     1E+10          0.1096      -0.2780       0.2034       0.1585
     1E+12         -0.9080      -0.6834       0.0517      -0.7966
```

```
     Tc=  6.E-9           SF=  270 MHz         DDCSA_004 FPHE ANALYSIS
     WOBBLE ANGLE=  0 DEGREES

      D1 // D2      1E+03         1E+08          1E+10          1E+12
     1E+03           .578          .605           .937          1.154
     1E+08           .578          .605           .937          1.154
T1   1E+10           .578          .605           .937          1.154
     1E+12           .578          .605           .937          1.154

     1E+03          5.462         3.918          2.555          2.485
     1E+08          5.462         3.918          2.555          2.485
Δν   1E+10          5.462         3.918          2.555          2.485
     1E+12          5.462         3.918          2.555          2.485

     1E+03        -0.8647       -0.7071        -0.6642        -0.8765
     1E+08        -0.8647       -0.7071        -0.6642        -0.8765
nOe  1E+10        -0.8647       -0.7071        -0.6642        -0.8765
     1E+12        -0.8647       -0.7071        -0.6642        -0.8765
     WOBBLE ANGLE=  45 DEGREES

      D1 // D2      1E+03         1E+08          1E+10          1E+12
     1E+03           .578          .605           .938          1.154
     1E+08           .611          .626          1.001          1.247
     1E+10           .857          .897          1.456          1.855
     1E+12           .894          .937          1.550          1.955

     1E+03          5.461         3.918          2.555          2.485
     1E+08          4.160         2.977          1.847          1.778
     1E+10          3.601         2.468          1.527          1.475
     1E+12          3.585         2.452          1.512          1.465

     1E+03        -0.8647       -0.7071        -0.6642        -0.8765
     1E+08        -0.6786       -0.5312        -0.4824        -0.6638
     1E+10        -0.8142       -0.6372        -0.5851        -0.8158
     1E+12        -0.8616       -0.6787        -0.6416        -0.8752
     WOBBLE ANGLE=  90 DEGREES

      D1 // D2      1E+03         1E+08          1E+10          1E+12
     1E+03           .578          .605           .938          1.155
     1E+08           .637          .643          1.040          1.308
     1E+10          1.272         1.320          2.224          3.033
     1E+12          1.871         1.968          3.706          4.933

     1E+03          5.460         3.917          2.554          2.484
     1E+08          3.528         2.567          1.528          1.459
     1E+10          1.845         1.183           .662           .620
     1E+12          1.757         1.096           .599           .576

     1E+03        -0.8647       -0.7071        -0.6641        -0.8765
     1E+08        -0.6240       -0.4794        -0.4250        -0.6003
     1E+10        -0.4953       -0.3305        -0.2428        -0.4246
     1E+12        -0.8514       -0.6209        -0.5870        -0.8644
```

```
        Tc=  3.E-7            SF=  270 MHz   DDCSA_002      FTYR ANALYSIS
        WOBBLE ANGLE=  0 DEGREES

         D1 // D2      1E+03          1E+08          1E+10          1E+12

         1E+03        16.508          2.250          6.975         17.298
T1       1E+08        16.508          2.250          6.975         17.298
         1E+10        16.508          2.250          6.975         17.298
         1E+12        16.508          2.250          6.975         17.298

         1E+03       306.179        131.524        129.673        129.641
Δν       1E+08       306.179        131.524        129.673        129.641
         1E+10       306.179        131.524        129.673        129.641
         1E+12       306.179        131.524        129.673        129.641

         1E+03       -0.9418        -0.1284        -0.3979        -0.9869
nOe      1E+08       -0.9418        -0.1284        -0.3979        -0.9869
         1E+10       -0.9418        -0.1284        -0.3979        -0.9869
         1E+12       -0.9418        -0.1284        -0.3979        -0.9869

        WOBBLE ANGLE=  45 DEGREES

         D1 // D2      1E+03          1E+08          1E+10          1E+12

         1E+03        16.498          2.250          6.974         17.287
         1E+08         2.252          1.257          2.372          2.971
         1E+10        12.538          2.637          7.418         15.780
         1E+12        27.163          2.973         10.165         28.908

         1E+03       305.983        131.409        129.559        129.527
         1E+08       213.394         78.490         76.925         76.893
         1E+10       212.639         77.864         76.481         76.454
         1E+12       212.624         77.849         76.468         76.444

         1E+03       -0.9418        -0.1284        -0.3981        -0.9869
         1E+08       -0.3631        -0.2027        -0.3825        -0.4790
         1E+10       -0.3232        -0.0680        -0.1912        -0.4068
         1E+12       -0.9116        -0.0998        -0.3411        -0.9702

        WOBBLE ANGLE=  90 DEGREES

         D1 // D2      1E+03          1E+08          1E+10          1E+12

         1E+03        16.502          2.250          6.975         17.292
         1E+08         1.302           .894          1.330          1.563
         1E+10         3.969          2.278          4.630          6.613
         1E+12        57.533          4.821         18.531         65.506

         1E+03       305.920        131.374        129.524        129.492
         1E+08       119.247         33.468         32.040         32.008
         1E+10       115.213         30.936         30.084         30.060
         1E+12       115.128         30.852         30.027         30.013

         1E+03       -0.9418        -0.1284        -0.3981        -0.9869
         1E+08       -0.5812        -0.3993        -0.6162        -0.6980
         1E+10        0.0873         0.0501         0.1018         0.1454
         1E+12       -0.7375        -0.0618        -0.2375        -0.8397
```

```
         Tc=   6.E-9          SF=  270 MHz   DDCSA_002      FTYR ANALYSIS
         WOBBLE ANGLE=  0 DEGREES

          D1 // D2      1E+03         1E+08         1E+10         1E+12

         1E+03           .956          .719         1.051         1.154
T1       1E+08           .956          .719         1.051         1.154
         1E+10           .956          .719         1.051         1.154
         1E+12           .956          .719         1.051         1.154

         1E+03          6.303         3.962         2.771         2.740
Δν       1E+08          6.303         3.962         2.771         2.740
         1E+10          6.303         3.962         2.771         2.740
         1E+12          6.303         3.962         2.771         2.740

         1E+03        -0.7158       -0.5378       -0.7864       -0.8634
nOe      1E+08        -0.7158       -0.5378       -0.7864       -0.8634
         1E+10        -0.7158       -0.5378       -0.7864       -0.8634
         1E+12        -0.7158       -0.5378       -0.7864       -0.8634

         WOBBLE ANGLE=  45 DEGREES

          D1 // D2      1E+03         1E+08         1E+10         1E+12

         1E+03           .957          .719         1.051         1.154
         1E+08           .919          .715         1.109         1.224
         1E+10          1.444         1.039         1.636         1.851
         1E+12          1.539         1.087         1.739         1.955

         1E+03          6.302         3.962         2.771         2.739
         1E+08          4.946         3.053         1.990         1.958
         1E+10          4.379         2.561         1.652         1.626
         1E+12          4.364         2.546         1.639         1.616

         1E+03        -0.7158       -0.5377       -0.7864       -0.8634
         1E+08        -0.4825       -0.3754       -0.5821       -0.6422
         1E+10        -0.6260       -0.4504       -0.7091       -0.8023
         1E+12        -0.6792       -0.4798       -0.7674       -0.8624

         WOBBLE ANGLE=  90 DEGREES

          D1 // D2      1E+03         1E+08         1E+10         1E+12

         1E+03           .957          .719         1.051         1.154
         1E+08           .930          .724         1.152         1.276
         1E+10          1.919         1.451         2.492         2.969
         1E+12          3.454         2.170         4.149         4.937

         1E+03          6.301         3.961         2.770         2.739
         1E+08          4.256         2.656         1.637         1.606
         1E+10          2.437         1.289          .706          .682
         1E+12          2.353         1.206          .649          .635

         1E+03        -0.7158       -0.5377       -0.7863       -0.8634
         1E+08        -0.4207       -0.3275       -0.5214       -0.5774
         1E+10        -0.2657       -0.2008       -0.3450       -0,4110
         1E+12        -0.5970       -0.3752       -0.7173       -0.8535
```

B30423